https://doi.org/10.15388/vu.thesis.351
https://orcid.org/0000-0001-5503-4775

VILNIUS UNIVERSITY

Joana Smirnovienė

Switching inhibitor recognition by engineering isozymes of carbonic anhydrase

DOCTORAL DISSERTATION

Technological sciences,
Chemical engineering (T 005)

VILNIUS 2022

This dissertation was written between 2016 and 2022 at Vilnius university. The research was supported by the Research Council of Lithuania, Vilnius University, L'ORÉAL Baltic "For Woman in Science" program with the Lithuanian National Commission for UNESCO and the Lithuanian Academy of Sciences.

Academic supervisor – Prof. Dr. Daumantas Matulis (Vilnius University, Technological sciences, Chemical engineering, T 005).

This doctoral dissertation will be defended in a public meeting of the Dissertation Defence Panel:

Chairman – Prof. Dr. Gintaras Valinčius (Vilnius University, Natural sciences, Biochemistry, N 004).

Members:

Prof. Dr. Asta Juzėnienė (Oslo University Hospital, Norway, Technological sciences, Chemical engineering, T 005).

Dr. Giedrius Sasnauskas (Vilnius University, Natural sciences, Biochemistry, N 004).

Prof. Dr. Jolanta Sereikaitė (Vilnius Tech, Technological sciences, Chemical engineering, T 005).

Dr. Juozas Šiurkus (Thermo Fisher Scientific Baltics, Technological sciences, Chemical engineering, T 005).

The dissertation shall be defended at a public meeting of the Dissertation Defence Panel at 13:00 on 31st August 2022 in Room No. R401 of the Life Sciences Center (Vilnius University).

Address: Saulėtekio av. 7., Room No. R401, Vilnius, Lithuania
Tel. +370 678 43799; e-mail: joana.smirnoviene@gmc.vu.lt

The text of this dissertation can be accessed at the library of Vilnius University and on the website of Vilnius University: *www.vu.lt/lt/naujienos/ivykiu-kalendorius*

https://doi.org/10.15388/vu.thesis.351
https://orcid.org/0000-0001-5503-4775

VILNIAUS UNIVERSITETAS

Joana Smirnovienė

Slopiklių atpažinimo perjungimas, panaudojant chimerinių karboanhidrazių izofermentų inžineriją

DAKTARO DISERTACIJA

Technologijos mokslai,
Chemijos inžinerija (T 005)

VILNIUS 2022

Disertacija rengta 2016–2022 metais Vilniaus universitete.
Mokslinius tyrimus rėmė Lietuvos mokslo taryba; Vilniaus universitetas; L`ORÉAL Baltijos šalių "Moterims moksle" programa, vykdoma kartu su Lietuvos nacionaline UNESCO komisija ir Lietuvos mokslų akademija.

Mokslinis vadovas – prof. dr. Daumantas Matulis (Vilniaus universitetas, technologijos mokslai, chemijos inžinerija, T 005).

Gynimo taryba:
Pirmininkas – prof. dr. Gintaras Valinčius (Vilniaus universitetas, gamtos mokslai, biochemija, N 004).
Nariai:
prof. dr. Asta Juzėnienė (Oslo Universiteto ligoninė, Norvegija, technologijos mokslai, chemijos inžinerija, T 005).
dr. Giedrius Sasnauskas (Vilniaus universitetas, gamtos mokslai, biochemija, N 004).
prof. dr. Jolanta Sereikaitė (Vilnius Tech, technologijos mokslai, chemijos inžinerija, T 005).
dr. Juozas Šiurkus (UAB “Thermo Fisher Scientific Baltics”, technologijos mokslai, chemijos inžinerija, T 005).

Disertacija ginama viešame Gynimo tarybos posėdyje 2022 m. rugpjūčio mėn. 31 d. 13 val. Vilniaus universiteto Gyvybės mokslų centro R401 auditorijoje. Adresas: Saulėtekio al. 7, R401, Vilnius, Lietuva, tel. +370 678 43799 ; el. paštas joana.smirnoviene@gmc.vu.lt .

Disertaciją galima peržiūrėti Vilniaus universiteto bibliotekoje ir VU interneto svetainėje adresu: *https://www.vu.lt/naujienos/ivykiu-kalendorius*

ABBREVIATIONS

ANS	8-anilino-1-naphthalenesulfonate
CA	carbonic anhydrase
[*CA*]	carbonic anhydrase concentration
chCA	chimeric carbonic anhydrase
CHES	2-(cyclohexylamino)ethanesulfonic acid
DMSO	dimethyl sulfoxide
FTSA	fluorescent thermal shift assay
ΔG	Gibbs free energy change
h	Hill coefficient
ΔH	enthalpy change
HEPES	4-(2-hydroxyethyl)piperazine-1-ethanesulfonic acid
[*I*]	inhibitor concentration
IC_{50}	half-maximal inhibitory concentration
ITC	isothermal titration calorimetry
K_b	binding constant
k_{cat}	catalytic constant
$k_{cat\text{-}max}$	maximal catalytic constant
K_d	dissociation constant
$K_{d\text{-}obs.}$	observed dissociation constant
$K_{d\text{-}intr.}$	intrinsic dissociation constant
K_i	inhibition constant
K_M	Michaelis-Menten constant
MES	2-(N-morpholino)ethanesulfonic acid
MOPS	3-(N-morpholino)propanesulfonic acid
n_{CA}	number of protonated hydroxide ions bound to the CA active site's Zn
n_{sulf}	number of protons released during the deprotonation of the sulfonamide inhibitor
$pK_{a\text{-}CA}$	pK_a of CA's Zn-bound water molecule
$pK_{a\text{-}SA}$	pK_a of the compound's sulfonamide group
ΔS	entropy change
[*S*]	substrate concentration
SFA	stopped-flow CO_2 hydration assay
SPR	surface plasmon resonance
TRIS	tris(hydroxymethyl)aminomethane

TABLE OF CONTENT

INTRODUCTION 8
1. LITERATURE OVERVIEW 11
1.1. Catalytic mechanism 11
1.2. Inhibitor binding mechanism 13
1.3. Carbonic anhydrase II 14
1.4. Carbonic anhydrase VI 15
1.5. Carbonic anhydrase XII 15
2. METHODS 17
2.1. Fluorescent thermal shift assay 17
2.2. Isothermal titration calorimetry 18
2.3. Stopped-flow CO_2 hydration assay 19
2.4. Synthesis of sulfonamide inhibitors 20
2.5. Production of carbonic anhydrases 21
3. SUMMARY OF RESULTS 22
3.1. MANUSCRIPT 1: A standard operating procedure for an enzymatic activity inhibition assay 22
3.2. MANUSCRIPT 2: Picomolar inhibitors of carbonic anhydrase: Importance of inhibition and binding assays 23
3.3. MANUSCRIPT 3: Experimental approaches to identify selective picomolar inhibitors for carbonic anhydrase IX 24
3.4. MANUSCRIPT 4: Engineered carbonic anhydrase VI-mimic enzyme switched the structure and affinities of inhibitors 25
3.5. MANUSCRIPT 5: Switching the inhibitor – enzyme recognition profile via chimeric carbonic anhydrase XII 25
3.6. MANUSCRIPT 6: Isoform-selective enzyme inhibitors by exploring pocket size according to the Lock-and-Key principle 26
4. GENERAL DISCUSSION 28
4.1. Importance of combining biophysical and enzymatic inhibition methods 28
4.2. Switching inhibitor recognition 30

4.2.1. Kinetic studies 31
4.2.2. Binding and inhibition studies 32
5. CONCLUDING REMARKS AND FUTURE PROSPECTIVES 34
6. SUMMARY IN LITHUANIAN LANGUAGE 36
7. ACKNOWLEDGEMENTS 54
8. PUBLICATIONS INCLUDED IN THE DISSERTATION 55
9. PUBLICATIONS NOT INCLUDED IN THE DISSERTATION 57
10. LIST OF SCIENTIFIC EVENTS 59
11. CURRICULUM VITAE 61
12. REFERENCES 63
13. COPIES OF PUBLICATIONS 75

INTRODUCTION

Enzymes are common targets for the discovery of small-molecule drugs. Scientists worldwide discovered numerous enzyme inhibitors to prevent or treat a wide range of diseases. Rational drug design exploits the knowledge about structure-activity relationships. Generally, inhibitors' chemical groups are modified, and interactions with target protein are measured under various experimental conditions to determine the inhibitory activity. Affinity and selectivity towards the target enzyme are the main parameters describing an inhibitor's potency to become a drug.

This thesis focuses on the carbonic anhydrase-sulfonamide recognition mechanism. Humans have 12 active isoforms of carbonic anhydrases (CA) that share high structural homology but have different physiological functions. More than 30 CA inhibitors, mostly primary sulfonamides, are used in clinics to treat glaucoma, altitude sickness, epilepsy, congestive heart failure, idiopathic intracranial hypertension, congestive heart failure, and other diseases. However, most of them lack selectivity towards a particular isozyme and cause side effects such as panting, depression, vomiting, diarrhea, and collapse. There is a huge demand for novel CA inhibitors with higher selectivity and affinity towards particular isoforms to ensure higher efficiency and fewer side effects.

For designing the highly selective and extremely strong drug candidates, we must understand the inhibitor recognition mechanism. To investigate how carbonic anhydrase recognises the sulfonamide (classical CA inhibitor), we did the following research:

I) Modified the chemical groups of inhibitors.
II) Engineered the active site of CA II to generate chimeric CA (chCA).
III) Measured affinities by fluorescent thermal shift assay (FTSA), isothermal titration calorimetry (ITC), and stopped-flow CO_2 hydration (SFA).
IV) Performed structural studies by X-ray crystallography and molecular modeling.

My colleagues at the Institute of Biotechnology, Life Sciences Center, Vilnius University did a large amount of work, including synthesizing sulfonamide compounds, producing recombinant CAs, performing molecular modeling, and X-ray crystallographic studies. My contribution was to characterize CA and chCA catalytic activity, thermal stability, as well as

binding and inhibition by chemical compounds. I have applied FTSA, ITC and SFA methods to characterize the binding parameters and investigate the recognition mechanism. The techniques have advantages and limitations, especially when working with tight-binding inhibitors. Therefore, I highlighted the importance of combining several methods to obtain reliable binding parameters.

The dissertation contains two main parts. The first part describes the advantages and disadvantages of enzymatic activity inhibition and biophysical methods. The second part is devoted to analyzing the engineered carbonic anhydrases and their recognition profiles for a series of inhibitors. The principal scheme of constructing chimeric carbonic anhydrase XII is shown in Figure 1.

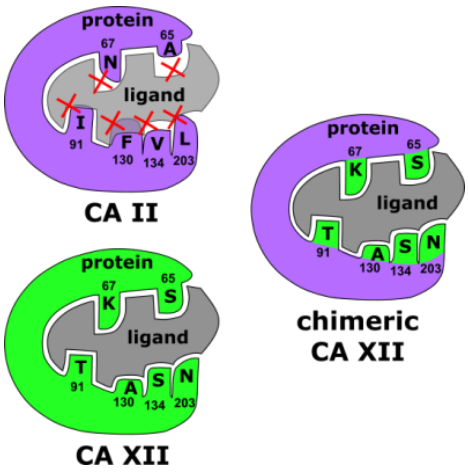


Figure 1. Chimeric carbonic anhydrase XII (chCA XII) is based on CA II with six CA XII-specific amino acids in the active site. Therefore, chCA XII bound ligands as CA XII but not CA II.

Goal:

The main aim of this thesis was to investigate the switching of inhibitor recognition by engineering isozymes of carbonic anhydrase.

Objectives:

We have set the following objectives to achieve a dissertation's goal:

1. To characterize chCAVI's and chCA XII's thermal stability, catalytic activity, and inhibition by sulfonamide compounds.
2. To evaluate the switching of inhibitor recognition from CA II to CA XII using chCA XII.

3. To compare FTSA, ITC, and SFA assays by measuring chemical compound interactions with target and chimeric CA isozymes and explain the advantages and limitations of these techniques for determining affinities of tight-binding inhibitors.

Scientific novelty:

This study has shown that a chemical compound is being recognized by a rather small set of up to six amino acids located in the active site of a protein. Mutation of the six amino acids in the active site of CA II caused the enzyme to begin recognizing different chemical compounds. The mutations were designed to resemble the active site of isozyme CA XII. The chCA XII bound the same ligands that the native CA XII binds. However, the affinity for those compounds that CA II preferred to bind was significantly diminished. Thus, the mutated CA II protein switched into CA XII in its small molecule compound recognition profile. The structures of carbonic anhydrases were rather rigid and did not significantly change during inhibitor binding. Engineered chCA XII allowed us to determine the fundamental structural difference between CA II and CA XII. The research resulted in designing the CA XII-selective nanomolar inhibitor EA12-7.

Defending statements:

1. A chemical compound is being recognized in the active site of CA VI or CA XII by a set of up to six key amino acids.
2. The chCA VI and chCA XII are good models of target isozymes and could be used to design CA isozyme-selective inhibitors.
3. Combining biophysical and enzymatic activity inhibition assays is essential to determine picomolar compound binding affinities.

1. LITERATURE OVERVIEW

A family of human carbonic anhydrase (CAs; EC 4.2.1.1) catalyzes carbon dioxide's reversible hydration ($CO_2 + H_2O \leftrightarrow HCO_3^- + H^+$). CAs are distributed in all kingdoms of life and are listed in eight categories: α, β, γ, δ, ζ, η, θ, and ι[1–8]. They are found in almost any live organism and are essential for an endless list of physiological and biochemical processes all over the body. In this thesis, I will focus on human CAs, called α-CAs. They contain 15 members, of which 12 are catalytically active. They differ in their physiological role, organ and tissue distribution, expression levels, kinetic properties, thermal stability, and inhibitor binding affinities[9]. CAs differently localize in the cell: five are cytosolic (isoforms I, II, II, VII, and XIII), two are mitochondrial (isozymes VA and VB), four are membrane-bound (isoforms IV, IX, XII, and XIV), and one is secreted (isozymeVI). Three members of CA family - VIII, IX, and X are catalytically inactive due to the absence of one or more critical Zn-coordinating histidines[10,11]. They are termed carbonic anhydrase-related proteins – CARP VIII, IX, and X[12].

1.1. Catalytic mechanism

The active site of carbonic anhydrase II is coned-shaped with a diameter of about 12 Å and a depth of about 13 Å[13]. One side is hydrophobic (Val121, Val143, Leu198, Val207, and Trp209), and the other is hydrophilic (Tyr7, Asn62, His64, Asn67, Thr199, and Thr200)[14]. The crystal structure (PDB code 6LUU), including the entrance conduit, and hydrophilic and hydrophobic residues, is shown in figure 2A. A catalytic zinc ion is tetrahedrally coordinated in the active site by imidazole groups of three histidine residues (His94, His96, and His119) and a water molecule/hydroxide ion[15]. The proton transfer and substrate/product/water exchange occur via water networks during catalytic reaction, as demonstrated in figure 2B. The catalytic mechanism of CO_2 hydration is represented in figure 2C.

Firstly, CO_2 hydration occurs in the hydrophobic part of the active site. A nucleophilic attack by the zinc-bound hydroxyl ion onto CO_2 produces a bicarbonate ion. The formed HCO_3^- is subsequently displaced by the water molecule[16]. In this way, a catalytically inactive form is obtained. Secondly, Zn-H_2O loses a proton, transferred to His64 via a water network. His64 is called the "proton shuttle"[17] and has two pH-dependent conformations: "in" and "out"[18]. His64 adopts an "in" orientation to closely bring delta nitrogen (Nδ) to the catalytic Zn atom. The proton transfer from Zn-H_2O to His64 is a

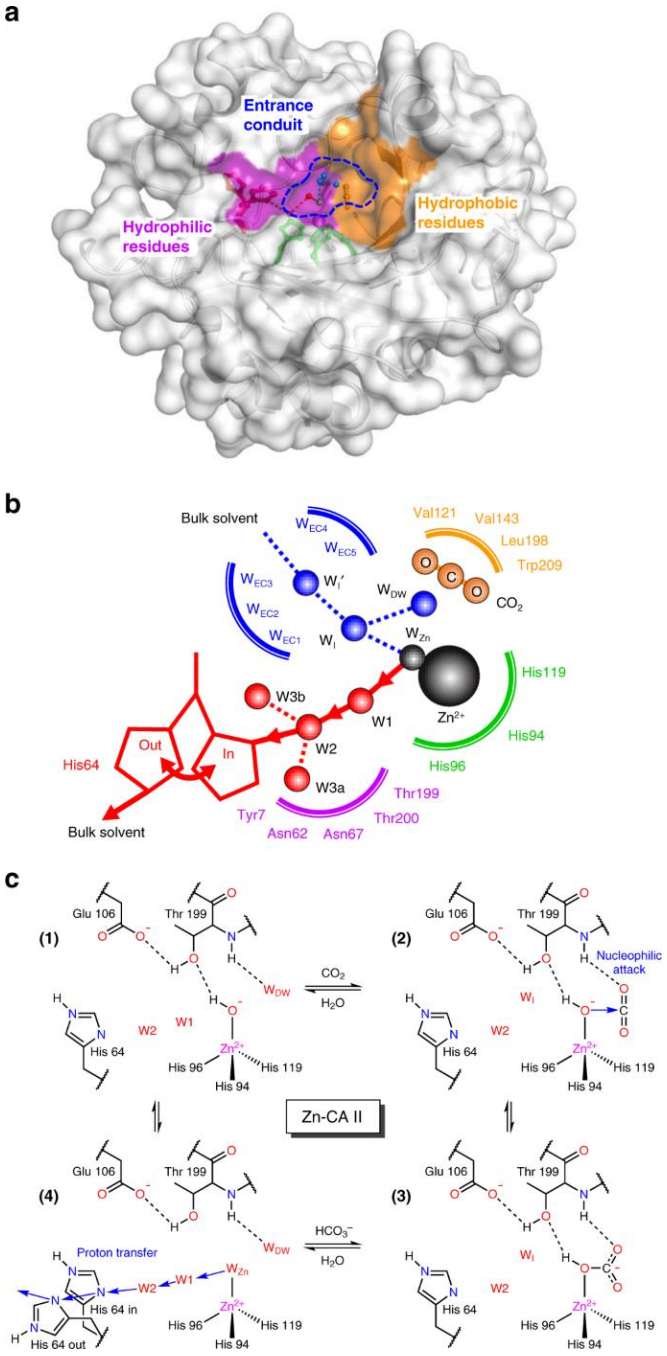


Figure 2. Structure of carbonic anhydrase II (PDB code 6LUU) and its catalytic mechanism[16]. (A) The active site consists of hydrophilic and hydrophobic sites and an entrance conduit. (B) Water networks during the catalysis. (C) The CO_2 hydration reaction mechanism.

rate-limiting step of the reaction with the free energy barrier of 10.4 kcal/mol[19]. After its protonation, His64 rotates to an "out" orientation to release N_δ's excess proton from the imidazole ring into the bulk solvent. The cycle continues as Zn-bound water becomes deprotonated and His64 reorients to "out" conformation[20].

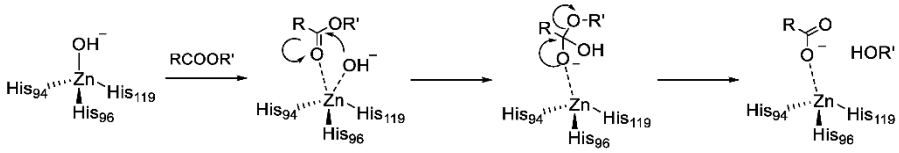


Figure 3. Catalytic mechanism of CA esterase activity[21].

Carbonic anhydrases catalyze not only CO_2 hydration activity but also hydrolysis of esters[21]. The reaction occurs in the active site of CA, and the mechanism is shown in figure 3. It is pretty similar to the hydration of carbon dioxide. The esters are hydrolyzed by the nucleophilic attack of a zinc-coordinated OH^- to the carbonyl CO with the formation of an oxyanionic intermediate. Experimentally, the catalytic reaction is usually measured using *p*-nitrophenyl acetate as a substrate[22].

1.2. Inhibitor binding mechanism

Patients have been using CA inhibitors as treatment options in many disease areas, including glaucoma drugs[23,24], diuretics[25], and antiepileptic drugs[26–29]. However, most inhibitors used clinically lack selectivity towards targeted CA isozymes and have various side effects. Thus, there is a demand for selective inhibitors that target only the disease-associated CA isoform, such as CA IX or CA XII, that regulate the pH of the tumor microenvironment[30]. However, the high homology amino acid sequence between isozymes complicates the design and development of CA isoform-selective inhibitors. The sequence identity of CAs catalytic domain is more than 30 %[20]. The active sites of CA isoforms are conical in shape and differ by only a few amino acids. The top of the binding site is variable, and the most conserved residues are found deep in the active site and close to the zinc ion[31]. Thermodynamic, kinetic, and structural analysis of interactions between more than 400 inhibitors and 12 CA isozymes revealed that minor structural differences between CA isoforms cause unpredictable effects how the ligand is recognized[9].

Primary sulfonamides are the substrate's (carbon dioxide) hydration transition state analogs. They are classical inhibitors and interact with carbonic anhydrases in the simplest case of reversible competitive 1:1

inhibition. A single sulfonamide molecule competes with the carbon dioxide and binds reversibly (non-covalently) to the CA's active site.

The binding occurs when the inhibitor's sulfonamide group is deprotonated and the Zn-bound water molecule is protonated. The process is highly pH-dependent. The calculations are provided in subsection 2.1 and the principal scheme is shown in figure 4.

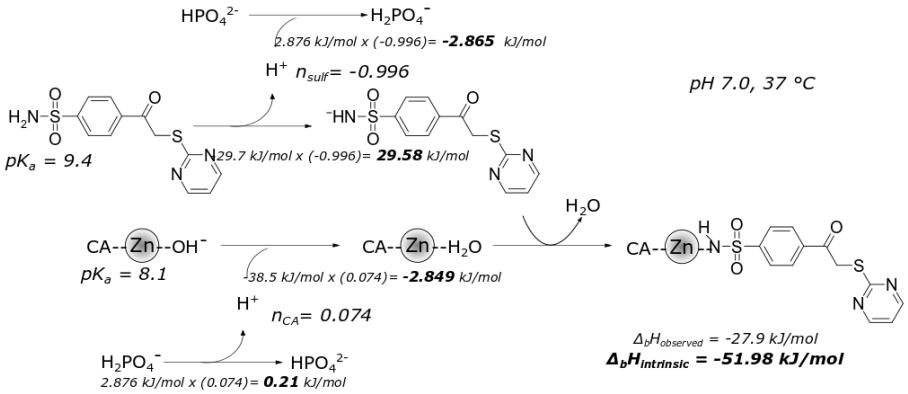


Figure 4. The principle scheme of the sulfonamide inhibitor binding to CA I[32]. The phosphate buffer participates as a proton donor or acceptor. Here, n_{sulf} is the number of protons released during the deprotonation of the sulfonamide inhibitor, and n_{CA} is the number of protonated hydroxide ions bound to the active site's Zn. The "n" values are calculated using the Henderson-Hasselbalch equation and multiplied by enthalpies of an each related reaction yields the observed enthalpic contribution of each reaction at pH 7.0, 37 °C.

All protonation events should be subtracted from the observed reaction to evaluate the intrinsic binding parameters of the CA-sulfonamide interaction.

1.3. Carbonic anhydrase II

Carbonic anhydrase II is the best-studied and most abundant isoform of CAs. CA II is a 29 kDa monomeric protein with dimensions of 40 × 42 × 56 Å. The cytosolic CA II has a large expression in *E. coli* bacteria and purification yield, highest catalytic efficiency among CAs ($k_{cat\text{-}max}$ = 0.6–1.4 μs^{-1})[33–35], moderate thermal stability (T_m 55–59 °C)[36–38] and is easily crystallized. The CA II is usually studied as a model protein[13]. In addition, scientists consider CA II and CA I as off-target isozymes because they are found in erythrocytes and play a significant role in respiration and regulating blood ion concentration[10,39–41].

1.4. Carbonic anhydrase VI

CA VI is the only isozyme of human CA produced by salivary and mammary glands[42,43]. It has a dimeric structure[44]. Researchers also found the CA VI in serum, respiratory airways, and gastrointestinal tract[45–49]. In addition, it is involved in saliva pH regulation, bitter taste perception, and tooth formation[43,50]. Increased salivary CA VI activity is related to the amount of supragingival dental calculus[51] and the development of dental caries in school children[50,52,53]. Recently, Pemmari et al. assessed the regenerative potential of CA VI for animal wound healing. However, the study showed that CA is not responsible for the licking-associated improved wound healing in animals[54].

Our laboratory team has produced recombinant CA VI in *E. coli* bacteria, and mammalian FreeStyle 293-F suspension cells, and directly purified it from human saliva. Biophysical studies showed that CA VI from all three sources bound a class of inhibitors with identical affinities within the error margin[55]. In addition, this study confirmed that recombinant CA VI's from bacteria or mammalian cells are good models of the native isozyme VI.

Recombinant and native CA VI have a low purification yield, which complicates the screening of inhibitors and the determination of the first crystal structure of CA VI bound to a ligand. For this reason, we need an additional model of CA VI to accelerate the discovery of novel CA VI-selective compounds.

1.5. Carbonic anhydrase XII

CA XII is an essential isozyme in cancer development because it controls the extracellular pH of cancer cells and acts as a hypoxia-induced tumor marker. Estrogen receptors in breast cancer regulate CA XII[56]. High expression of CA XII correlates with favorable survival of patients having invasive breast or resectable non-small cell lung cancers[57,58]. However, it is associated with poor prognosis in patients with colorectal, hepatocellular carcinomas, and diffuse astrocytomas[59–61]. Furthermore, CA XII is considered as a pharmacological target for overcoming chemoresistance in cancer cells[62]. The lower wide-spread expression of CA XII has also been detected in the human eye, gut, kidney, pancreas, gastric mucosa, epithelial components of skin, endometrial epithelium, and male excurrent ducts[47,63–67]. Additional roles of CA XII in the human body include glaucoma progression, salt uptake in sweat glands, and pH regulation of nucleus pulposus cells[66,68,69]. Waheed and Sly, in great detail, reviewed CA XII's functional role in diseases[70].

CA XII is a highly challenging drug target. Traditional screening and drug design protocols are limited because it is a membrane-associated dimeric enzyme containing an N-terminal extracellular catalytic domain, a membrane-spanning α-helix, and a 30-residue intracellular C-terminal region. Therefore, CA XII has been the target of many studies to determine its structure and function at the atomic level. Whittington et al. solved the first crystallographic structure of CA XII with a resolution of 1.55 Å in 2001[71]. The composition of the active site is analogous to the CA II: His94, His96, His119, and a water molecule coordinates the zinc ion. The pK_a of the zinc-bound water molecule at 25°C is 7.0–7.1[72,73]. Our research group deposited to Protein Data Bank the structural data for 24 crystal structures of chlorinated/ fluorinated mono-/di-substituted benzenesulfonamides bound to CA XII complexes, forming a valuable resource for CA XII-selective inhibitor design.

2. METHODS

I used and compared FTSA, ITC, and SFA methods in my dissertation.

2.1. Fluorescent thermal shift assay

Salemme and co-workers introduced fluorescent thermal shift assay (FTSA, also termed ThermoFluor® or differential scanning fluorimetry) in miniaturized format in 2001[74]. The method is gaining popularity in academic and industrial laboratories due to its precision, simplicity, and rapidity. The protein thermal stability is measured upon heat-induced protein unfolding[75] by recording the fluorescence of a solvatochromic dye, such as SyproOrange[76,77] or 1-anilino-8-naphthalene sulfonate (ANS)[78,79]. ANS is more suitable for measuring the CA-sulfonamide interactions[80]. The ANS dye binds to CA, forming ionic bonds via negatively charged sulfonate and cationic groups of the soluble enzyme[81]. The fluorescence of ANS highly increases as it attaches to the hydrophobic interior of the protein while water quenches it strongly[82]. FTSA allowed us to characterize thermal stability profiles of recombinant human CA I – CA XIV [38,55,72,83–85], and chCA XII[86]. Furthermore, FTSA has also been effectively used in inhibitor binding studies since the shift in protein melting temperature upon adding a ligand is related to the binding affinity[79,80,87].

Experimental conditions:

I carried out CA or chCA thermal stability and inhibitor binding experiments using a Corbett Rotor-Gene 6000 (QIAGEN Rotor-Gene Q) instrument. The protein solution was heated from 25 to 99 °C (heating rate - 1 °C/min). The melting temperature T_m was determined by following the fluorescence of ANS (λ_{ex} - 365 ± 20 nm, λ_{em} - 460 ± 15 nm) or SyproOrange (λ_{ex} - 470 ± 20 nm, λ_{em} - 610 ± 15 nm). I used SyproOrange when ANS was not suitable due to highly-fluorescent inhibitors. ANS stock solution was prepared by dissolving its powder in DMSO at 10 mM concentration while SyproOrange was bought as a commercial liquid solution with unavailable information about concentration of the active molecules. The FTSA experiment samples consisted of a constant 5 μM concentration of CA (except 10 μM for CA IV) or chCA, 0–200 μM concentrations of a chemical compound, 50 μM ANS or 2000–3000-fold diluted from stock SyproOrange and 50 mM sodium phosphate buffer (at pH 7.0) containing 100 mM sodium chloride and 2% (v/v) of DMSO. In addition, several experiments were performed in a pH range of 5–10 using sodium phosphate or universal (50 mM

sodium acetate, 25 mM sodium borate, 50 mM sodium phosphate, and 50 mM sodium chloride) buffers. I obtained protein-ligand dosing curves as described in Ref.[80]. Parameters used to fit dosing curves: the temperature was 37 °C, the heat capacity of unfolding was 17 kJ/(mol·K), enthalpy of binding was -42 kJ/mol, the heat capacity of binding was -0.8 kJ/(molK), enthalpy of unfolding was 602.5 kJ/mol for CA I, 690 kJ/mol for CA II, chCA VI, chCA XII, 480 kJ/mol for CA III, CA IV, CA VI, and CA VII, 400 kJ/mol for CA VA, 300 kJ/mol for CA VB, 501.6 kJ/mol for CA IX, 520 kJ/mol for CA XII, 460 kJ/mol for CA XIII, and 450 kJ/mol for CA XIV.

The observed dissociation constants ($K_{\text{d-obs.}}$) were compared with intrinsic values ($K_{\text{d-intr.}}$) independent of pH. The $K_{\text{d-intr.}}$ was calculated using an equation[32]:

$$K_{d-intr.} = K_{d-obs.} \times \frac{10^{pH-pK_{a-SA}}}{1+10^{pH-pK_{a-SA}}} \times \frac{10^{pH-pK_{a-CA}}}{1+10^{pH-pK_{a-CA}}}$$

Here $pK_{\text{a-SA}}$ – pK_a of the compound's sulfonamide group; $pK_{\text{a-CA}}$ – pK_a of CA's Zn-bound water molecule.

2.2. Isothermal titration calorimetry

The isothermal titration calorimeter directly measures the heat absorbed or released by the biochemical reactions. Due to high sensitivity, ITC is especially suitable for characterizing typical non-covalent biomolecular interactions[88]. Thus, ITC is a powerful method for observing the enthalpy changes (ΔH), entropy changes (ΔS), Gibbs free energy changes (ΔG), and stoichiometry of binding partners in a single experiment[89,90]. Thermodynamic parameters ΔH and ΔG are measured directly, while ΔS is calculated. Moreover, researchers could determine the heat capacity of binding by measuring binding affinities at several temperatures (e. g. 13, 25, 37, 49 °C)[91]. To consider protonation effects, investigators could also perform experiments in broad-range pH and several buffers with varying ionization enthalpies[9,92,93].

Experimental conditions:

ITC experiments were carried out at 37 °C using VP-ITC or ITC-200 calorimeters. The solution containing 6–20 μM CA or chCA in the cell and was titrated with 60–200 μM inhibitor solution in the syringe. Experiments were performed in 50 mM sodium phosphate buffer containing 100 mM sodium chloride at pH 7.0 with a final DMSO concentration of 2 %. CAs were dialyzed in the reaction buffer before the titrations. Experimental setup used for VP-ITC instrument: 25 injections of 10 μL every 180 s at reference power of 4 μcal/s and stirring speed of 260 rpm; ITC200 instrument: 19 injections of

2 µL every 180 s at reference power of 5 µcal/s and stirring speed of 750 rpm. The binding thermodynamic parameters (ΔH, ΔS, and ΔG) were determined using MicroCal Origin software. The single binding model was applied to fit the experimental data after deleting the first injection point.

2.3. Stopped-flow CO_2 hydration assay

The stopped-flow apparatus was introduced in 1950 by Chance[94]. Since then, the SFA method has been the most popular for determining CA catalytic activity and chemical compounds' inhibitory effect[33,73,95–99]. Researchers use the pH indicators to follow the absorbance change while CA acidifies the pH. Firstly, Gibbons and Edsall[100,101], and later Khalifah[33] introduced a buffer factor and models, which correlate the activity of CA with the indicator's absorbance change. The indicator and buffer pairs should be chosen according to their pK_a values and reaction pH. For example, if pH is 7.5, phenol red (pK_a 7.5) and Hepes buffer (pK_a 7.5) are used. Substrate concentration is considered to be 17 mM at 25 °C[73,102,103]. However, gaseous CO_2 is lost when filling the syringes and during the experiment (visually seen pistons moving up). The unknown exact CO_2 concentration complicates determining the enzyme's catalytic parameters – catalytic constant k_{cat} and Michaelis-Menten constant K_M.

Experimental conditions:

I performed SFA experiments using Applied Photophysics SX.18 MV-R Stopped-Flow Spectrometer at 24 °C. I prepared the saturated substrate solution by bubbling CO_2 gas into milli-Q water for 1 hour at room temperature. I selected 25 mM buffer and 30–100 µM indicator pairs with similar pK_a values as follows: MES and bromocresol purple at pH 6.0–6.4 (λ_{590}), MOPS and bromothymol blue at pH 6.8–7.1 (λ_{615}), HEPES and phenol red at pH 7.2–7.8 (λ_{557}), TRIS and *m*-cresol purple at pH 8.1–8.4 (λ_{575}), CHES and thymol blue at pH 8.6–9.0 (λ_{595}), sodium carbonate and phenolphthalein pH 9.5–9.8 (λ_{595}). Solutions also contained 0.2 M sodium sulfate for maintaining ionic strength. Chosen CA concentration was directly related to its activity: 200–600 nM for CA I and CA XIII, 10–100 nM for CA II and CA IX, 200–800 nM for CA III, 50–200 nM for CA IV, chCA VI, CA VI, CA VII, chCA XII, CA XII, and CA XIV. I chose inhibitor concentrations according to their IC_{50}.

I determined kinetic parameters k_{cat} and K_M by performing experiments at varying CO_2 concentrations. First, I diluted the saturated carbon dioxide solution with milli-Q water and determined the final substrate concentrations according to Ref.[99]. Then, I obtained the kinetic parameters using

Lineweaver-Burk and Michaelis-Menten plots. In addition, I determined the pK_a values of His64 (CA II, chCA VI, CA VI, chCA XII, and CA XII) using a single ionization model:

$$k_{cat} = \frac{k_{cat-max}}{1 + 10^{pH-pK_a}}$$

Here $k_{cat-max}$ – maximal catalytic constant, k_{cat} – catalytic constant.

CA I has two pK_avalues, and I obtained them by applying a two-site ionization model:

$$k_{cat} = \frac{k_{cat-max1} \cdot 10^{-(pH+pK_{a1})} + k_{cat-max2} \cdot 10^{-(pK_{a1}+pK_{a2})}}{10^{-2pH} + 10^{-(pH+pK_{a1})} + 10^{-(pK_{a1}+pK_{a2})}}$$

Here $k_{cat-max}$ – maximal catalytic constant, k_{cat} – catalytic constant.

Inhibition constants were determined by varying inhibitor concentrations at pH 7.5. I used two models to determine the dissociation constant. Firstly, Hill's equation[104] was applied:

$$CA\ act.(\%) = \left(1 - \frac{1}{1+(\frac{IC_{50}}{[I]})^h}\right) \cdot 100\ \%$$

Here [IC_{50}] – half-maximal inhibitory concentration; h – Hill coefficient, [I] – inhibitor concentration.

Cheng-Prusoff equation is used to determine the inhibition constant K_i:

$$K_i = \frac{IC_{50}}{1+\frac{[S]}{K_M}}$$

Here [K_i] – inhibition constant; K_M – Michaelis-Menten constant, [S] – substrate concentration.

For comparison, the Morrison's model[105] was used:

$$CA\ act.(\%) = (1 - \frac{([CA] + [I] + K_d - \sqrt{([CA] + [I] + K_d)^2 - 4[CA][I]}}{2[CA]}) \cdot 100\%$$

Here [CA] – carbonic anhydrase concentration, [I] – inhibitor concentration, K_d – dissociation constant.

2.4. Synthesis of sulfonamide inhibitors

Commercial inhibitors were purchased from Sigma-Aldrich (St. Louis, MO, USA). Dr. Virginija Dudutienė, dr. Edita Čapkauskaitė, Audrius Zakšauskas, and their students synthesized sulfonamide compounds. Synthesis of them was published in Refs.[86,106–118]. All used chemical compounds are insoluble in water. I have dissolved all chemical compounds in DMSO at 10–50 mM concentration and diluted in buffers prior to the FTSA,

SFA, and ITC experiments. The final DMSO concentration was 2 % in FTSA and ITC experiments, and it was up to 1 % in SFA experiments. DMSO concentration of 1–2% increases the solubility of chemical compounds in buffers but do not significantly affect the stability and catalytic activity of the CA (unpublished data).

2.5. Production of carbonic anhydrases

I used in-house recombinant carbonic anhydrases in the study. Aurelija Mickevičiūtė, dr. Vaida Juozapaitienė, Vilma Michailovienė, dr. Jurgita Matulienė, Jelena Jachno, dr. Justina Kazokaitė-Adomaitienė and their students produced the CAs. Productions of CA's is described in Refs.[55,72,83–85,87,119–122]. CA VI, CA IX and CA XII have dimeric structure, but in-house they were recombinantly produced as monomers: amino acids 21 to 290 for CA VI, 138 to 390 for CA IX, 30 to 291 for CA XII. I determined the concentration of CA isozymes spectrophotometrically using extinction coefficients: 44920 $M^{-1}cm^{-1}$ for CA I, 50420 $M^{-1}cm^{-1}$ for CA II, 56045 $M^{-1}cm^{-1}$ for CA III, 55872.5 $M^{-1}cm^{-1}$ for CA IV, 71515 $M^{-1}cm^{-1}$ for CA VA, 57597.5 $M^{-1}cm^{-1}$ for CA VB, 55872.5 $M^{-1}cm^{-1}$ for CA VI, 46535 $M^{-1}cm^{-1}$ for CA VII, 35075 $M^{-1}cm^{-1}$ for CA IX, 42985 $M^{-1}cm^{-1}$ for CA XII, 50420 $M^{-1}cm^{-1}$ for CA XIII, and 41432.5 $M^{-1}cm^{-1}$ for CA XIV. The extinction coefficients were calculated using the Expasy ProtParam tool (https://web.expasy.org/protparam/protparam-doc.html).

3. SUMMARY OF RESULTS

I have included six manuscripts in this thesis. In this part, I have summarized the results of each publication and listed them not chronologically to show the related outcomes of the dissertation in a sequence. SFA, FTSA, and ITC methods in the manuscripts 1–3 are described. Next, publications 4–5 are dedicated to chCA VI and chCA XII. Finally, the recognition of an inhibitor according to the Lock-and-Key principle is represented in a Manuscript 6.

3.1. MANUSCRIPT 1: A standard operating procedure for an enzymatic activity inhibition assay

The Standard Operating Procedure describes the critical steps of the experimental setup and data analysis for the enzymatic activity inhibition assay to obtain highly reliable results. In addition, the protocol notifies the correct selection of the following parameters:

- **Enzyme-specific assay.** The rates of enzymatically catalyzed reactions could be measured by recording the product's appearance or the substrate's disappearance over a period of time. Carbonic anhydrases are one of the fastest known enzymes with k_{cat} of up to 10^6 s^{-1}, and for this reason, a rapid mixing technique such as stopped-flow [123,124] is needed to follow the kinetic reaction. As the concentration of inhibitor increases, the rates of catalytic reactions decrease until complete inhibition of the CA is achieved. Complete inhibition of the CA could be detected when the inhibited reaction's rate becomes equal to the rate of spontaneous CO_2 hydration.
- **Optimal experimental conditions.** Optimal conditions for the maximal catalytic efficiency of an enzyme should be determined to reduce the CA concentration in a sample. The rates of catalysis are affected by temperature, pH, ionic strength, buffer, and other additives. Some buffer components and solvents may inhibit the enzyme and must be tested before inhibition assays.
- **Enzyme concentration.** The enzymatic reaction rate linearly depends on enzyme concentration. Thus, the CA concentration should be large enough to detect the signal in an assay but significantly lower than the IC_{50}.
- **Substrate concentration.** Enzymes catalyze reactions when excess substrate exceeds enzyme concentration ([S] >> [E])[125]. The

Michaelis-Menten plot describes the dependence of the rate of enzymatic reaction on substrate concentration. Furthermore, when comparing the affinities of a series of inhibitors, enzyme inhibition experiments should be performed at a constant substrate concentration.

- **Inhibitor concentration.** Typically, a set of inhibitor concentrations is obtained by a serial dilution, depending on the expected affinity and enzyme concentration. For example, a three-fold dilution and nine points of inhibitor concentration are optimal for determining dose-response curves. The middle data point should be around $IC_{50,}$ and the last data point should affect >90 % enzyme inhibition.
- **Positive and negative controls.** Experiments without the enzyme or substrate provide the background of a tested reaction. Therefore, the observed signals of positive and negative controls have to be subtracted from catalyzed reactions.
- **Fitting models.** For simple cases, linear regression models can be used to fit the rates of reactions, but more complex reactions require nonlinear multi-parameter equations. In addition, dose-response curves are usually fitted using a simple Hill's or more complex Morrison's equation. The Hill coefficient must be 1, and the fitted curve should represent experimental data points correctly when the Hill model is applied.

3.2. MANUSCRIPT 2: Picomolar inhibitors of carbonic anhydrase: Importance of inhibition and binding assays

The manuscript compares enzyme activity inhibition and biophysical methods for studying protein-ligand interactions and highlights their advantages and limitations. Stopped-flow CO_2 hydration assay is the most popular for directly following CA enzymatic activity inhibition. However, the method has several limitations.

Firstly, the exact concentration of substrate – carbon dioxide dissolved in water is unknown. Several authors declare up to 17 mM CO_2 concentration at 25 °C[126,127]. However, the CO_2 gas spontaneously evaporates from samples. In this paper, we developed a new model for determining the CO_2 concentration in the sample. Moreover, I observed the K_M and k_{cat} of CA I and CA II in a wide range of pHs. CA II is one of the fastest enzymes with maximal k_{cat} - $6 \cdot 10^5$ s^{-1}, while CA I is less active with maximal k_{cat} - $2 \cdot 10^5$ s^{-1}. CA's activity increases as pH increases and reaches the maximal value. The K_M values are 1.4 ± 0.8 mM for CA I and 4.6 ± 1.0 mM for CA II in the pH range of 7.0–

9.0. Two-ionization groups were observed in the active site of CA I, yielding pK_a values of 6.9 ± 0.1 and 8.8 ± 0.1. CA II has a single-ionization group with a pK_a of 7.3 ± 0.2.

Secondly, the determination of inhibition constants by SFA is limited by enzyme activity and concentration. A series of dose-response curves were collected and fitted using Hill[104] and Morrison[105] equations. In the case of weak to moderate inhibition, both models provided the same IC_{50} values. However, the analysis demonstrated that only the Morrison[105] model is applicable for determining the K_d of tight-binding inhibitors.

In comparison, ITC is the only direct method to observe thermodynamic parameters of inhibitor binding to protein. However, Wiseman's "*c*-factor"[128] limits the binding constant determination, and ITC could not be used to measure very weak or tight interactions. Only the fluorescent thermal shift assay is applicable to determine picomolar affinities of ligand binding. All three assays need to be combined to characterize the CA-inhibitor interactions fully, especially when binding is extremely strong.

3.3. MANUSCRIPT 3: Experimental approaches to identify selective picomolar inhibitors for carbonic anhydrase IX

The review presents the design and identification of the nano- to picomolar inhibitors VD11-4-2, VD12-09, and VR16-09 that selectively target carbonic anhydrase IX. The review's part of biochemical and biophysical assays for *in vitro* measurements of inhibitor affinity is related to this dissertation.

Here, we discussed the structure-affinity relationship of 6 structurally similar compounds. Firstly, 4-substituted-2,3,5,6-benzenesulfonamides (VD10-13, VD10-35, and VR16-05) were discovered as nanomolar and selective inhibitors of the off-target CA isozyme I[114,115]. Substitution of a fluorine atom to cyclooctylamino group at the *ortho*- position in benzenesulfonamide ring (compound VD12-09) radically (>450 000-fold) decreased binding affinity to CA I. The same substituent at *meta*- position (compound VD11-4-2) resulted in a thousand-fold strengthened binding with CA IX (K_d 0.05 nM). Substitution to even more bulky and hydrophobic substituent – cyclododecylamino – at *ortho*- position (compound VR16-09) resulted in high affinity (K_d 0.16 nM) towards CA IX and loss of affinity for off-target isozymes I and II (K_d > 200 μM). The tight-binding of *para*-substituted compounds to CA I was enthalpy-driven, while *para*-, *meta*- and *para*-, *ortho*- substituted inhibitors bound to CA IX with dominated entropy[91,129]. A combination of FTSA, ITC, and SFA assays was necessary to

characterize such tight-binding inhibitors. However, only the FTSA method was suitable for determining the dissociation constants of the lead compounds.

3.4. MANUSCRIPT 4: Engineered carbonic anhydrase VI-mimic enzyme switched the structure and affinities of inhibitors

The paper describes the design and characterization of chimeric CA VI (chCA VI) protein. Kazokaitė et al. engineered this model protein via site-directed mutagenesis[165]. CA II was selected as a core isozyme, and five point mutations - A65T, N67Q, F130Y, V134Q, L203T, were introduced to the active site. The study aimed to evaluate a chCA VI as a model for X-ray crystallographic studies and inhibitor screening. To my knowledge, there have been no CA VI-selective inhibitors discovered or crystal structures of CA VI solved until now. I carried out SFA experiments to determine enzymatic activity and inhibition of chCA VI and CA VI, and compared the kinetic parameters to CA II. I observed the maximum catalytic activity of CA VI at pH 7.0–8.0 with catalytic constant k_{cat} – $1.9 \cdot 10^5$ $s^{-1,}$ and it dropped at higher pHs. ChCA VI had a similar pK_a value (7.3) and catalytic activity as CA II (k_{cat} – $1.9 \cdot 10^5$ s^{-1}), and in the pH range 7.1-8.4, Michaelis-Menten constant K_M (6.8 ± 2.0 mM) was closer to CA II (4.7 ± 1.0 mM) than to CA VI (11.3 ± 0.7 mM).

Observed and intrinsic thermodynamics were consistent with structural results that confirmed chCA VI as a relevant model of CA VI. In addition, most of the tested benzenesulfonamides consistently interacted with chCA VI as with CA VI, but not CA II. Therefore, we confirmed chCA VI as a suitable model for the design and screening of CA VI-selective inhibitors.

3.5. MANUSCRIPT 5: Switching the inhibitor – enzyme recognition profile via chimeric carbonic anhydrase XII

In this paper, we used a protein engineering method to obtain a chCA XII that recapitulates the CA XII enzyme activity and inhibitor binding. First, we aligned the sequences of CA II and CA XII, which share 34% sequence identity[130]. Then, we detected six amino acids in the vicinity of the ligand-binding site that differs between the two isozymes. Finally, we created a CA II-based mutant with six CA XII-specific residues (A65S, N67K, I91T, F130A, V134S, and L203N). To elucidate the role of crucial amino acids in the active site of CA XII, I measured the catalytic activity and thermal stability of chCA XII. Also, we performed ligand binding and inhibition studies with 63 small molecule compounds using SFA, FTSA, and ITC assays.

Furthermore, we obtained nine crystal structures of inhibitors bound to chCA XII and compared the inhibitors' binding positions and affinities to CA II and CA XII.

The catalytic properties of chCA XII had similarities with both CA isoforms – II and XII. Six mutations in the active site of CA II slightly stabilized the protein by 0.5 °C in the pH range 4.5–10.0 and retained the catalytic efficiency (k_{cat} = 6.0 · 10^5 s^{-1}). CA XII's catalytic constant was k_{cat} = 4.1·10^5. However, a proton shuttle' His64 pK_a has increased by 0.6 units (pK_a= 7.9 ± 0.2 for chCA XII, pK_a= 7.3 ± 0.2 for CA II, and pK_a= 7.6 ± 0.2 for CA XII) while the K_M value decreased from 4.7 ± 1.0 mM to 3.6 mM ± 2.0 mM to approach CA XII (K_M = 3.6 ± 1.5 mM). We hypothesized that I91T mutation increased the pK_a of the mutant enzyme, and Thr88 (CA XII numbering) played a major role in the catalytic mechanism of CA XII.

The binding, inhibition, and structural studies revealed that the engineered chCA XII protein mimicked the active site of CA XII. ChCA XII bound inhibitors with similar affinities as CA XII. There was a strong correlation between pK_d's of chCA XII and CA XII with a coefficient of determination R^2 = 0.90 and a nearly absent correlation between binding affinities of chCA XII and CA II with R^2 = 0.24. The correlations of intrinsic values were also similar to those observed. Moreover, chCA XII and CA XII accommodated large compounds with bulky substituents in the active site that hardly or did not fit in the active site of CA II.

In this study, we designed and synthesized the new inhibitor – EA12-7, an analog of the lead compound EA12-3[116]. I measured binding affinities with all 12 catalytically active CAs and showed that compound EA12-7 bound all CAs with lower affinity than EA12-3 but significantly increased selectivity. It had 155-fold selectivity towards CA XII (K_d = 19 nM) over CA II (K_d = 3000 nM) and weakly bound or did not bind CAs I, III, VA, VB, VI, VII, and XIII (K_d ≥ 10–200 μM). As a result, we have shown that chCA XII is a valuable model for developing CA XII-specific inhibitors, such as lead compound EA12-3 and its newly synthesized analog EA12-7.

3.6. MANUSCRIPT 6: Isoform-selective enzyme inhibitors by exploring pocket size according to the Lock-and-Key principle

The paper discussed the strategy for developing selective inhibitors by augmenting the chemical compound's size and exploring the dimensions and shape of CA's active site in this way. Di-*ortho*- and di-*meta*-substituted benzenesulfonamides with gradually increasing hydrophobic substituents were synthesized, and binding to CAs was measured. In most cases, as the

inhibitor size increased, the binding affinity also increased until reaching the border when the CA could not accommodate the compound due to the binding pocket's limited size. The study showed that anticancer target CA IX has the most spacious active sites in volume and shape and can bind the inhibitors with the largest diameter, such as compound VD17-18 (**15b**), possessing up to 2000-fold selectivity over other CA isozymes. On the other hand, the active site of another anticancer target CA XII was less spacious than CA IX, but accommodated compound VD16-22 (**15a**), which did not fit in the active site of CA II. Furthermore, I observed that a well-known compound dansylamide, used for fluorescent competition assay, is a selective inhibitor of CA IX (K_d = 0.4 nM).

The study showed that the mechanism of inhibitor binding to CA follows the Lock-and-Key principle. The CA enzyme is structurally relatively rigid and does not undergo significant conformational changes while binding sulfonamide compounds. Therefore, the inhibitor must have an optimal size and shape to fit the binding pocket of CA.

Moreover, in this paper, two types of recombinant human CA IX - produced in mammalian FreeStyle 293-F suspension cells[84] and yeast (*Pichia pastoris*) cells[131] - were compared, how they bind inhibitors. The commercial compound naphthalene-2-sulfonamide bound both CA IX, expressed in mammalian or yeast cells, with the same K_d of 130 nM by SFA method and similar K_d's of 240 nM (mammalian) and 140 nM (yeast) by FTSA assay. CA IX, expressed in yeast, was used in structural studies because the crystallographers could not crystallize the human CA IX produced in mammalian cells. CA IX produced in yeast had two mutations - C174S and N346Q to avoid glycosylation to make easier crystallization. Binding and inhibition studies confirmed that both forms of CA IX are suitable for structure-activity relationship analysis and new CA IX-selective inhibitor design.

4. GENERAL DISCUSSION

The dissertation consisted of two main parts: comparing biophysical and enzyme inhibition methods to determine picomolar affinities (I) and investigating engineered chCA VI and chCA XII for inhibitor recognition (II). Both parts of the dissertation are essential for a deeper understanding of the CA-inhibitor recognition mechanism.

4.1. Importance of combining biophysical and enzymatic inhibition methods

Scientists worldwide test novel inhibitors for potential inhibitory properties towards disease-related enzyme targets every day. They choose binding and/or inhibition assays according to their protein-ligand system, available instruments, and budget. Most popular techniques in drug design are UV-Vis spectrophotometry, isothermal titration calorimetry, surface plasmon resonance (SPR), microscale thermophoresis, etc. Miniaturized assays save reagents and time. Sometimes fast reactions require a rapid mixing device such as the stopped-flow[123,124] or quench-flow[132,133] instruments. However, all assays have advantages and limitations.

Compared to biophysical assays, the enzyme inhibition assays data confirm that inhibitors alter the enzyme's catalytic activity. Enzyme inhibition assays are usually specific for each enzyme. In this work, I performed a specific stopped-flow CO_2 hydration assay. Enzyme-inhibitor binding can proceed with a wide range of affinities that require significant differences in the design of the enzyme inhibition assay. CAs catalyze a spontaneous CO_2 hydration reaction. Uncatalyzed reaction rate is 0.037 s^{-1} [133,101]. The CA concentration should be sufficient to detect the difference between uncatalyzed and catalyzed reactions enabling accurate measurement of the catalyzed reaction rate. The sufficient CA concentration is practically 10–500 nM depending on the CA isoform, with different catalytic activity. However, the concentration is usually unacceptable for measuring the picomolar affinities. In tight-binding inhibition, an active site titration occurs that gives the K_d value equal to half CA concentration (K_d = [CA concentration] / 2)[99,134–136]. For this reason, CA activity and concentration limit the determination of tight-binding inhibitors by SFA. The problem could be partly overcomed by applying Morrison's equation instead of Hill's model. Morrison's equation considers the CA concentration and provides a more exact K_d value. Data reability could be enhanced by determining at least several data points near

the expected K_d value. In this case, the 2-fold serial dilution of inhibitor concentrations is preffered over 3-fold serial dilution.

The ITC method is also limited by CA concentration. However, a limitation is described by the Wiseman *c*-factor ($c = K_b \times$ [CA concentration], $5 < c < 500$)[128]. Using 5–20 μM protein allows measuring the micromolar to nanomolar affinity range. Protein-ligand interactions with higher affinity can be measured indirectly by the displacement ITC assay[137,138]. This biophysical method is time-consuming, requires a significant amount of purified protein (~300 μg), and thus the technique is quite expensive. However, this is the only method for direct determination of thermodynamic parameters of binding (ΔH, ΔG, ΔS). In addition, the target protein used in an assay does not need to be chemically modified, labeled, or immobilized[139].

FTSA assay also requires micromolar CA concentration (5–10 μM), but this does not limit the determination of the CA's melting temperature without or bound with an inhibitor. For FTSA experiments, proteins and chemical compounds should be sufficiently stable and soluble[140], and the melting temperatures must be below water boiling temperature. Unfortunately, some benzenesulfonamide inhibitors, even having several aromatic rings, have high fluorescence and make determining the protein unfolding curve challenging. For this reason, I used SyproOrange dye instead of ANS to obtain CA unfolding curves. Despite the discussed obstacles, FTSA allows measuring the binding affinities from the millimolar to the picomolar range. Therefore, we calculate the inhibitor affinities from changes in melting temperatures from the unbound and inhibitor-bound protein. It is the most accurate method compared to ITC and SFA because CA activity and concentration in the sample do not limit the determination of ligand binding affinities.

This thesis showed a good correlation between inhibitor affinities determined by FTSA, SFA, and ITC assays under comparable conditions and in the micromolar to nanomolar range. Previously, my colleagues showed that the SPR[9] assay yielded the same K_d within the error margin as those three methods. In addition, for testing a class of chlorinated pyrrolidinone-bearing benzenesulfonamides[106], I also performed a *p*-nitrophenyl acetate assay[141]. Again, the observed K_d's were in line with those determined by FTSA, SFA, and ITC[106]. However, CAs exhibit weak esterase activity towards esters; therefore, *p*-nitrophenyl acetate assay requires a large concentration (micromolar) of CA. The advantage of this assay is that a standard UV/Vis spectrophotometer is suitable for an experimental setup. The experiments could be accelerated using multi-plate readers.

Scientists usually claim that the error margin of the K_d value is 5–10 %. However, the K_d value is a reverse unit of binding constant K_b ($K_d = 1/ K_{b)}$,

and is a logarithmic number. For this reason, the 2-fold error margin of the binding/dissociation constant is normal[142] and could not be expected to be less. Furthermore, up to a 10-fold difference in binding affinities was observed while using and comparing several assays. Therefore, lead compounds suitable for further development should possess at least 100–1000-fold selectivity towards desired CA isoform over the other 11 CA isozymes.

Moreover, scientists usually assume that a *p*-value of <0.05 provides statistically significant results. However, American Statistical Association stated that "No single index should substitute for scientific reasoning"[143]. To get reliable results, scientists must have logical considerations, correctly design the assay format, analyze results using several models and apply as many techniques as possible. Third-party testing is always a good choice in the drug design process to confirm the inhibitor binding properties.

4.2. Switching inhibitor recognition

Drug discovery begins in a tube while measuring interactions between the target enzyme, responsible for disease development, and drug-candidate molecules. Therefore, it is always a question of how to produce a recombinant protein that would be equally biologically active as a native human body. Usually, scientists use *E. coli* bacteria, mammalian cells, or yeast to make recombinant human proteins or find ways to purify the native protein from human blood, milk, saliva, etc. This thesis showed that recombinant human CA IX, produced in mammalian and yeast cells, bound inhibitors with similar affinities, and both could be used alternatively for inhibitors screening. However, CA IX produced in yeast is less catalytically active than that from mammalian cells, and researchers should use a larger concentration of it in the SFA assay. Earlier our laboratory group compared the binding properties of native CA VI from human saliva with recombinant CA VI from *E. coli* bacteria and mammalian cells[55]. All three forms of CA VI bound a class of inhibitors with the same binding affinities confirming recombinant proteins as suitable models of the native one.

Despite biotechnological progress, some proteins are still challenging and expensive to produce in E. *coli* bacteria, especially in large amount. In addition and partly as a consequence, some crystal structures of proteins or protein-ligand complexes are unavailable. Here, I present the engineering of chCA VI and chCA XII as a solution for complex enzyme production and crystallization. First, my colleagues constructed chCA VI and chCA XII, and then I conducted the kinetic and ligand binding studies to evaluate them as models of target isozymes.

4.2.1. Kinetic studies

During the study, I have determined the catalytic parameters of CA I, CA II, chCA VI, CA VI, chCA XII, and CA XII using the SFA method. I have summarized the data in Table 1. First, I used our derived model[99] to determine the exact substrate concentration in a sample. Then, I applied Lineweaver-Burk and Michelis-Menten equations to observe the $k_{cat,}$ K_M, and pK_a. Those parameters were consistent with previously published data, including those determined by other methods such as *p*-nitrophenyl acetate hydrolysis, ^{18}O-mass spectrometry, and Nuclear Magnetic Resonance[33,34,71,144–147]. Catalytic constants differed up to 2–3-fold, and pK_a values differed up to 0.6 units.

Table 1. The catalytic parameters of CA I, CA II, chCA VI, CA VI, chCA XII, and CA XII at 23 °C.

CA	**pK_a**	**k_{cat}, s^{-1}**	**K_M, mM**
CA I	6.9 ± 0.1 (I) 8.8 ± 0.1 (II)	$2.0 \cdot 10^5$	4.7 ± 1.0
CA II	7.3 ± 0.2	$6.0 \cdot 10^5$	4.7 ± 1.0
chCA VI	7.3 ± 0.2	$6.0 \cdot 10^5$	6.8 ± 2.0
CA VI	6.6 ± 0.2	$1.9 \cdot 10^5$	11.3 ± 0.7
chCA XII	7.9 ± 0.2	$6.0 \cdot 10^5$	3.6 ± 2.0
CA XII	7.6 ± 0.2	$4.1 \cdot 10^5$	3.6 ± 1.5

ChCA XII contained the same five-point mutations (A65S, N67K, I91T, F130A, V134S) as chCA VI (A65T, N67Q, F130Y, V134Q, L203T) and one – additional (I91T). Replacement of CA II active site amino acids to CA VI-specific amino acids did not affect the pK_a value of His64, but it increased in the chCA XII protein. For this reason, I assumed that I91T mutation increased the pK_a of chCA XII and Thr88 (CA XII numbering) was a key member in the catalytic mechanism of CA XII.

In the study K_M values were determined with a large error margin. Most studies claim that K_M is pH-independent[33,148]. However, in this study, K_M was independent of pH only in a narrow range of near-neutral pH. At acidic and basic pHs, the K_M values were larger than at neutral pH. A similar profile was described in Ref.[100] in 1964. Interestingly, the literature analysis was fruitless in finding the graphs of experimental data for K_M dependence on pH.

4.2.2. Binding and inhibition studies

We conducted binding and inhibition studies to evaluate the "switch" of chCA VI and chCA XII. To the best of my knowledge, no CA VI-selective inhibitors have been discovered yet. Screening of our more than 1000 compounds library showed that all inhibitors bind stronger to CA II than CA VI. Moreover, no crystal structures of inhibitors bound to CA VI are available. Only the crystal structure of the human CA VI catalytic domain with resolution of 1.9Å was determined in 2012[44]. ChCA VI resembled the active site of CA VI and was confirmed as a suitable model for inhibitor screening and X-ray crystallographic studies. In that way, chCA VI has provided a deeper insight into the efficiency of CA VI inhibitors. In addition, it could be used to reveal the biological role of CA VI.

Carbonic anhydrase XII already had been crystalized with more than 20 inhibitors that possess micromolar to nanomolar affinities. ChCA XII was used to understand key differences between CA II and CA XII for benzenesulfonamide binding. The studies resulted in the synthesis of a new compound EA12-7 that possesses significant selectivity towards CA XII over other CA isoforms. Therefore, it could be selected as a lead compound for further development in preclinical studies. Inhibitor binding analysis included a well-known inhibitor 4-(4-fluorophenylureido)-benzenesulfonamide (U-104/SLC-0111) that had been tested in patients with advanced solid tumors and has finished clinical trial phase I[149]. The Phase Ib/II trials[150] are ongoing of SLC-0111 compound with a recommended dosage of 1000 mg/day. It has been previously published as a strong inhibitor of CA XII (K_i = 4.5 nM) and a moderate inhibitor of CA II (K_i = 96 nM)[151]. However, we have observed that the binding affinities of compound SLC-0111 were 17-fold stronger for CA II than for CA XII, and the K_d's are in the micromolar range, as confirmed by three different assays (SFA, FTSA, and ITC). The data were consistent with other published studies[106,108,114,152,153] that *para*-substituted benzenesulfonamides bind to CA II with more than ten-fold higher affinity than to CA XII. Recently, Jonsson and Liljas have published a paper[154] expressing doubts about proper experimental data for promoting the SLC-0111 compound in preclinical research. Many scientists performed preclinical assays[155,156] or molecular docking[157] studies with SLC-0111, but no other biochemical or biophysical assay than SFA was used to verify the binding affinities of the compound. As many techniques as possible are needed to confirm the validity of the binding affinities, mainly because the enzyme inhibition assay is limited by the enzyme activity and concentration in a sample.

A similar protein engineering approach has been used to construct CA models that mimic CA I, CA III, and CA IX[113,158–161]. The first active site mutants of carbonic anhydrase II were generated in the early 1990s[158,161]. Behravan et al.[158] replaced the active site residues in CA II with the isozyme I-specific amino acids (V62N, H67N, and H200T). It showed that His200 has a dominant influence on the catalytic activity of CA I while Val62 and His67 are insignificant. Ren et al.[161] mutated the active site of CA II with residues characterizing CA III (H64K, N67R, L198F, and V207I); however, none of the mutations were responsible for the low catalytic activity and low sulfonamide affinity of CA III. In 2009–2014 double mutant (A65S, N67Q)[159], and septuplet mutant (A65S, N67Q, E69T, I91L, F131V, K170E, and L204A)[160] of CA II were made to mimic the anticancer target CA IX. They were reported as effective models for rapid screening of CA IX-targeting novel compounds and X-ray crystallographic studies. The main reason for constructing ch CA IX was its application for structural studies because until then, only one crystal structure of CA IX bound to an inhibitor was published[162]. Our laboratory also made the chCA IX with 7 point mutations (A65S, N67Q, I91L, F130V, V134L, and L204A)[113]. I have measured interactions with six fluorinated benzenesulfonamides, including the anticancer lead compound VD11-4-2, and showed that chimeric CA IX partly switched binding affinities from CA II to CA IX.

The detailed studies confirmed that isozyme engineering is a good strategy for the design of selective inhibitors. The strategy could be applied for the production of other chimeric CA isoforms that have low expression and purification yields, and crystal structures are unavailable.

5. CONCLUDING REMARKS AND FUTURE PROSPECTIVES

Drug discovery is a very long and costly process that includes four main milestones: *in vitro* studies (I), preclinical studies (II), clinical studies (III), and the drug launch to the market (IV). The later the stage, the more complex and costly it is. For this reason, it is imperative to choose the right drug-candidate molecule in the "*in vitro* stage" in order not to fail in later preclinical and clinical studies. In addition, a deep understanding of the protein-drug-candidate recognition mechanism could accelerate the drug discovery process.

Medicinal chemists could apply the strategy discussed in this thesis to other enzyme-inhibitor systems. Engineering chimeric isozymes could solve drug discovery challenges such as low purification quantity and difficult crystallization conditions. As published in the literature, there are no available crystal structures of mitochondrial CA VA and CA VB, and they are purified in insufficient quantities. Engineering of chCA VA and chCA VB would help design novel inhibitors as anti-obesity drugs since CA VA and CA VB play a role in obesity[163].

The engineering of chimeric isozymes provides key structural differences between several isozymes and give insights for design of isoform-selective inhibitors. The approach could lead to discoveries of novel drug candidates. For example, the lead compound EA12-7 was designed during the studies. This nanomolar inhibitor selectively binds CA XII and is a suitable candidate for preclinical anticancer studies.

I would recommend continuing molecular recognition studies as a key to the genuinely rational design of high-affinity and high-selectivity drug candidates. In the carbonic anhydrase field, the sulfonamide inhibitors have the potential to become drugs for epilepsy, obesity, cancer and others diseases treatment.

Conclusions:

1. Five to six mutations of the active site residues of CA II required to generate chCA VI and chCA XII did not affect the maximal catalytic activity of the enzyme, and had moderate effects on its melting temperatures and Michaelis-Menten constants.
2. ChCA VI and chCA XII switched the inhibitor recognition profile from CA II to CA VI and CA XII, confirming that chimeric CAs are good models for the design of isozyme-selective inhibitors.
3. There is a good correlation between protein-ligand binding affinities determined by FTSA, SFA, and ITC assays under comparable

conditions and in the micromolar to nanomolar affinity range. However, the fluorescent thermal shift assay is the most accurate method to measure picomolar affinities.

6. SUMMARY IN LITHUANIAN LANGUAGE

SANTRUMPOS

ANS	8-anilino-1-naftalensulfonatas
CA	karboanhidrazė
[*CA*]	karboanhidrazės koncentracija
chCA	chimerinė karboanhidrazė
CHES	2-(cikloheksilamino)etansulfoninė rūgštis
DMSO	dimetil sulfoksidas
FTSA	fluorescentinis terminio poslinkio metodas
ΔG	Gibso laisvosios energijos pokytis
h	Hilo koeficientas
ΔH	entalpijos pokytis
HEPES	4-(2-hidroksietil)piperazino-1-etansulfoninė rūgštis
[*I*]	slopiklio koncentracija
IC_{50}	pusė didžiausios slopinančios koncentracijos
ITC	izoterminio titravimo kalorimetrija
K_b	jungimosi konstanta
k_{cat}	katalizinė konstanta
$k_{cat\text{-}max}$	didžiausia katalizinė konstanta
K_d	disociacijos konstanta
K_i	slopinimo konstanta
K_M	Michaelis-Menten konstanta
MES	2-(N-morfolino)etansulfoninė rūgštis
MOPS	3-(N-morfolino)propansulfoninė rūgštis
ΔS	entropijos pokytis
[*S*]	substrato koncentracija
SFA	sustabdytos srovės CO_2 hidratacijos metodas
SPR	paviršiaus plazmono rezonansas
TRIS	tris(hidroksimetil)aminometanas

ĮVADAS

Fermentai yra patrauklūs taikiniai mažamolekulinių vaistų kūrimui. Racionalus vaistų kūrimas pagrįstas struktūros-aktyvumo sąryšių tyrimais. Cheminių junginių slopinamasis aktyvumas dažniausiai nustatomas modifikuojant slopiklių chemines grupes ir matuojant jų sąveikas su tiksliniais fermentais. Pagrindiniai parametrai, apibūdinantys slopiklio potencialą tapti vaistu, yra gimiringumas ir atrankumas tiksliniam fermentui.

Šioje disertacijoje didžiausias dėmesys skiriamas karboanhidrazės (CA) ir sulfonamidinio slopiklio atpažinimo mechanizmui. Žmogaus organizme yra 12 aktyvių CA izoformų, kuris pasižymi didele struktūrine homologija, tačiau atlieka skirtingas fiziologines funkcijas. Šiuo metu daugiau nei 30 CA slopiklių, daugiausia pirminių sulfonamidų, yra naudojama glaukomos, aukštumos ligos, epilepsijos, stazinio širdies nepakankamumo, idiopatinės intrakranijinės hipertenzijos, ir kitų ligų gydymui. Deja, dauguma jų nepasižymi atrankumu tam tikrai CA izoformai ir dėl šios priežasties sukelia šalutinius poveikius - dusimą, depresiją, vėmimą, viduriavimą ir pan. Tam kad sukurti efektyvesnius vaistus su retesniais šalutiniais poveikiais, būtina ieškoti naujų slopiklių, pasižyminčių didesniu atrankumu ir gimingumu tiksliniam CA izofermentui.

Siekiant išsiaiškinti, kaip karboanhidrazė atpažįsta sulfonamidą (klasikinį slopiklį), buvo atlikti šie tyrimai:

I) Slopiklių cheminių grupių modifikavimas.

II) CA II aktyvaus centro inžinerija chimerinių karboanhidrazių (chCA) sukūrimui.

III) Gimiringumo nustatymas taikant fluorescentinio terminio poslinkio metodą (FTSA), izoterminio titravimo kalorimetriją (ITC) ir sustabdytos srovės CO_2 hidratacijos (SFA) metodą.

IV) Struktūriniai tyrimai, taikant rentgeno kristalografiją ir molekulinį modeliavimą.

Mano kolegos Vilniaus universiteto Gyvybės mokslų centro Biotechnologijos institute atliko didelę dalią darbų, įskaitant sulfonamidinių junginių bibliotekos sintezę, rekombinantinių CA ir chCA gamybą, molekulinį modeliavimą, rentgeno kristalografinius tyrimus. Mano indėlis yra žmogaus CA ir chCA katalizinio aktyvumo ir terminio stabilumo charakterizavimas bei sąveikos su slopikliais tyrimai. Jungimosi ir slopinimo parametrų nustatymui bei atpažinimo mechanizmo tyrimui taikiau FTSA, ITC ir SFA metodus. Šie metodai turi savų pranašumų ir trūkumų, ypač dirbant su labai stipriai besijungiančiais slopikliais. Dėl to išryškinau kelių metodų

kombinavimo svarbą, siekiant nustatyti patikimus jungimosi ir/ar slopinimo parametrus.

Disertaciją sudaro dvi pagrindinės dalys. Pirmoje dalyje aprašomi fermentinio aktyvumo slopinimo ir biofizikinių metodų privalumai ir apribojimai. Antroji dalis skirta chimerinių karboanhidrazių ir jų slopiklių atpažinimo perjungimui.

Tikslas:

Disertacijos tikslas - ištirti slopiklio atpažinimo perjungimą, panaudojant chimerinių karboanhidrazių izofermentų inžineriją.

Uždaviniai:

Tikslui pasiekti buvo iškelti šie uždaviniai:

1. Charakterizuoti chCA VI ir chCA XII terminį stabilumą, katalizinį aktyvumą ir slopinimą sulfonamidiniais junginiais.
2. Įvertinti slopiklio atpažinimo perjungimą iš CA II į CA XII, panaudojant chCA XII.
3. Palyginti biofizikinius ir fermentinio aktyvumo slopinimo metodus (FTSA, ITC ir SFA), matuojant cheminių junginių sąveikas su CA ir chCA, bei paaiškinti jų privalumus ir apribojimus nustatant ypač stiprių slopiklių gimiringumo konstantas.

Mokslinis naujumas:

Disertacijos tyrimai parodė, kad cheminį junginį CA VI ar CA XII aktyviajame centre atpažįsta tik iki 6 pagrindinių aminorūgščių rinkinys. Dėl 5−6 aminorūgščių mutacijų CA II aktyviajame centre, fermentas pradeda atpažinti skirtingus cheminius junginius. Tyrime mutacijos buvo parinktos taip, kad atitiktų CA VI ar CA XII aktyviuosius centrus. CA II pagrindu sukonstruotas chimerinis fermentas, aktyviajame centre turintis CA XII būdingas šešias aminorūgštis, jungėsi su cheminiais junginiais taip, kaip ir CA XII. Be to, CA II-atrankių slopiklių grupės gimiringumas CA II ženkliai sumažėjo. Tai parodo, kad CA II baltymas įgavo CA XII būdingą mažamolekulinių junginių atpažinimo profilį. CA pasižymėjo gana standžia struktūra, kuri ženkliai nekito jungiantis slopikliui. Sukurta chCA XII leido mums nustatyti esminius struktūrinius skirtumus tarp CA II ir CA XII. Tyrimų dėka sukūrėme CA XII-atrankų nanomolinį slopiklį EA12-7.

Ginamieji teiginiai:

1) Cheminis junginys CA VI ar CA XII aktyviajame centre yra atpažįstamas tik iki šešių pagrindinių aminorūgščių rinkinio.
2) Chimerinės karboanhidrazės VI and XII yra geri tikslinių izofermentų modeliai ir gali būti naudojami izoformai atrankių slopiklių kūrime.
3) Pikomolinių slopiklių jungimosi konstantų nustatymui būtina kombinuoti biofizikinius ir fermentų aktyvumo slopinimo metodus.

LITERATŪROS APŽVALGA

Žmogaus karboanhidrazės šeima (CA; EC 4.2.1.1)) katalizuoja grįžtamąją anglies dioksido hidratacijos reakciją ($CO_2 + H_2O \leftrightarrow HCO_3^- + H^+$). Karboanhidrazės aptinkamos visose gamtos karalystėse ir yra skirtomos į 8 kategorijas: α, β, γ, δ, ζ, η, θ, ir ι[1–8]. Jos dalyvauja daugybėje fiziologinių ir biocheminių procesų. Šiame darbe dėmesį skyriau žmogaus α-CA. Jas sudaro 15 šeimos narių, iš kurių 12 yra kataliziškai aktyvios. CA skiriasi savo fiziologiniu vaidmeniu, pasiskirstymu audiniuose ir organuose, raiškos lygiais, kinetinėmis savybėmis, terminiu stabilumu ir slopiklių jungimosi gimiringumu[9]. Ląstelėje jos išsidėsčiusios skirtingai: penkios yra citozolinės (I, II, II, VII ir XIII izoformos), dvi yra mitochondrinės (VA ir VB izoformos), keturios yra prisijungusios prie membranos (IV, IX, XII ir XIV izoformos), o viena yra sekretuojama (VI izoforma). Trys CA izofermentai - VIII, IX, ir X yra kataliziškai neaktyvūs.

KATALIZINIS MECHANIZMAS

CA II aktyvus centras yra kūgio formos, jo skersmuo apie 12 Å, o gylis apie 13 Å[13]. Viena pusė yra hidrofobinė, o kita – hidrofilinė[14]. Aktyviajame centre katalizinį cinko joną koordinuoja trijų histidinų (His94, His96 ir His119) imidazolo grupės ir vandens molekulė/hidroksido jonas[15]. Protonų pernaša ir substrato / produkto / vandens mainai katalizinės reakcijos metu vyksta per vandens molekulių tinklą (žr. "figure 2 A−C").

Pirma, CO_2 hidratacija vyksta aktyvaus centro hidrofobinėje dalyje. Nukleofilinė $Zn\text{-}OH^-$ ataka į CO_2 sugeneruoja bikarbonato joną. Susidariusį HCO_3^- vėliau pakeičia vandens molekulė[16]. Tokiu būdu gaunama kataliziškai neaktyvi forma. Antra, $Zn\text{-}H_2O$ praranda protoną, kuris per vandens molekulių tinklą perduodamamas į His64. His64 vadinamas "protonų šaudykle"[17] ir turi dvi nuo pH priklausančias konformacijas: "į" ir "iš"[18]. His64 perima "į" konformaciją, kad delta azotą (Nδ) priartintų prie katalizinio Zn atomo.

Protono perdavimas iš Zn-H_2O į His64 yra greitį limituojantis reakcijos etapas. Po šio protono perdavimo His64 persisuka į "iš" orientaciją, kad iš imidazolo žiedo atpalaiduotų Nδ protono perteklių į reakcijos tirpiklį. Ciklas tęsiasi, kai prie cinko prisijungusi vandens molekulė deprotonizuojasi, o His64 persiorientuoja į "iš" konformaciją[20].

Karboanhidrazės katalizuoja ne tik CO_2 hidrataciją, bet ir esterių hidrolizę[21]. Reakcija vyksta CA aktyviajame centre (žr. "figure 3"). Ji gana panaši į anglies dioksido hidrataciją. Esteriai hidrolizuojami dėka Zn-OH^- nukleofilinės atakos į karbonilinį CO, susidarant oksianijono tarpiniam junginiui. Eksperimentiškai katalizinė reakcija matuojama naudojant *p*-nitrofenilacetatą, kaip substratą[22].

Slopiklių jungimosi mechanizmas

Didelė aminorūgščių homologija (>30 %[30]) tarp skirtingų CA izoformų apsunkina atrankių slopiklių kūrimą ir vystymą. CA izoformų aktyvūs centrai yra kūginės formos ir skiriasi tik keliomis aminorūgštimis. Slopiklio surišimo vietos viršus yra kintamas, o labiausiai konservatyvios aminorūgščių liekanos aptinkamos aktyvaus centro gilumoje ir arti cinko jono[31]. Daugiau nei 400 slopiklių ir 12 CA izoformų sąveikos termodinaminė, kinetinė ir struktūrinė analizė atskleidė, kad maži struktūriniai skirtumai tarp CA izoformų sukelia nenuspėjamus efektus, kaip ligandas bus atpažįstamas[9].

Pirminiai sulfonamidai yra substrato (anglies dioksido) hidratacijos pereinamosios būsenos analogai. Jie yra klasikiniai slopikliai ir sąveikauja su karboanhidrazėmis per grįžtamąjį konkurentinį 1:1 slopinimą. Viena sulfonamido molekulė konkuruoja su anglies dioksidu ir grįžtamai (nekovalentiškai) jungiasi viename CA aktyviajame centre.

Prisijungimas vyksta, kai slopiklio sulfonamido grupė yra deprotonizuota, o prie Zn prisijungusi vandens molekulė yra protonizuota. Procesas yra priklausomas nuo pH (žr. "figure 4"). Visi protonizacijos reiškiniai turi būti atimti iš stebimosios jungimosi reakcijos, tam, kad nustatyti tikrinę (angl. *intrinsic*) CA-slopiklio sąveikos jungimosi konstantą.

Karboanhidrazė II

CA II yra labiausiai ištyrinėta ir daugiausia paplitusi CA izoforma. Tai 29 kDa, 40 × 42 × 56 Å dydžio baltymas. Citozolinė CA II pasižymi didele raiška *E. coli* bakterijose ir gryninimo išeiga, didžiausiu iš visų CA kataliziniu aktyvumu (k_{cat} 0.6–1.4 μs^{-1})[33–35], vidutiniu terminiu stabilumu (T_m 55–59 °C)[36–38] ir yra lengvai kristalinama. Taip pat, mokslininkai CA II ir CA I

vadina "netaikininėmis" (angl. *off-target*) izoformomis, kurių gyvajame organizme nereikia slopinti, nes jos yra aptinkamos eritrocituose ir atlieka svarbų vaidmenį tiek kvėpavime, tiek kraujo jonų koncentracijos reguliavime[10,39–41].

Karboanhidrazė VI

CA VI yra vienintelė žmogaus CA izoforma, kurią gamina seilių ir pieno liaukos[42,43]. Ji yra dimerinės struktūros[44]. Tyrėjai taip pat aptiko CA VI izoformą serume, kvėpavimo takuose ir virškinimo trakte[45–49]. Be to, ji dalyvauja reguliuojant seilių pH, kartaus skonio suvokimą ir dantų formavimąsi[43,50]. Padidėjęs seilių CA VI aktyvumas yra susijęs su dantų akmenų dydžiu[51] ir mokyklinio amžiaus vaikų dantų ėduonies išsivystymu[50,52,53].

Mūsų laboratorijos komanda pagamino rekombinantinę CA VI *E. coli* bakterijose, žinduolių ląstelėse ir tiesiogiai išskyrė iš žmogaus seilių. Biofizikiniai tyrimai parodė, kad CA VI, išgauta iš visų trijų šaltinių, jungėsi su slopikliais paklaidų ribose su identišku gimingumu[55]. Šie tyrimai patvirtino, kad rekombinantinės žmogaus CA VI, pagamintos bakterijų ar žinduolių ląstelių, yra geri natyvios CA VI modeliai.

Rekombinantinės ir natyvi CA VI turi mažą gryninimo išeigą, o tai apsunkina atrankių slopiklių kūrimą ir pirmosios CA VI kristalinės struktūros, prisijungusios cheminį junginį, nustatymą. Dėl šios priežasties reikalingas papildomas CA VI modelis, kad paspartinti naujų CA VI-atrankių slopiklių sukūrimą.

Karboanhidrazė XII

CA XII kontroliuoja vėžinių ląstelių ekstraląstelinį pH ir veikia kaip hipoksijos sukeltas naviko žymuo. Krūties vėžio estrogenų receptoriai reguliuoja CA XII[56]. Didelė CA XII raiška koreliuoja su palankiu pacientų, sergančių agresyviu krūties arba nesmulkialąsteliniu plaučių vėžiu, išgyveninamumu[57,58]. Pacientams, turintiems kolorektalines, kepenų ląstelių karcinomas ir difuzines astrocitomas[59–61], CA XII raiška asocijuojasi prasta prognoze. Be to, CA XII laikoma farmakologiniu taikiniu vėžinių ląstelių cheminiam atsparumui įveikti[62]. Mažesnė CA XII raiška taip pat buvo aptikta žmogaus akyje, žarnyne, inkstuose, kasoje, skrandžio gleivinėje, odos epitelio komponentuose, ir kt.[47,63–67]. Papildomai CA XII dalyvauja glaukomos vystymesi, druskos įsisavinime prakaito liaukose ir kt.[66,68,69]. Waheed ir Sly išsamiai apibūdino CA XII funkcinę rolę apžvalgoje[70].

CA XII yra sudėtingas vaistų taikinys. Tradiciniai vaistų kūrimo būdai yra riboti, nes tai su membrana susijęs dimerinis fermentas, turintis N-galinį ekstraląstelinį katalizinį domeną. Whittington ir kt. 2001 m. išsprendė pirmąją CA XII kristalinę struktūrą. Aktyvaus centro struktūra yra analogiška CA II: His94, His96, His119 ir vandens molekulė koordinuoja cinko joną[71]. Mūsų tyrėjų grupė patalpino į baltymų duomenų banką (PDB) 24 CA XII-slopiklių kristalines struktūras, suteikdama nemenką duomenų šaltinį slopiklių kūrimui.

METODAI

Fluorescentinis terminio poslinkio metodas

Salemme su kolegomis 2001 m. pristatė miniatiūrizuotą fluorescentinio terminio poslinkio metodą (FTSA, dar vadinamą ThermoFluor® arba diferencine skenavimo fluorimetrija)[74]. Baltymų terminis stabilumas nustatomas, kai veikiant karščiui, baltymas išsivynioja[75] ir registruojama solvatochrominio dažo, pvz. SyproOrange[76,77] arba 1-anilino-8-naftaleno sulfonatą (ANS)[78,79], fluorescencija. FTSA efektyviai naudojamas slopiklių jungimosi tyrimuose, nes baltymų lydymosi temperatūros T_m pokytis pridedant ligandą yra susijęs su jungimosi konstanta[79,80,87]. FTSA metodo eksperimentinės sąlygos aprašytos moksliniuose straipsniuose[86,99,106,111], o tikrinių parametrų nustatymas - publikacijoje[32].

Izoterminė titravimo kalorimetrija

Izoterminio titravimo kalorimetras tiesiogiai matuoja biocheminių reakcijų metu sugeriamą arba išskiriamą šilumą. Dėl didelio jautrumo ITC ypač tinka tipinėms nekovalentinėms biomolekulinėms sąveikoms charakterizuoti[88]. Taigi, ITC yra efektyvus metodas, leidžiantis vieno eksperimento metu nustatyti entalpijos (ΔH), entropijos (ΔS), ir Gibso laisvosios energijos (ΔG) pokyčius bei jungimosi partnerių stechiometriją[89,90]. Termodinaminiai parametrai ΔH ir ΔG yra matuojami tiesiogiai, o ΔS yra apskaičiuojamas. Doktorantūros studijų metu atliktų ITC eksperimentų sąlygos aprašytos publikacijoje[99].

Sustabdytos srovės CO_2 hidratacijos metodas

Sustabdytos srovės CO_2 hidratacijos metodas yra pats populiariausias CA kataliziniam aktyvumui nustatyti ir cheminių junginių slopikliniam efektui tirti[33,73,95–99]. Mokslininkai naudoja pH indikatorius, kad nustatytų optinio

tankio pokyčius CA rūgštinant pH. Indikatoriaus ir buferinio tirpalo poros turi būti parenkamos pagal jų pK_a ir reakcijos pH vertes. Pvz., jei reakcijos pH yra 7.5, tai turi būti naudojami fenolio raudonasis (pK_a 7.5) ir Hepes buferinis tirpalas (pK_a 7.5). Dažnai teigiama, kad substrato koncentracija yra 17 mM[73,102,103]. Deja, dujinis CO_2 garuoja užpildant švirkštus ir eksperimento metu. Nežinoma tiksli CO_2 koncentracija apsunkina CA katalizinių parametrų nustatymą. CA aktyvumo ir slopinimo matavimų eksperimentinės sąlygos aprašytos publikacijose[86,99,111,164,165]. IC_{50} nustatymui buvo panaudoti Hilo[104] ir Morisono[105] modeliai.

Sulfonamidinių slopiklių sintezė

Komerciniai slopikliai buvo nupirkti iš Sigma-Aldrich tiekėjo. Kitus sulfonamidinius junginius[86,106–118] susintetino dr. V. Dudutienė, dr. E. Čapkauskaitė, A. Zakšauskas ir jų studentai (-ės).

Karboanhidrazių gamyba

Šiame tyrime naudojau VU GMC BTI Biotermodinamikos ir vaistų tyrimo skyriuje pagamintas rekombinantines CA ir chCA[55,72,83–85,87,119–122]. Jas gamino A. Mickevičiūtė, dr. V. Juozapaitienė, V. Michailovienė, dr. J. Matulienė, J. Jachno, dr. J. Kazokaitė-Adomaitienė ir jų studentai (-ės). CA koncentraciją nustatinėjau spektrofotometriškai.

REZULTATŲ SANTRAUKA

Į disertaciją įtraukiau 6 publikacijas. Šioje dalyje apibendrinau kiekvienos publikacijos rezultatus ir išvardijau juos ne chronologiškai, bet nuosekliai.

PUBLIKACIJA 1: Standartinė fermentinio aktyvumo slopinimo nustatymo darbo procedūra

Standartinėje darbo procedūroje aprašomi kritiniai eksperimentinio planavimo žingsniai ir duomenų analizė, skirta fermentinio aktyvumo slopinimo nustatymui. Be to, procedūra aprašo tinkamų parametrų pasirinkimą:

- **Fermentui specifinis metodas.** Fermentų katalizuojamų reakcijų greitis gali būti matuojamas registruojant produkto susidarymą arba substrato išnykimą per tam tikrą laikotarpį. Didėjant slopiklio

koncentracijai, katalizinės reakcijos greitis mažėja, kol pasiekiamas visiškas CA slopinimas, t. y., kai slopinamos reakcijos greitis tampa lygus spontaninės CO_2 hidratacijos reakcijos greičiui.

- **Optimalios eksperimentinės sąlygos.** Norint sumažinti CA koncentraciją mėginyje, reikia optimizuoti sąlygas $k_{cat\text{-}max}$ nustatymui. Katalizės greitį veikia temperatūra, pH, joninė jėga, buferiniai tirpalai ir kiti priedai. Kai kurie buferinio tirpalo komponentai ir tirpikliai gali slopinti fermentą, todėl turi būti patikrintas jų slopiklinis efektas prieš atliekant cheminių junginių slopinimo tyrimus.
- **Fermento koncentracija.** Fermentinės reakcijos greitis tiesiškai priklauso nuo CA koncentracijos, kuri turi būti pakankama, kad detektuoti signalą, bet ženkliai mažesnė, nei IC_{50}.
- **Substrato koncentracija.** Tam, kad palyginti kelių slopiklių gimiringumus, fermentų aktyvumo slopinimo eksperimentai turi būti atlikti pastovioje substrato koncentracijoje.
- **Slopiklio koncentracija.** Ji parenkama atsižvelgiant į numatomą gimingumą ir CA koncentraciją, o gaunamos atliekant serijinį skiedimą. Vidurinis eksperimentinių duomenų taškas turėtų būti apie IC_{50}, o paskutinis - slopinti >90 % fermento katalizinio aktyvumo.
- **Teigiamos ir neigiamos kontrolės.** Šios kontrolės turi būti atliktos reakcijos "fonui" nustatyti ir atimtos iš katalizuojamos reakcijos.
- **Duomenų apdorojimo modeliai.** Reakcijų greičių nustatymui taikomi tiesinės regresijos modeliai arba netiesinės kelių kintamųjų parametrų lygtys, priklausomai nuo reakcijos sudėtingumo. Taikant Hilo modelį, Hilo koeficientas būtinai turi būti 1, o teorinė kreivė privalo gerai atitikti eksperimentinius taškus.

PUBLIKACIJA 2: Pikomoliniai karboanhidrazių slopikliai: slopinimo ir jungimosi metodų svarba

Šiame moksliniame straipsnyje buvo lyginami fermentų aktyvumo slopinimo ir biofizikiniai baltymų-ligandų sąveikos tyrimo metodai bei pabrėžiami jų privalumai ir trūkumai. SFA metodas yra pats populiariausias tiesioginiam CA katalizinio aktyvumo slopinimo nustatymui, tačiau turi keletą apribojimų.

Pirmiausia, nėra žinoma tiksli vandenyje ištirpusio anglies dioksido koncentracija. Keli autoriai deklaruoja iki 17 mM CO_2 koncentraciją[126,127], tačiau CO_2 dujos spontaniškai garuoja iš mėginių. Šiame darbe sukūrėme naują modelį CO_2 koncentracijai mėginyje nustatyti. Be to, nustačiau CA I ir

II K_M ir k_{cat} plačiame pH intervale. CA II yra vienas iš greičiausių fermentų su $k_{cat\text{-}max}$ - $6 \cdot 10^5$ s^{-1}, o CA I yra mažiau aktyvi su $k_{cat\text{-}max}$ - $2 \cdot 10^5$ s^{-1}. CA aktyvumas auga didėjant pH vertei, kol pasiekia didžiausią vertę. CA I K_M vertė yra 1.4 ± 0.8 mM, o CA II - 4.6 ± 1.0 pH intervale 7.0–9.0. CA I aktyviajame centre nustatytos dvi besijonizuojančios grupės, kurių pK_a vertės - 6.9 ± 0.1 ir 8.8 ± 0.1. CA II turi vieną jonizacijos grupę, kurios pK_a yra 7.3 ± 0.2.

Antra, slopinimo konstantų nustatymas SFA metodu yra ribojamas CA aktyvumu ir koncentracija. Surinktos dozavimo kreivės buvo apdorotos naudojant Hilo ir Morisono lygtis. Silpno ir vidutinio slopinimo atveju, abu modeliai pateikė vienodas IC_{50}. Visgi, analizė parodė, labai stipriai besijungiančių slopiklių atveju tik Morisono modelis yra tinkamas IC_{50} nustatymui.

Palyginimui, ITC yra vienintelis tiesioginis metodas, skirtas nustatyti termodinaminius slopiklio prisijungimo prie baltymo parametrus. Deja, Vaismano "*c*-faktorius"[128] riboja jungimosi konstantų nustatymą. Dėl to ITC negali būti naudojamas labai silpnai ar stipriai sąveikai matuoti. Tik FTSA metodas buvo tinkamas pikomoliniam ligandų jungimosi gimiringumui nustatyti. Visi trys metodai turi būti kombinuojami, siekiant išsamiai apibūdinti CA-slopiklio sąveiką, ypač kai jungimasis yra labai stiprus.

PUBLIKACIJA 3: Eksperimentiniai metodai, skirti nustatyti atrankius pikomolinius karboanhidrazės IX slopiklius

Apžvalgoje pristatomas slopiklių VD11-4-2, VD12-09 ir VR16-09, kurie atrankiai ir ypač stipriai jungiasi su CA IX, kūrimas ir charakterizavimas. Apžvalginė biocheminių ir biofizinių metodų, skirtų slopiklių gimingumo matavimams *in vitro*, dalis yra susijusi su šia disertacija.

Čia mes aptarėme 6 struktūriškai panašių cheminių junginių struktūros-gimininingumo sąryšius. Pirmiausia, 4-pakeisti-2,3,5,6-benzensulfonamidai (VD10-13, VD10-35 ir VR16-05) buvo atrasti kaip nanomoliniai ir atrankūs netaikininės (angl. *off-target*) CA I slopikliai[114,115]. Fluoro atomo pakeitimas benzensulfonamido žiedo *orto*- pozicijoje į ciklooktilamino grupę (junginys VD12-09) radikaliai (>450 000 kartų) sumažino gimingumą CA I. Toks pat pakeitimas *meta*- pozicijoje tūkstantį kartų sustiprino jungimąsi su CA IX (K_d = 0.05 nM). O pakeitimas į dar didesnių gabaritų hidrofobinį pakaitą – ciklododecilaminą *orto*- padėtyje (junginys VR16-09) suteikė didelį gimingumą CA IX (K_d = 0.16 nM) ir panaikino jungimąsi su netaikininėmis CA I ir CA II (K_d > 200 μM). Norint apibūdinti taip stipriai besijungiančius slopiklius, buvo būtinas FTSA, ITC ir SFA metodų kombinavimas. Visgi, tik

FTSA metodas buvo tinkamas lyderinių junginių disociacijos konstantoms nustatyti.

PUBLIKACIJA 4: Sukonstruotas CA VI imitacinis fermentas perjungė slopiklių struktūras ir giminingumą

Publikacijoje aptariamas chCA VI sukūrimas ir charakterizavimas. Kazokaitė ir kt. palygino CA II ir CA VI sekas ir sukonstravo chCA VI, taikydami taškinę mutagenezę[165]. CA II buvo pasirinkta kaip šerdis ir 5 taškinės mutacijos - A65T, N67Q, F130Y, V134Q, L203T buvo įvestos į aktyvų centrą. Tyrimo tikslas buvo įvertinti chCA VI, kaip modelio, tinkamumą rentgeno kristalografijai ir slopiklių skenavimui (angl. *screening*). Mano žiniomis lyg šiolei nėra sukurta CA VI-atrankių slopiklių ir nėra išspręsta CA VI kompleksų su slopikliais kristalinių struktūrų. Aš atlikau SFA eksperimentus, kad nustatyčiau chCA VI ir CA VI katalizinius aktyvumus ir slopinimą sulfonamidais. Nustačiau, kad CA VI didžiausia katalizinė konstanta yra k_{cat} – $1.9 \cdot 10^5$ s^{-1} pH 7–8 intervale, o aukštesniame pH fermento aktyvumas ženkliai mažėja. ChCA VI turėjo tokią pačią pK_a vertę (7.3) ir didžiausią katalizį aktyvumą kaip CA II (k_{cat} – $1.9 \cdot 10^5$ s^{-1}), o pH intervale 7.1–8.4, K_M vertė (6.8 ± 2.0 mM) buvo artimesnė CA II (4.7 ± 1.0 mM) nei CA VI (11.3 ± 0.7 mM). Dauguma tirtų benzensulfonamidų sąveikavo su chCA VI, kaip ir su CA VI, bet ne su CA II. Tyrimais patvirtinome, kad chCA VI yra tinkamas CA VI modelis ir gali būti naudojamas slopiklių kūrimui ir atrankai.

PUBLIKACIJA 5: Slopiklio–baltymo atpažinimo profilio perjungimas panaudojant chimerinę karboanhidrazę XII

Šioje publikacijoje aprašoma chCA XII. Pirmiausia, mes palyginome CA II ir CA XII sekas ir nustatėme šešias aminorūgštis slopiklio jungimosi vietoje, kurios skiriasi tarp šių dviejų izoformų. Tuomet, sukūrėme CA II mutantą su šešiomis CA XII-specifinėmis aminorūgštimis (A65S, N67K, I91T, F130A, V134S, ir L203N). Siekdama išsiaiškinti esminių aminorūgščių vaidmenį CA XII aktyviajame centre, pamatavau chCA XII katalizinį aktyvumą ir terminį stabilumą. Taip pat su kolegemis atlikome jungimosi ir slopinimo tyrimus su 63 cheminiais junginiais.

ChCA XII katalizinės savybės buvo panašios į abiejų CA izoformų – II ir XII. Šešios mutacijos CA II aktyviajame centre stabilizavo baltymą 0.5 °C pH intervale 4.5–10.0 ir išlaikė katalizinį efektyvumą (k_{cat} = $6.0 \cdot 10^5$ s^{-1}). CA XII katalizinė konstanta buvo mažesnė (k_{cat} = $4.1 \cdot 10^{5)}$. Vis tik, protonų šaudyklės His64 pK_a padidėjo 0.6 vieneto (chCA XII pK_a = 7.9 ± 0.2, CA II pK_a = 7.3 ±

0.2 ir CA XII pK_a= 7.6 ± 0.2), o K_M vertė sumažėjo nuo 4.7 ± 1.0 mM iki 3.6 mM ± 2.0 mM panašėjant į CA XII (K_M = 3.6 ± 1.5 mM). Iškėliau hipotezę, kad I91T mutacija padidino chCA XII His64 pK_a, o Thr88 (CA XII numeracija) atlieka svarbų vaidmenį CA XII kataliziniame mechanizme.

Jungimosi, slopinimo ir struktūriniai tyrimai atskleidė, kad sukonstruota chCA XII imitavo CA XII aktyvų centrą. ChCA XII jungėsi su slopikliais vienodu gimiringumu, kaip ir CA XII. Nustatyta stipri koreliacija tarp chCA XII ir CA XII stebimųjų pK_d verčių su determinacijos koeficientu R^2 = 0.90 ir beveik neaptikta koreliacijos tarp chCA XII ir CA II su R^2 = 0.24. Tikrinių verčių koreliacijos buvo panašios, kaip ir stebimųjų parametrų. Taip pat chCA XII ir CA XII "įsitalpino" stambius cheminius junginius su dideliais hidrofobiniais pakaitais, kurie sunkiai arba visai nesijungė CA II aktyviajame centre, nes netilpo jame pagal dydį.

Šiame tyrime sukūrėme ir susintetinome naują slopiklį EA12-7, lyderinio junginio EA12-3^{116} analogą. Slopiklis EA12-7 jungėsi su visomis 12 CA izoformų silpniau nei EA12-7, bet turėjo didesnį atrankumą. Jis jungėsi su CA XII (K_d = 19 nM) 155 kartus stipriau nei su CA II (K_d = 3000 nM), o su CA I, III, VA, VB, VI, VII, ir XIII jungėsi silpnai arba visai nesijungė ($K_d \geq$ 10–200 µM). Apibendrinant, mes parodėme, kad chCA XII yra vertingas modelis CA XII-atrankių slopiklių, tokių kaip EA12-3 ir jo naujai susintetinto analogo EA12-7, kūrimui.

PUBLIKACIJA 6: Izoformai atrankių slopiklių kūrimas, tikrinant kišenės dydį pagal Spynos-ir-Rakto modelį

Straipsnyje buvo aptarta atrankių slopiklių kūrimo strategija, didinant cheminio junginio dydį ir tokiu būdu tikrinant CA aktyvaus centro matmenis. Buvo susintetinti di-*orto* ir di-*meta* pakeisti benzensulfonamidai su palaipsniui didėjančiais hidrofobiniais pakaitais ir išmatuotas jų prisijungimas prie CA. Daugeliu atvejų, padidėjus slopiklio dydžiui, gimingumas fermentui taip pat padidėdavo, kol pasiekdavo ribą, kai CA nebegalėjo prisijungti cheminio junginio dėl riboto jungimosi kišenės dydžio. Tyrimai parodė, kad priešvėžinis taikinys CA IX turi erdviausią aktyvų centrą pagal tūrį ir formą, todėl gali surišti didžiausio skersmens slopiklius, kaip pvz. VD17-18 (**15b**). Kito priešvėžinio taikinio CA XII aktyvusis centras buvo mažesnis nei CA IX, tačiau jame dar tilpo junginys VD16-22 (**15a)**, kuris buvo per didelis jungimuisi su netaikinine CA II.

Tyrimas parodė, kad slopiklių prisijungimo prie CA mechanizmas atitinka "Spynos-ir-rakto" principą. CA fermentas yra struktūriškai santykinai

standus ir jungdamasis su sulfonamidais junginiais nepatiria reikšmingų konformacinių pokyčių.

Be to, šioje publikacijoje buvo parodyta, kad dvi žmogaus CA IX – pagamintos žinduolių ląstelėse[84] ir mielėse[131], jungiasi su slopikliais vienodu gimiringumu paklaidų ribose. Mielėse pagaminta CA IX turi dvi mutacijas glikozilinimo vietoje ir yra naudojama kristalografijoje. Šie tyrimai patvirtino, kad abi CA IX formos yra tinkamos naujų CA-IX atrankių slopiklių kūrimui.

BENDROJI DISKUSIJA

Disertacijoje palyginau biofizikinius ir fermentų slopinimo metodus pikomoliniam gimingumui nustatyti ir ištyriau slopiklių atpažinimo perjungimą, panaudojant chCA VI ir chCA XII.

Biofizikinių ir fermentinio aktyvumo slopinimo metodų derinimo svarba

Mokslininkai visame pasaulyje kiekvieną dieną kuria naujus cheminius junginius, kad jie slopintų su liga susijusius tikslinius fermentus. Jie renkasi ir taiko jungimosi ir/arba aktyvumo slopinimo metodus pagal savo baltymų-ligandų sistemą, turimus instrumentus ir biudžetą. Deja, visi tyrimo metodai turi privalumų ir apribojimų.

Lyginant su biofizikiniais tyrimo metodais, fermentinio aktyvumo slopinimo duomenys patvirtina, kad slopikliai keičia fermento katalizinį aktyvumą. Fermento-slopiklio sąveikos stiprumas gali stipriai skirtis, dėl to reikia tinkamai suplanuoti jungimosi eksperimentų atlikimą. CA katalizuoja savaiminę CO_2 hidratacijos reakciją, kurios greitis yra 0.037 s^{-1} [133,101]. Eksperimento metu turi būti naudojama tokia CA koncentracija, kad būtų detektuojamas ženklus greičių skirtumas tarp spontaninės ir katalizuojamos CO_2 hidratacijos reakcijos. Praktiškai, CA koncentracija turi būti 10–500 nM, priklausomai nuo izofermento katalizinio aktyvumo. Esant ypač stipriam jungimuisi (angl. *tight-binding*) stebimas CA aktyvaus centro nusititravimas, ir taikant Hilo modelį nustatyta stebimoji K_d būna lygi pusei CA koncentracijos ($K_d = [CA] / 2$)[99,134–136]. Dėl šios priežasties CA aktyvumas ir koncentracija riboja labai stipriai besijungiančių slopiklių gimiringumo konstantos nustatymą, naudojant SFA. Problemą iš dalies galima išspręsti taikant Morisono lygtį, kuri atsižvelgia į CA koncentraciją ir pateikia tikslesnę K_d reikšmę.

Disociacijos konstantos nustatymą ITC metodu taip pat riboja CA koncentracija. Naudojama 5–20 µM CA koncentracija leidžia išmatuoti

gimingumus intervale nuo mikromolinio iki nanomolinio. ITC reikalauja daug laiko, didelio baltymo kiekio (~300 μg) ir prietaisas yra gana brangus. Kita vertus, tai vienintelis metodas, leidžiantis įvertinti baltymo-ligando jungimosi termodinaminius parametrus (*ΔH, ΔG* ir *ΔS*).

FTSA metodui taip pat reikalingos mikromolinės CA koncentracijos (5–10 μM), tačiau tai neriboja fermento T_m nustatymo. Eksperimentuose baltymai ir cheminiai junginiai turi būti pakankamai stabilūs ir tirpūs, o vienintelis metodo apribojimas yra vandens virimo temperatūra. Deja, kai kurie benzensulfonamidai, ypač turintys kelis aromatinius žiedus, pasižymi didele fluorescencija, todėl apsunkina baltymų išsivyniojimo kreivės stebėjimą. Tokiu atveju vietoj ANS naudojau SyproOrange dažą, kad galėčiau gauti CA išsivyniojimo kreives. Nepaisant aptartų kliūčių, FTSA leidžia išmatuoti jungimosi konstantas nuo milimolinio iki pikomolinio diapazono. Tai tiksliausias metodas, lyginant su ITC ir SFA, nes CA aktyvumas ir koncentracija mėginyje neriboja K_d nustatymo.

Šis darbas parodė gerą koreliaciją tarp slopiklių gimingumų, nustatytų FTSA, SFA ir ITC metodais panašiomis sąlygomis, diapozone nuo mikromolinio iki nanomolinio. Anksčiau mano kolegos parodė, kad SPR[9] metodu nustatytos tokios pačios K_d paklaidų ribose kaip ir aptartais trimis metodais. Analogišką rezultatą gavau ir taikydama *p*-nitrofenilacetato metodą[106].

Slopiklio atpažinimo perjungimas

Vaistų atradimas prasideda mėgintuvėlyje, įvairiais tyrimo metodais matuojant sąveikas tarp tikslinio fermento, atsakingo už ligos vystymąsi, ir vaistų-kandidatų molekulių. Dėl to visada kyla klausimas, kaip pagaminti rekombinantinį baltymą, kuris būtų toks pat biologiškai aktyvus kaip ir esantis žmogaus organizme. Paprastai mokslininkai naudoja *E. coli* bakterijas, žinduolių ląsteles ar mieles rekombinantiniams žmogaus baltymams gaminti arba randa būdų, kaip išgryninti natyvius baltymus iš žmogaus kraujo, pieno, seilių ir kt. Šis darbas parodė, kad rekombinantinė žmogaus CA IX, gaminama tiek žinduolių ląstelėse, tiek ir mielėse, jungiasi su slopikliais vienodu gimininguмu paklaidų ribose ir abi alternatyviai gali būti naudojamos slopiklių atrankai.

Nepaisant biotechnologijų pažangos, kai kuriuos baltymus vis dar sudėtinga ir brangu gaminti *E. coli* bakterijose, o ypač dideliais kiekiais. Be to, dalies baltymų ir jų kompleksų su ligandais vis dar nepavyksta iškristalinti. Čia pristatau chCA VI ir chCA XII inžineriją, kaip sudėtingos fermentų gamybos ir kristalinimo sprendimą. Pirmiausia, mano kolegos sukonstravo

chCA VI ir chCA XII, o tada aš atlikau kinetinius ir ligandų jungimosi tyrimus, kad įvertinčiau juos kaip tikslinių CA izofermentų modelius.

Kinetiniai tyrimai

Tyrimų metu naudodama SFA metodą nustačiau CA I, CA II, chCA VI, CA VI, chCA XII ir CA XII kinetinius parametrus. Duomenis apibendrinau 1 lentelėje. Pirmiausia pritaikiau mūsų modelį[99] tiksliai substrato koncentracijai mėginyje nustatyti, o tuomet pagal Lineweaver-Burk ir Michelis-Menten lygtis nustačiau $k_{cat,}$ K_M, ir pK_a. Gauti parametrai atitiko anksčiau paskelbtus rezultatus[33,34,71,144–147]. Katalizinės konstantos skyrėsi iki 2–3 kartų, o pK_a vertės kito iki 0.6 vieneto.

ChCA XII turėjo 5 mutacijas tose pačiose pozicijose (A65S, N67K, I91T, F130A, V134S) kaip ir chCA VI (A65T, N67Q, F130Y, V134Q, L203T) ir vieną - papildomą (I91T). CA II aktyvaus centro aminorūgščių pakeitimas CA VI-specifinėmis aminorūgštimis neturėjo įtakos His64 pK_a vertei, tačiau ji padidėjo chCA XII baltyme. Dėl šios priežasties manau, kad I91T mutacija padidino chCA XII pK_a, o Thr88 (CA XII numeracija) dalyvauja CA XII kataliziniame mechanizme.

Tyrimų metu K_M vertės buvo nustatytos su didelėmis paklaidomis. Dauguma studijų teigia, kad K_M nuo pH nepriklauso. Nepaisant to, šiame tyrime K_M nepriklausė nuo pH tik siaurame intervale, artimo neutraliam pH. Rūgštinėse ir bazinėse sąlygose K_M vertės buvo didesnės nei neutraliame pH. Panašaus profilio rezultatai buvo paskelbti 1964 m. publikacijoje[100]. Įdomu tai, kad atliekant literatūros analizę nepavyko rasti K_M priklausomybės nuo pH eksperimentinių duomenų paveikslų.

Jungimosi ir slopinimo tyrimai

Mes atlikome jungimosi ir slopinimo tyrimus, kad įvertintume chCA VI ir chCA XII ligandų atpažinimo perjungimą. Mano žiniomis, iki šiol nėra atrasta CA VI atrankių slopiklių. Mūsų laboratorijos daugiau nei 1000 cheminių junginių bibliotekos skenavimas (angl. *screening*) parodė, kad visi slopikliai stipriau jungiasi su CA II nei su CA VI. Be to, nėra su CA VI-slopiklių kompleksų kristalų struktūrų. 2012 m. buvo nustatyta tik žmogaus CA VI katalizinio domeno kristalinė struktūra[44]. ChCA VI atitiko CA VI ir buvo patvirtinta kaip tinkamas modelis slopiklių atrankos ir rentgeno kristalografiniams tyrimams. Tokiu būdu chCA VI suteikė žinių apie CA VI slopiklių efektyvumą. Be to, ji galėtų būti panaudojama biologiniam CA VI vaidmeniui nustatyti.

ChCA XII buvo tyrinėjama siekiant suprasti pagrindinius CA II ir CA XII struktūrinius skirtumus, susijusius su sulfonamidinių slopiklių jungimusi. Remiantis tyrimų rezultatais buvo sukurtas ir susintetintas naujas junginys EA12-7, pasižymintis dideliu atrankumu CA XII, lyginant su kitomis 11 CA izoformų. Dėl to jis galėtų būti pasirinktas kaip lyderinis junginys ir toliau vystomas ikiklinikiniuose tyrimuose. Slopiklių jungimosi analizė apėmė ir gerai žinomą slopiklį 4-(4-fluorfenilureido)-benzensulfonamidą (U-104 arba SLC-0111), su kuriuo yra atliekami Ib/II fazės[150] klinikiniai tyrimai vėžio gydymui. Anksčiau buvo paskelbta, kad jis stipriai sąveikauja su CA XII (K_i = 4.5 nM), o sąveika su CA II yra vidutinio stiprumo (K_i = 96 nM). Visgi, mes nustatėme, kad junginio SLC-0111 jungimosi gimingumas CA II buvo 17 kartų stipresnis nei CA XII, o K_d yra mikromoliniame intevale, kaip tai patvirtino rezultatai, gauti taikant tris skirtingus tyrimo metodus (SFA, FTSA ir ITC). Rezultatai atitiko kitus anksčiau paskelbtus tyrimus[106,108,114,152,153], kad *para*-pakeisti benzensulfonamidai jungiasi su CA II daugiau nei dešimt kartų stipriau nei su CA XII. Neseniai paskelbtoje publikacijoje[154] išreiškiamos abejonės dėl eksperimentinių duomenų kokybės, kurie lėmė SLC-0111 junginio pasirinkimą klinikiniams tyrimams. Norint validuoti jungimosi konstantų vertes, būtina naudoti kuo daugiau tyrimo metodų.

Panašus baltymų inžinerijos metodas anksčiau buvo panaudotas CA modelių, kurie imituoja CA I, CA III ir CA IX[113,158–161], kūrimą. Pirmieji CA II mutantai buvo sugeneruoti apie 1990 m.[158,161]. Behravan ir kt.[158] pakeitė CA II aktyviajame centre tris aminorūgštas į tas, kurios būdingos CA I, o Ren ir kt.[161] mutavo CA II aminorūgštis į tas, kurios būdingos CA III. 2009–2014 m. buvo sukurti du CA II mutantai su dviejomis[159] arba septyniomis[160] mutacijomis, kurie imituoja priešvėžinį taikinį CA IX. ChCA IX buvo pagrinde kuriamos kristalografiniams tyrimams, kadangi iki tol buvo išspręsta tik viena CA IX kristalinė struktūra[162]. Mūsų laboratorijoje taip pat buvo sukurta chCA IX, kurios sąveikos stiprumus išmatavau su 6 fluorintais benzensulfonamidais. Nustačiau, kad chCA IX dalinai perjungė slopiklių atpažinimą iš CA II į CA IX.

Išsami analizė patvirtino izofermentų inžineriją, kaip tinkamą strategiją atrankių slopiklių kūrimui. Ji galėtų būti pritaikoma kitų CA izoformų, pvz, mitochondrinių CA VA ir CA VB, sukūrimui, kurios pasižymi ypač mažomis raiškos ir gryninimo išeigomis, ir vis dar nėra jų kristalinių struktūrų.

BAIGIAMOSIOS NUOSTATOS IR ATEITIES PERSPEKTYVOS

Vaistų kūrimas yra labai ilgas ir brangus procesas, apimantis keturis pagrindinius etapus: *in vitro* tyrimus (I), ikiklinikinius tyrimus (II), klinikinius

tyrimus (III) ir vaistų patekimą į rinką (IV). Kuo vėlesnis etapas, tuo jis sudėtingesnis ir brangesnis. Dėl šios priežasties "*in vitro* stadijoje" būtina pasirinkti tinkamą vaisto-kandidato molekulę, kad vėlesniuose ikiklinikinių ir klinikinių tyrimų etapuose pavyktų gauti sėkmingus rezultatus.

Medicininės chemijos specialistai gali pritaikyti šiame darbe aptartą izofermentų inžinerijos strategiją kitoms fermentų-slopiklių sistemoms. Chimerinių izofermentų inžinerija galėtų spręsti vaistų kūrimo iššūkius, tokius kaip maža baltymo raiška ir gryninimo išeiga bei sudėtingos kristalinimo sąlygos. Mitochondrinių CA VA ir CA VB kristalinių struktūrų vis dar nėra, o jos išgryninamos labai mažais kiekiais. ChCA VA ir chCA VB sukūrimas padėtų sukurti naujus slopiklius, kaip vaistus-kandidatus nuo nutukimo[163].

Chimerinių izofermentų inžinerija suteikia informaciją apie pagrindinius struktūrinius kelių izoformų skirtumus ir pateikia įžvalgų izoformai atrankių slopiklių kūrimui. Ši strategija gali padėti sukurti naujus vaistus-kandidatus. Pavyzdžiui, šių tyrimų metu buvo sukurtas lyderinis junginys EA12-7. Šis nanomolinis slopiklis atrankiai jungiasi su CA XII ir yra tinkamas kandidatas ikiklinikiniams priešvėžiniams tyrimams.

Rekomenduočiau tęsti molekulinio atpažinimo tyrimus, kurie yra esminis pagrindas tikrai racionaliam didelio gimingumo ir atrankumo vaistų-kandidatų kūrimui. CA srityje, sulfonamidiniai slopikliai turi potencialą tapti vaistais epilepsijos, nutukimo, vėžio ir kitų ligų gydymui.

Išvados:

1. 5–6 aminorūgščių CA II aktyviajame centre mutacijos, reikalingos chCA VI ir chCA VI sugeneravimui, neturėjo įtakos fermento didžiausiam kataliziniam aktyvumui, tačiau turėjo vidutinį poveikį lydymosi temperatūroms ir Michaelis-Menten konstantoms.
2. ChCA VI ir chCA XII baltymai perjungė slopiklių atpažinimo profilį iš CA II į CA VI ir CA XII, patvirtindami, kad chimerinės CA yra geri modeliai izoformai atrankių slopiklių kūrime.
3. Nustatyta gera koreliacija tarp baltymo-ligando gimininguмo konstantų, išmatuotų FTSA, SFA ir ITC metodais, esant palyginamoms sąlygoms ir gimininguмo diapazonui nuo mikromolinio iki nanomolinio. Visgi, pikomolinių konstantų nustatymui tinkamiausias buvo FTSA metodas.

7. ACKNOWLEDGEMENTS

I would like to thank my supervisor and colleagues at the Institute of Biotechnology in Vilnius University Life Sciences Center:

- **Prof. Daumantas Matulis** for teaching me science, broader thinking, and lifetime things; opportunities to participate at international conferences.
- **Dr. Asta Zubrienė**, **dr. Lina Baranauskienė** for kindness and constant help to solve everyday practical issues.
- **Dr. Vytautas Petrauskas** for teaching to prepare and present high-quality scientific data, discussions, and critical thinking.
- **MD Agnė Petrošiūtė** for daily talks on feminine things.
- **Dr. Justina Kazokaitė–Adomaitienė** for collaborations on investigating chimeric carbonic anhydrase VI and writing the review about experimental approaches.
- **Dr. Jurgita Matulienė, dr. Vaida Juozapaitienė, Vilma Michailovienė, Aurelija Mickevičiūtė, Jelena Jachno, David Timm, and their students** for the production of recombinant human and chimeric carbonic anhydrases.
- **Dr. Virginija Dudutienė, dr. Edita Čapkauskaitė, Audrius Zakšauskas and their students** for the synthesized benzenesulfonamides.
- **Dr. Alexey Smirnov, dr. Elena Manakova and prof. Saulius Gražulis** for X-ray crystallographic studies.
- **Dr. Visvaldas Kairys** for molecular modeling studies.

In addition, huge thanks to my husband **dr. Vytautas Smirnovas** for sharing his expertise, love, trust, logical thinking, and everyday support.

I am grateful to the community of the Vilnius University Life Sciences Center for a friendly and supportive work atmosphere.

8. PUBLICATIONS INCLUDED IN THE DISSERTATION

I have included six publications in the dissertation:

1. **Smirnovienė, J.**, Baranauskienė, L., Zubrienė, A., Matulis, D. A standard operating procedure for an enzymatic activity inhibition assay. Eur. Biophys. J. (2021) 50, 345–352. https://doi.org/10.1007/s00249-021-01530-8

I prepared all figures and wrote a significant part the first draft of a publication.

2. **Smirnovienė, J.**, Smirnov, A., Zakšauskas, A., Zubrienė, A., Petrauskas, V., Mickevičiūtė, A., Michailovienė, V., Čapkauskaitė, E., Manakova, E., Gražulis, S., Baranauskienė, L., Chen, W.-Y., Ladbury, J. E., Matulis, D. Switching the inhibitor – enzyme recognition profile via chimeric carbonic anhydrase XII. *ChemistryOpen* (2021) 10(5):567–580. https://doi.org/10.1002/open.202100042

I designed and conducted significant parts of FTSA and SFA experiments, analyzed the data, proposed to synthesize inhibitors EA11-7 and EA12-7, and wrote the first draft of a publication.

3. Kazokaitė-Adomaitienė, J., Becker, H. M., **Smirnovienė, J.**, Dubois, L. J., Matulis, D. Experimental approaches to identify selective picomolar inhibitors for carbonic anhydrase IX. *Curr. Med. Chem.* (2021) 28(17):3361–3384. https://doi.org/10.1038/s41598-019-49094-0

I prepared the section "2. Biochemical and biophysical assays to determine inhibitor affinity in vitro".

4. Dudutienė, V., Zubrienė A., Kairys V., Smirnov A., **Smirnovienė, J.**, Leitans J., Kazaks A., Tars K., Manakova L., Gražulis S., Matulis D. Isoform-selective enzyme inhibitors by exploring pocket size according to the Lock-and-Key principle. *Biophys J.* (2020) 119(8):1513–1524. https://doi.org/10.1016/j.bpj.2020.08.037

I designed and conducted all SFA and several FTSA experiments and prepared figures S1 and S2.

5. Kazokaitė, J., Kairys, V., **Smirnovienė, J.**, Smirnov, A., Manakova, E., Tolvanen, M., Parkkila, S., Matulis, D. Engineered Carbonic Anhydrase VI-Mimic Enzyme Switched the Structure and Affinities

of Inhibitors, *Sci. Rep.* 9(1):12710 (2019). https://doi.org/10.1038/s41598-019-49094-0

I designed and conducted all SFA experiments, analyzed the data, and prepared figures 2 and 4.

6. **Smirnovienė, J.**, Smirnovas, V., and Matulis, D. Picomolar inhibitors of carbonic anhydrase: Importance of inhibition and binding assays. Anal. Biochem. 522 (2017) 61-72. https://doi.org/10.1016/j.ab.2017.01.022

I designed and conducted all experiments, analyzed data, prepared all figures, and wrote the first draft of a publication.

9. PUBLICATIONS NOT INCLUDED IN THE DISSERTATION

1. Balandis, B., Ivanauskaitė, G., **Smirnovienė, J.**, Kantminienė, K., Matulis, D., Mickevičius, V., Zubrienė, A. Synthesis and structure–affinity relationship of chlorinated pyrrolidinone bearing benzenesulfonamides as human carbonic anhydrase inhibitors, *Bioorg. Chem.* 97 (2020) 103658. https://doi.org/10.1016/j.bioorg.2020.103658
2. Toleikis, Z., Sirotkin V. A., Skvarnavičius, G., **Smirnovienė, J.**, Roumenstand, Ch., Matulis, D., and Petrauskas, V. Volume of Hsp90 Protein-Ligand Binding Determined by Fluorescent Pressure Shift Assay, Densitometry, and NMR. *J. Phys. Chem. B* 120 (2016) 9903–9912. https://doi.org/10.1021/acs.jpcb.6b06863
3. Zubrienė, A., **Smirnovienė, J.**, Smirnov, A., Morkūnaitė, V., Michailovienė, V., Jachno, J., Juozapaitienė, V., Norvaišas, P., Manakova, E., Gražulis, S., and Matulis, D. Intrinsic thermodynamics of 4-substituted-2,3,5,6-tetrafluorobenezenesulfonamides binding to carbonic anhydrases by isothermal titration calorimetry. *Biophys. Chem.*, 205 (2015) 51–65. https://doi.org/10.1016/j.bpc.2015.05.009
4. Kazokaitė, J., Milinavičiūtė, G., **Smirnovienė, J.**, Matulienė, J., Matulis, D. Intrinsic Binding of 4-Substituted-2,3,5,6-tetrafluorobenezenesulfonamides to Native and Recombinant Human Carbonic Anhydrase VI. *FEBS J.* (2015) 972–983. https://doi.org/10.1111/febs.13196
5. Dudutienė, V., Zubrienė, A., Smirnov, A., Timm, D. D**., Smirnovienė, J.**, Kazokaitė, J., Michailovienė, V., Zakšauskas, A., Manakova, E., Gražulis, S., and Matulis, D. Functionalization of fluorinated benzenesulfonamides and their inhibitory properties of carbonic anhydrases. *Chem. Med. Chem.* (2015) 662–687. https://doi.org/10.1002/cmdc.201402490
6. Morkūnaitė, V., **Gylytė, J.**, Zubrienė, A., Baranauskienė, L., Kišonaitė, M., Michailovienė, V., Juozapaitienė, V., Todd, M. J., and Matulis, D. Intrinsic thermodynamics of sulfonamide inhibitor binding to human carbonic anhydrases I and II. *J. Enz. Inhib. Med. Chem.* (2015) 204–211. https://doi.org/10.3109/14756366.2014.908291
7. Dudutienė, V., Matulienė, J., Smirnov, A., Timm, D. D., Zubrienė, A., Baranauskienė, L., Morkūnaitė, V., **Smirnovienė, J.**, Michailovienė, V., Juozapaitienė, V., Mickeviciūtė, A., Kazokaitė, J., Bakšytė, S., Kasiliauskaiė, A., Jachno, J., Revuckienė, J., Kišonaitė, M., Pilipuitytė, V., Ivanauskaitė, E., Milinavičiūtė, G., Smirnovas, V., Petrikaitė, V., Kairys, V., Petrauskas, V., Norvaišas, P., Lingė, D., Gibieža, P., Čapkauskaitė, E., Zakšauskas, A., Kazlauskas, E., Manakova, E., Gražulis, S., Ladbury, J. E., and Matulis, D. Discovery

and characterization of novelselective CAIX inhibitors. *J. Med. Chem.* (2014) 9435–9446. https://doi.org/10.1021/jm501003k

8. Kišonaitė, M., Zubrienė, A., Čapkauskaitė, E., Smirnov, A., **Smirnovienė, J.**, Kairys, V., Michailovienė, V., Manakova, E., Gražulis, S., Tumkevičius, S., and Matulis, D. Intrinsic thermodynamics and structure correlation of benzenesulfonamides with a pyrimidine moiety binding to carbonic anhydrases I, II, VII, XII, and XIII. *PLoS One* 9 (12) (2014), e114106. https://doi.org/10.1371/journal.pone.0114106
9. Zubrienė, A., Čapkauskaitė, E., **Gylytė, J.**, Kišonaitė, M., Tumkevičius, S., Matulis, D. Benzenesulfonamides with benzimidazole moiety as inhibitors of carbonic anhydrases I, II, VII, XII and XIII. *J. Enz. Inhib. Med. Chem.* (2014) 124–131. https://doi.org/10.3109/14756366.2012.757223
10. Čapkauskaitė, E., Zubrienė, A., Smirnov, A., Torresan, J., Kišonaitė, M., Kazokaitė, J., **Gylytė, J.**, Michailovienė, V., Jogaitė, V., Manakova,E. , Gražulis, S., Tumkevičius, S., and Matulis, D. Benzenesulfonamides with pyrimidine moiety as inhibitors of human carbonic anhydrases I, II, VI, VII, XII, and XIII. *Bioorg. Med. Chem.*, 21 (2013) 6937–6947. https://doi.org/10.1016/j.bmc.2013.09.029
11. Dudutienė, V., Zubrienė, A., Smirnov, A., **Gylytė, J.**, Timm, D. D., Manakova, E., Gražulis, S., Matulis, D. 4-Substituted-2,3,5,6-Tetrafluorobenzenesulfonamides as Inhibitors of Carbonic Anhydrases I, II, VII, XII, and XIII. *Bioorg. Med. Chem.*, 21 (2013) 2093–2106; https://doi.org/10.1016/j.bmc.2013.01.008
12. Petrauskas, V., **Gylytė, J.**, Toleikis, Z., Cimmperman, P., Matulis, D. Volume of Hsp90 ligand binding and the unfolding phase diagram as a function of pressure and temperature. *Eur. Biophys. J.*, 42 (2013) 355–362; https://doi.org/10.1007/s00249-012-0884-7
13. Jogaitė, V., Zubrienė, A., Michailovienė, V., **Gylytė, J.**, Morkūnaitė, V., Matulis, D. 2012. Characterization of Human Carbonic Anhydrase XII Stability and Inhibitor Binding. *Bioorg. Med. Chem.*, 21 (2013) 1431–1436; https://doi.org/10.1016/j.bmc.2012.10.016

10. LIST OF SCIENTIFIC EVENTS

I have presented the results of the dissertation at twelve scientific events:

1. **J. Smirnovienė**, J. Kazokaitė, A. Smirnov, V. Kairys, A. Mickevičiūtė, V. Michailovienė, E. Manakova, L. Baranauskienė, D. Matulis. "Engineering of chimeric carbonic anhydrases for designing isoform-selective inhibitors", FEBS3+ conference of Estonian, Latvian, and Lithuanian and Biochemical Societies, Tallinn, Estonia, 15–17th June 2022 (poster presentation);
2. **J. Smirnovienė**, V. Dudutienė, A. Zubrienė, and D. Matulis. "Picomolar inhibitors of carbonic anhydrase: Importance of inhibition and binding assays", XXI Conference of the International Society for Biological Calorimetry "ISBC-2022", Vilnius, Lithuania, 8–10th June 2022 (poster presentation);
3. **J. Smirnovienė**, A. Smirnov, V. Kairys, J. Kazokaitė-Adomaitienė, A. Mickevičiūtė, V. Michailovienė, E. Manakova, L. Baranauskienė, D. Matulis. "Engineering of chimeric carbonic anhydrases for designing isoform-selective inhibitors", "13th European Biophysics Conference", Vienna, Austria, 24–28th July 2021 (poster presentation);
4. **J. Smirnovienė**, J. Kazokaitė, V. Kairys, A. Smirnov, V. Michailovienė, E. Manakova, L. Baranauskienė, D. Matulis. "Engineered chimeric carbonic anhydrases switched the structure and affinities of inhibitors. "4th COST Action ARBRE-MOBIEU plenary meeting "Living molecules: towards integrative Biophysics of the Cell", Prague, Czech Republic, 24–26th February 2020 (flash poster presentation);
5. **J. Smirnovienė**, D. Matulis. "Picomolar inhibitors of carbonic anhydrase: Importance of inhibition and binding assays. 6th Prague-Weismann summer school "Advances in Drug Discovery. Drug discovery and development from basic research through preclinical and clinical phases", Prague, Czech Republic, 2–6th September 2019 (poster presentation);
6. **J. Smirnovienė**, D. Matulis. "Picomolar inhibitors of carbonic anhydrase: Importance of inhibition and binding assays. "Affinity", Stockholm, Sweden, 26–28th June 2019 (poster presentation);
7. **J. Smirnovienė**, D. Matulis. "Tight-binding inhibitors of carbonic anhydrase: necessity to combine inhibition and binding assays", FEBS3+ conference of Latvian, Lithuanian and Estonian Biochemical Societies, Riga, Latvia, 17–20th June 2019 (oral presentation);
8. **J. Smirnovienė**, A. Zubrienė, V. Dudutienė, V. Juozapaitienė, V. Michailovienė, D. Matulis. "Intrinsic structure-thermodynamics correlations of fluorinated benzenesulfonamide as inhibitors of human carbonic anhydrases", Lithuanian chemists conference

"Chemistry and Chemical Technology", Vilnius, Lithuania, 16th May 2019 (poster presentation);

9. **J. Smirnovienė**, D. Matulis. "Picomolar inhibitors of carbonic anhydrase: Importance of inhibition and binding assays." 62nd international conference for students of physics and natural sciences "Open Readings 2019", Vilnius, Lithuania, 19–22nd March 2019 (poster presentation);
10. **J. Smirnovienė**, D. Matulis. "Picomolar inhibitors of carbonic anhydrase: Importance of inhibition and binding assays", 14th international conference of life sciences "The COINS 2019", Vilnius, Lithuania, 26–28th February 2018 (poster presentation);
11. **J. Smirnovienė**, D. Matulis, "Picomolar inhibitors of carbonic anhydrase: Importance of inhibition and binding assays", Baltic Biophysics Conference, Kaunas, Lithuania, 5–6th October 2018 (poster presentation);
12. **J. Smirnovienė**, D. Matulis, "Picomolar inhibitors of carbonic anhydrase: Importance of inhibition and binding assays", XVth International Conference of Lithuanian Biochemical Society, Dubingiai, Lithuania, 26–29th June 2018 (poster presentation).

11. CURRICULUM VITAE

Education

2016 – 2022	Doctoral (Ph.D.) studies in Chemical Engineering, Vilnius University
2013 – 2015	M. Sc. Biochemistry, Vilnius University
2009 – 2013	B. Sc. Bioengineering, Vilnius Gediminas Technical University

Research experience

Since 2018	*Junior Scientist.* Department of Biothermodynamics and Drug Design, Institute of Biotechnology, Life Sciences Center, Vilnius University
2011 – 2018	*Research Assistant*. Department of Biothermodynamics and Drug Design, Institute of Biotechnology, Vilnius University

Research projects

2021 – 2023	EU Structural Fund project "Development of a prototype technology for evaluating the efficacy of compounds in inhibiting SARS CoV-2 recombinant viral enzymes"(01.2.2-LMT-K-718-05-0011), principal member.
2020 – 2023	EU Structural Fund project "Design of anti-Alzheimer's Drug Candidates that Inhibit BACE1 Enzymatic Activity and Aggregation of A Peptide "(01.2.2-LMT-K-718-03-0003), principal member.
2020 – 2023	EU Structural Fund project "Screening for new methods for treatment of neurodegenerative disorders" (01.2.2-LMT-K-718-03-0021), principal member.
2019 – 2020	Vilnius University project "Target enzyme engineering for research of protein-small molecule interactions" (MSF-JM-6), principal member.

Awards

- ✓ Fellowship of L'Oréal Baltic Program "For Women in Science" (2021)
- ✓ Research Council of Lithuania scholarships for academic achievements (2018–2022)
- ✓ Life Sciences Center scholarship for academic achievements (2020)
- ✓ Vilnius university one-off earmarked scholarships for academic achievements (2018–2021)

Pedagogical activities

Supervision of one bachelor thesis and seven invited lectures for school children.

Science promotion activities

One interview on the TV show "Labas rytas" by Lithuanian National Television and Radio; four interviews in news portals, one interview in a magazine "Moteris"; participation at Vilnius University Science Communication Competition "Science Sprint".

12. REFERENCES

1. Capasso, C. & Supuran, C. T. An overview of the alpha-, beta- and gamma-carbonic anhydrases from Bacteria: can bacterial carbonic anhydrases shed new light on evolution of bacteria? *J Enzyme Inhib Med Chem* 325–332 (2014).
2. Cronk, J. D., O'Neill, J. W., Cronk, M. R., Endrizzi, J. A. & Zhang, K. Y. Cloning, crystallization and preliminary characterization of a beta-carbonic anhydrase from Escherichia coli. *Acta Crystallogr D Biol Crystallogr* **56**, 1176–1179 (2000).
3. De Luca, V. *et al.* Expression and characterization of a recombinant psychrophilic γ-carbonic anhydrase (NcoCA) identified in the genome of the Antarctic cyanobacteria belonging to the genus Nostoc. *J Enzyme Inhib Med Chem* 1–8 (2015).
4. Del Prete, S. *et al.* Discovery of a new family of carbonic anhydrases in the malaria pathogen Plasmodium falciparum—The η-carbonic anhydrases. *Bioorganic Med Chem Lett* **24**, 4389–4396 (2014).
5. Hewett-Emmett, D. & Tashian, R. E. Functional diversity, conservation, and convergence in the evolution of the alpha-, beta-, and gamma-carbonic anhydrase gene families. *Mol Phylogenet Evol* **5(1)**, 50–77 (1996).
6. Kikutani, S. *et al.* Thylakoid luminal θ-carbonic anhydrase critical for growth and photosynthesis in the marine diatom Phaeodactylum tricornutum. *PNAS* **113**, 9828–9833 (2016).
7. Del Prete, S. *et al.* Sulfonamide Inhibition Profile of the β-Carbonic Anhydrase from Malassezia restricta, An Opportunistic Pathogen Triggering Scalp Conditions. *Metabolites* **10**, 39 (2020).
8. Hirakawa, Y. *et al.* Characterization of a novel type of carbonic anhydrase that acts without metal cofactors. *BMC Biology* **19**, 105 (2021).
9. Linkuvienė, V. *et al.* Thermodynamic, kinetic, and structural parameterization of human carbonic anhydrase interactions toward enhanced inhibitor design. *Q Rev Biophys* **51**, 1–48 (2018).
10. Occhipinti, R. & Boron, W. F. Role of Carbonic Anhydrases and Inhibitors in Acid–Base Physiology: Insights from Mathematical Modeling. *Int J Mol Sci* **20**, 3841 (2019).
11. Picaud, S. S. *et al.* Crystal structure of human carbonic anhydrase-related protein VIII reveals the basis for catalytic silencing. *Proteins* **76**, 507–511 (2009).
12. Aspatwar, A., Tolvanen, M. E. E. & Parkkila, S. An update on carbonic anhydrase-related proteins VIII, X and XI. *J Enzyme Inhib Med Chem* **28(6)**:1129–1142 (2013).

13. Krishnamurthy, V. M. *et al.* Carbonic Anhydrase as a Model for Biophysical and Physical-Organic Studies of Proteins and Protein−Ligand Binding. *Chem Rev* **108**, 946–1051 (2008).
14. Aggarwal, M., Boone, C. D., Kondeti, B. & McKenna, R. Structural annotation of human carbonic anhydrases. *J Enzyme Inhib Med Chem* **28**, 267–277 (2013).
15. Sjöblom, B., Polentarutti, M. & Djinović-Carugo, K. Structural study of X-ray induced activation of carbonic anhydrase. *PNAS* **106**, 10609–10613 (2009).
16. Kim, J. K. *et al.* Elucidating the role of metal ions in carbonic anhydrase catalysis. *Nature Comm* **11**, 4557 (2020).
17. Nair, S. K. & Christianson, D. W. Unexpected pH-dependent conformation of His-64, the proton shuttle of carbonic anhydrase II. *J. Am Chem Soc* **113**, 9455–9458 (1991).
18. Maupin, C. M. & Voth, G. A. Preferred Orientations of His64 in Human Carbonic Anhydrase II. *Biochemistry* **46**, 2938–2947 (2007).
19. Fu, Y., Fan, F., Zhang, Y., Wang, B. & Cao, Z. Conformational Change of H64 and Substrate Transportation: Insight Into a Full Picture of Enzymatic Hydration of CO2 by Carbonic Anhydrase. *Front Chem* **0**, (2021).
20. Aggarwal, M., Kondeti, B. & McKenna, R. Insights towards sulfonamide drug specificity in a-carbonic anhydrases. *Bioorg Med Chem* **21**, 1526–1533 (2013).
21. Angeli, A., Carta, F. & Supuran, C. T. Carbonic Anhydrases: Versatile and Useful Biocatalysts in Chemistry and Biochemistry. *Catalysts* **10**, 1008 (2020).
22. Pocker, Y. & Stone, J. T. The Catalytic Versatility of Erythrocyte Carbonic Anhydrase. The Enzyme-Catalyzed Hydrolysis of p-Nitrophenyl Acetate. *ACS Publications* (1965).
23. Ingram, C. J. & Brubaker, R. F. Effect of brinzolamide and dorzolamide on aqueous humor flow in human eyes. *Am J Ophthalmol* **128**, 292–296 (1999).
24. Silver, L. H. Clinical efficacy and safety of brinzolamide (Azopt™), a new topical carbonic anhydrase inhibitor for primary open-angle glaucoma and ocular hypertension. *Am J Ophthalmol* **126**, 400–408 (1998).
25. Wile, D. Diuretics: a review. *Ann Clin Biochem* **49**, 419–431 (2012).
26. Brigo, F., Lattanzi, S., Igwe, S. C., Behzadifar, M. & Bragazzi, N. L. Zonisamide add-on therapy for focal epilepsy. *Cochrane Database Syst Rev* **10**, CD001416 (2018).
27. Kothare, S. V. & Kaleyias, J. Zonisamide: review of pharmacology, clinical efficacy, tolerability, and safety. *Expert Opin Drug Metab Toxicol* **4**, 493–506 (2008).

28. Leniger, T., Thöne, J. & Wiemann, M. Topiramate modulates pH of hippocampal CA3 neurons by combined effects on carbonic anhydrase and Cl-/HCO3- exchange. *Br J Pharmacol* **142**, 831–842 (2004).
29. Perucca, E. A pharmacological and clinical review on topiramate, a new antiepileptic drug. *Pharmacol Res* **35**, 241–256 (1997).
30. Y. Mboge, M., McKenna, R. & C. Frost, S. Advances in Anti-Cancer Drug Development Targeting Carbonic Anhydrase IX and XII. in *Topics in Anti-Cancer Research* (eds. Atta-ur-Rahman & Zaman, K.) 3–42 (Bentham Science Publishers, 2016).
31. Pinard, M. A., Mahon, B. & McKenna, R. Probing the Surface of Human Carbonic Anhydrase for Clues towards the Design of Isoform Specific Inhibitors. *Biomed Res Int* **2015**, 1–15 (2015).
32. Kišonaitė, M. *et al.* Intrinsic Thermodynamics and Structure Correlation of Benzenesulfonamides with a Pyrimidine Moiety Binding to Carbonic Anhydrases I, II, VII, XII, and XIII. *PLoS ONE* **9**, e114106 (2014).
33. Khalifah, R. G. The carbon dioxide hydration activity of carbonic anhydrase. I. Stop-flow kinetic studies on the native human isoenzymes B and C. *J Biol Chem* **246**, 2561–2573 (1971).
34. Mikulski, R. *et al.* Water Networks in Fast Proton Transfer during Catalysis by Human Carbonic Anhydrase II. *Biochemistry* **52**, 125–131 (2013).
35. Smirnovienė, J., Smirnovas, V. & Matulis, D. Picomolar inhibitors of carbonic anhydrase: Importance of inhibition and binding assays. *Anal Biochem* **522**, 61–72 (2017).
36. Avvaru, B. S. *et al.* Apo-human carbonic anhydrase II revisited: implications of the loss of a metal in protein structure, stability, and solvent network. *Biochemistry* **48**, 7365–7372 (2009).
37. Fisher, Z. *et al.* Kinetic and structural characterization of thermostabilized mutants of human carbonic anhydrase II. *Protein Eng Des Sel* **25**, 347–355 (2012).
38. Zubrienė, A. & Matulis, D. Characterization of Carbonic Anhydrase Thermal Stability. in *Carbonic Anhydrase as Drug Target: Thermodynamics and Structure of Inhibitor Binding* (ed. Matulis, D.) 51–59 (Springer International Publishing, 2019).
39. Esbaugh, A. J. & Tufts, B. L. The structure and function of carbonic anhydrase isozymes in the respiratory system of vertebrates. *Respir Physiol Neurobiol* **154**, 185–198 (2006).
40. Henry, R. P. The Role of Carbonic Anhydrase in Blood Ion and Acid-Base Regulation. *Am Zool* **24**, 241–251 (1984).
41. Tufts, B. L., Esbaugh, A. & Lund, S. G. Comparative physiology and molecular evolution of carbonic anhydrase in the erythrocytes of early vertebrates. *Comp Biochem Physiol A Mol Integr Physiol* **136**, 259–69 (2003).

42. Nishita, T. *et al.* Isolation and sequencing of swine carbonic anhydrase VI, an enzyme expressed in the swine kidney. *BMC Research Notes* **7**, 116 (2014).
43. Patrikainen, M., Pan, P., Kulesskaya, N., Voikar, V. & Parkkila, S. The role of carbonic anhydrase VI in bitter taste perception: evidence from the Car6−/− mouse model. *J Biomed Sci* **21**, 82 (2014).
44. Pilka, E. S., Kochan, G., Oppermann, U. & Yue, W. W. Crystal structure of the secretory isozyme of mammalian carbonic anhydrases CA VI: implications for biological assembly and inhibitor development. *Biochem Biophys Res Commun* **419**, 485–489 (2012).
45. Karhumaa, P. *et al.* The Identification of Secreted Carbonic Anhydrase VI as a Constitutive Glycoprotein of Human and Rat Milk. *PNAS* **98**, 11604–11608 (2001).
46. Kaseda, M., Ichihara, N., Nishita, T., Amasaki, H. & Asari, M. Immunohistochemistry of the bovine secretory carbonic anhydrase isozyme (CA-VI) in bovine alimentary canal and major salivary glands. *J Vet Med Sci* **68**, 131–135 (2006).
47. Kivela, J., Parkkila, S., Parkkila, A. K., Leinonen, J. & Rajaniemi, H. Salivary carbonic anhydrase isoenzyme VI. *J Physiol* **520 Pt 2**, 315–20 (1999).
48. Leinonen, J. S., Saari, K. A., Seppänen, J. M., Myllylä, H. M. & Rajaniemi, H. J. Immunohistochemical demonstration of carbonic anhydrase isoenzyme VI (CA VI) expression in rat lower airways and lung. *J Histochem Cytochem* **52**, 1107–1112 (2004).
49. Murakami, H. & Sly, W. S. Purification and characterization of human salivary carbonic anhydrase. *J Biol Chem* **262**, 1382–1388 (1987).
50. Esberg, A., Haworth, S., Brunius, C., Lif Holgerson, P. & Johansson, I. Carbonic Anhydrase 6 Gene Variation influences Oral Microbiota Composition and Caries Risk in Swedish adolescents. *Sci Rep* **9**, 452 (2019).
51. Arabacı, T., Çiçek, Y., Beydemir, Ş., Çanakçı, C. F. & Çanakçı, V. Are increased salivary carbonic anhydrase VI levels related to the amount of supragingival dental calculus formation and clinical periodontal scores? *J Dent Sci* **10**, 123–127 (2015).
52. Picco, D. de C. R. *et al.* Children with a Higher Activity of Carbonic Anhydrase VI in Saliva Are More Likely to Develop Dental Caries. *CRE* **51**, 394–401 (2017).
53. Picco, D. C. R., Marangoni-Lopes, L., Parisotto, T. M., Mattos-Graner, R. & Nobre-dos-Santos, M. Activity of Carbonic Anhydrase VI is Higher in Dental Biofilm of Children with Caries. *Int. J. Mol. Sci.* **20**, 2673 (2019).
54. Pemmari, T., Laakso, J., Patrikainen, M. S., Parkkila, S. & Järvinen, T. A. H. Carbonic Anhydrase VI in Skin Wound Healing Study on Car6 Knockout Mice. *IJMS* **21**, 5092 (2020).

55. Kazokaitė, J., Milinavičiūtė, G., Smirnovienė, J., Matulienė, J. & Matulis, D. Intrinsic binding of 4-substituted-2,3,5,6-tetrafluorobenezenesulfonamides to native and recombinant human carbonic anhydrase VI. *FEBS Journal* **282**, 972–983 (2015).
56. Barnett, D. H. *et al.* Estrogen receptor regulation of carbonic anhydrase XII through a distal enhancer in breast cancer. *Cancer Res.* **68**, 3505–3515 (2008).
57. Ilie, M. I. *et al.* Overexpression of carbonic anhydrase XII in tissues from resectable non-small cell lung cancers is a biomarker of good prognosis. *Int J Cancer* **128**, 1614–1623 (2011).
58. Watson, P. H. *et al.* Carbonic anhydrase XII is a marker of good prognosis in invasive breast carcinoma. *Br J Cancer* **88**, 1065–1070 (2003).
59. Gu, X.-F., Shi, C.-B. & Zhao, W. Prognostic value of carbonic anhydrase XII (CA XII) overexpression in hepatocellular carcinoma. *Int J Clin Exp Pathol* **12**, 2173–2183 (2019).
60. Haapasalo, J. *et al.* Carbonic anhydrase II in the endothelium of glial tumors: a potential target for therapy. *Neuro Oncol* **9**, 308–313 (2007).
61. Viikilä, P. *et al.* Carbonic anhydrase enzymes II, VII, IX and XII in colorectal carcinomas. *WJG* **22**, 8168 (2016).
62. Kopecka, J. *et al.* Carbonic anhydrase XII is a new therapeutic target to overcome chemoresistance in cancer cells. *Oncotarget* (2015).
63. Karhumaa, P. Identification of carbonic anhydrase XII as the membrane isozyme expressed in the normal human endometrial epithelium. *Mol. Hum Reprod* **6**, 68–74 (2000).
64. Karhumaa, P. *et al.* Expression of the transmembrane carbonic anhydrases, CA IX and CA XII, in the human male excurrent ducts. *Mol Hum Reprod* **7**, 611–616 (2001).
65. Leppilampi, M. *et al.* Carbonic anhydrase isozymes IX and XII in gastric tumors. *World J Gastroenterol* **9**, 1398–403 (2003).
66. Liao, S.-Y. Expression of cell surface transmembrane carbonic anhydrase genes CA9 and CA12 in the human eye: overexpression of CA12 (CAXII) in glaucoma. *J Med Gen* **40**, 257–261 (2003).
67. Parkkila, S. *et al.* Expression of the Membrane-associated Carbonic Anhydrase Isozyme XII in the Human Kidney and Renal Tumors: *J. Histochem. & Cytochem.* (2016)
68. Muhammad, E. *et al.* Autosomal recessive hyponatremia due to isolated salt wasting in sweat associated with a mutation in the active site of Carbonic Anhydrase 12. *Hum Genet* **129**, 397–405 (2011).
69. Power, K. A. *et al.* Identification of cell surface-specific markers to target human nucleus pulposus cells: expression of carbonic anhydrase XII varies with age and degeneration. *Arthritis Rheum* **63**, 3876–3886 (2011).
70. Waheed, A. & Sly, W. S. Carbonic anhydrase XII functions in health and disease. *Gene* **623**, 33–40 (2017).

71. Whittington, D. A. *et al.* Crystal structure of the dimeric extracellular domain of human carbonic anhydrase XII, a bitopic membrane protein overexpressed in certain cancer tumor cells. *Proc Natl Acad Sci U.S.A.* **98**, 9545–9550 (2001).
72. Jogaitė, V. *et al.* Characterization of human carbonic anhydrase XII stability and inhibitor binding. *Bioorg & Med Chem* **21**, 1431–1436 (2013).
73. Ulmasov, B. *et al.* Purification and kinetic analysis of recombinant CA XII, a membrane carbonic anhydrase overexpressed in certain cancers. *PNAS.* **97**, 14212–14217 (2000).
74. Pantoliano, M. W. *et al.* High-density miniaturized thermal shift assays as a general strategy for drug discovery. *J Biomol Screen* **6**, 429–440 (2001).
75. Niesen, F. H., Berglund, H. & Vedadi, M. The use of differential scanning fluorimetry to detect ligand interactions that promote protein stability. *Nat Protoc* **2**, 2212–2221 (2007).
76. Abbott, J. A., Livingston, N. M., Egri, S. B., Guth, E. & Francklyn, C. S. Characterization of aminoacyl-tRNA synthetase stability and substrate interaction by differential scanning fluorimetry. *Methods* **113**, 64–71 (2017).
77. Lo, M.-C. *et al.* Evaluation of fluorescence-based thermal shift assays for hit identification in drug discovery. *Anal Biochem* **332**, 153–159 (2004).
78. Lavinder, J. J., Hari, S. B., Sullivan, B. J. & Magliery, T. J. High-Throughput Thermal Scanning: A General, Rapid Dye-Binding Thermal Shift Screen for Protein Engineering. *J Am Chem Soc* **131**, 3794–3795 (2009).
79. Matulis, D., Kranz, J. K., Salemme, F. R. & Todd, M. J. Thermodynamic Stability of Carbonic Anhydrase: Measurements of Binding Affinity and Stoichiometry Using ThermoFluor. *Biochemistry* **44**, 5258–5266 (2005).
80. Petrauskas, V., Zubrienė, A., Todd, M. J. & Matulis, D. Inhibitor Binding to Carbonic Anhydrases by Fluorescent Thermal Shift Assay. in *Carbonic Anhydrase as Drug Target: Thermodynamics and Structure of Inhibitor Binding* (ed. Matulis, D.) 63–78 (Springer International Publishing, 2019).
81. Matulis, D. & Lovrien, R. 1-Anilino-8-Naphthalene Sulfonate Anion-Protein Binding Depends Primarily on Ion Pair Formation. *Biophys J* **74**, 422–429 (1998).
82. Matulis, D., Baumann, C. G., Bloomfield, V. A. & Lovrien, R. E. 1-Anilino-8-naphthalene sulfonate as a protein conformational tightening agent. *Biopolymers* **49**, 451–458 (1999).
83. Kasiliauskaitė, A. *et al.* Thermodynamic characterization of human carbonic anhydrase VB stability and intrinsic binding of compounds. *J Therm Anal Calorim* **123**, 2191–2200 (2016).

84. Linkuvienė, V. *et al.* Intrinsic thermodynamics of inhibitor binding to human carbonic anhydrase IX. *Biochim et Biophys Acta (BBA) - General Subjects* **1860**, 708–718 (2016).
85. Mickevičiūtė, A. *et al.* Intrinsic thermodynamics of high affinity inhibitor binding to recombinant human carbonic anhydrase IV. *Eur Biophys J* **47**, 271–290 (2018).
86. Smirnovienė, J. *et al.* Switching the Inhibitor-Enzyme Recognition Profile via Chimeric Carbonic Anhydrase XII. *ChemistryOpen* **10**, 567–580 (2021).
87. Cimmperman, P. *et al.* A Quantitative Model of Thermal Stabilization and Destabilization of Proteins by Ligands. *Biophys J* **95**, 3222–3231 (2008).
88. Bastos, M. & Velazquez-Campoy, A. Isothermal titration calorimetry (ITC): a standard operating procedure (SOP). *Eur Biophys J* (2021) doi:10.1007/s00249-021-01509-5.
89. de Azevedo, W. F. & Dias, R. Experimental approaches to evaluate the thermodynamics of protein-drug interactions. *Curr Drug Targets* **9**, 1071–1076 (2008).
90. Paketurytė, V., Zubrienė, A., Ladbury, J. E. & Matulis, D. Intrinsic Thermodynamics of Protein-Ligand Binding by Isothermal Titration Calorimetry as Aid to Drug Design. in *Microcalorimetry of Biological Molecules* (ed. Ennifar, E.) vol. 1964 61–74 (Springer New York, 2019).
91. Zubrienė, A. *et al.* Intrinsic thermodynamics of 4-substituted-2,3,5,6-tetrafluorobenzenesulfonamide binding to carbonic anhydrases by isothermal titration calorimetry. *Biophys Chem* **205**, 51–65 (2015).
92. Baker, B. M. & Murphy, K. P. Evaluation of Linked Protonation Effects in Protein Binding Reactions Using Isothermal Titration Calorimetry. *Biophys J* **71**, 2049–2055 (1996).
93. Zubrienė, A. & Matulis, D. Observed Versus Intrinsic Thermodynamics of Inhibitor Binding to Carbonic Anhydrases. in *Carbonic Anhydrase as Drug Target: Thermodynamics and Structure of Inhibitor Binding* (ed. Matulis, D.) 107–123 (Springer International Publishing, 2019).
94. Chance, B. The reactions of catalase in the presence of the notatin system. *Biochem J* **46**, 387–402 (1950).
95. Heck, R. W. *et al.* Structure-Based Design of an Intramolecular Proton Transfer Site in Murine Carbonic Anhydrase V. *Biochemistry* **35**, 11605–11611 (1996).
96. Hurt, J. D., Tu, C., Laipis, P. J. & Silverman, D. N. Catalytic Properties of Murine Carbonic Anhydrase IV. *J Bio Chem* **272**, 13512–13518 (1997).
97. Jewell, D. A. *et al.* Enhancement of the catalytic properties of human carbonic anhydrase III by site-directed mutagenesis. *Biochemistry* **30**, 1484–1490 (1991).

98. Kernohan, J. A method for studying the kinetics of the inhibition of carbonic anhydrase by sulphonamides. *Biochim Biophys Acta (BBA)-Enzymol Biol Oxid* **118**, 405–412 (1966).
99. Smirnovienė, J., Smirnovas, V. & Matulis, D. Picomolar inhibitors of carbonic anhydrase: Importance of inhibition and binding assays. *Anal Biochem* **522**, 61–72 (2017).
100. Gibbons, B. H. & Edsall, J. T. Kinetic Studies of Human Carbonic Anhydrases B and C. *J Biol Chem* **239**, 2539–2544 (1964).
101. Gibbons, B. H. & Edsall, J. T. Rate of hydration of carbon dioxide and dehydration of carbonic acid at 25 degrees. *J Biol Chem* **238**, 3502–3507 (1963).
102. Kernohan, J. The pH-activity curve of bovine carbonic anhydrase and its relationship to the inhibition of the enzyme by anions. *Biochim Biophys Acta (BBA)-Enzymol Biol Oxid* **96**, 304–317 (1965).
103. La Regina, G. *et al.* Discovery of 1,1′-Biphenyl-4-sulfonamides as a New Class of Potent and Selective Carbonic Anhydrase XIV Inhibitors. *J Med Chem* **58**, 8564–8572 (2015).
104. Hill, A. V. The possible effects of the aggregation of the molecules of hæmoglobin on its dissociation curves. *Physiol J* **40**, i–vii (1910).
105. Morrison, J. F. Kinetics of the reversible inhibition of enzyme-catalysed reactions by tight-binding inhibitors. *Biochim BiophysActa (BBA) - Enzymol* **185**, 269–286 (1969).
106. Balandis, B. *et al.* Synthesis and structure–affinity relationship of chlorinated pyrrolidinone-bearing benzenesulfonamides as human carbonic anhydrase inhibitors. *Bioorg Chem* **97**, 103658 (2020).
107. Čapkauskaitė, E. *et al.* Benzimidazole design, synthesis, and docking to build selective carbonic anhydrase VA inhibitors. *Bioorg & Med Chem* **26**, 675–687 (2018).
108. Čapkauskaitė, E. *et al.* Thiazole-substituted benzenesulfonamides as inhibitors of 12 human carbonic anhydrases. *Bioorg Chem* **77**, 534–541 (2018).
109. Čapkauskaitė, E. *et al.* Benzenesulfonamides with pyrimidine moiety as inhibitors of human carbonic anhydrases I, II, VI, VII, XII, and XIII. *Bioorg & Med Chem* **21**, 6937–6947 (2013).
110. Čapkauskaitė, E. *et al.* Design of [(2-pyrimidinylthio)acetyl]benzenesulfonamides as inhibitors of human carbonic anhydrases. *Eur J Med Chem* **51**, 259–270 (2012).
111. Dudutienė, V. *et al.* Isoform-Selective Enzyme Inhibitors by Exploring Pocket Size According to the Lock-and-Key Principle. *Biophys J* **119**, 1513–1524 (2020).
112. Dudutienė, V. *et al.* Functionalization of Fluorinated Benzenesulfonamides and Their Inhibitory Properties toward Carbonic Anhydrases. *ChemMedChem* **10**, 662–687 (2015).
113. Dudutienė, V. *et al.* Discovery and characterization of novel selective inhibitors of carbonic anhydrase IX. *J Med Chem* **57**, 9435–9446 (2014).

114. Dudutienė, V. *et al.* 4-Substituted-2,3,5,6-tetrafluorobenzenesulfonamides as inhibitors of carbonic anhydrases I, II, VII, XII, and XIII. *Bioorg Med Chem* **21**, 2093–2106 (2013).
115. Kazokaitė, J. *et al.* Novel fluorinated carbonic anhydrase IX inhibitors reduce hypoxia-induced acidification and clonogenic survival of cancer cells. *Oncotarget* **9**, (2018).
116. Zakšauskas, A. *et al.* Halogenated and di-substituted benzenesulfonamides as selective inhibitors of carbonic anhydrase isoforms. *Eur J Med Chem* **185**, 111825 (2020).
117. Zakšauskas, A. *et al.* Design of two-tail compounds with rotationally fixed benzenesulfonamide ring as inhibitors of carbonic anhydrases. *Eur J Med Chem* **156**, 61–78 (2018).
118. Zubrienė, A. *et al.* Benzenesulfonamides with benzimidazole moieties as inhibitors of carbonic anhydrases I, II, VII, XII and XIII. *J Enz Inh Med Chem* **29**, 124–131 (2014).
119. Baranauskienė, L. *et al.* Inhibition and binding studies of carbonic anhydrase isozymes I, II and IX with benzimidazo[1,2-c][1,2,3]thiadiazole-7-sulphonamides. *J Enzyme Inhib Med Chem* **25**, 863–870 (2010).
120. Baranauskienė, L. & Matulis, D. Intrinsic thermodynamics of ethoxzolamide inhibitor binding to human carbonic anhydrase XIII. *BMC biophys* **5**, 12 (2012).
121. Juozapaitienė, V. *et al.* Purification, enzymatic activity and inhibitor discovery for recombinant human carbonic anhydrase XIV. *J Biotechnol* **240**, 31–42 (2016).
122. Pilipuitytė, V. & Matulis, D. Intrinsic thermodynamics of trifluoromethanesulfonamide and ethoxzolamide binding to human carbonic anhydrase VII: thermodynamics of TFS and EZA binding to CA VII. *J Mol Recog* **28**, 166–172 (2015).
123. Fink, A. L. & Meehan, P. Detection and accumulation of tetrahedral intermediates in elastase catalysis. *Proc Natl Acad Sci U S A* **76**, 1566–1569 (1979).
124. Zhao, P., Geyer, R. R. & Boron, W. F. A Novel Stopped-Flow Assay for Quantitating Carbonic-Anhydrase Activity and Assessing Red-Blood-Cell Hemolysis. *Front Physiol* **8**, (2017).
125. Strelow, J. *et al.* Mechanism of Action Assays for Enzymes. in *Assay Guidance Manual* (eds. Sittampalam, G. S. et al.) (Eli Lilly & Company and the National Center for Advancing Translational Sciences, 2004).
126. Bozdag, M. *et al.* Combining the tail and the ring approaches for obtaining potent and isoform-selective carbonic anhydrase inhibitors: Solution and X-ray crystallographic studies. *Bioorg & Med Chem* **22**, 334–340 (2014).
127. Ghorab, M. M., Alsaid, M. S., Ceruso, M., Nissan, Y. M. & Supuran, C. T. Carbonic anhydrase inhibitors: Synthesis, molecular docking, cytotoxic and inhibition of the human carbonic anhydrase isoforms I, II,

IX, XII with novel benzenesulfonamides incorporating pyrrole, pyrrolopyrimidine and fused pyrrolopyrimidine moieties. *Bioorg & Med Chem* **22**, 3684–3695 (2014).
128. Wiseman, T., Williston, S., Brandts, J. F. & Lin, L. N. Rapid Measurement of Binding Constants and Heats of Binding Using a New Titration Calorimeter. *Anal Biochem* **179**, 131–137 (1989).
129. Zubrienė, A. *et al.* Intrinsic Thermodynamics and Structures of 2,4- and 3,4-Substituted Fluorinated Benzenesulfonamides Binding to Carbonic Anhydrases. *ChemMedChem* **12**, 161–176 (2017).
130. Bhatt, A. *et al.* Structure-Activity Relationships of Benzenesulfonamide-Based Inhibitors towards Carbonic Anhydrase Isoform Specificity. *ChemBioChem* **18**, 213–222 (2017).
131. Leitans, J. *et al.* Efficient Expression and Crystallization System of Cancer-Associated Carbonic Anhydrase Isoform IX. *J Med Chem* **58**, 9004–9009 (2015).
132. Ruangchan, N., Tongsook, C., Sucharitakul, J. & Chaiyen, P. pH-dependent Studies Reveal an Efficient Hydroxylation Mechanism of the Oxygenase Component of p-Hydroxyphenylacetate 3-Hydroxylase. *J Biol Chem* **286**, 223–233 (2011).
133. Liu, M.-S., Gong, S., Yu, H.-H., Taylor, D. W. & Johnson, K. A. Chapter Thirteen - Kinetic characterization of Cas9 enzymes. in *Methods in Enzymology* (ed. Bailey, S.) vol. 616 289–311 (Academic Press, 2019).
134. Copeland, R. A. Evaluation of enzyme inhibitors in drug discovery: a guide for medicinal chemists and pharmacologists. (Wiley-Interscience, 2005).
135. Copeland. Evaluation of Enzyme Inhibitors in Drug Discovery a Guide for Medicinal Chemists and Pharmacologists. (John Wiley & Sons, inc., 2013).
136. Kuzmič, P. Optimal design for the dose-response screening of tight-binding enzyme inhibitors. *Analy Biochem* **419**, 117–122 (2011).
137. Krainer, G., Broecker, J., Vargas, C., Fanghänel, J. & Keller, S. Quantifying High-Affinity Binding of Hydrophobic Ligands by Isothermal Titration Calorimetry. *Anal Chem* **84**, 10715–10722 (2012).
138. Krainer, G. & Keller, S. Single-Experiment Displacement Assay for Quantifying High-Affinity Binding by Isothermal Titration Calorimetry. *Methods (San Diego, Calif.)* **76**, 116–123 (2015).
139. Garbett, N. C. & Chaires, J. B. Thermodynamic studies for drug design and screening. *Expert Opin Drug Discov* **7**, 299–314 (2012).
140. Kazlauskas, E., Petrauskas, V., Paketurytė, V. & Matulis, D. Standard operating procedure for fluorescent thermal shift assay (FTSA) for determination of protein–ligand binding and protein stability. *Eur Biophys J* **50**, 373–379 (2021).
141. Tu, C. K., Thomas, H. G., Wynns, G. C. & Silverman, D. N. Hydrolysis of 4-nitrophenyl acetate catalyzed by carbonic anhydrase III from bovine skeletal muscle. *J Biol Chem* **261**, 10100–10103 (1986).

142. Paketurytė, V. *et al.* Uncertainty in protein–ligand binding constants: asymmetric confidence intervals versus standard errors. *Eur Biophys J* **50**, 661–670 (2021).
143. Wasserstein, R. L. & Lazar, N. A. The ASA Statement on *p* -Values: Context, Process, and Purpose. *Am Stat* **70**, 129–133 (2016).
144. Boone, C. D., Pinard, M., McKenna, R. & Silverman, D. Catalytic Mechanism of α-Class Carbonic Anhydrases: CO_2 Hydration and Proton Transfer. in *Subcell Biochem* **75** 31–52 (2014).
145. Krebs, J. F. & Fierke, C. A. Determinants of catalytic activity and stability of carbonic anhydrase II as revealed by random mutagenesis. *J Biol Chem* **268**, 948–954 (1993).
146. Nishimori, I. *et al.* Carbonic anhydrase activators: the first activation study of the human secretory isoform VI with amino acids and amines. *Bioorg Med Chem* **15**, 5351–7 (2007).
147. Ren, X. & Lindskog, S. Buffer dependence of CO2 hydration catalyzed by human carbonic anhydrase I. *Biochim Biophys Acta* **1120**, 81–6 (1992).
148. Supuran, C. T. Carbonic anhydrases: novel therapeutic applications for inhibitors and activators. *Nat Rev Drug Discov* **7**, 168–181 (2008).
149. McDonald, P. C. *et al.* A Phase 1 Study of SLC-0111, a Novel Inhibitor of Carbonic Anhydrase IX, in Patients With Advanced Solid Tumors: *Am J Clin Oncol* 1 (2020)
150. Supuran, C. T. Carbonic anhydrase inhibitors: an update on experimental agents for the treatment and imaging of hypoxic tumors. *Expert Opin Investig Drugs* **0**, 1–12 (2021).
151. Pacchiano, F. *et al.* Ureido-substituted benzenesulfonamides potently inhibit carbonic anhydrase IX and show antimetastatic activity in a model of breast cancer metastasis. *J Med Chem* **54**, 1896–1902 (2011).
152. Rutkauskas, K. *et al.* 4-Amino-substituted Benzenesulfonamides as Inhibitors of Human Carbonic Anhydrases. *Molecules* **19**, 17356–17380 (2014).
153. Rutkauskas, K. *et al.* Benzenesulfonamides bearing pyrrolidinone moiety as inhibitors of carbonic anhydrase IX: synthesis and binding studies. *Med Chem Res* **26**, 235–246 (2017).
154. Jonsson, B.-H. & Liljas, A. Perspectives on the Classical Enzyme Carbonic Anhydrase and the Search for Inhibitors. *Biophys J* **119**, 1275–1280 (2020).
155. Andreucci, E. *et al.* The carbonic anhydrase IX inhibitor SLC-0111 sensitises cancer cells to conventional chemotherapy. *J Enzyme Inhib Med Chem* **34**, 117–123 (2019).
156. Peppicelli, S. *et al.* The Carbonic Anhydrase IX inhibitor SLC-0111 as emerging agent against the mesenchymal stem cell-derived pro-survival effects on melanoma cells. *J Enzyme Inhib Med Chem* **35**, 1185–1193 (2020).

157. Chahal, V., Nirwan, S. & Kakkar, R. A comparative study of the binding modes of SLC-0111 and its analogues in the hCA II and hCA IX active sites using QM/MM, molecular docking, MM-GBSA and MD approaches. *Biophys Chem* **265**, 106439 (2020).
158. Behravan, G., Jonasson, P., Jonsson, B.-H. & Lindskog, S. Structural and functional differences between carbonic anhydrase isoenzymes I and II as studied by site-directed mutagenesis. *Eur J Biochem* **198**, 589–592 (1991).
159. Genis, C. *et al.* Design of a carbonic anhydrase IX active-site mimic to screen inhibitors for possible anticancer properties. *Biochemistry* **48**, 1322–1331 (2009).
160. Pinard, M. A., Boone, C. D., Rife, B. D., Supuran, C. T. & McKenna, R. Structural study of interaction between brinzolamide and dorzolamide inhibition of human carbonic anhydrases. *Bioorg Med Chem* **21**, 7210–7215 (2013).
161. Ren, X., Jonsson, B.-H. & Lindskog, S. Some properties of site-specific mutants of human carbonic anhydrase II having active-site residues characterizing carbonic anhydrase III. *Eur J Biochem* **201**, 417–420 (1991).
162. Alterio, V. *et al.* Crystal structure of the catalytic domain of the tumor-associated human carbonic anhydrase IX. *PNAS.* **106**, 16233–16238 (2009).
163. Queen, A., Khan, P. & Hassan*, A. A. and M. I. Understanding the Role and Mechanism of Carbonic Anhydrase V in Obesity and Its Therapeutic Implications. *Curr Protein & Pept Sci* (2018).
164. Smirnovienė, J., Baranauskienė, L., Zubrienė, A. & Matulis, D. A standard operating procedure for an enzymatic activity inhibition assay. *Eur Biophys J* **50**, 345–352 (2021).
165. Kazokaitė, J. *et al.* Engineered Carbonic Anhydrase VI-Mimic Enzyme Switched the Structure and Affinities of Inhibitors. *Sci Rep* **9**, 12710 (2019).

13. COPIES OF PUBLICATIONS

European Biophysics Journal
https://doi.org/10.1007/s00249-021-01530-8

BIOPHYSICS LETTER

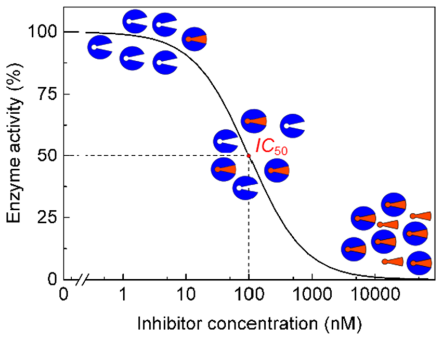
A standard operating procedure for an enzymatic activity inhibition assay

Joana Smirnovienė[1] · Lina Baranauskienė[1] · Asta Zubrienė[1] · Daumantas Matulis[1]

Received: 23 December 2020 / Revised: 12 March 2021 / Accepted: 26 March 2021
© European Biophysical Societies' Association 2021

Abstract
This Standard Operating Protocol (SOP) describes the key steps of experimental setup for an inhibition assay of enzymatic activity. The protocol begins with the design of an experiment, including the choice of a catalytic reaction, optimal conditions, fraction and concentration of the active enzyme, substrate and inhibitor concentrations and the positive and negative controls. The protocol ends with the data analysis followed by a typical example of an experiment. Despite an apparently standard procedure, the assay has a number of possible pitfalls such as low fraction of the active enzyme or errors in the analysis such as application of an improper model or incorrect determination of the inhibition constant while not recognizing the dependence on enzyme concentration. The protocol provides examples of necessary steps and controls to avoid these problems and obtain highly reliable results.

Graphic abstract



Keywords Enzyme inhibition · Tight binding · Hill equation · Morrison equation

Introduction

Enzymes are attractive molecular targets for small molecule drug discovery. Numerous enzyme inhibitors are being used as small molecule drugs to treat or prevent different diseases. Many new compounds are analyzed in laboratories worldwide for possible inhibitory properties towards new enzyme targets. Enzyme inhibition assays can be used both as primary or confirmative methods for the analysis of small molecule libraries.

Special Issue: COST Action CA15126, MOBIEU: Between atom and cell.

✉ Daumantas Matulis
matulis@ibt.lt; daumantas.matulis@bti.vu.lt

[1] Department of Biothermodynamics and Drug Design, Institute of Biotechnology, Life Sciences Center, Vilnius University, Saulėtekio 7, 10257 Vilnius, Lithuania

Published online: 16 April 2021

Biophysical binding assays usually employ universal design and observed signal, which can be directly applied for various protein–compound (ligand) systems, while enzyme activity assays are usually specific for each enzyme. A general requirement for enzyme activity measurement is to quantify either the appearance of reaction products, or decay of the substrate (Fig. 1a). Inhibition of the catalytic activity of target enzymes directly shows that a small molecule compound not only binds to it, but also alters its biological function by affecting the catalytic activity. A great variety of techniques can be used to monitor the time-dependent spectrophotometric, fluorometric, chemiluminescent, mass spectrometric (Greis 2007), calorimetric (Todd and Gomez 2001), electrochemical or other signal of the enzymatic reaction progression. Standard instruments could be applied to monitor simple slow reactions,

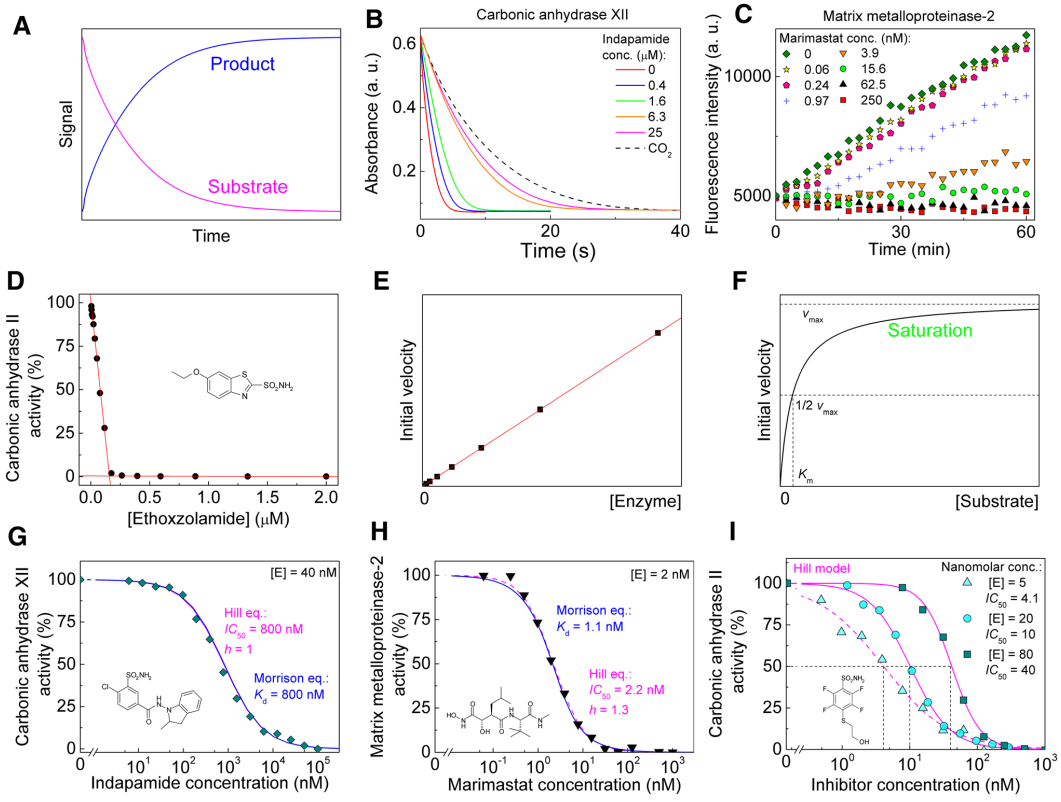


Fig. 1 Measurements of enzyme catalytic activity and its inhibition. **a** Theoretical curves showing formation of the product or consumption of the substrate over time in a catalyzed reaction. **b** Raw curves of 40 nM carbonic anhydrase XII inhibition by drug indapamide. Observed signal—absorption of pH indicator phenol red at 557 nm, occurring due to protons formed in the enzymatic or spontaneous carbon dioxide hydration reaction. The steepest curve indicates the fastest reaction. **c** Raw curves of 2 nM matrix metalloproteinase-2 inhibition by a drug inhibitor marismastat. The cleavage of fluorogenic substrate Mca–Pro–Leu–Gly–Leu–Dpa–Ala–Arg–NH_2, where Mca is 7-methoxycoumarin-4-yl-acetyl and Dpa is N-3-(2,4-dinitrophenyl)-L-α,β-diaminopropionyl by MMP-2 between Gly-Leu generates the fluorogenic product Mca-Pro-Leu-Gly, whose fluorescence is measured at 393 nm (λ_{ex} = 325 nm). **d** Example for the determination of the concentration of enzyme active sites. Here, the inhibition of carbonic anhydrase II with drug ethoxzolamide is shown. **e** Theoretical plot showing linear dependence between the catalyzed reaction rate and the enzyme concentration. **f** Theoretical Michaelis–Menten plot showing enzyme saturation with the substrate. **g** Dose–response curve of carbonic anhydrase XII inhibition with drug indapamide obtained after fitting curves such as in panel B. **h** Dosing curves of matrix metalloproteinase-2 inhibition with marismastat. **i** Dose–response curves for carbonic anhydrase II inhibition with tight-binding chemical compound VD10-13 (Dudutienė et al. 2013) at three enzyme concentrations: 5.0, 20 and 80 nM yielding different apparent IC_{50}'s: 4.1, 10 and 40 nM. These values are not representing the inhibition, but rather the concentration of the enzyme. In panels **g**, **h** and **i**, experimental data-points shown in light/dark cyan while models used for fitting are pink (Hill equation) and blue (Morrison equation) lines

but miniaturization using multi-well plate readers could save reagents and time. Following the kinetics of fast enzyme reactions requires a rapid mixing device such as the stopped-flow (Fink and Meehan 1979; Zhao et al. 2017) or quench-flow (Liu et al. 2019; Ruangchan et al. 2011) instruments.

An inhibitor can bind to an enzyme either reversibly or irreversibly (covalently). The reversible inhibition may be competitive, uncompetitive, noncompetitive or of a mixed type (Ramsay and Tipton 2017; Strelow et al. 2004). All the experimental considerations in this SOP will be provided for the simplest case of the reversible competitive 1:1 inhibition, when a single inhibitor molecule binds reversibly (non-covalently) to the active site of the enzyme and competes with the substrate. While the catalytic activity and its detection are specific for every target enzyme, there are general principles for the design of enzyme inhibition assays that we will discuss here.

The enzymatic activity inhibition assay requires an optimization process that could be cost-effectively speeded up using Fisher's Factorial, Taguchi and/or Shainin DoE (Design of Experiments) approaches instead of a OFAT (One Factor At a Time) approach (Kowang and Long 2015; Onyeogaziri and Papaneophytou 2019). DoE methodology builds a multidimensional space to read the relationships between multiple factors such as enzyme concentration, temperature, pH, salt type, salt concentration, solvent, and many others.

Target protein-small molecule binding can proceed with a wide range of affinities (Fig. 2). Different ranges of affinity may require significant differences in the design of the enzyme inhibition assay to obtain reliable results. It is very important to have more datapoints around the inhibitor concentrations range near the expected IC_{50} to enhance the data robustness.

When planning an enzyme inhibition or any other experiment, it is usually assumed that experimental factors should be statistically significant when p value is < 0.05. However, the American Statistical Association stated that "No single index should substitute for scientific reasoning" (Wasserstein and Lazar 2016). A qualified design and conduct of an experiment, proper data analysis and logical considerations lead to advanced results of the study.

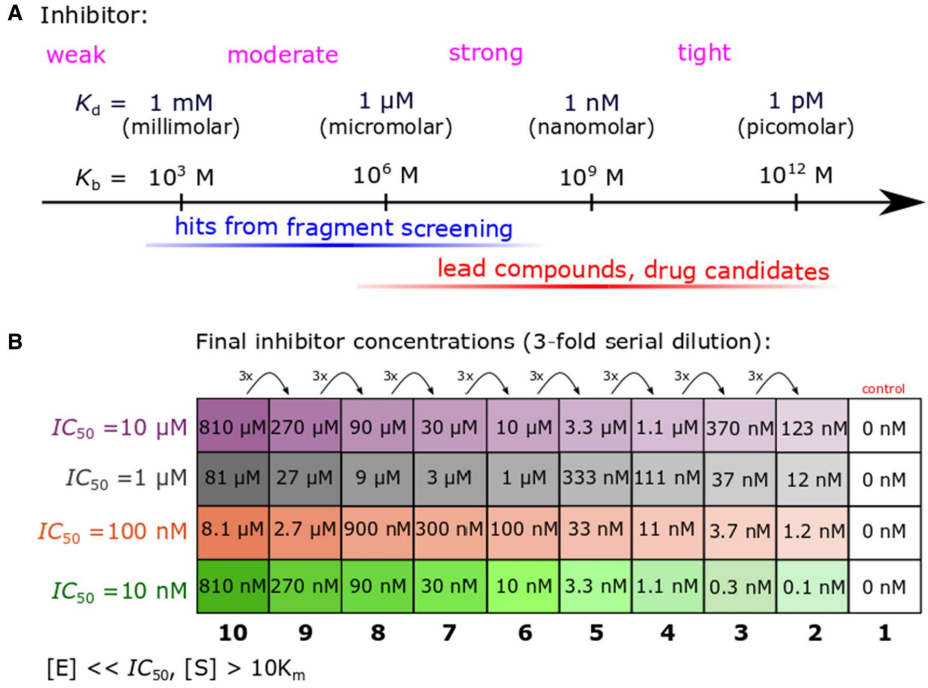


Fig. 2 Selection of inhibitor concentration range for an enzyme inhibition experiment. **a** Range of affinities between an enzyme and an inhibitor. **b** Recommended inhibitor concentrations for a given IC_{50}

Protocol

Design of experiment

- Choose a suitable assay to determine the catalytic reaction rates of the target enzyme

The rates of enzymatically catalyzed reactions could be measured by recording the appearance of the product or disappearance of the substrate over a period of time (Fig. 1a). Increasing inhibitor concentrations slow down the rates of catalytic reactions until full inhibition of the enzyme is achieved. Figure 1b and c show practical examples of the following enzymatic reactions: (I) fast consumption of carbon dioxide by carbonic anhydrase XII (Jogaitė et al. 2013) and its inhibition with the drug indapamide by following the absorbance of a pH indicator phenol red and (II) slow production of fluorogenic peptide Mca-Pro-Leu-Gly· where Mca is 7-methoxycoumarin-4-yl-acetyl by matrix metalloproteinase-2 and its inhibition with marimastat. Full inhibition of the enzyme could be detected when the reaction rate becomes equal to the rate of spontaneous reaction involving the substrate (e.g. CO_2 hydration, Fig. 1b) or the signal does not change within the time scale (Fig. 1c).

- Define optimal experimental conditions for maximal initial velocity

Determination of the inhibition constant is limited by enzyme activity and its concentration (Smirnovienė et al. 2017). For this reason, it is advisable to determine optimal conditions for the maximal catalytic efficiency of an enzyme. The main factors affecting the catalytic activity are temperature, pH, ionic strength and various other additives. Some enzymes also require specific cofactor(s) to be present in the reaction mixture to perform their catalytic functions. Suggestions would be to use the pH near the physiological value (~ 7.5), 0.05–0.2 M buffer and salt concentration with buffer pK_a value near the optimal pH of the enzyme, and choose 25, 30 or 37 °C temperature according to the stability profile of the enzyme and thermostatting possibilities (Bisswanger 2014). However, suggested conditions could be completely unsuitable for thermophilic, halophilic, or other specific enzymes and should be determined separately. Moreover, some buffer components and solvents, in which inhibitors are dissolved, could inhibit the catalytic activity of the enzyme, and should be tested before the inhibition studies with chemical compounds.

- Determine the fraction of active enzyme

Commercially available enzymes usually are provided with the characterized specific activity of the sample and can be used without validation. Target enzymes can also be purified from a natural source, or produced recombinantly. It is advisable to identify the fraction of catalytically active enzyme preparation prior to its application for the inhibition assay, since incorrect enzyme concentration can cause large errors in the determination of affinity. Catalytically active enzyme fraction can be specified by performing the active site titration using any available tight binding inhibitor and relatively high enzyme concentration: $[E]_T/K_i^{App} \geq 200$ (here $[E]_T$– total enzyme concentration, K_i^{App}—apparent inhibition constant). This can be performed either by maintaining a constant enzyme concentration $[E]_T$ and titrating the inhibitor (as in Fig. 1d) or by maintaining a constant inhibitor concentration and titrating the enzyme. Both methods are equally accurate (Copeland 2013). Alternative strategy to determine tight-binding affinity constants and enzyme concentration from a single dose–response curve has also been described (Kuzmič et al. 2000).

- Select the enzyme concentration

It is useful to determine the region of suitable enzyme concentration for the inhibition assay. The rate of a catalytic reaction should depend linearly on the enzyme concentration within a certain range (Fig. 1e). The enzyme concentration should be much lower than the substrate and inhibitor concentrations to satisfy the Michaelis–Menten conditions. If this is not possible, the measurements of apparent inhibition constants may still be practical to compare the binding affinities of different inhibitors under the same experimental conditions including the same enzyme concentration. However, it should be kept in mind that it may be impossible to accurately determine affinities of inhibitors when their affinities are much tighter than the applied enzyme concentration. For example, inhibitors possessing pM affinities cannot be determined while applying nM enzyme concentrations.

An optimal enzyme concentration for the inhibition assay should be chosen to obtain a reliable difference between the catalyzed and a spontaneous (Fig. 1b) or fully inhibited (Fig. 1c) reactions, together with the reasonable duration of the measurement. Since the enzyme concentration limits the highest affinity to be determined (Smirnovienė et al. 2017; Straus et al. 1943), it should be as low as possible to detect a wide enough window between the catalyzed and a spontaneous or 100% inhibited reaction. Figure 1i shows that the apparent half-maximal inhibitory constant IC_{50} strongly depends on the used enzyme concentration when tight binding occurs. The IC_{50} is then equal to half the enzyme concentration. Furthermore, Kuzmič et al. demonstrated that under very tight-binding conditions ($K_i^{App} = 0.1 \times [E]_0$ or $0.01 \times [E]_0$) only 10–20% error in presumed enzyme

concentration might cause more than an order of magnitude discrepancy in the apparent inhibition constant (Kuzmič et al. 2000).

- Select the substrate concentration

Enzymes act catalytically at the large excess of substrate over enzyme concentration ([S] > > [E]) (Strelow et al. 2004). Michaelis–Menten plot describes the enzymatic reaction rate dependence on the substrate concentration in a hyperbolic fashion (Fig. 1f). At the beginning, the initial velocity gradually increases as a function of substrate concentration. When the enzyme's active site becomes saturated with the substrate, the reaction rate reaches a maximum value (close to maximal initial velocity) and does not change as the substrate concentration increases further.

Enzyme inhibition experiments should be performed at a constant substrate concentration when comparing inhibitory effect of a series of small molecules. The inhibitor competes with the substrate and the inhibition constant is dependent on the substrate concentration (Holdgate et al. 2018): $IC_{50} = K_i\left(1 + \frac{[S]}{K_m}\right)$.

- Include negative and positive controls

Negative and positive controls help validate the method. Perform the assay without the substrate and without the enzyme for determination of the background. Some substrates undergo spontaneous reactions, such as carbon dioxide hydration (Fig. 1b). Rates of such spontaneous reactions must be subtracted from the catalyzed reaction rates.

- Select proper concentration range for the studied inhibitor

To determine enzyme inhibition, a series of samples with a constant enzyme and substrate concentrations and varied inhibitor concentration are prepared and an enzyme-specific assay for its catalytic activity is applied. The stock solution of an inhibitor is prepared in water or in an organic solvent such as dimethyl sulfoxide (DMSO), acetonitrile, methanol, etc. at the concentration of 10–50 mM. The final solvent concentration should be determined by simple titration for possible inhibitory effect before the measurements of IC_{50}. Widely used DMSO solvent is a highly hygroscopic liquid. Note that if DMSO solution does not get frozen in a lab refrigerator at + 4 °C, it means that it contains more than 9% water (Rasmussen and MacKenzie 1968) and should not be used for making compound stock solutions. Absorbed water molecules decrease the solubility of hydrophobic compounds and can lead to an incorrect final inhibitor concentration. Typically, a set of inhibitor concentrations is produced by a serial dilution procedure, according to the expected affinity and enzyme concentration (Fig. 2a, b). The inhibition of enzyme activity is expressed as follows:

$$\text{Inhibition } (\%) = \frac{[I]}{[I] + IC_{50}} \times 100\%,$$

where [I]—total added inhibitor concentration, IC_{50}—half maximal inhibitory concentration. The inhibitor concentrations should be chosen to cover full enzyme inhibition from 0 to 100%. We advise to design the serial dilution scheme according to these rules (as shown in Fig. 2b):

- Use a series of at least 9 inhibitor concentrations.
- Use twofold, threefold or fourfold serial dilutions to obtain the dose–response inhibition plot. Higher fold dilutions could be used only for initial rough determination of the IC_{50} range. To assay tight-binding inhibitors, twofold serial dilution is preferred or specific design of non-serial dilution scheme with smaller intervals in a lower concentration range has been proposed (Kuzmič 2011).
- The minimal inhibitor concentration should be at least tenfold lower than the expected IC_{50}.When $[I] = 0.1 \times IC_{50}$, exactly 9.1% of the enzyme activity should be inhibited:

$$\begin{aligned}\text{Inhibition } (\%) &= \frac{[I]}{[I] + IC_{50}} \times 100\% \\ &= \frac{0.1 \times IC_{50}}{0.1 \times IC_{50} + IC_{50}} \times 100\% \\ &= \frac{0.1}{1.1} \times 100\% = 9.1\%\end{aligned}$$

- The middle inhibitor concentration (well 6 in Fig. 2b) should be very close to the expected $IC_{50.}$ When $[I] = IC_{50}$, 50% of enzyme molecules are inhibited:

$$\begin{aligned}\text{Inhibition } (\%) &= \frac{IC_{50}}{IC_{50} + IC_{50}} \times 100\% \\ &= \frac{1}{2} \times 100\% = 50\%\end{aligned}$$

- The maximal inhibitor concentration should be at least tenfold higher than the determined IC_{50}. When $[I] = 10 \times IC_{50}$, exactly 91% of the enzyme activity is inhibited:

$$\begin{aligned}\text{Inhibition } (\%) &= \frac{[I]}{[I] + IC_{50}} \times 100\% \\ &= \frac{10 \times IC_{50}}{10 \times IC_{50} + IC_{50}} \times 100\% \\ &= \frac{10}{11} \times 100\% = 91\%\end{aligned}$$

It is important to choose optimal pipetting volumes when preparing serial-dilution samples. As sample size decreases, the margin of error increases. Small error of the volume in the first well plate would result in increasing the volume error in every next sample and the final concentration of the inhibitor could be misleading due to incorrect pipetting. Furthermore, the samples containing enzyme and inhibitor should be pre-incubated to form the enzyme-inhibitor complex prior to adding substrate and performing enzymatic reaction (Kuzmič 2020).

Data analysis

- Ensure data reproducibility

Experiments should be performed at least in duplicate or triplicate with independent preparations of enzyme and inhibitor batches to ensure data reproducibility. It is suggested to obtain the values of individual experiments and avoid fitting the averaged values of replicates, because it hides the information about reliability of each measurement (Tonge 2019).

- Choose an appropriate model to fit initial velocities

Usually a linear regression model is used to fit the initial velocities of enzymatic reaction. This model is suitable for slow enzymatic reactions as shown in Fig. 1c. However, for more complex reactions, such in Fig. 1b, nonlinear multi-parameter equations are required. In fast mixing experiments, some noisy data-points are sometimes observed at the beginning of a progressive curve. These data-points should not be included in the fitting or additional variables should be added to the equation used to fit the curves.

- Analyze the dose–response curves using appropriate model

The most widely used model to fit a dose response curve and determine the binding affinity is the Hill equation:

$$\text{Enzyme activity } (\%) = \left(1 - \left(\frac{1}{1 + (\frac{IC_{50}}{[I]})^h}\right)\right) \times 100\%,$$

where IC_{50}—concentration of inhibitor that achieves inhibition of half enzymatic activity, [I] – total added inhibitor concentration, and h—Hill coefficient. This coefficient may correlate with the cooperativity of interacting molecules to produce a physiological response (Weiss 1997). However, when a simple 1:1 enzyme-inhibitor binding occurs, the Hill coefficient must be 1. Interestingly, H. Prinz analyzed the NIH database and stated that in a classical enzyme inhibition assay for HSD14B4 activity less than 1% of dose–response curves (out of 5650) were fitted with a Hill coefficient of 1 (Prinz 2009). When tight-binding occurs and the enzyme concentration in an assay is higher than the apparent IC_{50}, the dose–response curve becomes steeper and could be better fitted with $h > 1$. Such curves usually provide incorrect estimations of the inhibition constants, because the enzyme concentration is not considered in the Hill equation above.

The apparent inhibition constant could also be determined using a competitive inhibition equation (Walsh 2018):

$$v = \frac{[S]}{[S] + K_M\left(1 + \frac{[I]}{K_i}\right)} v_{max}$$

However, this equation also does not take into account the concentration of active enzyme. For tight-binding inhibitors it is better to apply the quadratic Morrison equation (Kuzmič 2015; Morrison 1969; Williams and Morrison 1979), which takes into account the enzyme concentration:

$$\text{Enzyme activity } (\%) = \left(1 - \frac{([E] + [I] + K_d - \sqrt{([E] + [I] + K_d)^2 - 4[E][I]}}{2[E]}\right) \times 100\%$$

where [E]—total added concentration of active enzyme, [I] – total added inhibitor concentration, and K_d—dissociation constant.

When the applied enzyme concentration is much lower than the IC_{50} ($[E] << IC_{50}$), both models, Hill and Morrison, predict similar affinity as provided in Fig. 1g ($[E] = 40$ nM, IC_{50} or $K_d = 800$ nM). However, when the enzyme concentration is similar to IC_{50}, the analysis becomes more complex. Figure 1h shows an example, when the applied enzyme concentration is 2.0 nM, the Hill equation provides $IC_{50} = 2.2$ nM with $h = 1.3$ and the Morrison equation yields a more accurate value $K_d = 1.1$ nM.

The Hill equation does not take into account the enzyme concentration and provides incorrect IC_{50} for tight-binding inhibition. In Fig. 1i there is an example of tight-binding inhibition, when the apparent IC_{50} is equal to half enzyme concentration ($IC_{50} = [E]/2$). More detailed examination of the correlations between enzyme concentration, observed IC_{50}, and the true affinities is provided in several articles (Copeland 2005; Straus et al. 1943). Analysis of the dose–response curves should always start from considering and comparing three main parameters: [E], IC_{50} and h. If $[E] > IC_{50}$ and $h > 1$, then the Morrison equation should be used instead of the Hill equation. Alternatively, the experiment may be repeated with smaller enzyme concentration, if possible.

Example of a typical enzyme inhibition experiment

Protocol for the measurement of inhibition of matrix metalloproteinase 2 (MMP2) enzymatic activity by marimastat drug

The experiment of inhibition of MMP2 activity is performed in a total volume of 200 µL per well in black-walled, clear-bottom 96-microwell plates. Plate reader with fluorescence detection is used for the monitoring of formation of enzymatic reaction product. Raw experimental data and dose–response curves of MMP2 inhibition by marimastat drug are shown in Fig. 1c and h.

Materials:

Inhibitor: marimastat (MedChemExpress, Cat.No: HY-12169/CS-3456). Prepare 10 mM marimastat stock solution in dimethylsulfoxide (DMSO) and store the solution at −20 ºC.

Substrate: Mca–Pro–Leu–Gly–Leu–Dpa–Ala–Arg–NH_2, where Mca is 7-methoxycoumarin-4-yl)acetyl and Dpa is N-3-(2,4-dinitrophenyl)-L-α,β-diaminopropionyl (Enzo Life Sciences, Cat.No: BML-P126-0001). Prepare 1 mM stock solution in DMSO. Dispense the prepared stock peptide solution into smaller aliquots (20 or 50 µl) and store at −20 ºC.

Enzyme: recombinant human MMP-2 catalytic domain (GiottoBiotech), stock concentration 0.15 mg/ml or 8.4 µM (MW 17.9 kDa). Store the solution at −80 ºC.

Assay buffer: 50 mM TRIS (pH 7.5), 150 mM NaCl, 10 mM $CaCl_2$.

Reagent working solutions:

- Dilute 1 mM substrate solution 1:125 with assay buffer yielding 8 µM concentration of the substrate.
- Prepare 8 nM concentration of MMP2 in the assay buffer from the 8.4 µM enzyme stock solution (1050-fold dilution).
- Prepare 16 inhibitor concentrations in DMSO following a twofold serial dilution scheme, from a maximum concentration of 200 µM with the last one containing only DMSO (no inhibitor). For this, add 49 µL of DMSO and 1 µL of the 10 mM marimastat solution to the first well and mix (50-fold dilution). Then add 5 µL DMSO to all 15 following tubes.
- Transfer 5 µL of 200 µM marimastat solution from the first tube to the second one, mix, then transfer 5 µL of this mix to the third tube, and so on. After this, dilute the prepared 16 inhibitor samples with the assay buffer: mix 2 µL of each inhibitor sample prepared in DMSO with 98 µL of assay buffer (50-fold dilution). The prepared 16 inhibitor working solutions in 2% (v/v) DMSO starts from the maximum concentration of 4 µM and decreases 2-fold down to 0.24 nM.

Measuring the inhibition of MMP2 by marimastat:

1. Add 50 µL of 8 nM MMP2 solution to 16 wells.
2. Add 50 µL of each inhibitor working solution to the designated wells. Mix by shaking the plate gently.
3. Incubate at room temperature for 30 min.
4. Add 100 µL of 8 µM substrate to each well. Mix by shaking plate gently.
5. Note that final concentrations of enzyme, substrate and inhibitor are 2 nM MMP2, 4 µM substrate and 0–1 µM marimastat.
6. Monitor the hydrolysis of the substrate at 37 ºC temperature every 2.5 min for 60 min, by measuring the increase in fluorescence (Fig. 1c) with a plate reader (in this case Synergy H4) at an excitation wavelength of 325 nm and an emission wavelength of 393 nm.
7. Analyze the data to evaluate the rate of substrate hydrolysis (Fig. 1c) and to determine IC_{50} values (Fig. 1h).

Key points

- Ensure that enzyme concentration used in an assay is significantly smaller than the IC_{50};
- Ensure to achieve > 90% inhibition of enzyme catalytic activity by the studied compound;
- Ensure that the Hill coefficient $h = 1$ and the arrangement of the dosing data-points is well represented by the fitted curve.

Acknowledgements Authors acknowledge the COST project ARBRE-MOBIEU CA15126.

References

Bisswanger H (2014) Enzyme assays. Perspect Sci 1:41–55. https://doi.org/10.1016/j.pisc.2014.02.005

Copeland RA (2005) Evaluation of enzyme inhibitors in drug discovery: a guide for medicinal chemists and pharmacologists, Methods of biochemical analysis. Wiley-Interscience, Hoboken, NJ

Copeland RA (2013) Evaluation of enzyme inhibitors in drug discovery a guide for medicinal chemists and pharmacologists. John Wiley & Sons, Inc

Dudutienė V, Zubrienė A, Smirnov A, Gylytė J, Timm D, Manakova E, Gražulis S, Matulis D (2013) 4-Substituted-2,3,5,6-tetrafluorobenzenesulfonamides as inhibitors of carbonic anhydrases I, II, VII, XII, and XIII. Bioorg Med Chem 21:2093–2106. https://doi.org/10.1016/j.bmc.2013.01.008

Fink AL, Meehan P (1979) Detection and accumulation of tetrahedral intermediates in elastase catalysis. Proc Natl Acad Sci U S A 76:1566–1569. https://doi.org/10.1073/pnas.76.4.1566

Greis KD (2007) Mass spectrometry for enzyme assays and inhibitor screening: an emerging application in pharmaceutical research. Mass Spectrom Rev 26:324–339. https://doi.org/10.1002/mas.20127

Holdgate GA, Meek TD, Grimley RL (2018) Mechanistic enzymology in drug discovery: a fresh perspective. Nat Rev Drug Discov 17:115–132. https://doi.org/10.1038/nrd.2017.219

Jogaitė V, Zubrienė A, Michailovienė V, Gylytė J, Morkūnaitė V, Matulis D (2013) Characterization of human carbonic anhydrase XII stability and inhibitor binding. Bioorg Med Chem 21:1431–1436. https://doi.org/10.1016/j.bmc.2012.10.016

Kowang TO, Long CS (2015) Design of experiment—an integration of Fisher, Taguchi and Shainin DOE methodology [WWW Document]. Appl Mech Mater. https://doi.org/10.4028/www.scientific.net/AMM.789-790.1201

Kuzmič P (2011) Optimal design for the dose–response screening of tight-binding enzyme inhibitors. Anal Biochem 419:117–122. https://doi.org/10.1016/j.ab.2011.06.013

Kuzmič P (2015) History, variants and usage of the "Morrison equation" in enzyme inhibition kinetics, BioKin Technical Note TN-2015-01, Biokin Ltd., Watertown, MA [Online]. http://www.biokin.com/TN/2015/01

Kuzmič P (2020) Optimal duration of the preincubation phase in enzyme inhibition experiments. https://doi.org/10.26434/chemrxiv.12016974.v1

Kuzmič P, Elrod KC, Cregar LM, Sideris S, Rai R, Janc JW (2000) High-throughput screening of enzyme inhibitors: simultaneous determination of tight-binding inhibition constants and enzyme concentration. Anal Biochem 286:45–50. https://doi.org/10.1006/abio.2000.4685

Liu M-S, Gong S, Yu H-H, Taylor DW, Johnson KA (2019) Chapter Thirteen—Kinetic characterization of Cas9 enzymes, In: Bailey, S. (Ed.), Methods in enzymology, CRISPR-Cas Enzymes. Academic Press, pp 289–311. https://doi.org/10.1016/bs.mie.2018.10.022

Morrison JF (1969) Kinetics of the reversible inhibition of enzyme-catalysed reactions by tight-binding inhibitors. Biochim Biophys Acta 185:269–286. https://doi.org/10.1016/0005-2744(69)90420-3

Onyeogaziri FC, Papaneophytou C (2019) A general guide for the optimization of enzyme assay conditions using the design of experiments approach. SLAS Discov Adv Life Sci R D 24:587–596. https://doi.org/10.1177/2472555219830084

Prinz H (2009) Hill coefficients, dose–response curves and allosteric mechanisms. J Chem Biol 3:37–44. https://doi.org/10.1007/s12154-009-0029-3

Ramsay RR, Tipton KF (2017) Assessment of enzyme inhibition: a review with examples from the development of monoamine oxidase and cholinesterase inhibitory drugs. Mol Basel Switz. https://doi.org/10.3390/molecules22071192

Rasmussen DH, MacKenzie AP (1968) Phase diagram for the system water-dimethylsulphoxide. Nature 220:1315–1317

Ruangchan N, Tongsook C, Sucharitakul J, Chaiyen P (2011) pH-dependent studies reveal an efficient hydroxylation mechanism of the oxygenase component of p-Hydroxyphenylacetate 3-Hydroxylase. J Biol Chem 286:223–233. https://doi.org/10.1074/jbc.M110.163881

Smirnovienė J, Smirnovas V, Matulis D (2017) Picomolar inhibitors of carbonic anhydrase: importance of inhibition and binding assays. Anal Biochem 522:61–72. https://doi.org/10.1016/j.ab.2017.01.022

Straus OH, Goldstein A, With the Technical Assistance of Plachte FL (1943). Zone behavior of enzymes. J Gen Physiol 26:559–585. https://doi.org/10.1085/jgp.26.6.559

Strelow J, Dewe W, Iversen PW, Brooks HB, Radding JA, McGee J, Weidner J (2004). Mechanism of action assays for enzymes. In: Sittampalam GS, Grossman A, Brimacombe K, Arkin M, Auld D, Austin CP, Baell J, Bejcek B, Caaveiro JMM, Chung TDY, Coussens NP, Dahlin JL, Devanaryan V, Foley TL, Glicksman M, Hall MD, Haas JV, Hoare SRJ, Inglese J, Iversen Philip W, Kahl SD, Kales SC, Kirshner S, Lal-Nag M, Li Z, McGee J, McManus O, Riss T, Saradjian P, Trask OJ, Weidner JR, Wildey MJ, Xia M, Xu X (Eds.), Assay guidance manual. Eli Lilly & Company and the National Center for Advancing Translational Sciences, Bethesda, MD

Todd MJ, Gomez J (2001) Enzyme kinetics determined using calorimetry: a general assay for enzyme activity? Anal Biochem 296:179–187. https://doi.org/10.1006/abio.2001.5218

Tonge PJ (2019) Quantifying the interactions between biomolecules: guidelines for assay design and data analysis. ACS Infect Dis 5:796–808. https://doi.org/10.1021/acsinfecdis.9b00012

Walsh R (2018) Comparing enzyme activity modifier equations through the development of global data fitting templates in Excel. PeerJ 6:e6082. https://doi.org/10.7717/peerj.6082

Wasserstein RL, Lazar NA (2016) The ASA statement on p -values: context, process, and purpose. Am Stat 70:129–133. https://doi.org/10.1080/00031305.2016.1154108

Weiss JN (1997) The Hill equation revisited: uses and misuses. FASEB J 11:835–841. https://doi.org/10.1096/fasebj.11.11.9285481

Williams JW, Morrison JF (1979) [17] The kinetics of reversible tight-binding inhibition. In: Methods in enzymology, enzyme kinetics and mechanism part a initial rate and inhibitor methods. Academic Press, pp 437–467. https://doi.org/10.1016/0076-6879(79)63019-7

Zhao P, Geyer RR, Boron WF (2017) A novel stopped-flow assay for quantitating carbonic-anhydrase activity and assessing red-blood-cell hemolysis. Front Physiol. https://doi.org/10.3389/fphys.2017.00169

Publisher's Note Springer Nature remains neutral with regard to jurisdictional claims in published maps and institutional affiliations.

Analytical Biochemistry 522 (2017) 61–72

Contents lists available at ScienceDirect

Analytical Biochemistry

journal homepage: www.elsevier.com/locate/yabio

Picomolar inhibitors of carbonic anhydrase: Importance of inhibition and binding assays

Joana Smirnovienė, Vytautas Smirnovas, Daumantas Matulis*

Department of Biothermodynamics and Drug Design, Institute of Biotechnology, Life Sciences Center, Vilnius University, Saulėtekio al. 7, LT-10257 Vilnius, Lithuania

ARTICLE INFO

Article history:
Received 2 November 2016
Received in revised form
23 January 2017
Accepted 25 January 2017
Available online 31 January 2017

Keywords:
Carbonic anhydrase
Tight-binding inhibitors
Stopped-flow CO_2 hydration assay
Fluorescent thermal shift assay
Differential scanning fluorimetry
Isothermal titration calorimetry

ABSTRACT

The K_i of carbonic anhydrase (CA) inhibitors is often determined by the stopped- flow CO_2 hydration assay, the method that directly follows the inhibition of CA enzymatic activity. However, the assay has limitations, such as largely unknown concentration of CO_2 and the inability to determine the K_i below several nM. The widely used direct binding assay, isothermal titration calorimetry, also does not determine the K_d below several nM. In contrast, the thermal shift assay can accurately determine picomolar affinities.

New equations estimating CO_2 concentration were developed for the determination of k_{cat} and K_M of CA I and CA II. The inhibitor dose-response curves were analyzed using Hill and Morrison equations demonstrating that only the Morrison model is applicable for the determination of tight-binding inhibitor K_i. The measurements of interactions between ten inhibitors and seven CA isoforms showed the limitations and advantages of all three techniques. Inhibitor **6** exhibited the K_d of 50 pM and was highly selective towards human CA IX, an isoform which is nearly absent in healthy human, but highly overexpressed in numerous cancers. Combination of inhibition and binding techniques was necessary for precise determination of CA-high-affinity inhibitor interactions and future drug design.

© 2017 Elsevier Inc. All rights reserved.

1. Introduction

The carbonic anhydrases (CAs; EC 4.2.1.1) are a family of mostly zinc metalloenzymes that catalyze reversible hydration of carbon dioxide into bicarbonate and protons: $CO_2 + H_2O \Leftrightarrow HCO_3^- + H^+$. CAs are widely distributed in all kingdoms of life and are categorized in six classes: α, β, γ, δ, ζ, and η [1–5]. Only the α-CAs are found in human body. Out of 15 human CA isoforms, 12 are catalytically active and differ in their subcellular localization, distribution in organs and tissues, expression levels, kinetic properties, and inhibitor binding affinities [6,7]. Five isoforms are cytosolic (CA I, CA II, CA III, CA VII, and CA XIII), two are mitochondrial (CA VA and CA VB), one is secreted (CA VI), and four are membrane-bound (CA IV, CA IX, CA XII, and CA XIV). The CA is a highly efficient catalyst of reversible interconversion of carbon dioxide and bicarbonate ion. The rate constant of uncatalyzed reaction is 0.037 s^{-1} while CA increases the rate by approximately 10^6 times [8,9]. The catalysis proceeds via the two-step ping-pong mechanism [10–14]:

$$1.\ \text{E-Zn-OH}^- + CO_2 + H_2O \rightleftharpoons \text{E-Zn-HCO}_3^- + H_2O \rightleftharpoons \text{E-Zn-H}_2O + HCO_3^-$$

$$2.\ \text{E-Zn-H}_2O \rightleftharpoons H^+\text{-E-Zn-OH}^- + \text{Buffer} \rightleftharpoons \text{E-Zn-OH}^- + \text{BufferH}^+$$

In the first step, the active form of the enzyme (CA bearing the hydroxide bound to catalytic Zn(II) ion) catalyzes CO_2 interconversion to HCO_3^-. The resulting zinc-coordinated HCO_3^- is displaced by a water molecule leading to an acidic form of the enzyme, which is catalytically inactive. In the next step, the proton from zinc-bound water is transferred to the imidazole ring of His 64 or another base via the water molecules in the active site, the rate-limiting step [10]. The proton leaves the base for the buffer

Abbrevation: ANS, 8-anilino-1-naphthalenesulfonate; AZM, acetazolamide; CA, carbonic anhydrase; CHES, 2-(cyclohexylamino)ethanesulfonic acid; EZA, ethoxzolamide; FTSA, fluorescent thermal shift assay; HEPES, 4-(2-hydroxyethyl)piperazine-1-ethanesulfonic acid; ITC, isothermal titration calorimetry; MES, 2-(N-morpholino)ethanesulfonic acid; MOPS, 3-(N-Morpholino)-propanesulfonic acid; SFA, stopped-flow CO_2 hydration assay; SULFA, sulfanilamide; TRIS, tris(hydroxymethyl)aminomethane.

* Corresponding author.
E-mail addresses: gylyte@ibt.lt (J. Smirnovienė), vytautas@smirnovas.info, vytautas.smirnovas@bti.vu.lt (V. Smirnovas), daumantas.matulis@bti.vu.lt, matulis@ibt.lt (D. Matulis).

http://dx.doi.org/10.1016/j.ab.2017.01.022
0003-2697/© 2017 Elsevier Inc. All rights reserved.

completing the catalytic cycle.

A wide range of chemical compounds have been reported to inhibit the activity of CAs. The classical inhibitors are primary benzenesulfonamides bearing various substituents, which bind to zinc ion in a deprotonated form (RSO_2NH^-) by exchanging a water molecule. Sulfonamides have numerous clinical applications and have been used as drugs to treat glaucoma, epileptic seizures, obesity, altitude sickness, and as diuretics [6,7,15,16]. Clinically approved sulfonamides lack selectivity towards CA isoforms and result in various side effects. Recently, extensive studies have been performed in search of selective inhibitors targeting CA IX, which is a therapeutic target for cancer treatment [17–22].

Accurate and precise determination of inhibition and binding constants is an important task in drug discovery, especially in the building of structure-activity relationships. A variety of assays have been used to measure interactions between CAs and inhibitors [23]. Most common are the surface plasmon resonance spectroscopy (SPR), stopped-flow CO_2 hydration assay (SFA), isothermal titration calorimetry (ITC), and fluorescent thermal shift assay (FTSA) [24,25]. While studying CA-inhibitor interactions, it has already been shown that there is a good correlation between K_ds determined by SPR, FTSA [26], and ITC [27]. In this study we have determined the binding affinities of 7 synthetic compounds to CA I, CA II, CA VI, CA VII, CA IX, CA XII, and CA XIII by SFA, FTSA, and ITC. The binding and inhibitory properties of these compounds were compared to conventional CA inhibitors – acetazolamide (AZM), ethoxzolamide (EZA), and sulfanilamide (SULFA).

SFA is based on measuring the absorbance change of an indicator while the CA acidifies the pH. The calculation of the hydration rate of carbonic acid was first proposed by Gibbsons and Edsall [8,28] and later by Khalifah [9]. They suggested to use the buffer factor in order to correlate the absorbance change of an indicator with the activity of CA. It is usually considered that CO_2 concentration in the sample of the stopped-flow syringe is 17 mM at 25 °C [29–31]. However, some amount of gas is lost during the filling of the syringes in SFA and during the experiment. In this study we describe modified Khalifah equations [9] for the determination of $[CO_2]$ in the sample. Not only CO_2 concentration is important in the SFA, but also an appropriate model for the determination of inhibition constant. SFA as all enzymatic methods is limited by an enzyme activity and concentration (Table 1). The Hill model is very popular to fit the dose-response data, but in case of tight-binding inhibitors often lead to inaccurate results, because total concentration of an active enzyme is not considered. The Morrison equation [32,33] takes into account the total active enzyme concentration and better prognoses the affinity of tight-binding inhibitors. A number of publications discuss the Hill and Morrison equations in great details [34,35,36]. In this study we analyzed the dose-response curves using both equations and compared SFA results with FTSA and ITC data.

The FTSA, also known as the differential scanning fluorimetry (DSF) or ThermoFluor®, is quite popular in industrial and academic laboratories due to its precision, simplicity, rapidity and low amount of protein required. The protein thermal stability is measured by recording the fluorescence of a solvatochromic dye upon heat-induced protein unfolding [37–40]. Furthermore, FTSA is also effectively used in ligand binding studies since the shift in protein melting temperature upon addition of a ligand is related to the binding affinity [41,42]. FTSA is not limited in measuring the binding affinities since ligands and proteins are soluble and the melting temperatures are below water boiling temperature (Table 1).

ITC is a method that directly measures the heat absorbed or released by the reaction. In a single experiment, three thermodynamic parameters are determined, the binding constant K_b (Gibbs energy ΔG), the enthalpy ΔH, and entropy ΔS. ITC is very useful in thermodynamic studies for building the structure-thermodynamics relationships [43,44,20]. For ITC experiments, the target protein does not need to be chemically modified, labeled or immobilized [45]. However, the method is time-consuming, requires a significant amount of purified protein (~300 μg) and thus the technique is quite expensive (Table 1). Determination of the binding constant K_d by ITC is limited by the Wiseman c-factor ($c = K_b \cdot$ [Protein concentration], $1 < c < 1000$) [46]. Using 5–20 μM protein allows to measure the affinity in the micromolar to nanomolar range. For higher affinities the displacement ITC could be used [47].

Here we show the determination of the lead compound **6** [21,48,49,26], binding affinity and inhibition potency towards the anticancer CA IX. The compound is highly potent, exhibiting the K_d of 50 pM and it is difficult to determine such affinity by any technique. Only the combination of SFA, ITC, and FTSA could fully characterize interaction between **6** and CA IX, necessary for its further development as an anticancer drug candidate.

2. Materials and methods

2.1. Protein preparation

Recombinant human carbonic anhydrases were prepared as previously described: CA I - [50], CA II – [42], CA VI – [51], CA VII and CA XIII – [52], CA IX – [21], CA XII – [53]. Protein identity was confirmed by MS, purity - by SDS-PAGE, and the concentration - spectrophotometrically.

2.2. Synthesis of inhibitors

The synthesis of chemical compounds has been previously described: **1** - [54], **2**–**5** - [55], **6,7** - [21,56]. EZA, AZM, and SULFA was purchased from Sigma-Aldrich (St. Louis, MO, USA) and used without further purification. Instant JChem was used for structure database management, search and prediction, Instant JChem 6.1.3, 2013, ChemAxon (http://www.chemaxon.com).

2.3. Stopped-flow CO_2 hydration assay (SFA)

The stopped-flow CO_2 hydration assay was performed using Applied Photophysics SX.18 MV-R instrument at 25 °C. Saturated CO_2 solution was prepared by bubbling the gas into milli-Q water at room temperature for 1 h.

Table 1
Comparison of enzymatic vs biophysical assays for determination of K_d/IC_{50}, when 8 points are used in the dosing curve (FTSA and SFA).

	SFA	FTSA	ITC
Parameters	k_{cat}, K_M, IC_{50}, K_i, K_d	T_m, K_d, ΔG	ΔH, ΔG, ΔS, K_d, n
Amount of enzyme	1.2–120 μg	24–96 μg	240–3000 μg
Concentration	5–500 nM	5–20 μM	4–50 μM
Volume	8 ml	0.16 ml	2 ml
Time	~60 min	9 K_d per 90 min	60–150 min
Limitations	Enzyme activity & concentration	Water boiling temperature	Solubility of proteins, ligands & c-factor

2.3.1. The equations to determine CO_2 concentration in the sample

In this study we report a model for the determination of CO_2 concentration in the stopped-flow apparatus syringe. Catalytic activity of CAs is measured as a change in indicator absorbance per time. Hydration of CO_2 releases protons that acidify the pH. For this reason it is important to relate the absorbance of indicator with the pH of a buffer. Coefficient k relates initial fraction of indicator's deprotonated form f_{In0} with the initial pH of the sample. The k is calculated according to the initial absorbance A_0 of indicator and initial pH_0:

$$k = \frac{A_0}{f_{In_0}} = \frac{A_0}{1 - \frac{1}{10^{pH_0 - pK_{a(In)}} + 1}} \tag{1}$$

Absorbance A is being measured experimentally and is expressed as:

$$A = k \cdot f_{In} = k\left(1 - \frac{1}{10^{pH - pK_{a(In)}} + 1}\right) \tag{2}$$

The pH may be calculated from the absorbance A:

$$pH = \lg\left(\frac{A}{k - A}\right) + pK_{a(In)} \tag{3}$$

Buffer also participates in the reaction of CO_2 hydration, so concentrations of acidic and basic forms of the buffer ($[B]_{acidic}$, $[B]_{basic}$) are calculated using a Henderson-Hasselbalch equation:

$$[B]_{acidic} = \frac{[B]_{total}}{1 + 10^{pH - pK_{a(B)}}} \tag{4}$$

$$[B]_{basic} = [B]_{total} - [B]_{acidic} \tag{5}$$

where $[B]_{total}$ is the total buffer concentration. Then the equations derived by Khalifah [9] are applied. The first pH-dependent CO_2 hydration equilibrium constant $K_{a1(CO2)}$ is:

$$K_{a1(CO_2)} = \frac{[H^+]_f \left[HCO_3^-\right]_f}{[CO_2]_f + [H_2CO_3]_f} \approx \frac{[H^+]_f \left[HCO_3^-\right]_f}{[CO_2]_f} \tag{6}$$

where subscript f means equilibrium conditions at the end of the hydration reaction. The second equilibrium reaction is buffer ionization. At near neutral pH, equal amounts of HCO_3^- and H^+ are produced, and the equilibrium constant of buffer is:

$$K_{a(B)} = \frac{[H^+]_f [B]_{basic-f}}{[B]_{acidic-f}} = \frac{[H^+]_f \left([B]_{basic-0} - \left[HCO_3^-\right]_f\right)}{[B]_{acidic-0} + \left[HCO_3^-\right]_f} \tag{7}$$

where subscripts 0 and f refer to the conditions at the beginning and completion of the hydration reaction. From this equation the concentration of HCO_3^- is expressed as:

$$\left[HCO_3^-\right]_f = \frac{[H^+]_f [B]_{basic-0} - K_{a(B)} [B]_{acidic-0}}{[H^+]_f + K_{a(B)}} \tag{8}$$

At higher pH, the CO_3^{2-} ions and more than 1 proton are released. The ratio R of produced protons at high pH compared to production of protons at low pH is:

$$R = 1 - \frac{K_{a2(CO_2)}}{[H^+] + 2K_{a2(CO_2)}} \tag{9}$$

At pH > 12, two protons are produced, so this equation approaches $R = 1/2$. Concentration of HCO_3^- ions at pH > 8 is:

$$\left[HCO_3^-\right]_{pH\ >\ 8} = \frac{\left[HCO_3^-\right]_f}{R} \tag{10}$$

The concentration of HCO_3^- ions produced by spontaneous uncatalyzed reaction ($k_{CO2} = 0.037\ s^{-1}$ [8,9]) is subtracted from the total amount of $[HCO_3^-]$.

Substituting eq. (8) (at pH < 8) and eq. (10) (at pH > 8) with eq. (3–5), the production of $[HCO_3^-]$ as a function of time is obtained. The $[HCO_3^-]$ dependence on time is fitted with an exponential equation:

$$y = a\left(1 - e^{-bx}\right) + c \tag{11}$$

Despite very rapid mixing of solutions in stopped-flow apparatus, the speed is insufficient and some noise is seen at the beginning of the curve. Variable c in eq. (11) eliminates the influence of this noisy data jump. The initial velocity v_0 is expressed as the product of multiplication of a and b:

$$v_0 = ab \tag{12}$$

At acidic and neutral pH, not all CO_2 converts to HCO_3^- at equilibrium. The concentration of unconverted CO_2 is calculated while eliminating $[H^+]_f$ variable from carbon dioxide and buffer equilibrium constants in equations (6) and (7):

$$[CO_2]_f = \frac{K_{a(B)}\left([B]_{acidic-0} + \left[HCO_3^-\right]_f\right)\left[HCO_3^-\right]_f}{K_{a1(CO_2)}\left([B]_{basic-0} - \left[HCO_3^-\right]_f\right)} \tag{13}$$

Initial CO_2 concentration is equal to the sum of $[CO_2]_f$ and $[HCO_3^-]_f$:

$$[CO_2]_0 = [CO_2]_f + \left[HCO_3^-\right]_f \tag{14}$$

The described model was used to determine the initial velocity of enzymatic reaction and calculate the initial carbon dioxide concentration. The obtained data was essential for the study of CA kinetic parameters.

Graphical representation of the derived model and experimentally obtained data is shown in Fig. 1. Fig. 1A illustrates typical raw data of the stopped-flow assay – the change of bromthymol blue (BTB) absorbance in the 0–7 s timescale. The absorbance of deprotonated BTB increases in basic pH with a peak maximum at 615 nm (inset of Fig. 1A). At 615 nm, the BTB absorbance is sigmoidally dependent on pH in the range 2–12 (inset of Fig. 1B), but a linear dependence is seen in a narrow pH interval such as 1–2 pH unit. Hydration of CO_2 drops the pH up to 2 units, so coefficient k in eq. (1) is used to correlate the change of absorbance with the pH. The pH dependence on time is calculated using eq. (3) and shown in Fig. 1B. Release of HCO_3^- ions is then observed using eq. (8) (at pH < 8 or, alternatively, eq. (10), valid at pH > 8, may be used) and is represented in Fig. 1C. In the inset of Fig. 1C an enlarged view of $[HCO_3^-]$ vs. time plot shows a noisy data jump at the beginning of the reaction. The influence of this noisy data is eliminated using $+ c$ variable in the exponential fitting curve (eq. (11)). Fig. 1D shows that the rate of CO_2 hydration reaction drops in the timescale and its inset represents the noisy data jump in more clear way. Because the reaction rate is decreasing, taking initial 5–10% data points of the curve for fitting the initial velocity, as usually done in CA studies, may lead to inaccurate results. Exponential fit is much more reliable in this case.

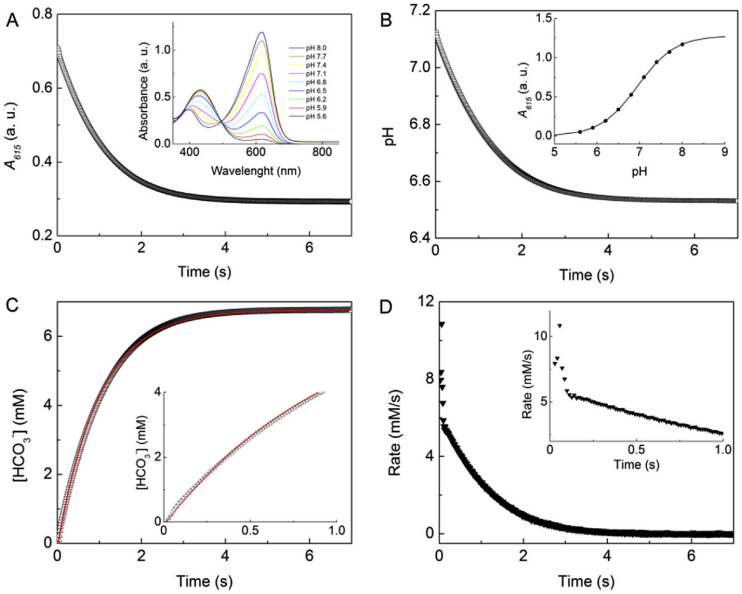


Fig. 1. Graphical representation of the model for the determination of HCO_3^- concentration in the stopped-flow syringe. The experiment was performed using 490 nM CA I, 25 mM MOPS buffer, 200 mM Na_2SO_4, 50 μM bromthymol blue (BTB, λ - 615 nm), pH 7.124, 25 °C. (A) Raw data of a typical SFA experiment - the change of BTB absorbance as a function of time. The inset shows BTB absorbance spectra in the range of pH 5.6–8.0, 20 mM phosphate buffer and 20 mM NaCl. (B) Calculated pH dependence on time using eq. (3). The inset shows a sigmoidal BTB absorbance dependence on pH. (C) The plot of HCO_3^- concentration as a function of time, obtained using eq. (8). The red line represents an exponential fit of eq. (11) for the determination of initial velocity. (D) Drop of reaction rate in the timescale. Insets of (C) and (D) show a noisy data jump at the beginning of the reaction, due to the mixing of samples in the stopped-flow apparatus. (For interpretation of the references to colour in this figure legend, the reader is referred to the web version of this article.)

2.3.2. Studies of catalytic properties

Catalytic constants k_{cat} and Michaelis constants K_M of CAs were determined in a wide pH range using 25 mM buffer and 30–300 μM indicator systems with similar pK_a values: MES (pK_a 6.1) and Bromocresol Purple (pK_a 6.4, λ - 590 nm, pH 6.0–6.4), MOPS (pK_a 7.2) and Bromothymol Blue (pK_a 7.1, λ - 615 nm, pH 6.8–7.1), HEPES (pK_a 7.5) and Phenol Red (pK_a 7.5, λ - 557 nm, pH 7.3–7.5), Tris (pK_a 8.06) and *m*-Cresol Purple (pK_a 8.3, λ - 575 nm, pH 8.0–8.4), CHES (pK_a 9.3) and Thymol Blue (pK_a 8.9, λ - 595 nm, pH 8.9–9.3), Sodium Carbonate (pK_a 10.25) and Phenolphthalein (pK_a 9.7, λ - 595 nm, pH 9.5–9.8). CA concentration was 400–600 nM for CA I and 16.6–60 nM for CA II. The ionic strength of solution was maintained at 0.2 M by the addition of sodium sulfate. Data was analyzed as described in the next subsection.

2.3.3. Determination of pK_a of CAs

Single ionization event model was used to fit the k_{cat} values and obtain the pK_a of CA II:

$$k_{cat} = \frac{k_{cat-max}}{1 + 10^{\mathrm{pH}-\mathrm{p}K_a}} \quad (15)$$

Two-site ionization model was used to fit the k_{cat} values and obtain the two pK_a values of CA I:

$$k_{cat} = \frac{k_{cat-max1}10^{-(\mathrm{pH}+\mathrm{p}K_{a1})} + k_{cat-max2}10^{-(\mathrm{p}K_{a1}+\mathrm{p}K_{a2})}}{10^{-2\mathrm{pH}} + 10^{-(\mathrm{pH}+\mathrm{p}K_{a1})} + 10^{-(\mathrm{p}K_{a1}+\mathrm{p}K_{a2})}} \quad (16)$$

2.3.4. Inhibition experiments

Inhibition experiments were performed in a sample containing the CA, 0–50 μM inhibitor, ≤0.1% DMSO, and the reaction buffer. Majority of experiments were performed using 25 mM HEPES buffer containing 200 mM Na_2SO_4, 30 μM Phenol-Red indicator (λ - 557 nm), pH 7.5. Compound **3** binding to CA II was tested using 10 mM HEPES buffer with 40 μM Bromthymol Blue (λ - 615 nm) indicator and 10 mM NaCl added, pH 7.4. The inhibition of CAs by compound **1** was tested using 25 mM MOPS buffer containing 50 μM Bromthymol Blue, 100 mM NaCl, pH 7.0. CA concentration was chosen according to its activity – 33–500 nM CA I, 5–100 nM CA II, 50 nM CA VI, 50 nM CA VII, 10–20 nM CA IX, 40–100 nM CA XII, and 23–500 nM CA XIII. Raw curves were fitted using a single exponential model and the inhibition constants were determined using Hill (eq. (17)), Cheng-Prusoff (eq. (18)) and Morrison (eq. (19)) equations.

2.3.4.1. Determination of the inhibition constants. The maximum velocity was assigned 100% CA activity. The IC_{50} was determined by fitting the dosing curve to the experimental data using the Hill equation:

$$\text{CA activity}(\%) = 1 - \frac{100}{1 + (\frac{IC_{50}}{[\mathrm{I}]})^h} \quad (17)$$

where [I] is the total added inhibitor concentration, *h* is the Hill coefficient.

The inhibition constant K_i was calculated from the IC_{50} using the Cheng-Prusoff [57] equation:

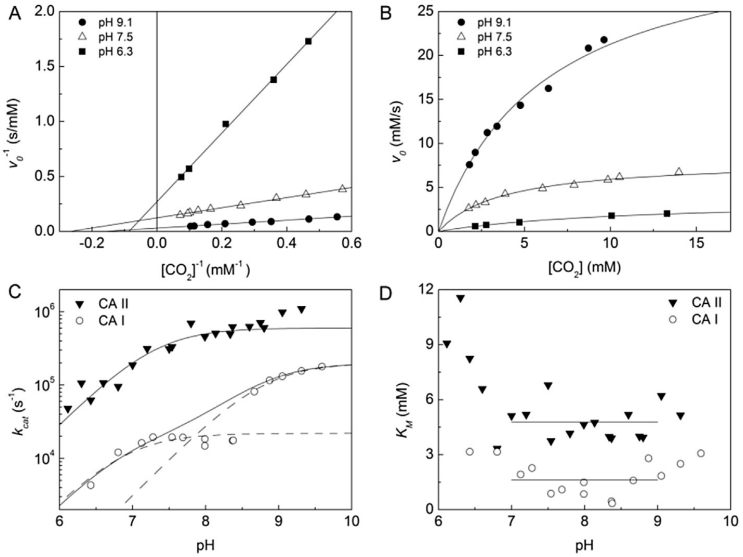


Fig. 2. Determination of the kinetic parameters of CA I and CA II at 25 °C. (A) The Lineweaver-Burk plot for the experiment using 35 nM CA II at pH 6.3 (■), 7.5 (△), and 9.1 (●). (B) Michaelis-Menten plot using the same data points and fitting parameters as in (A). (C) The k_{cat} dependence on pH for CA I (○) and CA II (▼). Dots represent the experimental values and the solid lines were fit using eq. (16) for CA I and eq. (15) to CA II. The dashed lines represent the single-ionization event model fit using eq. (15) (D) The plot of K_M versus pH for CA I (○) and CA II (▼). In the pH range 7.0–9.0, the K_M is approximately independent of pH.

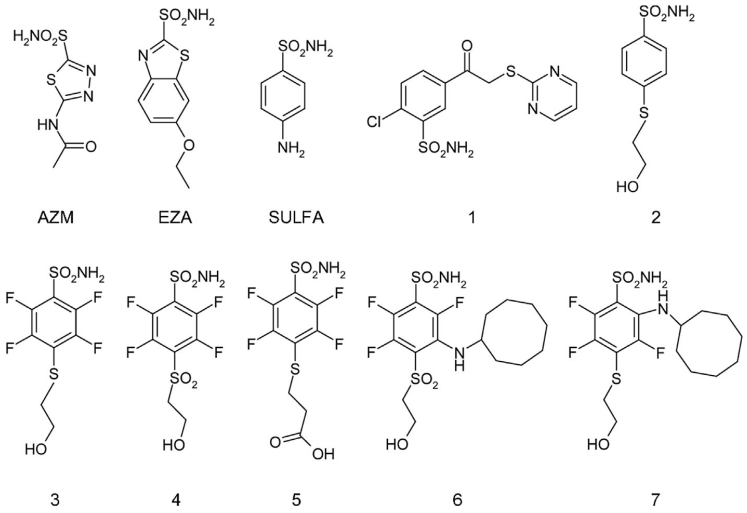


Fig. 3. Chemical structures of compounds used in this manuscript.

$$K_i = \frac{IC_{50}}{1 + \left(\frac{[CO_2]}{K_M}\right)} \quad (18)$$

where $[CO_2]$ is carbon dioxide concentration determined using the model described above and K_M is the Michaelis constant.

For comparison, the Morrison equation [32,33] was used that takes into account the CA concentration:

$$\text{CA act.}(\%) = \left(1 - \frac{([\text{CA}] + [\text{I}] + K_d) - \sqrt{([\text{CA}] + [\text{I}] + K_d)^2 - 4[\text{CA}][\text{I}]}}{2[\text{CA}]}\right) 100\% \quad (19)$$

Table 2
Binding and inhibition of CAs by SFA (pH 7.0–7.5, 25 °C), FTSA, and ITC (pH 7.0, 37 °C). The K_M values were 1.4 mM (CA I), 4.7 mM (CA II), 6.9 mM (CA VI), 11.4 mM (CA VII), 6.9 mM (CA IX), 12.0 mM (CA XII), and 13.8 mM (CA XIII) [6] except CA I, CA II. Values are shown in regular font when the results match among all three methods, in bold to point the most reliable result when significant differences are observed, and in italic to emphasize methodologically unreliable results.

Inhibitor	CA	SFA						FTSA	ITC
		[CA] (nM)	[CO_2] (mM)	*h* coef.	IC_{50-SFA} (nM) Hill	K_{i-SFA} (nM) Hill + Cheng-Prusoff	K_{d-SFA} (nM) Morrison	K_{d-FTSA} (nM) [CA] = 5–10 μM	K_{d-ITC} (nM) [CA] = 4–10 μM
AZM[a]	CA I	300	11	1	400	45	290	1400	810
	CA II	12.5	14	1.3	14	4.6	10	38	46
		50	13	1.1	*≤35*	*≤9.2*	**10**	38	46
		100	16	2	*≤50*	*≤12*	10	38	46
	CA IX	20	12	1.3	18	6.4	6.7	20	22
	CA XII	40	9.9	1.4	45	25	25	130	130
	CA XIII	100	7.9	2	*≤60*	*≤38*	*≤10*	**50**	60
EZA	CA VI[b]	50	13	1	55	19	40	33	53
	CA XIII[c]	200	15	2	*≤100*	*≤48*	**17**	13	*≤10*
SULFA[d]	CA VII	50	14	1	40000	17900	40000	50000	ND
	CA XII	50	14	1	3800	1760	3800	67000	ND
1[e]	CA I	500	8.6	1	5550	780	5550	3100	2300
	CA II	20	8.9	1	220	76	220	330	430
	CA VII	50	7.3	1	830	470	830	710	660
	CA XII	100	8.6	1	1100	640	1100	1300	370
	CA XIII	500	11	1	450	250	250	330	270
2[f]	CA I	230	17	1	250	19	125	200	790
	CA II	20	21	1	60	11	44	130	330
	CA XII	40	13	1	3000	1420	3000	2500	1500
	CA XIII	310	14	1	1000	500	1000	1400	1000
3[a]	CA I	300	12	2	*≤150*	*≤15*	*≤20*	**0.11**	*≤10*
	CA II	5.0	16	0.9	4.1	0.9	*≤5*	**6.7**	*≤10*
		20	20	1.5	*≤10*	*≤1.9*	*≤5*	6.7	*≤10*
		80	14	2.1	*≤40*	*≤10*	*≤5*	6.7	*≤10*
	CA IX	10	11	1	35	14	25	32	57
	CA XII	40	11	1	110	58	110	220	94
	CA XIII	100	12	2	*≤50*	*≤26*	*≤10*	**8.3**	18
4[f]	CA II	9.5	23	1	*≤4*	*≤0.7*	**1.0**	17	*≤12*
	CA XII	85	23	1	120	41	83	250	143
	CA XIII	23	22	2	*≤10*	*≤3.9*	*≤1*	**29**	74
5[i]	CA I	33	16	1.1	*≤12*	*≤0.9*	*≤2*	**0.4**	*≤12*
		100	11	1.5	*≤50*	*≤5.5*	*≤10*	0.4	*≤12*
		300	11	2	*≤150*	*≤17*	*≤20*	0.4	*≤12*
6[a]	CA I	300	14	1	700	65	560	710	1100
	CA II	20	14	1	29	7.4	29	60	59
	CA IX	10	14	3	*≤5*	*≤1.7*	*≤10*	**0.05**	*≤10*
		20	17	3	*≤10*	*≤2.9*	*≤10*	0.05	*≤10*
	CA XII	40	10	2	*≤20*	*≤11*	*≤10*	**3.3**	20
	CA XIII	54	9.7	2	*≤25*	*≤15*	*≤10*	**3.6**	42
7[a]	CA I	500	13	1	46000	4500	46000	50000	*≥10000*
	CA II	40	13	1	910	240	910	1300	730
	CA IX	20	10	2	*≤13*	*≤5.2*	*≤5.0*	**1.1**	15
	CA XII	40	12	1	170	86	170	330	230
	CA XIII	150	14	1.3	180	90	130	140	420

SFA, FTSA, ITC data from [a] – [21], [b] – [59], [e] – [43]; FTSA, ITC data from [c] – [60], [f] – [55]; FTSA data from [d] – [61], [i] – [55]; ND - not determined; the standard error of K_d measurements is ±2 times [24], [62].

Where [CA] is the total concentration of the active CA molecules, [I] is the total added inhibitor concentration, and K_d is the apparent inhibition constant equal to the protein–ligand dissociation constant under assumption of one inhibitor binding to one protein molecule. A dose-response curve was fitted using fixed enzyme concentration and assuming that the total CA concentration is equal to the active CA concentration.

2.4. Fluorescent thermal shift assay (FTSA)

During a FTSA experiment, the protein melting temperature is determined by following the fluorescence of 8-anilino-1-naphthalene sulfonate (ANS), an extrinsic probe of hydrophobic surfaces in proteins, as a function of temperature. Addition of an inhibitor shifts the melting temperature in a concentration-

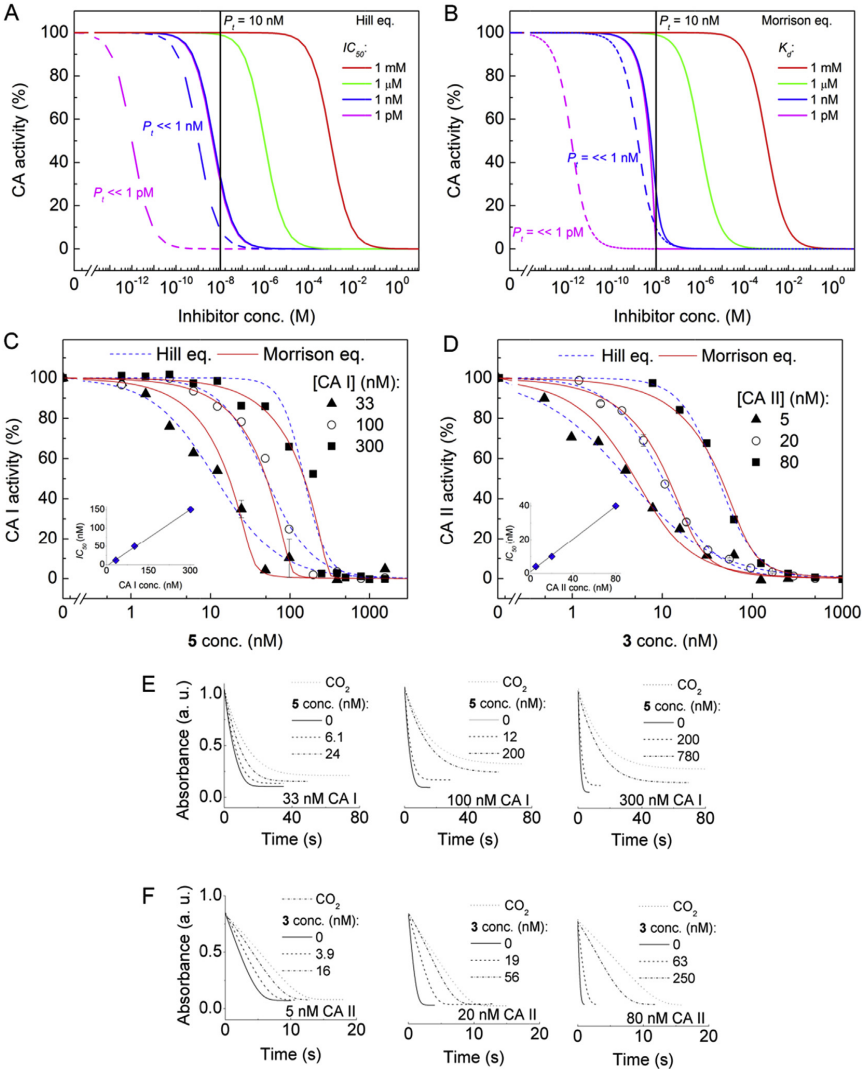


Fig. 4. Theoretical and experimental dosing curves by SFA. (A, B) Modeling of Hill (A) and Morrison (B) equations when the protein concentration P_t is 10 nM and the apparent IC_{50} are 1 mM, 1 μM, 1 nM, and 1 pM (red, green, blue, pink solid lines). The P_t should be reduced to less than 1 nM or 1 pM to obtain reliable dosing curves (dashed blue and pink lines) of nanomolar or picomolar affinity. (C, D) Experimental data of interactions between CA I-**5** and CA II-**3** at several CA concentrations. Data points were fitted to the Hill (blue dashed line) and Morrison (red solid line) equations. The insets show linear apparent IC_{50} dependence on CA concentration and the intercept of *y*-axis should be the true IC_{50}. (E, F) Raw data of CA I-**5** and CA II-**3** pairs. (For interpretation of the references to colour in this figure legend, the reader is referred to the web version of this article.)

dependent manner that is fit to an equation [41,42] and the affinity is determined. FTSA experiments were performed using a Corbett Rotor-Gene 6000 (QIAGEN Rotor-Gene Q) instrument (excitation 365 ± 20, detection 460 ± 15 nm). Samples consisted of 5–10 μM CA, 0–200 μM inhibitor, 2% DMSO, 50 μM ANS, and 50 mM sodium phosphate buffer (pH 7.0) containing 100 mM NaCl. The samples were heated from 25 to 99 °C with a heating rate of 1/min. Protein unfolding profiles and the melting temperatures were determined at each inhibitor concentration while recording extrinsic fluorescence of ANS. Data was analyzed as previously described [41,50].

2.5. Isothermal titration calorimetry (ITC)

ITC experiments were performed using VP-ITC instrument (Microcal, Inc., Northampton, USA) with 4–10 μM CA in the cell and 40–100 μM of the inhibitor in the syringe at 37 °C. The buffer contained 50 mM sodium phosphate (pH 7.0) and 100 mM NaCl. Final DMSO concentration was 2% in the cell and the syringe. The protein stock solution was dialyzed against the reaction buffer before the ITC experiment. A typical experiment consisted of 25 injections (10 μl each, except initial injection of 3 μl) added at 3 min

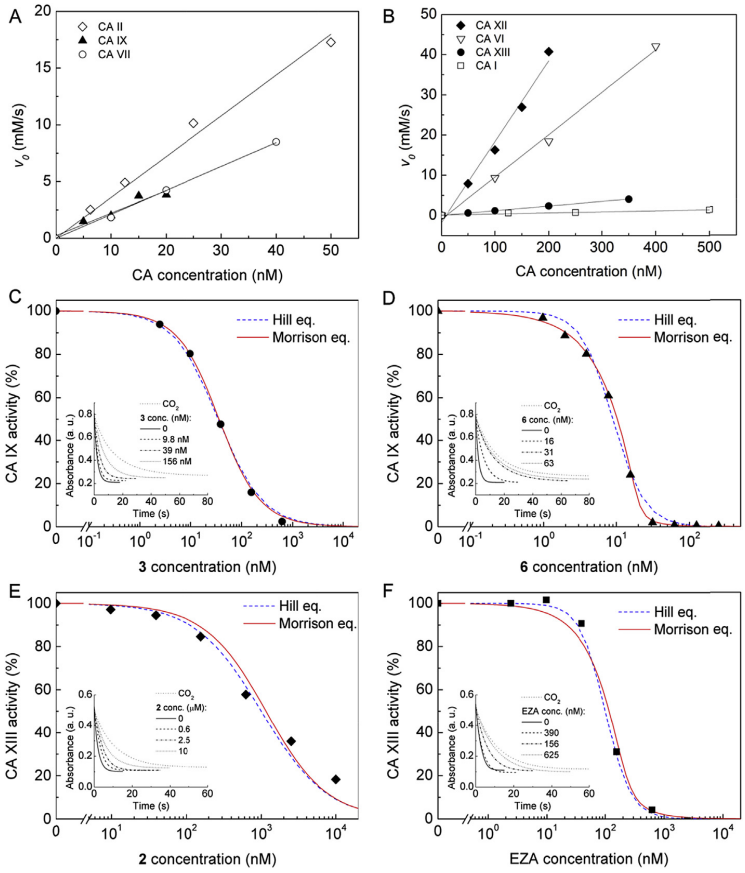


Fig. 5. Relative activity of used CAs and several examples of SFA dose-response curves fitted with the Hill (eq. (17), dashed blue lines) and Morrison (eq. (19), straight red lines) equations. (A, B) Initial velocity dependence on CA concentration at constant CO_2 concentration. Data points represent different CA: CA I (□), CA II (◇), CA VI (▽), CA VII (○), CA IX (▲), CA XII (◆), and CA XIII (●), the straight lines are linear fits. CA II, VII, and CA IX are much more active than CA I, VI, CA XII, and CA XIII. (C, E) Typical SFA dosing curves when [CA]<IC_{50} and the Hill coefficient $h = 1$. (D, F) Examples of tight-binding when [CA]>IC_{50} and $h > 1$. The used CA IX, CA XIII and CO_2 concentrations, observed IC_{50}/K_d and fitting parameters are listed in Table 2. (For interpretation of the references to colour in this figure legend, the reader is referred to the web version of this article.)

intervals. The pre-titration delay was set to 200–600 s, the reference power - 4 μcal s^{-1} and the stirring rate - 260 rpm. Data analysis was performed using MicroCal Origin software. The first point of integrated data was removed and the thermodynamic parameters of binding were estimated by fitting the data with the single binding site model.

3. Results

3.1. Determination of CA activity: k_{cat}, K_M, and pK_a

Using the model described in the methods part for the determination of [CO_2] in the sample, the catalytic activity of CA I and CA II was measured in a wide pH interval. At the highest dissolved CO_2 concentration at room temperature, the CAs are not fully saturated with the substrate and reach only 60% of its maximal activity compared to the saturated enzyme [29]. Therefore, the Lineweaver-Burk coordinates were used to obtain the maximal velocity v_{max} and the Michaelis constants K_M (Fig. 2A). To confirm these parameters, the Michaelis-Menten plot was constructed using the same fitting parameters (Fig. 2B). The catalytic constant k_{cat} of CA I and CA II increases at increasing pH and reaches maximum values of $k_{cat} = 2 \cdot 10^5$ s^{-1} for CA I and $k_{cat} = 6 \cdot 10^5$ s^{-1} for CA II (Fig. 2C). For CA II, the single-ionization model yielded the pK_a value of 7.3 ± 0.2. However, two ionizable groups in the active site of CA I were observed yielding the pK_a values of 6.9 ± 0.1 and 8.8 ± 0.1. Fig. 2D shows that in the pH range 7.0–9.0, the K_M values are independent of pH and are 1.4 ± 0.8 mM for CA I and 4.6 ± 1.0 mM for CA II. In the acidic and basic (pH > 9) solutions, the substrate has less affinity to CA than in neutral and slightly basic pH.

3.2. SFA, FTSA, and ITC for the determination of inhibition and binding

Inhibition and binding of acetazolamide (AZM), ethoxzolamide (EZA) and sulfanilamide (SULFA) and compounds **1**–**7**, structures

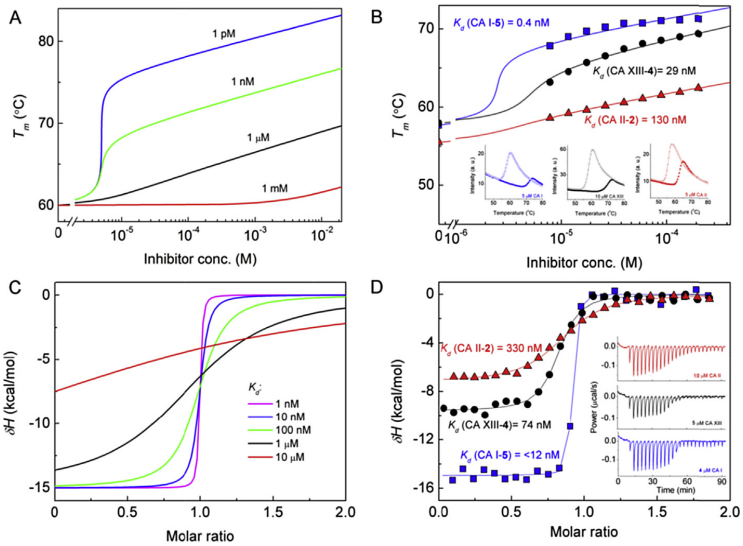


Fig. 6. Theoretical and experimental dosing curves obtained by FTSA and ITC. (A) Simulated FTSA dosing curves according to previously published equations in [41,42] for weak to strong binding affinity: 1 mM (red line), 1 μM (black line), 1 nM (green line), and 1 pM (blue line). The curves were drawn for a hypothetical but common situation when the temperature is 37 °C, protein concentration is 10 μM, enthalpy of unfolding is 690 kJ/mol, heat capacity of unfolding is 17 kJ/(molK), enthalpy of binding is −42 kJ/mol, heat capacity of binding is −0.8 kJ/(molK), and the reference melting temperature T_m without added ligand is 60 °C. (B) Experimental FTSA data of CA I-**5** (■), CA II-**2** (▲), CA XIII-**5** (●) pairs. The insets show CA unfolding curves at 0 and 200 μM inhibitor concentrations. (C) Simulated ITC curves using single binding site model of weak to strong binding affinity: 10 μM (red line), 1 μM (black line), 100 nM (green line), 10 nM (blue line), and 1 nM (pink line) when the protein concentration is 10 μM. Red line is too flat while the pink line is too steep to determine accurate dissociation constants. (D) Experimental ITC curves of the same binding interactions as in panel B. Affinity of CA I-**5** is too strong to be determined by ITC but FTSA assay provides accurate K_d. (For interpretation of the references to colour in this figure legend, the reader is referred to the web version of this article.)

listed in Fig. 3, to recombinant human CA I, II, VI, VII, IX, XII, and XIII was measured using SFA, FTSA, and ITC techniques.

The observed IC_{50}, K_i, and K_d are listed in Table 2. Sulfanilamide (SULFA) and compounds **1** and **2** are weak binders and weak inhibitors of CA and thus good examples when both the Hill and Morrison equations yield nearly equal inhibition constants. When $IC_{50} \gg [CA]$, the Hill coefficient $h = 1$, while $h > 1$ indicates that IC_{50} is below [CA] and should be verified by the Morrison equation or other methods. Fluorinated *para*-substituted compounds **3**–**5** are stronger inhibitors of CAs than a non-fluorinated compound **2**. Addition of fluorine atoms to the benzenesulfonamide ring lowers the pK_a value of the compound and it leads to stronger binding affinity to CAs, because sulfonamides bind to the active site in the deprotonated form. The observed K_ds of compound **3** and **5** binding to CA I are 0.1 and 0.4 nM. Substitution of cyclooctyl groups in *meta*- or *orto*- positions (compounds **6** and **7**) increases the selectivity towards CA IX. The K_d of compound **6** binding to CA IX is 50 pM and that is one the strongest known protein–small molecule interactions. The compound **7** bound to CA IX with weaker affinity, 1.1 nM, than compound **6**, but is 100–50000 times more selective for CA IX over CA isoforms I, II, XII, and XIII. *In vivo* studies have already shown low toxicity [49] and high inhibitory potency of compound **6** against hypoxic CA IX in MDA-MB-231 breast cancer cells, and intracellularly and extracellularly expressed CA IX in *Xenopus* oocytes while possessing selectivity over CA II, CA IV, and CA XII [48]. The described fluorinated compounds are more effective CA inhibitors than clinically used acetazolamide (AZM) and ethoxzolamide (EZA) because they show stronger binding affinities and selectivities towards CA I and CA IX. The observed inhibition constants K_is of CA I, II, IX, XII, XIII by AZM and CA VI by EZA are in good agreement (differ by less than 6 times) with the K_is published by Supuran group [6, 58].

Inhibitors, bearing the inhibition constant K_i that is at or below the enzyme concentration [K_i]«[E] used in the enzymatic assay are considered tight-binding inhibitors [34]. Both the Hill and Morrison models could be applied for the determination of such compound's inhibition constant as shown in Fig. 4. Panels A and B represent simulated curves using Hill and Morrison equations at fixed protein concentration $P_t = 10$ nM and several inhibition/dissociation IC_{50}/K_d constants in the range of 1 pM–1 mM. Since the enzyme concentration is not considered in the Hill equation, the observed IC_{50} would be half of the active enzyme concentration [E], in this case $IC_{50} = 5$ nM. To measure the true inhibition constant, the [E] should be reduced dramatically to 1 nM or to 1 pM. Unfortunately, it is experimentally impossible to get a reliable signal, even using such active enzymes as CAs. Another way is to perform experiments at several enzyme concentrations and extrapolate the IC_{50} to the zero [E] value. The Morrison equation allows to overcome these difficulties and obtain a more realiable K_d value in a single experiment. This equation takes into account the active enzyme concentration and yields the K_d quite well and irrespective of used [E] as shown in Table 2.

Several interactions between tight-binding inhibitors and CA isoforms were measured at three CA concentrations as shown in Fig. 4C and D. For the CA II-**3** pair, the IC_{50} fitted with the Hill equation and extrapolated to zero [CA] was 1.1 nM (inset of Fig. 4C), and Morrison equation yielded the K_d - 0.4 nM. The FTSA and ITC methods confirmed the constant to be 0.4 nM and ≤10 nM, respectively. For the CA I-**5** interaction, the extrapolation of IC_{50} to zero [CA] was impossible because CA I is less active than CA II (Figs. 2C, 5A and 5B) and a large concentration of CA I was used to detect a reasonable signal. For reliable determination of inhibition

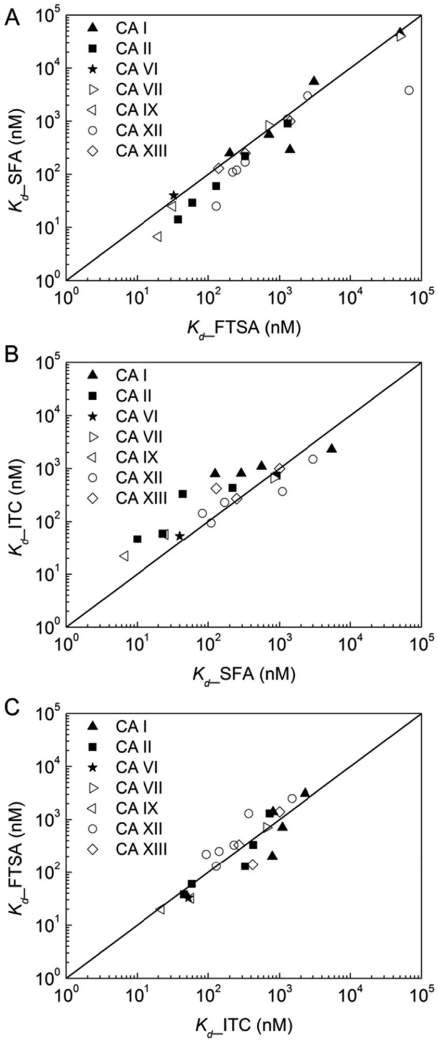


Fig. 7. Comparison of the K_d values determined by SFA, FTSA, and ITC for CA-inhibitor interactions when ITC observed K_ds are not limited by the Wiseman *c*-factor and are more than 12 nM. Data points represent different CAs: CA I (▲), CA II (■), CA VI (★), CA VII (▷), CA IX (◁), CA XII (○), and CA XIII (◇), and the straight line shows where the perfect match between K_d values would line. The K_ds observed by FTSA and SFA or ITC and SFA slightly differ because of used pH values (pH 7.0 in FTSA/ITC and pH 7.5 in SFA) and temperature (37 °C in FTSA/ITC and 25 °C in SFA). The error of K_d measurements is ±2 times [24,62].

constant, the [E]/IC_{50} ratio should be less than 50 [36]. However, the observed K_d by SFA method and Morrison equation was ≤5 nM and K_ds by FTSA and ITC assays were 6.7 nM and ≤10 nM. Raw data of both interactions between CA I-**5** and CA II-**3** are shown in Fig. 5E and F. Increase of CA concentration gives a wider window between CA catalyzed and a spontaneous CO_2 hydration reactions and leads to a better quality data. Using too small concentrations of CA is not recommended because it decreases the signal-to-noise ratio dramatically. First, the catalytic activity of each CA isoform should be determined to choose appropriate CA concentration for the inhibition experiments. Relative catalytic activities of used CA isoforms are shown in Fig. 5A and B and are arranged in the order of a decreasing catalytic activity: CA II, CA IX, CA VII, CA XII, CA VI, CA XIII, and CA I. A rather similar order of catalytic activities has been published by Supuran [6, 63]. Several examples of weak and strong inhibitor binding to catalytically highly efficient CA IX and having low catalytic activity CA XIII are shown in Fig. 5C–F. To detect a reliable signal and get a wide window between the catalyzed and a spontaneous CO_2 hydration reactions in the raw data, an enzyme concentration should be 10–20 nM for CA IX and as much as 50–300 nM for less active CA XIII. The enzyme activity and concentration limits the determination of a tight-binding compound inhibition constant. In the search for selective sub-nanomolar inhibitors for low catalytic activity CA isoforms such as CA I and CA XIII, other methods than enzymatic should be applied.

4. Discussion

The observed kinetic parameters of CA I and CA II are consistent with the results published by other scientific groups. The determined k_{cat} values compare reasonably well to the previously published k_{cat} values ranging 2.0–2.2 $\cdot 10^5$ s^{-1} for CA I and 0.8–1.4 $\cdot 10^6$ s^{-1} for CA II [6,9,10,64,65]. In addition, previously reported pK_a values of a proton shuttle His 64 in CA II were 6.8 by 4-nitrophenyl acetate hydrolysis [66], 6.8 by ^{18}O-mass spectrometry [65,67] and 7.1 by NMR [68]. The pK_a of zinc-bound water molecule in CA II was determined to be 7.1 by FTSA/ITC [69] and 7.0 by ^{18}O-mass spectrometry [67]. As in this study, complex kinetic patterns of CO_2 hydration by human CA I have been observed by Ren [64]. Futhermore, multiple proton-transfer pathways were also observed in murine CA IV [70], murine CA V [71], and murine CA VII [72]. Earnhardt et al. [72] assigned one pK_a to the zinc-bound water and another pK_a to His 64. In case of CA I the pK_a for the catalytic group was observed to be about 6.9 by NMR [73], 7.1 by 4-nitrophenyl acetate hydrolysis [74], and pK_a of zinc-bound water was determined to be 8.4 by FTSA/ITC methods [69]. Therefore, we interpret our SFA data and assign the pK_a value of 6.9 to His 64 and pK_a value of 8.8 to zinc-bound water molecule. The observed K_M dependence on pH is in agreement with the results obtained by Gibbons and Edsall [28] where at increasing pH (6.3, 7.05, 7.55) the K_M values decreased: 6.5, 2.6, and 1.0 mM for CA I and 18, 14, and 9.3 mM for CA II. However, it was later proposed that Michaelis constant of CAs is independent of pH and is 4.0 mM for CA I and 9.0–9.3 mM for CA II [6,9]. However, the K_M versus pH plots or tables in the literature are rather limited. Differences between the observed k_{cat}, K_M, and pK_a values for CA I and CA II as compared to previous works most likely arise from the uncertain CO_2 concentration in the previous studies. In this study, the model for the determination of CO_2 concentration in the sample was developed and the k_{cat} and K_M of CA I and CA II were obtained under well-characterized CO_2 concentration.

For binding studies we recommend to use FTSA since it has no limitations for determination of binding affinity and it is possible to measure the K_d from 1 pM to 1 mM in a single experiment without much adjustment of the protein concentration (Fig. 6A). ITC is also a method of choice to measure CA-ligand interactions, but observed affinities should fall in the nanomolar to micromolar range. Fig. 6C illustrates that K_d = 10 μM is too low to be observed by ITC and there is no significant difference between K_d = 1 nM and K_d = 10 nM to be determined experimentally. In Fig. 6B and D, the experimental dosing curves of several nanomolar and sub-nanomolar inhibitor binding to CA both by FTSA and ITC methods are shown. The fits match experimental data perfectly and allow to obtain the K_d values accurately. Moreover, the K_d values determined

by both FTSA and ITC methods are in good agreement. Fig. 7 illustrates the correlation between the K_ds observed by all three methods - SFA, FTSA, and ITC. The K_ds determined by SFA are a little smaller than measured by FTSA (Fig. 7A) and by ITC (Fig. 7B) but the differences are up to 5 times (except for CA XII-SULFA interaction where the difference is 18 times). The FTSA and ITC data is in better agreement and the K_ds vary up to 3 times. The reason could be due to slightly different experimental conditions. The SFA experiments were performed at pH 7.0–7.5, 25 °C, while FTSA and ITC experiments were done at pH 7.0, 37 °C.

5. Conclusions

The combined use of enzymatic and biophysical methods provides a greater precision of the protein–ligand interactions and helps to obtain the high-quality data. Despite different principles of the methods, the observed IC_{50} determined by an enzymatic stopped-flow CO_2 hydration assay correlated with the K_d obtained by biophysical fluorescent thermal shift assay and isothermal titration calorimetry within the ranges when all three methods are applied correctly. In enzymatic methods, the Morrison equation is more suitable than the Hill equation for the determination of K_d of tight-binding inhibitors. However, only the fluorescent thermal shift assay allowed to measure picomolar K_d and was essential for the development of compound **6** as a 50 pM inhibitor of CA IX, an anticancer target.

Funding

This research was funded by the Research Council of Lithuania [grant No. TAP LLT-1/2016].

Acknowledgements

We thank prof. S. Klimašauskas for providing access to the stopped-flow spectrophotometer and the COST projects CA15126, CA15135, CM1406, and CM1407.

References

[1] D. Hewett-Emmett, Evolution and distribution of the carbonic anhydrase gene families, New Horizons, Birkhäuser Basel, in: W.R. Chegwidden, N.D. Carter, Y.H. Edwards (Eds.), The Carbonic Anhydrases, 2000, pp. 29–76.
[2] J.D. Cronk, J.A. Endrizzi, M.R. Cronk, J.W. O'neill, K.Y. Zhang, Crystal structure of E. coli beta-carbonic anhydrase, an enzyme with an unusual pH-dependent activity, Protein Sci. 10 (2001) 911–922.
[3] S. Del Prete, D. Vullo, G.M. Fisher, K.T. Andrews, S.A. Poulsen, C. Capasso, C.T. Supuran, Discovery of a new family of carbonic anhydrases in the malaria pathogen Plasmodium falciparum–the η-carbonic anhydrases, Bioorg. Med. Chem. Lett. 24 (2014) 4389–4396.
[4] C.T. Supuran, C. Capasso, The η-class carbonic anhydrases as drug targets for antimalarial agents, Expert Opin. Ther. Targets 19 (2015) 551–563.
[5] C.T. Supuran, Structure and function of carbonic anhydrases, Biochem. J. 473 (2016) 2023–2032.
[6] C.T. Supuran, Carbonic anhydrases: novel therapeutic applications for inhibitors and activators, Nat. Rev. Drug. Discov. 7 (2008) 168–181.
[7] V. Alterio, A. Di Fiore, K. D'Ambrosio, C.T. Supuran, G. De Simone, Multiple binding modes of inhibitors to carbonic anhydrases: how to design specific drugs targeting 15 different isoforms? Chem. Rev. 112 (2012) 4421–4468.
[8] B.H. Gibbons, J.T. Edsall, Rate of hydration and dehydration of carbon dioxide and dehydration of carbonic acid at 25 degrees, J. Biol. Chem. 238 (1963) 3502–3507.
[9] R.G. Khalifah, The carbon dioxide hydration activity of carbonic anhydrase. I. Stop-flow kinetic studies on the native human isoenzymes B and C, J. Biol. Chem. 246 (1971) 2561–2573.
[10] H. Steiner, B.H. Jonsson, S. Lindskog, The catalytic mechanism of carbonic anhydrase. Hydrogen-isotope effects on the kinetic parameters of the human C isoenzyme, Eur. J. Biochem. 59 (1975) 253–259.
[11] D.N. Silverman, S. Lindskog, The catalytic mechanism of carbonic anhydrase: implications of a rate-limiting proteolysis of water, Acc. Chem. Res. 21 (1988) 30–36.
[12] C.K. Tu, D.N. Silverman, C. Forsman, B.H. Jonsson, S. Lindskog, Role of histidine 64 in the catalytic mechanism of human carbonic anhydrase II studied with a site-specific mutant, Biochemistry 28 (1989) 7913–7918.
[13] S. Lindskog, Structure and mechanism of carbonic anhydrase, Pharmacol. Ther. 74 (1997) 1–20.
[14] B. Sjöblom, M. Polentarutti, K. Djinović-Carugo, Structural study of X-ray induced activation of carbonic anhydrase, Proc. Natl. Acad. Sci. U. S. A. 106 (2009) 10609–10613.
[15] C.T. Supuran, Carbonic anhydrases as drug targets–an overview, Curr. Top. Med. Chem. 7 (2007) 825–833.
[16] C.T. Supuran, Drug interaction considerations in the therapeutic use of carbonic anhydrase inhibitors, Expert Opin. Drug Metab. Toxicol. 12 (2016) 423–431.
[17] O.O. Guler, G. De Simone, C.T. Supuran, Drug design studies of the novel antitumor targets carbonic anhydrase IX and XII, Curr. Med. Chem. 17 (2010) 1516–1526.
[18] C.T. Supuran, J.-Y. Winum, Carbonic anhydrase IX inhibitors in cancer therapy: an update, Future Med. Chem. 7 (2015) 1407–1414.
[19] M.R. Ambrosio, C. Di Serio, G. Danza, B.J. Rocca, A. Ginori, I. Prudovsky, N. Marchionni, M.T. Del Vecchio, F. Tarantini, Carbonic anhydrase IX is a marker of hypoxia and correlates with higher Gleason scores and ISUP grading in prostate cancer, Diagn. Pathol. 11 (2016) 45.
[20] V. Linkuvienė, J. Matulienė, V. Juozapaitienė, V. Michailovienė, J. Jachno, D. Matulis, Intrinsic thermodynamics of inhibitor binding to human carbonic anhydrase IX, Biochim. Biophys. Acta 1860 (2016) 708–718.
[21] V. Dudutienė, et al., Discovery and characterization of novel selective inhibitors of carbonic anhydrase IX, J. Med. Chem. 57 (2014) 9435–9446.
[22] J. Pastorek, S. Pastorekova, Hypoxia-induced carbonic anhydrase IX as a target for cancer therapy: from biology to clinical use, Semin. Cancer Biol. 31 (2015) 52–64.
[23] V.M. Krishnamurthy, G.K. Kaufman, A.R. Urbach, I. Gitlin, K.L. Gudiksen, D.B. Weibel, G.M. Whitesides, Carbonic anhydrase as a model for biophysical and physical-organic studies of proteins and protein–ligand binding, Chem. Rev. 108 (2008) 946–1051.
[24] V. Petrauskas, L. Baranauskienė, A. Zubrienė, D. Matulis, Isothermal titration calorimetry and fluorescent thermal and pressure shift assays in protein-ligand interactions, in: M. Bastos (Ed.), Biocalorimetry: Foundations and Contemporary Approaches, CRC Press, 2016, pp. 261–280.
[25] J.-P. Renaud, C.-W. Chung, U.H. Danielson, U. Egner, M. Hennig, R.E. Hubbard, H. Nar, Biophysics in drug discovery: impact, challenges and opportunities, Nat. Rev. Drug Discov. 15 (2016) 679–698.
[26] V.O. Talibov, V. Linkuvienė, D. Matulis, U.H. Danielson, Kinetically selective inhibitors of human carbonic anhydrase isozymes I, II, VII, IX, XII, and XIII, J. Med. Chem. 59 (2016) 2083–2093.
[27] T. Rogez-Florent, L. Duhamel, L. Goossens, P. Six, A.-S. Drucbert, P. Depreux, P.-M. Danzé, D. Landy, J.-F. Goossens, C. Foulon, Label-free characterization of carbonic anhydrase-novel inhibitor interactions using surface plasmon resonance, isothermal titration calorimetry and fluorescence-based thermal shift assays, J. Mol. Recognit. 27 (2014) 46–56.
[28] B.H. Gibbons, J.T. Edsall, Kinetic studies of human carbonic anhydrases B and C, J. Biol. Chem. 239 (1964) 2539–2544.
[29] J.C. Kernohan, The pH-activity of bovine carbonic anhydrase and its relationship to the inhibition of the enzyme by anions, Biochim. Biophys. Acta 96 (1965) 304–317.
[30] B. Ulmasov, A. Waheed, G.N. Shah, J.H. Grubb, W.S. Sly, C. Tu, D.N. Silverman, Purification and kinetic analysis of recombinant CA XII, a membrane carbonic anhydrase overexpressed in certain cancers, Proc. Natl. Acad. Sci. U. S. A. 97 (2000) 14212–14217.
[31] G. La Regina, A. Coluccia, V. Famiglini, S. Pelliccia, L. Monti, D. Vullo, E. Nuti, V. Alterio, G. De Simone, S.M. Monti, P. Pan, S. Parkkila, C.T. Supuran, A. Rossello, R. Silvestri, Discovery of 1,1'-biphenyl-4-sulfonamides as a new class of potent and selective carbonic anhydrase XIV inhibitors, J. Med. Chem. 58 (2015) 8564–8572.
[32] J.F. Morrison, Kinetics of the reversible inhibition of enzyme-catalysed reactions by tight-binding inhibitors, Biochim. Biophys. Acta 185 (1969) 269–286.
[33] J.W. Williams, J.F. Morrison, The kinetics of reversible tight-binding inhibition, Methods Enzymol. 63 (1979) 437–467.
[34] D.J. Murphy, Determination of accurate KI values for tight-binding enzyme inhibitors: an in silico study of experimental error and assay design, Anal. Biochem. 327 (2004) 61–67.
[35] P. Kuzmič, K.C. Elrod, L.M. Cregar, S. Sideris, R. Rai, J.W. Janc, High-throughput screening of enzyme inhibitors: simultaneous determination of tight-binding inhibition constants and enzyme concentration, Anal. Biochem. 286 (2000) 45–50.
[36] R.A. Copeland, in: Evaluation of Enzyme Inhibitors in Drug Discovery: a Guide for Medicinal Chemists and Pharmacologists, second ed., John Wiley & Sons, Inc., United States of America, 2013, pp. 245–285.
[37] M.W. Pantoliano, E.C. Petrella, J.D. Kwasnoski, V.S. Lobanov, J. Myslik, E. Graf, T. Carver, E. Asel, B.A. Springer, P. Lane, F.R. Salemme, High-density miniaturized thermal shift assays as a general strategy for drug discovery, J. Biomol. Screen 6 (2001) 429–440.
[38] F.H. Niesen, H. Berglund, M. Vedadi, The use of differential scanning fluorimetry to detect ligand interactions that promote protein stability, Nat. Protoc. 2 (2007) 2212–2221.
[39] D. Matulis, R. Lovrien, 1-Anilino-8-naphthalene sulfonate anion-protein

binding depends primarily on ion pair formation, Biophys. J. 74 (1998) 422–429.
[40] D. Matulis, C.G. Baumann, V.A. Bloomfield, R.E. Lovrien, 1-anilino-8-naphthalene sulfonate as a protein conformational tightening agent, Biopolymers 49 (1999) 451–458.
[41] D. Matulis, J.K. Kranz, F.R. Salemme, M.J. Todd, Thermodynamic stability of carbonic anhydrase: measurements of binding affinity and stoichiometry using ThermoFluor, Biochemistry 44 (2005) 5258–5266.
[42] P. Cimmperman, L. Baranauskienė, S. Jachimovičiūtė, J. Jachno, J. Torresan, V. Michailovienė, J. Matulienė, J. Sereikaitė, V. Bumelis, D. Matulis, A quantitative model of thermal stabilization and destabilization of proteins by ligands, Biophys. J. 95 (2008) 3222–3231.
[43] M. Kišonaitė, A. Zubrienė, E. Čapkauskaitė, A. Smirnov, J. Smirnovienė, V. Kairys, V. Michailovienė, E. Manakova, S. Gražulis, D. Matulis, Intrinsic thermodynamics and structure correlation of benzenesulfonamides with a pyrimidine moiety binding to carbonic anhydrases I, II, VII, XII, and XIII, PLoS One 9 (2014) e114106.
[44] A. Zubrienė, J. Smirnovienė, A. Smirnov, V. Morkūnaitė, V. Michailovienė, J. Jachno, V. Juozapaitienė, P. Norvaišas, E. Manakova, S. Gražulis, D. Matulis, Intrinsic thermodynamics of 4-substituted-2,3,5,6-tetrafluorobenzenesulfonamide binding to carbonic anhydrases by isothermal titration calorimetry, Biophys. Chem. 205 (2015) 51–65.
[45] N.C. Garbett, J.B. Chaires, Thermodynamic studies for drug design and screening, Expert Opin. Drug Discov. 7 (2012) 299–314.
[46] T. Wiseman, S. Williston, J.F. Brandts, L.N. Lin, Rapid measurement of binding constants and heats of binding using a new titration calorimeter, Anal. Biochem. 179 (1989) 131–137.
[47] G. Krainer, J. Broecker, C. Vargas, J. Fanghänel, S. Keller, Quantifying high-affinity binding of hydrophobic ligands by isothermal titration calorimetry, Anal. Chem. 84 (2012) 10715–10722.
[48] J. Kazokaitė, S. Ames, H.M. Becker, J.W. Deitmer, D. Matulis, Selective inhibition of human carbonic anhydrase IX in Xenopus oocytes and MDA-MB-231 breast cancer cells, J. Enzyme Inhib. Med. Chem. 31 (2016) 38–44.
[49] J. Kazokaitė, A. Aspatwar, V. Kairys, S. Parkkila, D. Matulis, Fluorinated benzenesulfonamide anticancer inhibitors of carbonic anhydrase IX exhibit lower toxic effects on zebrafish embryonic development than ethoxzolamide, Epub ahead of print, Drug Chem. Toxicol. (Sep 6, 2016). PMID: 27600313, DOI: http://dx.doi.org10.1080/01480545.2016.1223095.
[50] L. Baranauskienė, M. Hilvo, J. Matulienė, D. Golovenko, E. Manakova, V. Dudutienė, V. Michailovienė, J. Torresan, J. Jachno, S. Parkkila, A. Maresca, C.T. Supuran, S. Gražulis, D. Matulis, Inhibition and binding studies of carbonic anhydrase isozymes I, II and IX with benzimidazo[1,2-c][1,2,3]thiadiazole-7-sulphonamides, J. Enzyme Inhib. Med. Chem. 25 (2010) 863–870.
[51] E. Čapkauskaitė, A. Zubrienė, A. Smirnov, J. Torresan, M. Kišonaitė, J. Kazokaitė, J. Gylytė, V. Michailovienė, V. Jogaitė, E. Manakova, S. Gražulis, S. Tumkevičius, D. Matulis, Benzenesulfonamides with pyrimidine moiety as inhibitors of human carbonic anhydrases I, II, VI, VII, XII, and XIII, Bioorg. Med. Chem. 21 (2013) 6937–6947.
[52] J. Sūdžius, L. Baranauskienė, D. Golovenko, J. Matulienė, V. Michailovienė, J. Torresan, J. Jachno, R. Sukackaitė, E. Manakova, S. Gražulis, S. Tumkevičius, D. Matulis, 4-[N-(substituted 4-pyrimidinyl)amino]benzenesulfonamides as inhibitors of carbonic anhydrase isozymes I, II, VII, and XIII, Bioorg. Med. Chem. 18 (2010) 7413–7421.
[53] V. Jogaitė, A. Zubrienė, V. Michailovienė, J. Gylytė, V. Morkūnaitė, D. Matulis, Characterization of human carbonic anhydrase XII stability and inhibitor binding, Bioorg. Med. Chem. 21 (2013) 1431–1436.
[54] E. Čapkauskaitė, A. Zubrienė, L. Baranauskienė, G. Tamulaitienė, E. Manakova, V. Kairys, S. Gražulis, S. Tumkevičius, D. Matulis, Design of [(2-pyrimidinylthio)acetyl]benzenesulfonamides as inhibitors of human carbonic anhydrases, Eur. J. Med. Chem. 51 (2012) 259–270.
[55] V. Dudutienė, A. Zubrienė, A. Smirnov, J. Gylytė, D. Timm, E. Manakova, S. Gražulis, D. Matulis, 4-Substituted-2,3,5,6-tetrafluorobenzenesulfonamides as inhibitors of carbonic anhydrases I, II, VII, XII, and XIII, Bioorg. Med. Chem. 21 (2013) 2093–2106.
[56] V. Dudutienė, A. Zubrienė, A. Smirnov, D.D. Timm, J. Smirnovienė, J. Kazokaitė, V. Michailovienė, A. Zakšauskas, E. Manakova, S. Gražulis, D. Matulis, Functionalization of fluorinated benzenesulfonamides and their inhibitory properties toward carbonic anhydrases, ChemMedChem 10 (2015) 662–687.
[57] Y. Cheng, W.H. Prusoff, Relationship between the inhibition constant (Ki) and the concentration of inhibitor which causes 50 per cent inhibition (IC50) of an enzymatic reaction, Biochem. Pharmacol. 22 (1973) 3099–3108.
[58] M. Hilvo, A. Innocenti, S.M. Monti, G. De Simone, C.T. Supuran, S. Parkkila, Recent advances in research on the most novel carbonic anhydrases, CA XIII and XV, Curr. Pharm. Des. 14 (2008) 672–678.
[59] J. Kazokaitė, G. Milinavičiūtė, J. Smirnovienė, J. Matulienė, D. Matulis, Intrinsic binding of 4-substituted-2,3,5,6-tetrafluorobenezenesulfonamides to native and recombinant human carbonic anhydrase VI, FEBS J. 282 (2015) 972–983.
[60] L. Baranauskienė, D. Matulis, Intrinsic thermodynamics of ethoxzolamide inhibitor binding to human carbonic anhydrase XIII, BMC Biophys. 5 (2012) 12.
[61] K. Rutkauskas, A. Zubrienė, I. Tumosienė, K. Kantminienė, M. Kažemėkaitė, A. Smirnov, J. Kazokaitė, V. Morkūnaitė, E. Čapkauskaitė, E. Manakova, S. Gražulis, Z.J. Beresnevičius, D. Matulis, 4-amino-substituted benzenesulfonamides as inhibitors of human carbonic anhydrases, Molecules 19 (2014) 17356–17380.
[62] V. Linkuvienė, G. Krainer, W.Y. Chen, D. Matulis, Isothermal titration calorimetry for drug design: precision of the enthalpy and binding constant measurements and comparison of the instruments, Anal. Biochem. 515 (2016) 61–64.
[63] C.T. Supuran, Carbonic anhydrases–an overview, Curr. Pharm. Des. 14 (2008) 603–614.
[64] X. Ren, S. Lindskog, Buffer dependence of CO_2 hydration catalyzed by human carbonic anhydrase I, Biochim. Biophys. Acta 1120 (1992) 81–86.
[65] R. Mikulski, D. West, K.H. Sippel, B.S. Avvaru, M. Aggarwal, C. Tu, R. McKenna, D.N. Silverman, Water networks in fast proton transfer during catalysis by human carbonic anhydrase II, Biochemistry 52 (2013) 125–131.
[66] J.F. Krebs, C.A. Fierke, Determinants of catalytic activity and stability of carbonic anhydrase II as revealed by random mutagenesis, J. Biol. Chem. 268 (1993) 948–954.
[67] C.D. Boone, M. Pinard, R. McKenna, D. Silverman, Catalytic mechanism of α-class carbonic anhydrases: CO_2 hydration and proton transfer, Subcell. Biochem. 75 (2014) 31–52.
[68] I.D. Campbell, S. Lindskog, A.I. White, A study of the histidine residues of human carbonic anhydrase C using 270 MHz proton magnetic resonance, J. Mol. Biol. 98 (1975) 597–614.
[69] V. Morkūnaitė, J. Gylytė, A. Zubrienė, L. Baranauskienė, M. Kišonaitė, V. Michailovienė, V. Juozapaitienė, M.J. Todd, D. Matulis, Intrinsic thermodynamics of sulfonamide inhibitor binding to human carbonic anhydrases I and II, J. Enzyme Inhib. Med. Chem. 30 (2015) 204–211.
[70] J.D. Hurt, C. Tu, P.J. Laipis, D.N. Silverman, Catalytic properties of murine carbonic anhydrase IV, J. Biol. Chem. 272 (1997) 13512–13518.
[71] R.W. Heck, P.A. Boriack-Sjodin, M. Qian, C. Tu, D.W. Christianson, P.J. Laipis, D.N. Silverman, Structure-based design of an intramolecular proton transfer site in murine carbonic anhydrase V, Biochemistry 35 (1996) 11605–11611.
[72] J.N. Earnhardt, M. Qian, C. Tu, M.M. Lakkis, N.C. Bergenhem, P.J. Laipis, R.E. Tashian, D.N. Silverman, The catalytic properties of murine carbonic anhydrase VII, Biochemistry 37 (1998) 10837–10845.
[73] I. Simonsson, B.H. Jonsson, S. Lindskog, A 13C nuclear magnetic resonance study of CO_2/HCO_3^- exchange catalyzed by human carbonic anhydrase I, Eur. J. Biochem. 129 (1982) 165–169.
[74] C. Engstrand, B.H. Jonsson, S. Lindskog, Catalytic and inhibitor-binding properties of some active-site mutants of human carbonic anhydrase I, Eur. J. Biochem. 229 (1995) 696–702.

Send Orders for Reprints to reprints@benthamscience.net

REVIEW ARTICLE

Experimental Approaches to Identify Selective Picomolar Inhibitors for Carbonic Anhydrase IX

Justina Kazokaitė-Adomaitienė[1,4,*], Holger M. Becker[2], Joana Smirnovienė[1], Ludwig J. Dubois[3] and Daumantas Matulis[1]

[1]*Department of Biothermodynamics and Drug Design, Institute of Biotechnology, Life Sciences Center, Vilnius University, Vilnius, Lithuania;* [2]*Institute of Physiological Chemistry, University of Veterinary Medicine Hannover, Hannover, Germany;* [3]*The M-Lab, Department of Precision Medicine, GROW – School for Oncology and Developmental Biology, Maastricht University, The Netherlands;* [4]*Present address: Division of Biochemistry, the Netherlands Cancer Institute, Amsterdam, the Netherlands*

Abstract: ***Background*:** Carbonic anhydrases (CAs) regulate pH homeostasis via the reversible hydration of CO_2, thereby emerging as essential enzymes for many vital functions. Among 12 catalytically active CA isoforms in humans, CA IX has become a relevant therapeutic target because of its role in cancer progression. Only two CA IX inhibitors have entered clinical trials, mostly due to low affinity and selectivity properties.

***Objective*:** The current review presents the design, development, and identification of the selective nano- to picomolar CA IX inhibitors VD11-4-2, VR16-09, and VD12-09.

***Methods and results*:** Compounds were selected from our database, composed of over 400 benzensulfonamides, synthesized at our laboratory, and tested for their binding to 12 human CAs. Here we discuss the CA CO_2 hydratase activity/inhibition assay and several biophysical techniques, such as fluorescent thermal shift assay and isothermal titration calorimetry, highlighting their contribution to the analysis of compound affinity and structure-activity relationships. To obtain sufficient amounts of recombinant CAs for inhibitor screening, several gene cloning and protein purification strategies are presented, including site-directed CA mutants, heterologous CAs from *Xenopus* oocytes, and native endogenous CAs. The cancer cell-based methods, such as clonogenicity, extracellular acidification, and mass spectrometric gas-analysis are reviewed, confirming nanomolar activities of lead inhibitors in intact cancer cells.

***Conclusions*:** Novel CA IX inhibitors are promising derivatives for *in vivo* explorations. Furthermore, the simultaneous targeting of several proteins involved in proton flux upon tumor acidosis and the disruption of transport metabolons might improve cancer management.

ARTICLE HISTORY

Received: April 14, 2020
Revised: August 14, 2020
Accepted: October 29, 2020

DOI:
10.2174/0929867327666201102112841

Keywords: drug development, organic chemistry, cancer, sulfonamide, thermal shift assay, isothermal titration calorimetry, CA IX.

1. INTRODUCTION

The goal of target-based drug discovery is to identify the key compounds which could induce a therapeutically relevant response via modulation of the disease-associated proteins [1, 2]. Nowadays, the development of numerous therapeutics often fails in clinical trials, most likely because of their improper selection during the preclinical stage. To successfully translate *in vitro* data to a clinical disease setting, the combination of different experimental assays is required to sufficiently characterize the inhibitor affinity properties and mode of action.

* Address correspondence to this author at the Division of Biochemistry, the Netherlands Cancer Institute, Amsterdam, the Netherlands; Tel: +370-5-223-4364; Fax: +370-5-260-2116; E-mail: kazokaite@ibt.lt

0929-8673/21 $65.00+.00 **© 2021 Bentham Science Publishers**

Upon their discovery over 80 years ago [3], carbonic anhydrases (CAs, EC 4.2.1.1) have been involved in different research fields, such as basic enzymology as models for protein-ligand binding and clinical medicine as drug targets. Based on the structural features and predominant organisms of expression, CAs are grouped into six evolutionarily distinct genetic families [4-8]. In humans, fifteen α-CA isoforms have been described so far, with twelve catalytically active among them. Through the catalysis of reversible CO_2 hydration to bicarbonate and proton, CAs are involved in many physiological processes, including bone resorption, calcification, respiration, signal transduction, electrolyte secretion, and biosynthetic reactions [9].

The deregulation of expression levels or catalytic activities of human CAs has been linked with many diseases. CA I has emerged as a marker for hemolytic anemia [10], vision-impairing disorders [11], ankylosing spondylitis [12], and prostate cancer [13]. CA II has been linked with numerous pathologies, such as glaucoma [14], edema [15], epilepsy [16], atherosclerosis [17], osteoporosis [18], and certain forms of cancers [19, 20]. CA III has been introduced as a biomarker for several neuromuscular disorders [21] and a regulator of obesity [22]. CA IV has been associated with retinal degeneration [23] and renal injuries [24]. Both CA VA and CA VB isozymes are important for obesity [25], insulin resistance [26], and oxidative stress in the brain [27]. CA VI has been linked with certain cancers, such as that of salivary glands, although its role remains speculative [28]. CA VII has been shown to play a role in epileptic seizures [29] and neuropathic pain [30]. CA IX and CA XII have been associated with cancer progression [31, 32]. Down-regulated levels of CA XIII have been observed in colorectal cancer [33], whereas elevated amounts of CA XIV have been found in the hypertrophic myocardium [34]. Among the listed CA-associated pathologies, most attention has been directed toward tumorigenesis with a focus on CA IX and CA XII as important enzymes of many hypoxic tumors. To date, a broad library of CA IX and CA XII inhibitors has been published with the translation of two sulfonamide-based chemical derivatives, SLC-0111 and E7070/Indisulam, into clinical trials. Most difficulties in this area are caused by high structural homology among human CAs [35], leading to difficulties in the design of CA isoform-selective compounds.

The aim of this work is to summarize novel methods applied in the search for CA IX- or CA XII-selective inhibitors. The integrative set of molecular biology, cellular biology, and biophysical approaches is presented in the current review, highlighting their contributions to the characterization of CA-targeting inhibitors VD11-4-2, VR16-09, and VD12-09, which exhibit both great selectivity and up to picomolar affinity towards CA IX [36, 37].

2. BIOCHEMICAL AND BIOPHYSICAL ASSAYS TO DETERMINE INHIBITOR AFFINITY *IN VITRO*

The thermodynamics of binding of more than 400 benzenesulfonamides [38], synthesized at our laboratory, to all twelve catalytically active recombinant human CAs, was determined using enzymatic and biophysical methods such as stopped-flow CO_2 hydration assay (SFA), fluorescent thermal shift assay (FTSA), and isothermal titration calorimetry (ITC). The experiments were performed with various settings of assay conditions, including different buffers, pH values, and temperatures, to gain a more detailed picture of enzyme-inhibitor interactions and select the most potent molecules for further development. The chemical structures of lead compounds and their binding affinities to the anticancer target CA IX next to CA I and CA II that are undesirable to be inhibited (thus are off-target-s) are shown in Fig. (**1**).

Importantly, 4-substituted-2,3,5,6-benzenesulfonamides were discovered as extremely strong and selective inhibitors of the off-target CA I [39]. Substitution of a fluorine atom to cyclooctylamino group at *ortho-* or *metha-* in benzenesulfonamide ring resulted in increased binding affinity up to 1000-fold towards the anticancer target CA IX and up to 450000-fold decreased binding constants of the off-targets CA I and CA II [37]. Even more bulky and hydrophobic substituent at *ortho-* position allowed gaining high selectivity and affinity towards CA IX and losing affinity to the off--targets [36]. A combination of inhibition and binding assays was necessary for the identification of such tight-binding inhibitors. Representative raw and dose-response curves obtained by FTSA, SFA, and ITC techniques are displayed in Fig. (**2**), while dissociation constants (K_d's) of compound binding to all twelve recombinant human CAs are listed in Table **S1**.

2.1. Fluorescent Thermal Shift Assay

FTSA (differential scanning fluorimetry or ThermoFluor®) in miniaturized format was introduced by Salemme and co-workers [43] in 2001. This method is based on monitoring protein thermal denaturation upon addition of a fluorescent dye, mostly SyproOrange [44-46] or 1-anilino-8-naphthalene sulfonate (ANS)

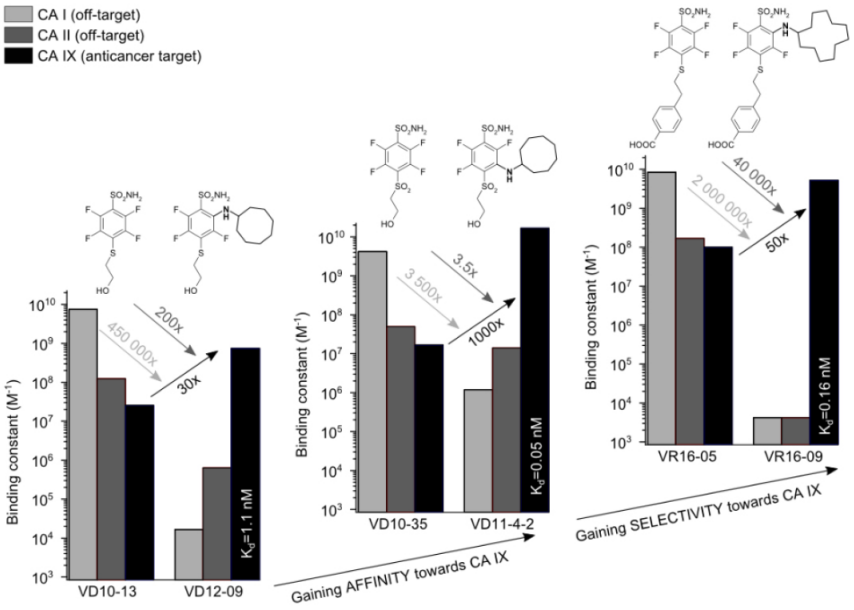


Fig. (1). Chemical structures and binding affinities of fluorinated benzenesulfonamides binding to CA I, CA II, and CA IX determined by FTSA. Numbers on arrows show fold difference in binding constants between *para*-substituted and *ortho/para*- or *meta/para*- disubstituted benzenesulfonamides. The figure was created originally according to previously published experimental data [36, 37]. (*A higher resolution / colour version of this figure is available in the electronic copy of the article*).

[47, 48]. For the CA-benzensulfonamide system, ANS is preferred [49]. The negatively charged sulfonate group of ANS binds to cationic groups of soluble proteins forming ion pairs [50]. The fluorescence of ANS is strongly quenched in water but significantly increased when the dye binds to the hydrophobic interior of the protein [51]. Application of FTSA allows characterizing thermal stability profiles of recombinant human CA I – CA XIV [52-57]. CA inhibitors cause a stabilization effect and result in increased CA melting temperature T_m. Fitting inhibitor dosing curves according to a quantitative model [40, 49] provide the estimation of binding affinity (binding/dissociation constant). The method is the first choice to screen the library of potential CA inhibitors due to rapidity, simplicity and low-cost. The main advantage of FTSA is the possibility to determine binding affinities from millimolar to picomolar range. Representative dose-response curves of weak to extremely strong affinities are shown in Fig. (**2B**). FTSA is the only suitable assay for measuring picomolar affinities of *para*-substituted compounds VD10-13, VD10-35, VR16-05 binding to CA I and *ortho/para*- or *meta/para*- disubstituted benzensulfonamides VD12-09, VD11-4-2, VR16-09 – to CA IX (Fig. **1**).

2.2. Stopped-flow CO_2 Hydration Assay

Since the introduction of the stopped-flow apparatus in 1950 by Chance [58], SFA has been most widely used to measure the CA catalytic activity and inhibitory effect of chemical compounds [59-70]. The CA catalyzed reaction ($CO_2 + H_2O \square HCO_3^- + H^+$) is followed by the absorbance change of pH-indicators, *e.g.* phenol red. To obtain high-quality results, it is important to choose an appropriate CA concentration at which the reaction rate r of the catalyzed reaction would be at least 10-fold higher than the reaction rate of spontaneous CO_2 hydration reaction ($r = 0.037\ s^{-1}$) [67, 71]. For this reason, the determination of nanomolar IC_{50} is limited by CA activity and concentration. Experiments of 20 nM CA IX inhibition with compound VD11-4-2 would give a steep curve with apparent $IC_{50} = 10$ nM, when the Hill equation is applied:

$$CA\ activity\ (\%) = 1 - \frac{100}{1 + (\frac{IC_{50}}{[I]})^h}$$

Where, IC_{50} is half-maximal inhibitory concentration, [I] is the total added inhibitor concentration and h is the Hill coefficient. When h> 1 and IC_{50} = [CA]/2, it is an indication of enzyme active site titration and misleading inhibitory constant. Lower CA IX concentrations decrease the signal-to-noise ratio and make it impossible to determine picomolar affinity, such as K_d = 0.05 nM of compound VD11-4-2. CA I possesses much lower catalytic activity than CA IX [68] and only micromolar inhibition constants could be measured as shown in Fig. (**2D**) (CA I inhibition with compound VD11-4-2). We recommend to fit dose-response curves using the Morrison equation [41, 42], as this takes into account the CA concentration and therefore provides a more accurate K_d:

$$CA\ activity\ (\%) = 1 - \frac{([CA] + [I] + K_d - \sqrt{([CA] + [I] + K_d)^2 - 4[CA][I]})}{2[CA]} \cdot 100\%$$

Where [CA] and [I] are total added active CA and inhibitor concentrations, K_d is dissociation constant. Several articles [72, 73] and a book [74] have discussed and evaluated the use of the Morrison equation for determining tight-binding inhibition constants. Tight-binding occurs when enzyme concentration in an assay is greater than the dissociation constant.

2.3. Isothermal titration calorimetry

ITC is a powerful method to study the thermodynamics of biomolecular interactions [75]. In a single experiment, the enthalpy, entropy, Gibbs free energy changes, and stoichiometry of binders are observed. Determination of binding affinity at several temperatures provides the heat capacity of binding. Moreover, it is applicable considering protonation effects upon inhibitor binding to the target protein [76, 77]. Performing ITC experiments of compounds VD10-13, VD12-09, VD10-35, VD11-4-2 binding to recombinant human CAs in broad-range pH and several buffers with varying ionization enthalpies provide intrinsic binding parameters [54, 56, 78, 79] that are not dependent on the experimental conditions. 4-substituted-2,3,5,6-benzenesulfonamides were characterized as extremely strong and selective binders of CA I [39](K_d = 0.11 - 0.20 nM, Table **S1**). In this case, the picomolar dissociation constant could not be observed by direct titration calorimetry due to Wiseman c-factor (c = [Protein conc.] · K_b, 5<c<500) [80], as shown in Fig. (**2F**). The displacement ITC experiments [81, 82] were performed to evaluate the binding energetics. ITC showed that extremely tight-binding of compounds VD10-13 and VD10-35 to CA I was associated with strong exothermic enthalpy ($\Delta H_{intr.}$ = -84.0 kJ/mol and -76.9 kJ/mol, 37 °C) and unfavorable entropy change ($-T\Delta S_{intr.}$ = 18.9 kJ/(mol · K) and 16.4 kJ/(mol · K), 37 °C) [79]. Contrarily, the extremely strong binding of disubstituted compounds VD12-09 and VD11-4-2 towards CA IX is an entropy-dominated process ($-T\Delta S_{intr.}$= -48.4 kJ/(mol · K) and -46.2 kJ/(mol · K), 37 °C) with contributing intrinsic enthalpy of one-third of Gibbs energy ($\Delta H_{intr.}$ = -18.7 kJ/mol and -24.9 kJ/mol, 37 °C) [78].

3. MOLECULAR BIOLOGICAL TECHNIQUES TO OBTAIN CARBONIC ANHYDRASE AS A MODEL PROTEIN

The affinity and biological outcome of the interaction between the inhibitor and mammalian protein can be evaluated through a number of biophysical and biochemical approaches [83], which employ the isolated recombinant proteins. Large quantities of recombinant proteins are necessary to determine the efficacy of compounds and to identify hits. These steps are essential for drug development because only proper compound characterization *in vitro* may lead to therapeutic benefit for patients during later clinical investigation.

The aim of our studies was to discover the compound exhibiting the most favorable properties against the anti-cancer target CA IX and low affinity toward other vital CA isoforms. Therefore, we put much effort into optimizing protocols to produce all 12 recombinant CAs, which are catalytically active in humans. Since yields of several recombinant CA isoforms, such as CA VI, CA IX or CA XII, are low, we applied a number of molecular biology-based procedures to get sufficient amounts of CA model proteins to screen our library composed of over 400 chemical derivatives [38]. Thus, we used not only recombinant CAs from *E. coli* or mammalian cells but also CA mutants, heterologous CAs, and native endogenous CAs, as presented in this section.

3.1. Generation of Site-directed Carbonic Anhydrase Mutants

Site-directed mutagenesis belongs to the group of versatile approaches applied for the functional and structural enzymatic studies. The goal is to alter DNA sequence via the polymerase chain reaction (PCR), thereby investigating the effect of target mutation on the protein properties. Among the extensively reviewed [84, 85] types of site-directed mutagenesis methods, the QuickChange™(from Agilent or Strategene) has been commonly used to carry out the point

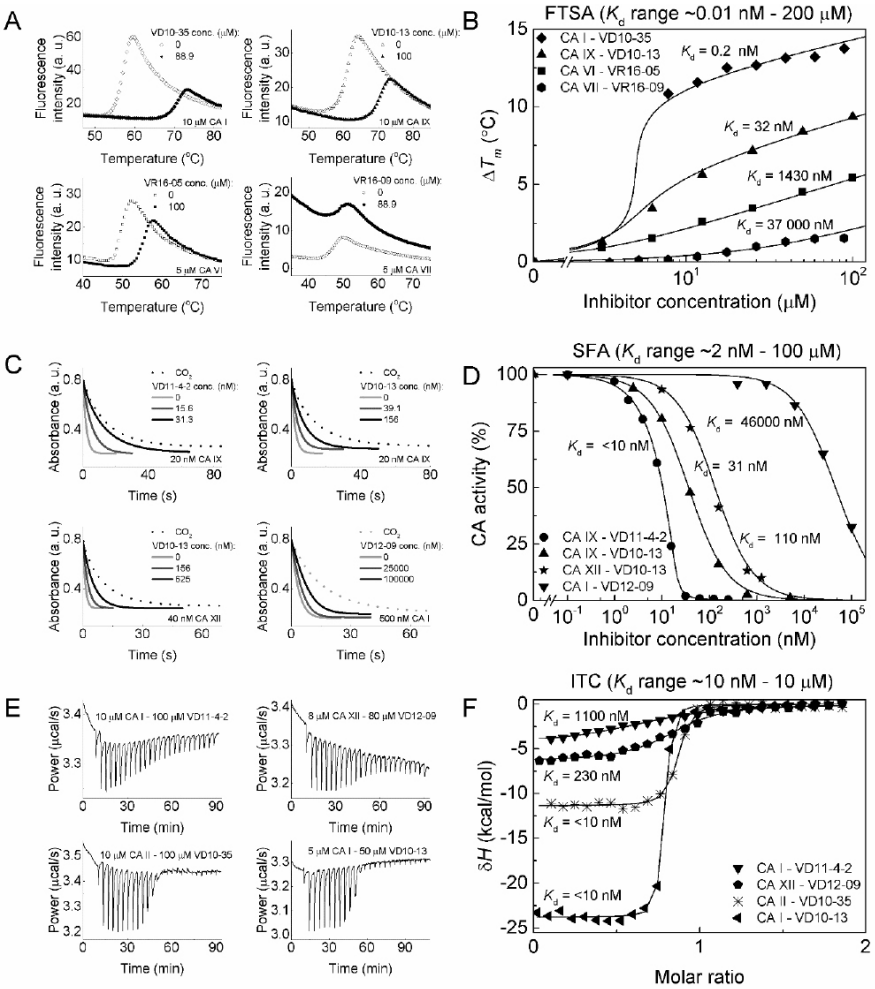


Fig. (2). Affinity determination ranges of FTSA (A-B, 50 mM sodium phosphate buffer, 100 mM NaCl, 50 μM 1,8-anilinonaphthalene sulfonate (ANS, fluorescent dye), pH 7.0, fitted at 37 °C), SFA (C-D, 25 mM Hepes buffer, 0.2 M sodium sulphate, 30 μM phenol-red (indicator) pH 7.5, 23 °C) and ITC (E-F, 50 mM Tris buffer, 100 mM sodium chloride, pH 7.0, 37 °C). The figure was created originally according to previously published experimental data [36, 37]. **(A)** Thermal melting curves of CA I (10 μM), CA IX (10 μM), CA VI (5 μM) and CA VII (5 μM) in the absence of inhibitor and added compound VD10-35 (88.9 μM), VD10-13 (100 μM), VR16-05 (100 μM) or VR16-09 (88.9 μM) concentration determined by FTSA. **(B)** The thermal shifts of CA I, CA IX and CA XII as a function of ligand VD10-13, VD10-35, VR16-05, VR16-09 concentrations. The dosing curves were fitted according to those referenced [40]. **(C)** Decrease of phenol red absorbance (λ - 557 nm) due to medium acidification during CO_2 hydration. The dashed lines represent CO_2 hydration in the absence of CAs. Decreasing transparency curves show CA IX (20 nM, red and blue), CA XII (40 nM, magenta) and CA I (500 nM, dark yellow) catalyzed CO_2 hydration reaction in the presence of several inhibitor concentrations (VD11-4-2 – 15.6, 31.3 nM; VD10-13 – 39.1, 156 or 156, 625 nM; VD12-09 – 25, 100 μM). The curves were fitted using a single exponential model. **(D)** Dose-response curves of CA I, CA IX and CA XII inhibition, fitted using Morrison equation [41, 42]. **(E)** Raw isothermal titration curves of CA I (10 μM and 5 μM), CA XII (8 μM), CA II (10 μM). (**F**) Integrated isothermal titration curves fitted using a single binding model. (*A higher resolution / colour version of this figure is available in the electronic copy of the article*).

mutations and delete or insert several bases. This strategy requires specifically designed primers, which have the desired mutations and are complementary to opposite strands of the target plasmid DNA. Upon the QuickChange™ experiment, DNA containing the desired mutation is amplified during the single PCR. This step is followed by digestion of the parental (methylated and hemimethylated) DNA template with endonuclease *Dpn I*.

In the CA research field, site-directed mutagenesis has been applied to identify residues which modulate catalytic properties [86, 87] and to discover anti-cancer compounds towards CA IX. High quantities of recombinant proteins are required for sufficient evaluation of compound efficacy and selectivity before studies in mammalians. However, the production of certain recombinant CA isoforms on a large scale is a complicated task [88]. Notably, human CAs are highly conserved [35]. The recombinant CA II has been used as a model protein for years due to the relatively easy production, the highest catalytic efficiency among the most enzymes in nature, and stability for structural investigations. Therefore, CA II has been selected as a core protein for site-directed mutagenesis studies aimed to design the target model CA protein featuring a low yield, as listed in Table **1**. The most widely investigated CA mutant is the CA II-based CA IX model protein, named CA IX-mimic. McKenna's group has reported a number of kinetic and structural studies which characterized CA II mutant with 2 mutations (S65A, Q67N) [89-91], 7 mutations (A65S, N67Q, E69T, I91L, F131V, K170E, L204A) [92-94] and 8 mutations (K9A, A65S, N67Q, E69T, I91L, F131V, K170E, L204A) [95]. They showed these proteins as suitable models for CA IX to determine the affinity and selectivity of novel CA IX-targeting inhibitors, such as sucrose, or well-defined drugs, such as acetazolamide, benzolamide, chlorzolamide, ethoxzolamide, methazolamide, brinzolamide, and dorzolamide.

Since we found difficulties in purifying recombinant CA IX and CA XII in high yield for inhibitor screening, we also started the production of CA II mutants mimicking CA IX and CA XII. Our group has published CA IX-mimic as CA II mutant with 6 mutations (A65S, N67Q, I91L, F130V, V134L, L203A) and CA XII as CA II mutant with 6 mutations (A65S, N67K, I91T, F130A, V134S, L203N) [37]. These mutants were applied for the kinetic and thermodynamic exploration of novel fluorinated CA IX inhibitors, including VD12-09 and VD11-4-2. The site-directed mutagenesis approach enabled us to show VD11-4-2 as the most selective compound for CA IX exhibiting 0.05 nM affinity and to implement further analyses on inhibitor selectivity towards CA isoforms. Furthermore, we did not manage to obtain recombinant CA VI on a high scale. Therefore, we have recently designed a CA II-based CA VI model protein with 5 mutations (A65T, N67Q, F130Y, V134Q, L203T) [70]. The CA VI-mimic has provided a deeper insight into the efficacy of CA VI-selective inhibitors and thus may be a useful model to reveal the biological role of CA VI because no crystallographic structures of inhibitors bound to CA VI are available so far. In addition, the low affinity of VD11-4-2 towards CA VI-mimic has been indicated, thereby confirming CA IX as the major target of VD11-4-2.

Table 1. Overview of studies on site-directed mutagenesis aimed to design model proteins mimicking the certain CA isoform to investigate inhibitor affinity and selectivity.

Core CA	Model CA	Mutations	Type of characterization	Refs.
CA II	CA VI	A65T, N67Q, F130Y, V134Q, L203T	Kinetic, thermodynamic, and structural	[70]
CA II	CA IX	S65A, Q67N	Kinetic, structural, and cell-biology based	[90]
CA II	CA IX	A65S, N67Q, E69T, I91L, F131V, K170E, L204A	Kinetic and structural	[94]
CA II	CA IX	K9A, A65S, N67Q, E69T, I91L, F131V, K170E, L204A	Kinetic and structural	[95]
CA II	CA IX	A65S, N67Q, I91L, F130V, V134L, L203A	Kinetic, thermodynamic, and structural	[37]
CA II	CA XII	A65S, N67K, I91T, F130A, V134S, L203N	Kinetic, thermodynamic, and structural	[37]

3.2. Heterologous Carbonic Anhydrases in *Xenopus laevis* Oocytes

The African clawed frog (*Xenopus laevis*) is a widely-used laboratory animal for biological and biomedical research. Until the 1960s, *Xenopus* females served as test animals in pregnancy diagnostics, after the finding of Shapiro & Zwarenstein [96] that injection of purified urine from pregnant women induces ovulation in the frog within a couple of hours. Today *Xenopus laevis* is used in zoological and physiological courses and its oocytes and larvae are the subjects of developmental studies. The frogs are easy to keep and breed at relatively low costs. *Xenopus* oocytes are frequently used

for heterologous expression of a variety of proteins. That *Xenopus* oocytes can efficiently express proteins upon injection of RNA was first shown by John Gurdon and colleagues [97] using rabbit hemoglobin. Today *Xenopus* oocytes are used for the expression of proteins from bacteria, plants and all kinds of animal species, including humans.

Oocytes, which are normally placed into the harsh environment of a pond or brackish water, are relatively robust to environmental changes, including alterations in the salinity and osmotic concentration of the incubation solution. Since post-vitellogenic oocytes are used for protein expression, they do not take up nutrients from the surrounding solution, instead they express only very few endogenous ion channels and transporters. However, various studies have demonstrated the endogenous expression of different membrane proteins like Na^+/H^+ exchangers [98] and a variety of ion channels which could interfere with the heterologously expressed proteins [99]. Therefore care should be taken to always test for possible interference of endogenous proteins with the expressed protein by use of adequate controls, like native or H_2O-injected oocytes.

Oogenesis in *Xenopus* occurs asynchronous, meaning that all developmental stages of oocytes present simultaneously. Six developmental stages of *Xenopus* oocytes have been classified by James Dumont [100], based on the cell's anatomy. Post-vitellogenic stage VI oocytes, which are preferentially used for protein expression, have a size of 1200 – 1300 μm, with a dark--brown pigmented animal hemisphere and a weak pigmented vegetal hemisphere, the two of which are separated by a near unpigmented equatorial band [100].

Oocytes are collected by surgically removing small parts of the ovary from anesthetized frogs. Given sufficient time, parts of the ovary can regenerate, allowing the repeated use of an animal. The oocytes are singularized and defolliculated either mechanically using fine forceps or by collagenase treatment. Single oocytes are handpicked for further treatment.

Protein expression is usually initiated by microinjection of cRNA, coding for the protein of interest into the oocyte's cytosol. The cRNA is produced by *in vitro* transcription. Therefore the gene of interest is cloned into a so-called "oocyte expression vector", like pGemHe, which carries the 3' and 5' untranscribed regions of the *Xenopus* β-globin, a well-translated *Xenopus* gene, flanking the multiple cloning site. It should be noted that the vectors are not expression vectors in the proper sense but are used for the production of cRNA by *in vitro* transcription. The procedure of protein expression in *Xenopus* oocytes has been described in detail in several reviews [101, 102]. An alternative to protein expression by injection of cRNA is the direct injection of the mature protein into the oocyte cytosol. For cytosolic proteins like CA II, this procedure could allow better control over the amount of protein within the cell.

Xenopus oocytes have been used to investigate the activity of various CA isoforms, including the intracellular isoforms CA I, CA II, CA III, the extracellular isoforms CA IV, CA IX, CA XII and also the catalytically inactive carbonic anhydrase-related proteins (CARPs) VIII, CARP X, and CARP XI [103-111]. Furthermore, *Xenopus* oocytes have been used to study functional interactions between CAs and different membrane proteins, including monocarboxylate transporters (MCTs, EC 2.1.3.1) [111-116], Na^+/HCO_3^- cotransporters (NBCe1) [104, 117], Cl^-/HCO_3^- exchangers [118] and aquaporins [103, 108]. No endogenous CA activity is observed in *Xenopus* oocytes [103], rendering them the ideal model for studying a specific CA without interference from other CA isoforms.

Catalytic activity of heterologously expressed CA can either be measured by mass spectrometric (MS) gas-analysis, as described in a subsequent 4.3.2 chapter, or by measuring pH changes in the cytosol or at the cell surface, using ion-sensitive microelectrodes. The use of pH-sensitive microelectrodes in *Xenopus* oocytes has been described in detail previously [101, 106, 119].

Xenopus oocytes have been successfully used to characterize newly developed CA IX inhibitors in several studies [36, 110, 120]. In a previous study [110], we investigated both potency and isoform-selectivity of the new CA IX inhibitor VD11-4-2 by measuring intracellular and surface pH in CA-expressing *Xenopus* oocytes with pH-sensitive microelectrodes. By this, we could determine IC_{50} values of 25 nM for CA IX at the extracellular side of the plasma membrane and of 15 nM for intracellular CA IX (*Xenopus* oocytes express significant amounts of cytosolic CA IX upon cRNA injection [109]). By the expression of different CA isoforms, we could demonstrate that VD11-4-2 is significantly less efficient against extracellular CA IV and CA XII, as well as intracellular CA II [110].

3.3. Native Endogenous Carbonic Anhydrases

Most α-CA isoforms were initially isolated as endogenous native proteins from diverse biological sources. For instance, CA I and CA II isoforms were purified from bovine and human blood [3, 121, 122].

The rabbit skeletal muscle was used to isolate CA III [123]. CA IV was purified from bovine lung [124] and human kidney [125]. The guinea pig liver was used to isolate mitochondrial CA V [126]. The secreted CA VI was purified from the saliva of sheep [127] and humans [128]. Other CA isoforms were mostly expressed in *E. coli*, mammalian or insect cells and isolated as recombinant proteins [129, 130].

For high-throughput inhibitor screening, the production of native proteins on a large scale is a complicated task owing to the lack of biological source or tricky procedure. Therefore, *E. coli* is usually applied as a host system because of low cost and relatively quick purification methods. However, proteins expressed in *E. coli* lack the post-translational modifications which might cause improper folding [131] and thus significantly affect the inhibitor binding affinity. Hence, it is fundamentally essential to assure that recombinant protein properly represents the native target of the human body for *in vitro* approaches. Interestingly, the comparison of inhibitor binding to both recombinant and respective endogenous native proteins can be carried out by using CA VI isozyme. In our study [54], CA VI was obtained from three sources; native CA VI was isolated from human saliva and two forms of recombinant CA VI were purified from *E. coli* and mammalian FreeStyle 293-F suspension cells. A series of sulfonamides bound with identical affinities towards CA VI isolated by three different methods were measured by FTSA and ITC. Thus, the recombinant CA VI from *E. coli* was characterized to be a suitable model of human native CA VI for *in vitro* inhibitors screening.

4. CELLULAR APPROACHES TO DETERMINE FUNCTIONAL INHIBITOR ACTIVITY

Next to biochemical and biophysical assays, there is a broad spectrum of methods to confirm compound efficacy and mode of action in the complex physiological environment of a cell. The quality, efficacy, and safety of the drug candidates are evaluated during this step of preclinical development using cell cultures and animal models. For anti-cancer compounds, the investigation mostly begins with viability and clonogenic survival assays in cancer cells followed by *in vivo* experiments using diverse mouse models [132]. The National Cancer Institute in the United States has a regulation to study the cytostatic or cytotoxic activity of a new derivative in eight cancer cell lines, which represent the most common human malignancies, and only afterwards, start investigation in mice [132]. In addition, large-scale toxicology studies focused on a rodent (rats) and a non-rodent (beagle dogs) species are commonly carried out before entering a clinical trial. If preclinical testing is prospective, the clinical development of a drug candidate is initiated.

Biological evaluation of our lead VD compounds was conducted via a number of cancer cell-based assays, including clonogenicity, extracellular acidification (pH), and MS gas-analysis. They provided significant clues for further exploration of anti-cancer activities of compounds *in vivo* using tumor-bearing mice.

4.1. Cell Viability Assay

Cytotoxicity of a derivative can be determined *in vitro* by various methods. Nowadays, the alamar blue method is a common choice over other cell viability and proliferation assays, such as 3-(4,5-dimethylthiazol-2-yl)-2,5-diphenyltetrazolium bromide dye, known as MTT, and 3H-thymidine incorporation. The principle of alamar blue method was initially applied by Pesch and Simmert to detect bacteria in milk [133], followed by a number of studies on milk quality [134]. Since that time, the alamar blue assay has been optimized for a broad range of cell types, including bacteria [135], yeast [136], fungi [137], protozoa [138],

Table 2. EC_{50} values (μM) for VR16-09, VD11-4-2, and VD12-09 determined by alamar blue viability assay. HeLa, H460, A549, and MDA-MB-231 cells were exposed to the compounds under normoxia (21% O_2) or hypoxia (0.2% O_2) for 72 h. Cytotoxic ratios (CR) of selectivity to hypoxia are indicated. Results of at least 3 independent repeats are shown (mean ± SD).

-	VR16-09			VD11-4-2			VD12-09		
[O_2]	21%	0.2%	CR	21%	0.2%	CR	21%	0.2%	CR
HeLa	20.2±4.3	40.8±9.6	0.46	47.8±9.6	92.2±8.3	0.52	21.6±4.1	46.9±7.0	0.44
H460	19.3±3.6	40.0±9.6	0.49	21.4±3.1	44.6±6.4	0.48	17.8±2.2	37.0±7.6	0.46
A549	17.0±1.0	76.7±2.9	0.22	43.8±2.5	105±6	0.42	33.8±2.5	98.8±8.5	0.34
MDA-MB-231	74.2±3.8	84.2±4.9	0.88	52.8±7.1	64.3±11.5	0.83	55.4±6.6	67.6±7.1	0.82

plants [139], and cultured mammalian cells [140]. The non-toxic and membrane-permeable resazurin is used for measurements by alamar blue, thereby enabling continuous monitoring of experiments without cell lysis. The reduction reaction of non-fluorescent resazurin to fluorescent resarufin is mostly catalyzed by mitochondrial enzymes [141]. Consequently, the experiment can be evaluated colorimetrically or fluorometrically according to the change of culture medium from indigo blue to fluorescent pink. However, the alamar blue method has several limitations. The investigated derivatives might affect the mitochondrial activity or reduce resazurin by themselves, resulting in misleading interpretations. Moreover, some cell lines exhibit the capability to reduce resorufin further until the highly toxic dihydroresorufin is obtained [140].

The anti-cancer activity *in vitro* of numerous CA IX-targeting derivatives has been evaluated by diverse viability methods, including MTT [142], 3H-thymidine incorporation [143], and alamar blue [144]. To investigate the cytotoxicity of our lead inhibitors VD11-4-2, VD12-09, and VR16-09, alamar blue assay was applied involving two-dimensional (2D) monolayer A549 (lung), AsPC-1 (pancreatic), MDA-MB-231 (breast), H460 (lung), and HeLa (cervical) cancer cells [36]. The increase of CA IX in these cell lines grown under hypoxia compared to normoxia was confirmed by Western blot analysis. Briefly, 96-well plates were used to seed cells in densities aiming to get 80% confluence after 96 h (the end of the experiment). Cells were allowed to attach overnight in normoxia. The next day, cells were exposed to normoxia or hypoxia (0.2% O_2) and the culture medium was replaced with pre-incubated normoxic or hypoxic medium containing 10-150 μM inhibitor or 0.25% DMSO. After 72 h, cells were incubated with 10% alamar blue reagent for 2 h, followed by measurements of fluorescence signal at 580 nm. For quantification, the sigmoidal dose-response curves were generated by a Hill fit to determine the concentration of inhibitor that leads to half-maximum viability response (EC_{50}). The tested inhibitors exhibited lower EC_{50} values for normoxic than hypoxic cells (Table **2**), thereby indicating the higher cytotoxicity for normoxic cells without/with significantly lower CA IX expression compared with CA IX-expressing hypoxic cells.

Our results are in line with several previous studies which showed the more efficacious cell kill in normoxia than hypoxia by CA IX inhibitors, such as SLC-0111 [145], sulfamate S4 [146], and dual-targeting compounds [147]. We speculate that the reason for this outcome might be the inhibitor binding towards CA XII, which is often upregulated to compensate CA IX absence, as demonstrated in many CA IX knockdown/-knockout cellular models [148-150]. Therefore, the development of single and double CA IX and/or CA XII knockout cell lines would significantly contribute to the identification of functional mechanisms of inhibitors.

4.2. Clonogenic Cell Survival Assay

The clonogenic assay monitors the ability of a single cell to grow into a colony composed of at least 50 cells. Over 60 years ago, this *in vitro* cellular technique was applied for the first time to evaluate the effect of radiation on the clonogenicity of HeLa cells [151, 152]. Since this experiment, the clonogenic assay has been adapted for a variety of cell lines [153] and different culture models. Next to 2D monolayers, clonogenic assay using three-dimensional (3D) cell culture models (spheroids) has been implemented to determine the reproductive viability under physiologically relevant microenvironment which is created by numerous important factors, including cell-cell interactions and oxygen gradients [154-156]. Upon the investigation of control untreated and treated groups, the impact of diverse treatments, including ionizing radiation and chemical agents, on clonogenic capacity can be evaluated. This information is valuable in radiation biology and drug development.

The 2D and 3D clonogenic assays have been widely applied in the development of CA IX-selective inhibitors. 2D cultures of canine kidney epithelial MDCK cells were used to show a significant reduction of clonogenicity by the derivative of temozolomide containing sulfonamide moiety which is important for targeting the active site of CA IX [147]. The 3-Hydrazinoisatin-based benzenesulfonamides significantly lowered the ability of HCT-116 monolayer colon cancer cells to proliferate [157]. Moreover, 3D clonogenic assay, using breast cancer MDA-MB-231 cells, was carried out to show the capability of CA IX inhibitor FC9403A, in combination with irradiation, to decrease colony formation in comparison to each separate treatments [146]. Several CA IX-targeting derivatives, such as acetazolamide, indanesulfonamide, and nitroimidazole-based compounds, were investigated in combination with irradiation by clonogenic survival of HT-29 colorectal carcinoma cells *in vitro* and further in tumor-bearing mice, resulting in the decreased tumor growth rate and sensitization of tumor to irradiation without toxic side effects [158, 159].

For our lead VD compounds, both 2D and 3D clonogenic assays were employed [36]. Briefly, 2D

HeLa cells were treated with 10-50 μM VR16-09, VD11-4-2, VD12-09 or 0.05% DMSO for 72 h upon normoxic or hypoxic conditions (0.2% O_2). Then cells were trypsinized, reseeded in triplicate with known cell densities and allowed to form colonies for 14 days. Colonies were stained and fixed with 0.4% methylene blue in 70% ethanol followed by quantification. In line with results obtained by alamar blue assay, 50 μM VR16-09 and 50 μM VD12-09 decreased clonogenic survival of normoxic HeLa cells (survival fraction 0.22 ± 0.10 and 0.67 ± 0.21, respectively) in a more efficient way than hypoxic cells (survival fraction 0.50 ± 0.18 and 0.85 ± 0.11, respectively), whereas the impact of VD11-4-2 on clonogenic survival of both normoxic (survival fraction 0.69 ± 0.18) and hypoxic cells (survival fraction 0.76 ± 0.18) did not differ significantly [36]. Furthermore, 3D clonogenic assay using H460 spheroids was applied. According to immunofluorescence, the overlap between CA IX expression and pimonidazole-positive hypoxia was investigated in sections of H460 spheroids grown for 11 days, whereas both factors were found in spheroids grown for 7 days. Therefore, non-hypoxic (grown for 4 days) and hypoxic (grown for 11 days) H460 spheroids were exposed to 5-15 μM VR16-09 or 0.25% DMSO for 24 h. Subsequently, single cell suspensions were made, followed by plating them in triplicate with known densities and allowing to form colonies for 14 days. After quantification, the effect of VR16-09 on clonogenic survival of 3D H460 cells was determined to be dependent on CA IX expression and hypoxia. After exposure to 15 μM VR16-09, the survival fraction was found to be 1.1 ± 0.10 for normoxic spheroids and 0.82 ± 0.12 for hypoxic spheroids, contrary to the results obtained by 2D viability and clonogenic survival methods.

4.3. Methods to Determine pH-linked Functional Activity

Upon progression of many cancers, overexpressed CA IX significantly contributes to the acidification of extracellular pH and alkalization of intracellular pH [31, 160]. Therefore, many strategies have been described in literature to aid in developing anti-cancer derivatives modulating CA IX catalytic activity. The most common *in vitro* method to evaluate the impact of inhibitor on catalytic activity of recombinant CA IX is the stopped-flow CO_2 hydration assay. At cellular level, the functional activities of CA-targeting inhibitors to reduce hypoxia-induced acidosis can be determined by two techniques: extracellular acidification assay by measuring pH directly inside a hypoxic chamber and MS gas-analysis following the ^{18}O depletion of doubly labeled $^{13}C^{18}O_2$.

4.3.1. Extracellular Acidification Assay

Cellular pH homeostasis under hypoxic conditions is mediated through several proteins, including CA IX. The elevated levels of extracellular H^+ ions lead to the tumor aggressiveness-promoting acidosis [161]. Gene silencing studies have confirmed that the depletion of CA IX decreases extracellular acidification *in vitro* [158]. Thus, measuring the rise of pH under normoxic conditions or directly inside a hypoxic chamber using a pH-meter is a convenient approach to evaluate the functional activity of new derivatives targeting extracellular CA IX. This type of extracellular acidification assay has been applied in a number of previous studies which showed the reduction of hypoxia-induced acidosis by fluorescein-labeled sulfonamide [162] and nitroimidazole-based inhibitors [159, 163].

We investigated the impact of our VD inhibitors on extracellular acidification of HeLa, H460, MDA-MB-231, and A549 cells [36]. HeLa, H460, and MDA-MB-231 cells were cultured in DMEM with 10% FBS, while A549 cells were grown in a home-made analogous medium containing a lower amount (10 mM) of sodium bicarbonate. Densities for each cell line were optimized to obtain 100% confluence after 96 h (the end of the experiment) in normoxia and hypoxia (0.2% O_2) after the exposure to 0.05% DMSO. These conditions were crucial to get the maximal level of CA IX-dependent extracellular acidification. Cells were plated in dishes (6 cm diameter) and allowed to attach for 24 h in normoxia. Subsequently, cells were treated with 5-50 μM of each inhibitor or DMSO for 72 h in parallel under normoxic or hypoxic conditions. The pH of the culture medium was measured at the end of the experiment using a pH-meter as previously published [162]. Hypoxia-induced acidification of cells was significantly reduced by VR16-09, VD11-4-2, and VD12-09 and was dependent on the concentration, whereas the effect of inhibitors on cellular acidification in normoxia was negligible (Table **3**). This functional property was the most prominent for VR16-09 at 50 μM, while VD12-09 featured the lowest activity among the tested compounds [36].

4.3.2. Mass Spectrometric Gas-analysis

Determination of CA catalytic activity *in vitro* by MS gas-analysis, using ^{18}O exchange technique, was first carried out by David Silverman and colleges in the early 1970s on CA from human erythrocytes [164]. Since then, this technique has served in numerous studies to determine the catalytic activity of various CA isoforms and CA mutants under a variety of chemical conditions. The technique is based on measuring

Table 3. The pH of culture medium after the treatment of HeLa, H460, A549, and MDA-MB-231 cells in parallel with 0.05% DMSO (pH) or 50 µM VR16-09, VD11-4-2 and VD12-09 (pH_i) for 72 h under hypoxia (0.2% O_2). Results of at least 3 independent repeats are shown (mean ± SD).

-	VD16-09			VD11-4-2			VD12-09		
-	pH	pH_i	ΔpH	pH	pH_i	ΔpH	pH	pH_i	ΔpH
HeLa	6.97 ± 0.06	7.44 ± 0.06	0.47	6.97 ± 0.06	7.21 ± 0.05	0.24	6.97 ± 0.06	7.22 ± 0.09	0.25
H460	6.67 ± 0.13	7.19 ± 0.14	0.52	6.67 ± 0.13	6.84 ± 0.14	0.17	6.67 ± 0.13	6.75 ± 0.28	0.08
A549	6.70 ± 0.04	6.79 ± 0.07	0.09	6.70 ± 0.04	6.81 ± 0.03	0.11	6.70 ± 0.04	6.72 ± 0.04	0.02
MDA-MB-231	6.37 ± 0.11	6.83 ± 0.20	0.46	6.37 ± 0.11	6.63 ± 0.07	0.26	6.37 ± 0.11	6.65 ± 0.11	0.28

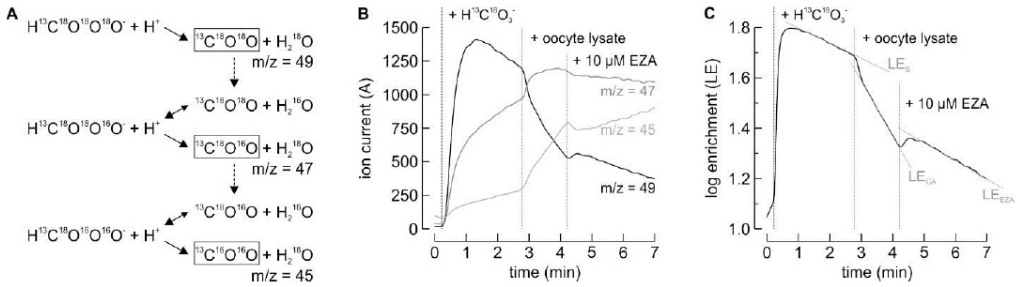


Fig. (3). Determination of CA activity by MS gas-analysis. The figure was created originally according to previously published experimental data [36]. (**A**) Simplified reaction sequence of ^{18}O exchange by the hydration and dehydration of CO_2 and HCO_3^-. (**B**) Original recording of the three CO_2 species $^{13}C^{18}O^{18}O$ (m/z=49), $^{13}C^{18}O^{16}O$ (m/z=47), and $^{13}C^{16}O^{16}O$ (m/z=45). (**C**) ^{18}O atom fraction (log enrichment), as calculated from the data shown in (B). The spontaneous ^{18}O exchange is determined from linear regression of the curve before the addition of CA (LE_S). Application of lysate from 20 CA II-expressing *Xenopus* oocytes increases the rate of ^{18}O exchange (LE_{CA}). Intact cancer cells also can be used here. Application of 10 µM 6-Ethoxy-2-benzothiazolesulfonamide (EZA) inhibits CA II catalytic activity, resulting in a reduction of the rate of ^{18}O exchange (LE_{EZA}).

the rate of isotopic depletion of ^{18}O-labelled bicarbonate using a gas-analysis mass spectrometer. This is usually achieved by measuring the ^{18}O to ^{16}O exchange from $^{13}C^{18}O_2$ caused by the hydration and dehydration of CO_2 and HCO_3^-, as shown in (Fig. **3A**).

Subsequent depletion of ^{18}O from CO_2 results in a subsequent change of the atomic weight from m/z=49 ($^{13}C^{18}O^{18}O$), over m/z=47 ($^{13}C^{18}O^{16}O$), to m/z=45 ($^{13}C^{16}O^{16}O$). The exchange is practically irreversible since the produced $H_2{}^{18}O$ is strongly diluted in $H_2{}^{16}O$. The concentration of the three CO_2 species is constantly recorded over the course of the experiment Fig. (**3B**). From these data, various kinetic parameters can be calculated, as described in numerous studies [164-167]. An easy method to calculate CA catalytic activity was described by Dieter Sültemeyer and colleagues [168]; first the ^{18}O atom fraction (also termed percent enrichment or log enrichment (LE)) is calculated from the three masses, using the formula:

$$LE = \log\frac{(^{13}C^{18}O_2)x100}{^{13}CO_2} = \log\frac{[49]x100}{[49]+[47]+[45]}.$$

The equation yields a curve, as shown in Fig. (**3C**). From the slopes of this curve, CA catalytic activity can be calculated as units of enzymatic activity (U), as defined by Badger and Price [169]:

$$U = \frac{LE_{CA} - LE_S}{LE_S} \quad \text{with}$$

LE_{CA} = CA catalyzed ^{18}O exchange

LE_S = spontaneous, unanalyzed ^{18}O exchange

The measurements are carried out in a measuring cuvette that is connected to a quadrupole mass spectrometer via a semipermeable membrane or by a direct inlet which is placed above the surface of the measuring solution. This setup allows to determine CA activity in a variety of samples, including purified protein [164, 170], lysates of CA-expressing *Xenopus* oocytes

[112, 171], cell suspensions of erythrocytes [172], cancer cells [36, 142], cardiomyocytes [173], hepatocytes [174] or intact oocytes [106, 109], isolated organelles like mitochondria [175] or chloroplasts [168], or even artificial phospholipid vesicles [176].

MS gas-analysis has been successfully used to characterize novel CA IX inhibitors in several studies [110, 120, 142]. In a recent study, we determined half-maximal inhibitory concentrations (IC_{50}) for three CA IX inhibitors VR16-09, VD11-4-2, and VD12-09 by measuring CA activity in hypoxic MDA-MB-231 breast cancer cells by MS gas-analysis. Results indicated a dose-dependent reduction of CA activity with IC_{50} values of 1.29 ± 0.11 nM for VR16-09, 2.95 ± 0.69 nM for VD11-4-2, and 167.4 ± 1.3 nM for VD12-09 [36]. Thereby, we could demonstrate that the tested derivatives inhibit CA IX activity at low nanomolar concentrations in intact cancer cells.

5. DISCUSSION

In recent years, the quantity of new drug approvals by the US Food and Drug Administration (FDA) and recommendations for authorization by the European Medicines Agency (EMA) has increased with a record number of 59 novel approved drugs in 2018 [177, 178]. Despite advances in molecular sciences, the development of many chemical or biological derivatives often fails so far with a rate of over 90% [179]. The outcome for 2016-2018 indicated that inaccurate studies on safety or efficacy cause 79% of clinical failures [180]. Therefore, there is a significant demand for the improved combination of biophysical, biochemical and cellular approaches in the initial stage of drug discovery, leading to deep insight into the characterization of drug candidates with promising clinical applications.

Herein, we have summarized the integrative set of our preclinical results obtained by enzymatic, biophysical, molecular, and cellular biology-based methods aiming to develop CA-targeting benzenesulfonamides VD11-4-2, VD12-09, and VR16-09 as anti-cancer drug candidates. The recent studies presenting the development of these compounds are listed in Table **4**. In humans, many vital functions are regulated by CA isoforms. The abnormal levels or activities of CAs are associated with diverse diseases. Thus, the development of chemical compounds targeting the specific CA isoform linked with certain pathology has been a major focus of attention over decades. Notably, CA IX has emerged as the relevant target for cancer therapy due to its unique expression pattern. CA IX is absent in normal tissues except for the epithelia of the gastrointestinal tract [181], whereas high overexpression of CA IX is detected in a wide spectrum of tumors. A number of reviews have already covered the biological significance of CA IX upon cancer progression [32, 182], a vast collection of compounds against CA IX [183], and diverse variations to deliver CA IX-targeting derivatives [184, 185]. The most successful strategies of modulating CA IX catalytic activity to date include the application of sulfonamide-based compounds. However, the design of CA isoform-selective compounds has been a challenging goal for many researchers because of the high conservation between human CA isoforms. Hence, only several chemical derivatives, such as sulfonamide SLC-0111, have progressed to clinical trials with unfavorable or unavailable results so far, indicating a need to improve preclinical characterization of compounds *in vitro* leading to more efficient CA IX--targeting options.

For the discovery of drug-lead compounds targeting CA IX, we have developed and analyzed a database of more than 400 benzensulfonamides to investigate their binding capacity to the twelve catalytically active recombinant human CA I – CA XIV isoforms [38]. Identification and characterization of picomolar affinities were challenging due to limitations of conventional enzymatic, calorimetric, or biosensing assays. Only several techniques, including fluorescence detected sedimentation velocity analytical ultracentrifugation (FDS-SV) [186, 187], microscale thermophoresis [188], and FTSA [189], are suitable for measuring dissociation constant below 1 nM. We applied FTSA as the primary technique to determine the affinities of a library of chemical compounds targeting CAs. In addition, SFA was used to validate the inhibition of CA catalytic activity and ITC was employed to dissect protonation events upon CA-ligand binding. Not only thermodynamic analysis but also kinetic studies have confirmed the potency of our lead compound VD11-4-2 to be suitable for clinical use. SPR experiments revealed that VD11-4-2 has a subnanomolar affinity with a low dissociation rate ($\sim 1 \cdot 10^{-3}$ s^{-1}) towards CA IX [190]. An excellent correlation has been observed between FTSA, ITC and SFA [68] and SPR [38] assays while studying CA-inhibitor interactions with a wide range of affinities. It was necessary to combine several biochemical and biophysical assays to obtain high-quality data and select potential drug molecules for further testing in biological systems.

Table 4. Timeline of discovery of benzenesulfonamides VD11-4-2, VD12-09, and VR16-09 as CA IX inhibitors.

Year	The Goal of the Study	Ref.
2013	Discovery of 4-substituted-2,3,5,6-tetrafluorobenzenesulfonamides (including VD10-13 and VD10-35) as selective picomolar inhibitors of CA I	[39]
2014	Discovery and characterization of lead compounds VD11-4-2 and VD12-09 as selective picomolar inhibitors of CA IX	[37]
2015	Evaluation of intrinsic thermodynamics of compounds VD10-13 and VD10-35 binding to CAs	[79]
2016	Biological evaluation of lead compounds VD11-4-2 and VD12-09 in *Xenopus* oocytes and human cancer cultures	[110]
2016	Thermodynamic characterization of human CA IX	[55]
2017	Evaluation of intrinsic thermodynamics of compounds VD11-4-2 and VD12-09 binding to CAs	[78]
2017	Comparison of inhibition and binding assays for the identification of picomolar inhibitors	[68]
2018	Thermodynamic, kinetic, and structural characterization of more than 400 inhibitors binding to 12 human CAs	[38]
2018	Biological evaluation of lead compounds VD11-4-2, VD12-09, and VR16-09 as selective inhibitors of CA IX in 2D and 3D models of human cancer cell cultures	[36]
2018	First *in vivo* study on the dual derivative composed of VD11-4-2 and tubulysin B	[143]
2019	Design of CA VI-mimic enzyme as a model for inhibitor screening	[70]

Next to biochemical approaches described in the present review, many other methods have been applied to determine the functional *in vitro* efficacy of CA IX inhibitors and their activated cellular programs. First, lactate dehydrogenase (LDH, EC 1.1.1.27) release assay allows evaluation of cytotoxicity, causing necrotic cell death. This colorimetric detection of serum LDH was applied by Mboge *et al.* to show that a series of ureido-substituted benzenesulfonamides inhibit cell growth without inducing cell death [142]. Second, detection of apoptotic markers, such as annexin V or cleaved caspases, is important to uncover apoptotic inhibitor-induced type of cell death. Several sulfonamide-based CA IX inhibitors have been reported by Koyuncu *et al.* to possess apoptotic roles in HeLa cells according to the increased amounts of cleaved caspase 3 (EC 3.4.22.56), caspase 8 (EC 3.4.22.61), caspase 9 (EC 3.4.22.62), and PARP (EC 2.4.2.30) [191]. Moreover, diamide-based benzenesulfonamides have been described by Abdelrahman *et al.* to induce apoptosis due to the increase of annexin V [192]. Third, the impact of CA IX-targeting compound on cell motility has been investigated by diverse migration and invasion assays, including wound healing assay [193], chemotaxis migration assay [194], and invasion through matrigel [194]. Taken together, the listed methods may provide detailed preclinical information on the mechanism of action of CA IX inhibitors, which would be essential for further *in vivo* investigations.

During cancer development, hypoxia induces many alterations in metabolic pathways, including the upregulation of CA IX and other proteins which are involved in cellular energetics. Recently, a number of studies have been actively pursued aimed at a synergistic effect through the combination of CA IX inhibitors with compounds directed against various proton and lactate exchangers and transporters, such as vacuolar ATPases (V-ATPases, EC 3.6.1.3), Na^+/H^+ exchangers (NHEs, EC 7.2.2.1), and MCTs [195]. The simultaneous targeting of CA IX by using sulfamate S4 or the ureido-sulfamate derivative FC9-399A and V-ATPase by applying lansoprazole has been reported to be more efficient than single treatments [196]. In addition, NHE1 inhibitor 5-(N,N-Dimethyl)amiloride hydrochloride (DMA) in combination with CA IX inhibitor FC9403A significantly reduced clonogenicity of MDA-MB-231 spheroids when combined with 0.5 Gy irradiation compared to either irradiation or single compound exposures [146]. However, the gene silencing study did not reveal the synergistic effect of both CA IX and NHE1 knockouts *in vivo* due to the upregulation of CA XII [150], emphasizing the cross-talk between CA isoforms and thus a need for the further investigation of molecular pH compensatory mechanisms.

Recently, CA IX has been identified to form diverse transport metabolons by interfering both directly and functionally with other proteins, such as NBCe1 [193], NHE1 [197], MCT1 [115], and MCT4 [115]. Thus, the disruption of transport metabolons has emerged as a promising anti-cancer strategy to disbalance cellular homeostasis and thus impair tumor progression [198]. Ames *et al*. have shown that MCT chaperone CD147 is necessary for the formation of

transport metabolon between MCT1/4 and CA IX [116]. Interestingly, antibodies recognizing CD147 or PG domain of CA IX have been demonstrated to significantly decrease CA IX-facilitated lactate flux by MCTs, resulting in a reduction of cellular proliferation [116, 171]. Furthermore, the compound KB-R7943, a selective inhibitor of type 1 Na^+/Ca^{2+} exchanger (NCX1), has been characterized by Liskova *et al.* to prevent the formation of NCX1-CA IX-NHE1 metabolon, leading to reduced cell motility [197]. These studies indicate that targeting the interaction of CA IX, a marker of hypoxic tumors, with widely expressed acid/base transporters might be a more efficient therapeutic option compared to targeting a single pH-regulating protein.

CONCLUSION

In conclusion, the newly designed fluorinated benzenesulfonamides VD11-4-2, VD12-09, and VR16-09 differ from previously reported CA IX inhibitors by bulky hydrophobic groups at *ortho*- and *meta*-positions. These groups ensure high selectivity and picomolar affinity towards CA IX as confirmed by the enzymatic inhibition, biophysical binding assays, and crystallographic analysis. Importantly, the combination of this data with results from biological assays significantly strengthens the conclusions of compound structure-activity relationships and is essential for sufficient *in vitro* characterization. For future directions, combinatorial approaches to applying our VD compounds with either biological derivatives, which suppress the formation of metabolons, or the standard treatment modalities may lead to improved biological efficacies. Indeed, the enhanced anti-tumor effect has recently been presented for a combination of SLC-0111 with gemcitabine to treat pancreatic cancer [199] (clinical Phase I/II trial: NCT03450018) and SLC-0111 with sunitinib to treat triple-negative breast cancer [200]. Furthermore, Marks *et al*. have reported the design of a dual derivative composed of VD11-4-2 and tubulysin B which impaired tumor growth *in vivo* and was not toxic [143], emphasizing that our lead VD compounds can be used as targeting moieties for the delivery of cytotoxic drugs and other diagnostic applications because of high affinity and great selectivity properties. Overall, we hope that the present review focusing on CA model proteins may serve as a constructive guideline to design and optimize picomolar hits in preclinical studies, leading to the development of therapeutically beneficial compounds without undesired side effects and thus the successful translation of basic research into clinic.

LIST OF ABBREVIATIONS

ANS	=	1,8- Anilinonaphthalene sulfonate
c	=	Wiseman c-factor
CA	=	carbonic anhydrase
EC_{50}	=	half-maximum viability response
EZA	=	6-Ethoxy-2-benzothiazolesulfonamide
FDS-SV	=	fluorescence detected sedimentation velocity analytical ultracentrifugation
FTSA	=	fluorescent thermal shift assay
h	=	Hill coefficient
$\Delta H_{intr.}$	=	intrinsic enthalpy change
Hepes	=	4-(2-Hydroxyethyl)piperazine-1-ethanesulfonic acid
$[I]$	=	total added inhibitor concentration
IC_{50}	=	half-maximal inhibitory concentration
ITC	=	isothermal titration calorimetry
K_b	=	binding constant
K_d	=	dissociation constant
LDH	=	lactate dehydrogenase
LE	=	log enrichment
MCT	=	monocarboxylate transporter
MTT	=	3-(4,5-dimethylthiazol-2-yl)-2,5-diphenyltetrazolium bromide
NBCe1	=	sodium bicarbonate co-transporter
NCX1	=	type 1 Na^+/Ca^{2+} exchanger
SFA	=	stopped-flow CO_2 hydration assay
$\Delta S_{intr.}$	=	intrinsic entropy change
SPR	=	surface plasmon resonance
Tris	=	2-Amino-2-(hydroxymethyl)-1,3-propanediol
VD10-13	=	2,3,5,6-Tetrafluoro-4-[(2-hydroxyethyl)thio] benzenesulfonamide
VD10-35	=	2,3,5,6-Tetrafluoro-4-[(2-hydroxyethyl)sulfonyl] benzenesulfonamide
VD11-4-2	=	3-(Cyclooctylamino)-2,5,6-trifluoro-4-[(2-hydroxyethyl)sulfonyl]benzenesulfonamide
VD12-09	=	2-(Cyclooctylamino)-3,5,6-trifluoro-4-[(2-hydroxyethyl)thio]benzenesulfonamide
VR16-05	=	4-(2-{[4-(Aminosulfonyl)-2,3,5,6-tetrafluorophenyl]thio}ethyl)benzoic acid
VR16-09	=	4-(2-{[4-(Aminosulfonyl)-3-(cyclododecylamino) -2,5,6-tetrafluorophenyl]thio}ethyl)benzoic acid

AUTHORS' CONTRIBUTION

Justina Kazokaitė-Adomaitienė has been involved in the conceptualization, methodology, visualization, and writing of original draft; Holger M. Becker in the

visualization and writing; Joana Smirnovienė in the visualization and writing; Ludwig J. Dubois in the writing, reviewing and editing of the manuscript and Daumantas Matulis also in writing, reviewing, and editing.

CONSENT FOR PUBLICATION

Not applicable.

FUNDING

This work was supported by the grant S-LLT-20-2 from the Research Council of Lithuania and by the Dutch Cancer Society (UM 2012-5394 and MAC 2013-6089).

CONFLICT OF INTEREST

DM declares that he has patents and patent applications pending on CA inhibitors. LD declares patents on CA IX inhibitors.

SUPPLEMENTARY MATERIALS

Supplementary material is available on the publisher's web site along with the published article.

ACKNOWLEDGEMENTS

Declared none.

REFERENCES

[1] Verma, S.; Prabhakar, Y.S. Target based drug design - a reality in virtual sphere. *Curr. Med. Chem.,* **2015**, *22*(13), 1603-1630. http://dx.doi.org/10.2174/0929867322666150209151209 PMID: 25666805

[2] Viayna, E.; Sola, I.; Di Pietro, O.; Muñoz-Torrero, D. Human disease and drug pharmacology, complex as real life. *Curr. Med. Chem.,* **2013**, *20*(13), 1623-1634. http://dx.doi.org/10.2174/0929867311320130002 PMID: 23410162

[3] Meldrum, N.; Roughton, F. Some Properties of Carbonic Anhydrase, the CO2 Enzyme Present in Blood. *J. Physiol.,* **1932**, *75*, 15-16.

[4] Del Prete, S.; Vullo, D.; De Luca, V.; Supuran, C.T.; Capasso, C. Biochemical characterization of the δ-carbonic anhydrase from the marine diatom Thalassiosira weissflogii, TweCA. *J. Enzyme Inhib. Med. Chem.,* **2014**, *29*(6), 906-911. http://dx.doi.org/10.3109/14756366.2013.868599 PMID: 24456295

[5] Samukawa, M.; Shen, C.; Hopkinson, B.M.; Matsuda, Y. Localization of putative carbonic anhydrases in the marine diatom, Thalassiosira pseudonana. *Photosynth. Res.,* **2014**, *121*(2-3), 235-249. http://dx.doi.org/10.1007/s11120-014-9967-x PMID: 24414291

[6] Kikutani, S.; Nakajima, K.; Nagasato, C.; Tsuji, Y.; Miyatake, A.; Matsuda, Y. Thylakoid luminal θ-carbonic anhydrase critical for growth and photosynthesis in the marine diatom Phaeodactylum tricornutum. *Proc. Natl. Acad. Sci. USA,* **2016**, *113*(35), 9828-9833. http://dx.doi.org/10.1073/pnas.1603112113 PMID: 27531955

[7] Zolfaghari Emameh, R.; Barker, H.R.; Syrjänen, L.; Urbański, L.; Supuran, C.T.; Parkkila, S. Identification and inhibition of carbonic anhydrases from nematodes. *J. Enzyme Inhib. Med. Chem.,* **2016**, *31*(sup4), 176-184. http://dx.doi.org/10.1080/14756366.2016.1221826 PMID: 27557594

[8] Zolfaghari Emameh, R.; Barker, H.R.; Tolvanen, M.E.E.; Parkkila, S.; Hytönen, V.P. Horizontal transfer of β-carbonic anhydrase genes from prokaryotes to protozoans, insects, and nematodes. *Parasit. Vectors,* **2016**, *9*, 152. http://dx.doi.org/10.1186/s13071-016-1415-7 PMID: 26983858

[9] Frost, S.C. Physiological functions of the alpha class of carbonic anhydrases. *Subcell. Biochem.,* **2014**, *75*, 9-30. http://dx.doi.org/10.1007/978-94-007-7359-2_2 PMID: 24146372

[10] Kuo, W-H.; Yang, S-F.; Hsieh, Y-S.; Tsai, C-S.; Hwang, W-L.; Chu, S-C. Differential expression of carbonic anhydrase isoenzymes in various types of anemia. *Clin. Chim. Acta,* **2005**, *351*(1-2), 79-86. http://dx.doi.org/10.1016/j.cccn.2004.07.009 PMID: 15563874

[11] Gao, B-B.; Clermont, A.; Rook, S.; Fonda, S.J.; Srinivasan, V.J.; Wojtkowski, M.; Fujimoto, J.G.; Avery, R.L.; Arrigg, P.G.; Bursell, S-E.; Aiello, L.P.; Feener, E.P. Extracellular carbonic anhydrase mediates hemorrhagic retinal and cerebral vascular permeability through prekallikrein activation. *Nat. Med.,* **2007**, *13*(2), 181-188. http://dx.doi.org/10.1038/nm1534 PMID: 17259996

[12] Chang, X.; Zheng, Y.; Yang, Q.; Wang, L.; Pan, J.; Xia, Y.; Yan, X.; Han, J. Carbonic anhydrase I (CA1) is involved in the process of bone formation and is susceptible to ankylosing spondylitis. *Arthritis Res. Ther.,* **2012**, *14*(4), R176. http://dx.doi.org/10.1186/ar3929 PMID: 22838845

[13] Takakura, M.; Yokomizo, A.; Tanaka, Y.; Kobayashi, M.; Jung, G.; Banno, M.; Sakuma, T.; Imada, K.; Oda, Y.; Kamita, M.; Honda, K.; Yamada, T.; Naito, S.; Ono, M. Carbonic Anhydrase I as a New Plasma Biomarker for Prostate Cancer. *ISRN Oncol,* **2012**, *2012* http://dx.doi.org/10.5402/2012/768190

[14] Mincione, F.; Starnotti, M.; Masini, E.; Bacciottini, L.; Scrivanti, C.; Casini, A.; Vullo, D.; Scozzafava, A.; Supuran, C.T. Carbonic anhydrase inhibitors: design of thioureido sulfonamides with potent isozyme II and XII inhibitory properties and intraocular pressure lowering activity in a rabbit model of glaucoma. *Bioorg. Med. Chem. Lett.,* **2005**, *15*(17), 3821-3827. http://dx.doi.org/10.1016/j.bmcl.2005.06.054 PMID: 16039853

[15] Lönnerholm, G.; Wistrand, P.J.; Bárány, E. Carbonic anhydrase isoenzymes in the rat kidney. Effects of chronic acetazolamide treatment. *Acta Physiol. Scand.,* **1986**, *126*(1), 51-60. http://dx.doi.org/10.1111/j.1748-1716.1986.tb07788.x PMID: 3082105

[16] Thiry, A.; Dogné, J-M.; Supuran, C.T.; Masereel, B. Anticonvulsant sulfonamides/sulfamates/sulfamides with carbonic anhydrase inhibitory activity: drug design and mechanism of action. *Curr. Pharm. Des.,* **2008**, *14*(7), 661-671. http://dx.doi.org/10.2174/138161208783877956 PMID: 18336312

[17] Oksala, N.; Levula, M.; Pelto-Huikko, M.; Kytömäki, L.; Soini, J.T.; Salenius, J.; Kähönen, M.; Karhunen, P.J.; Laaksonen, R.; Parkkila, S.; Lehtimäki, T. Carbonic anhydrases II and XII are up-regulated in osteoclast-like cells in advanced human atherosclerotic plaques-Tampere Vascular Study. *Ann. Med.,* **2010**, *42*(5), 360-370. http://dx.doi.org/10.3109/07853890.2010.486408 PMID: 20509747

[18] Kenny, A.D. Role of carbonic anhydrase in bone: plasma acetazolamide concentrations associated with inhibition of bone loss. *Pharmacology,* **1985**, *31*(2), 97-107. http://dx.doi.org/10.1159/000138104 PMID: 3927329

[19] Parkkila, S.; Lasota, J.; Fletcher, J.A.; Ou, W.B.; Kivelä, A.J.; Nuorva, K.; Parkkila, A-K.; Ollikainen, J.; Sly, W.S.; Waheed, A.; Pastorekova, S.; Pastorek, J.; Isola, J.; Miettinen, M. Carbonic anhydrase II. A novel biomarker for gastrointestinal stromal tumors. *Mod. Pathol.,* **2010**, *23*(5), 743-750. http://dx.doi.org/10.1038/modpathol.2009.189 PMID: 20081808

[20] Hynninen, P.; Parkkila, S.; Huhtala, H.; Pastorekova, S.; Pastorek, J.; Waheed, A.; Sly, W.S.; Tomas, E. Carbonic anhydrase isozymes II, IX, and XII in uterine tumors. *APMIS,* **2012**, *120*(2), 117-129. http://dx.doi.org/10.1111/j.1600-0463.2011.02820.x PMID: 22229267

[21] Heath, R.; Schwartz, M.S.; Brown, I.R.; Carter, N.D. Carbonic anhydrase III in neuromuscular disorders. *J. Neurol. Sci.,* **1983**, *59*(3), 383-388. http://dx.doi.org/10.1016/0022-510X(83)90023-0 PMID: 6410007

[22] Mitterberger, M.C.; Kim, G.; Rostek, U.; Levine, R.L.; Zwerschke, W. Carbonic anhydrase III regulates peroxisome proliferator-activated receptor-γ2. *Exp. Cell Res.,* **2012**, *318*(8), 877-886. http://dx.doi.org/10.1016/j.yexcr.2012.02.011 PMID: 22507175

[23] Rebello, G.; Ramesar, R.; Vorster, A.; Roberts, L.; Ehrenreich, L.; Oppon, E.; Gama, D.; Bardien, S.; Greenberg, J.; Bonapace, G.; Waheed, A.; Shah, G.N.; Sly, W.S. Apoptosis-inducing signal sequence mutation in carbonic anhydrase IV identified in patients with the RP17 form of retinitis pigmentosa. *Proc. Natl. Acad. Sci. USA,* **2004**, *101*(17), 6617-6622. http://dx.doi.org/10.1073/pnas.0401529101 PMID: 15090652

[24] Datta, R.; Shah, G.N.; Rubbelke, T.S.; Waheed, A.; Rauchman, M.; Goodman, A.G.; Katze, M.G.; Sly, W.S. Progressive renal injury from transgenic expression of human carbonic anhydrase IV folding mutants is enhanced by deficiency of p58IPK. *Proc. Natl. Acad. Sci. USA,* **2010**, *107*(14), 6448-6452. http://dx.doi.org/10.1073/pnas.1001905107 PMID: 20308551

[25] Scozzafava, A.; Supuran, C.T.; Carta, F. Antiobesity carbonic anhydrase inhibitors: a literature and patent review. *Expert Opin. Ther. Pat.,* **2013**, *23*(6), 725-735. http://dx.doi.org/10.1517/13543776.2013.790957 PMID: 23607332

[26] Parkkila, A-K.; Scarim, A.L.; Parkkila, S.; Waheed, A.; Corbett, J.A.; Sly, W.S. Expression of carbonic anhydrase V in pancreatic beta cells suggests role for mitochondrial carbonic anhydrase in insulin secretion. *J. Biol. Chem.,* **1998**, *273*(38), 24620-24623. http://dx.doi.org/10.1074/jbc.273.38.24620 PMID: 9733757

[27] Price, T.O.; Eranki, V.; Banks, W.A.; Ercal, N.; Shah, G.N. Topiramate treatment protects blood-brain barrier pericytes from hyperglycemia-induced oxidative damage in diabetic mice. *Endocrinology,* **2012**, *153*(1), 362-372. http://dx.doi.org/10.1210/en.2011-1638 PMID: 22109883

[28] Imtaiyaz Hassan, M.; Shajee, B.; Waheed, A.; Ahmad, F.; Sly, W.S. Structure, function and applications of carbonic anhydrase isozymes. *Bioorg. Med. Chem.,* **2013**, *21*(6), 1570-1582. http://dx.doi.org/10.1016/j.bmc.2012.04.044 PMID: 22607884

[29] Thiry, A.; Dogné, J-M.; Supuran, C.T.; Masereel, B. Carbonic anhydrase inhibitors as anticonvulsant agents. *Curr. Top. Med. Chem.,* **2007**, *7*(9), 855-864. http://dx.doi.org/10.2174/156802607780636726 PMID: 17504130

[30] Asiedu, M.; Ossipov, M.H.; Kaila, K.; Price, T.J. Acetazolamide and midazolam act synergistically to inhibit neuropathic pain. *Pain,* **2010**, *148*(2), 302-308. http://dx.doi.org/10.1016/j.pain.2009.11.015 PMID: 20007010

[31] Pastorek, J.; Pastorekova, S. Hypoxia-induced carbonic anhydrase IX as a target for cancer therapy: from biology to clinical use. *Semin. Cancer Biol.,* **2015**, *31*, 52-64. http://dx.doi.org/10.1016/j.semcancer.2014.08.002 PMID: 25117006

[32] Mboge, M.Y.; Mahon, B.P.; McKenna, R.; Frost, S.C. Carbonic Anhydrases: Role in pH Control and Cancer. *Metabolites,* **2018**, *8*(1), 8. http://dx.doi.org/10.3390/metabo8010019 PMID: 29495652

[33] Kummola, L.; Hämäläinen, J.M.; Kivelä, J.; Kivelä, A.J.; Saarnio, J.; Karttunen, T.; Parkkila, S. Expression of a novel carbonic anhydrase, CA XIII, in normal and neoplastic colorectal mucosa. *BMC Cancer,* **2005**, *5*, 41. http://dx.doi.org/10.1186/1471-2407-5-41 PMID: 15836783

[34] Vargas, L.A.; Alvarez, B.V. Carbonic anhydrase XIV in the normal and hypertrophic myocardium. *J. Mol. Cell. Cardiol.,* **2012**, *52*(3), 741-752. http://dx.doi.org/10.1016/j.yjmcc.2011.12.008 PMID: 22227327

[35] Aggarwal, M.; Boone, C.D.; Kondeti, B.; McKenna, R. Structural annotation of human carbonic anhydrases. *J. Enzyme Inhib. Med. Chem.,* **2013**, *28*(2), 267-277. http://dx.doi.org/10.3109/14756366.2012.737323 PMID: 23137351

[36] Kazokaitė, J.; Niemans, R.; Dudutienė, V.; Becker, H.M.; Leitāns, J.; Zubrienė, A.; Baranauskienė, L.; Gondi, G.; Zeidler, R.; Matulienė, J.; Tārs, K.; Yaromina, A.; Lambin, P.; Dubois, L.J.; Matulis, D. Novel fluorinated carbonic anhydrase IX inhibitors reduce hypoxia-induced acidification and clonogenic survival of cancer cells. *Oncotarget,* **2018**, *9*(42), 26800-26816. http://dx.doi.org/10.18632/oncotarget.25508 PMID: 29928486

[37] Dudutienė, V.; Matulienė, J.; Smirnov, A.; Timm, D.D.; Zubrienė, A.; Baranauskienė, L.; Morkūnaite, V.; Smirnovienė, J.; Michailovienė, V.; Juozapaitienė, V.; Mickevičiūtė, A.; Kazokaitė, J.; Bakšytė, S.; Kasiliauskaitė, A.; Jachno, J.; Revuckienė, J.; Kišonaitė, M.; Pilipuitytė, V.; Ivanauskaitė, E.; Milinavičiūtė, G.; Smirnovas, V.; Petrikaitė, V.; Kairys, V.; Petrauskas, V.; Norvaišas, P.; Lingė, D.; Gibieža, P.; Capkauskaitė, E.; Za-

kšauskas, A.; Kazlauskas, E.; Manakova, E.; Gražulis, S.; Ladbury, J.E.; Matulis, D. Discovery and characterization of novel selective inhibitors of carbonic anhydrase IX. *J. Med. Chem.,* **2014**, *57*(22), 9435-9446. http://dx.doi.org/10.1021/jm501003k PMID: 25358084

[38] Linkuvienė, V.; Zubrienė, A.; Manakova, E.; Petrauskas, V.; Baranauskienė, L.; Zakšauskas, A.; Smirnov, A.; Gražulis, S.; Ladbury, J.E.; Matulis, D. Thermodynamic, kinetic, and structural parameterization of human carbonic anhydrase interactions toward enhanced inhibitor design. *Q. Rev. Biophys.,* **2018**, *51*, e10. http://dx.doi.org/10.1017/S0033583518000082 PMID: 30912486

[39] Dudutienė, V.; Zubrienė, A.; Smirnov, A.; Gylytė, J.; Timm, D.; Manakova, E.; Gražulis, S.; Matulis, D. 4-Substituted-2,3,5,6-tetrafluorobenzenesulfonamides as inhibitors of carbonic anhydrases I, II, VII, XII, and XIII. *Bioorg. Med. Chem.,* **2013**, *21*(7), 2093-2106. http://dx.doi.org/10.1016/j.bmc.2013.01.008 PMID: 23394791

[40] Cimmperman, P.; Baranauskienė, L.; Jachimoviciūte, S.; Jachno, J.; Torresan, J.; Michailovienė, V.; Matulienė, J.; Sereikaitė, J.; Bumelis, V.; Matulis, D. A quantitative model of thermal stabilization and destabilization of proteins by ligands. *Biophys. J.,* **2008**, *95*(7), 3222-3231. http://dx.doi.org/10.1529/biophysj.108.134973 PMID: 18599640

[41] Morrison, J.F. Kinetics of the reversible inhibition of enzyme-catalysed reactions by tight-binding inhibitors. *Biochim. Biophys. Acta,* **1969**, *185*(2), 269-286. http://dx.doi.org/10.1016/0005-2744(69)90420-3 PMID: 4980133

[42] Williams, J.W.; Morrison, J.F. The Kinetics of Reversible Tight-Binding Inhibition. In: *Methods in Enzymology; Enzyme Kinetics and Mechanism Part A Initial Rate and Inhibitor Methods; Academic Press*; , **1979**, 63, p. 437–467.

[43] Pantoliano, M.W.; Petrella, E.C.; Kwasnoski, J.D.; Lobanov, V.S.; Myslik, J.; Graf, E.; Carver, T.; Asel, E.; Springer, B.A.; Lane, P.; Salemme, F.R. High-density miniaturized thermal shift assays as a general strategy for drug discovery. *J. Biomol. Screen.,* **2001**, *6*(6), 429-440. http://dx.doi.org/10.1177/108705710100600609 PMID: 11788061

[44] Abbott, J.A.; Livingston, N.M.; Egri, S.B.; Guth, E.; Francklyn, C.S. Characterization of aminoacyl-tRNA synthetase stability and substrate interaction by differential scanning fluorimetry. *Methods,* **2017**, *113*, 64-71. http://dx.doi.org/10.1016/j.ymeth.2016.10.013 PMID: 27794454

[45] Lo, M-C.; Aulabaugh, A.; Jin, G.; Cowling, R.; Bard, J.; Malamas, M.; Ellestad, G. Evaluation of fluorescence-based thermal shift assays for hit identification in drug discovery. *Anal. Biochem.,* **2004**, *332*(1), 153-159. http://dx.doi.org/10.1016/j.ab.2004.04.031 PMID: 15301960

[46] Niesen, F.H.; Berglund, H.; Vedadi, M. The use of differential scanning fluorimetry to detect ligand interactions that promote protein stability. *Nat. Protoc.,* **2007**, *2*(9), 2212-2221. http://dx.doi.org/10.1038/nprot.2007.321 PMID: 17853878

[47] Lavinder, J.J.; Hari, S.B.; Sullivan, B.J.; Magliery, T.J. High-throughput thermal scanning: a general, rapid dye-binding thermal shift screen for protein engineering. *J. Am. Chem. Soc.,* **2009**, *131*(11), 3794-3795. http://dx.doi.org/10.1021/ja8049063 PMID: 19292479

[48] Matulis, D.; Kranz, J.K.; Salemme, F.R.; Todd, M.J. Thermodynamic stability of carbonic anhydrase: measurements of binding affinity and stoichiometry using ThermoFluor. *Biochemistry,* **2005**, *44*(13), 5258-5266. http://dx.doi.org/10.1021/bi048135v PMID: 15794662

[49] Petrauskas, V.; Zubrienė, A.; Todd, M.J.; Matulis, D. Inhibitor Binding to Carbonic Anhydrases by Fluorescent Thermal Shift Assay.*Carbonic Anhydrase as Drug Target: Thermodynamics and Structure of Inhibitor Binding*; Matulis, D., Ed.; Springer International Publishing: Cham, **2019**, pp. 63-78. http://dx.doi.org/10.1007/978-3-030-12780-0_5

[50] Matulis, D.; Lovrien, R. 1-Anilino-8-naphthalene sulfonate anion-protein binding depends primarily on ion pair formation. *Biophys. J.,* **1998**, *74*(1), 422-429. http://dx.doi.org/10.1016/S0006-3495(98)77799-9 PMID: 9449342

[51] Matulis, D.; Baumann, C.G.; Bloomfield, V.A.; Lovrien, R.E. 1-anilino-8-naphthalene sulfonate as a protein conformational tightening agent. *Biopolymers,* **1999**, *49*(6), 451-458. http://dx.doi.org/10.1002/(SICI)1097-0282(199905)49:6<451::AID-BIP3>3.0.CO;2-6 PMID: 10193192

[52] Jogaitė, V.; Zubrienė, A.; Michailovienė, V.; Gylytė, J.; Morkūnaitė, V.; Matulis, D. Characterization of human carbonic anhydrase XII stability and inhibitor binding. *Bioorg. Med. Chem.,* **2013**, *21*(6), 1431-1436. http://dx.doi.org/10.1016/j.bmc.2012.10.016 PMID: 23159038

[53] Kasiliauskaitė, A.; Časaitė, V.; Juozapaitienė, V.; Zubrienė, A.; Michailovienė, V.; Revuckienė, J.; Baranauskienė, L.; Meškys, R.; Matulis, D. Thermodynamic Characterization of Human Carbonic Anhydrase VB Stability and Intrinsic Binding of Compounds. *J. Therm. Anal. Calorim.,* **2016**, *123*, 2191-2200. http://dx.doi.org/10.1007/s10973-015-5073-3

[54] Kazokaitė, J.; Milinavičiūtė, G.; Smirnovienė, J.; Matulienė, J.; Matulis, D. Intrinsic binding of 4-substituted-2,3,5,6-tetrafluorobenezenesulfonamides to native and recombinant human carbonic anhydrase VI. *FEBS J.,* **2015**, *282*(5), 972-983. http://dx.doi.org/10.1111/febs.13196 PMID: 25586768

[55] Linkuvienė, V.; Matulienė, J.; Juozapaitienė, V.; Michailovienė, V.; Jachno, J.; Matulis, D. Intrinsic thermodynamics of inhibitor binding to human carbonic anhydrase IX. *Biochim. Biophys. Acta,* **2016**, *1860*(4), 708-718. http://dx.doi.org/10.1016/j.bbagen.2016.01.007 PMID: 26794023

[56] Mickevičiūtė, A.; Timm, D.D.; Gedgaudas, M.; Linkuvienė, V.; Chen, Z.; Waheed, A.; Michailovienė, V.; Zubrienė, A.; Smirnov, A.; Čapkauskaitė, E.; Baranauskienė, L.; Jachno, J.; Revuckienė, J.; Manakova, E.; Gražulis, S.; Matulienė, J.; Di Cera, E.; Sly, W.S.; Matulis, D. Intrinsic thermodynamics of high affinity inhibitor binding to recombinant human carbonic anhydrase IV. *Eur. Biophys. J.,* **2018**, *47*(3), 271-290. http://dx.doi.org/10.1007/s00249-017-1256-0 PMID: 28975383

[57] Zubrienė, A.; Matulis, D. Characterization of Carbonic Anhydrase Thermal Stability.*Carbonic Anhydrase as Drug Target: Thermodynamics and Structure of Inhibitor Binding*; Matulis, D., Ed.; Springer International Publishing: Cham, **2019**, pp. 51-59. http://dx.doi.org/10.1007/978-3-030-12780-0_4

[58] Chance, B. The reactions of catalase in the presence of the

notatin system. *Biochem. J.,* **1950**, *46*(4), 387-402.
http://dx.doi.org/10.1042/bj0460387 PMID: 15420164

[59] Earnhardt, J.N.; Qian, M.; Tu, C.; Lakkis, M.M.; Bergenhem, N.C.H.; Laipis, P.J.; Tashian, R.E.; Silverman, D.N. The catalytic properties of murine carbonic anhydrase VII. *Biochemistry,* **1998**, *37*(30), 10837-10845.
http://dx.doi.org/10.1021/bi980046t PMID: 9692974

[60] Gibbons, B.H.; Edsall, J.T. Kinetic Studies of Human Carbonic Anhydrases B and C. *J. Biol. Chem.,* **1964**, *239*, 2539-2544.
PMID: 14235532

[61] Heck, R.W.; Boriack-Sjodin, P.A.; Qian, M.; Tu, C.; Christianson, D.W.; Laipis, P.J.; Silverman, D.N. Structure-based design of an intramolecular proton transfer site in murine carbonic anhydrase V. *Biochemistry,* **1996**, *35*(36), 11605-11611.
http://dx.doi.org/10.1021/bi9608018 PMID: 8794740

[62] Hurt, J.D.; Tu, C.; Laipis, P.J.; Silverman, D.N. Catalytic properties of murine carbonic anhydrase IV. *J. Biol. Chem.,* **1997**, *272*(21), 13512-13518.
http://dx.doi.org/10.1074/jbc.272.21.13512 PMID: 9153196

[63] Jewell, D.A.; Tu, C.K.; Paranawithana, S.R.; Tanhauser, S.M.; LoGrasso, P.V.; Laipis, P.J.; Silverman, D.N. Enhancement of the catalytic properties of human carbonic anhydrase III by site-directed mutagenesis. *Biochemistry,* **1991**, *30*(6), 1484-1490.
http://dx.doi.org/10.1021/bi00220a006 PMID: 1899618

[64] Juozapaitienė, V.; Bartkutė, B.; Michailovienė, V.; Zakšauskas, A.; Baranauskienė, L.; Satkūnė, S.; Matulis, D. Purification, enzymatic activity and inhibitor discovery for recombinant human carbonic anhydrase XIV. *J. Biotechnol.,* **2016**, *240*, 31-42.
http://dx.doi.org/10.1016/j.jbiotec.2016.10.018 PMID: 27773757

[65] Kernohan, J.C. A method for studying the kinetics of the inhibition of carbonic anhydrase by sulphonamides. *Biochim. Biophys. Acta,* **1966**, *118*(2), 405-412.
http://dx.doi.org/10.1016/S0926-6593(66)80049-8 PMID: 4960175

[66] Kernohan, J.C. The PH-Activity Curve of Bovine Carbonic Anhydrase and Its Relationship to the Inhibition of the Enzyme by Anions. *Biochimica et Biophysica Acta (B-BA)-. Biochim. Biophys. Acta,* **1965**, *96*, 304-317.
PMID: 14298834

[67] Khalifah, R.G. The carbon dioxide hydration activity of carbonic anhydrase. I. Stop-flow kinetic studies on the native human isoenzymes B and C. *J. Biol. Chem.,* **1971**, *246*(8), 2561-2573.
PMID: 4994926

[68] Smirnovienė, J.; Smirnovas, V.; Matulis, D. Picomolar inhibitors of carbonic anhydrase: Importance of inhibition and binding assays. *Anal. Biochem.,* **2017**, *522*, 61-72.
http://dx.doi.org/10.1016/j.ab.2017.01.022 PMID: 28153585

[69] Ulmasov, B.; Waheed, A.; Shah, G.N.; Grubb, J.H.; Sly, W.S.; Tu, C.; Silverman, D.N. Purification and kinetic analysis of recombinant CA XII, a membrane carbonic anhydrase overexpressed in certain cancers. *Proc. Natl. Acad. Sci. USA,* **2000**, *97*(26), 14212-14217.
http://dx.doi.org/10.1073/pnas.97.26.14212 PMID: 11121027

[70] Kazokaitė, J.; Kairys, V.; Smirnovienė, J.; Smirnov, A.; Manakova, E.; Tolvanen, M.; Parkkila, S.; Matulis, D. Engineered Carbonic Anhydrase VI-Mimic Enzyme Switched the Structure and Affinities of Inhibitors. *Sci. Rep.,* **2019**, *9*(1), 12710.
http://dx.doi.org/10.1038/s41598-019-49094-0 PMID: 31481705

[71] Gibbons, B.H.; Edsall, J.T. RATE OF HYDRATION OF CARBON DIOXIDE AND DEHYDRATION OF CARBONIC ACID AT 25 DEGREES. *J. Biol. Chem.,* **1963**, *238*, 3502-3507.
PMID: 14085409

[72] Kuzmic, P.; Elrod, K.C.; Cregar, L.M.; Sideris, S.; Rai, R.; Janc, J.W. High-throughput screening of enzyme inhibitors: simultaneous determination of tight-binding inhibition constants and enzyme concentration. *Anal. Biochem.,* **2000**, *286*(1), 45-50.
http://dx.doi.org/10.1006/abio.2000.4685 PMID: 11038272

[73] Murphy, D.J. Determination of accurate KI values for tight-binding enzyme inhibitors: an in silico study of experimental error and assay design. *Anal. Biochem.,* **2004**, *327*(1), 61-67.
http://dx.doi.org/10.1016/j.ab.2003.12.018 PMID: 15033511

[74] Copeland. *Evaluation of Enzyme Inhibitors in Drug Discovery a Guide for Medicinal Chemists and Pharmacologists;* ; JOHN WILEY & SONS, INC., **2013**.

[75] de Azevedo, W.F., Jr; Dias, R. Experimental approaches to evaluate the thermodynamics of protein-drug interactions. *Curr. Drug Targets,* **2008**, *9*(12), 1071-1076.
http://dx.doi.org/10.2174/138945008786949441 PMID: 19128217

[76] Baker, B.M.; Murphy, K.P. Evaluation of linked protonation effects in protein binding reactions using isothermal titration calorimetry. *Biophys. J.,* **1996**, *71*(4), 2049-2055.
http://dx.doi.org/10.1016/S0006-3495(96)79403-1 PMID: 8889179

[77] Leavitt, S.; Freire, E. Direct measurement of protein binding energetics by isothermal titration calorimetry. *Curr. Opin. Struct. Biol.,* **2001**, *11*(5), 560-566.
http://dx.doi.org/10.1016/S0959-440X(00)00248-7 PMID: 11785756

[78] Zubrienė, A.; Smirnov, A.; Dudutienė, V.; Timm, D.D.; Matulienė, J.; Michailovienė, V.; Zakšauskas, A.; Manakova, E.; Gražulis, S.; Matulis, D. Intrinsic Thermodynamics and Structures of 2,4- and 3,4-Substituted Fluorinated Benzenesulfonamides Binding to Carbonic Anhydrases. *ChemMedChem,* **2017**, *12*(2), 161-176.
http://dx.doi.org/10.1002/cmdc.201600509 PMID: 28001003

[79] Zubrienė, A.; Smirnovienė, J.; Smirnov, A.; Morkūnaitė, V.; Michailovienė, V.; Jachno, J.; Juozapaitienė, V.; Norvaišas, P.; Manakova, E.; Gražulis, S.; Matulis, D. Intrinsic thermodynamics of 4-substituted-2,3,5,6-tetrafluorobenzenesulfonamide binding to carbonic anhydrases by isothermal titration calorimetry. *Biophys. Chem.,* **2015**, *205*, 51-65.
http://dx.doi.org/10.1016/j.bpc.2015.05.009 PMID: 26079542

[80] Wiseman, T.; Williston, S.; Brandts, J.F.; Lin, L.N. Rapid measurement of binding constants and heats of binding using a new titration calorimeter. *Anal. Biochem.,* **1989**, *179*(1), 131-137.
http://dx.doi.org/10.1016/0003-2697(89)90213-3 PMID: 2757186

[81] Krainer, G.; Broecker, J.; Vargas, C.; Fanghänel, J.; Keller, S. Quantifying high-affinity binding of hydropho-

bic ligands by isothermal titration calorimetry. *Anal. Chem.,* **2012**, *84*(24), 10715-10722. http://dx.doi.org/10.1021/ac3025575 PMID: 23130786

[82] Sigurskjold, B.W. Exact analysis of competition ligand binding by displacement isothermal titration calorimetry. *Anal. Biochem.,* **2000**, *277*(2), 260-266. http://dx.doi.org/10.1006/abio.1999.4402 PMID: 10625516

[83] Kaczor, A.A.; Selent, J. Oligomerization of G protein-coupled receptors: biochemical and biophysical methods. *Curr. Med. Chem.,* **2011**, *18*(30), 4606-4634. http://dx.doi.org/10.2174/092986711797379285 PMID: 21864280

[84] Celie, P.H.; Parret, A.H.; Perrakis, A. Recombinant cloning strategies for protein expression. *Curr. Opin. Struct. Biol.,* **2016**, *38*, 145-154. http://dx.doi.org/10.1016/j.sbi.2016.06.010 PMID: 27391134

[85] Bachman, J. Site-directed mutagenesis. *Methods Enzymol.,* **2013**, *529*, 241-248. http://dx.doi.org/10.1016/B978-0-12-418687-3.00019-7 PMID: 24011050

[86] Behravan, G.; Jonasson, P.; Jonsson, B.H.; Lindskog, S. Structural and functional differences between carbonic anhydrase isoenzymes I and II as studied by site-directed mutagenesis. *Eur. J. Biochem.,* **1991**, *198*(3), 589-592. http://dx.doi.org/10.1111/j.1432-1033.1991.tb16054.x PMID: 1904817

[87] De Simone, G.; Di Fiore, A.; Truppo, E.; Langella, E.; Vullo, D.; Supuran, C.T.; Monti, S.M. Exploration of the residues modulating the catalytic features of human carbonic anhydrase XIII by a site-specific mutagenesis approach. *J. Enzyme Inhib. Med. Chem.,* **2019**, *34*(1), 1506-1510. http://dx.doi.org/10.1080/14756366.2019.1653290 PMID: 31431090

[88] Mickevičiūtė, A.; Juozapaitienė, V.; Michailovienė, V.; Jachno, J.; Matulienė, J.; Matulis, D. Recombinant Production of 12 Catalytically Active Human CA Isoforms.*Carbonic Anhydrase as Drug Target: Thermodynamics and Structure of Inhibitor Binding*; Matulis, D., Ed.; Springer International Publishing: Cham, **2019**, pp. 15-37. http://dx.doi.org/10.1007/978-3-030-12780-0_2

[89] Tars, K.; Vullo, D.; Kazaks, A.; Leitans, J.; Lends, A.; Grandane, A.; Zalubovskis, R.; Scozzafava, A.; Supuran, C.T. Sulfocoumarins (1,2-benzoxathiine-2,2-dioxides): a class of potent and isoform-selective inhibitors of tumor-associated carbonic anhydrases. *J. Med. Chem.,* **2013**, *56*(1), 293-300. http://dx.doi.org/10.1021/jm301625s PMID: 23241068

[90] Genis, C.; Sippel, K.H.; Case, N.; Cao, W.; Avvaru, B.S.; Tartaglia, L.J.; Govindasamy, L.; Tu, C.; Agbandje-McKenna, M.; Silverman, D.N.; Rosser, C.J.; McKenna, R. Design of a carbonic anhydrase IX active-site mimic to screen inhibitors for possible anticancer properties. *Biochemistry,* **2009**, *48*(6), 1322-1331. http://dx.doi.org/10.1021/bi802035f PMID: 19170619

[91] Sippel, K.H.; Stander, A.; Tu, C.; Venkatakrishnan, B.; Robbins, A.H.; Agbandje-McKenna, M.; Fourie, J.; Joubert, A.M.; McKenna, R. Characterization of Carbonic Anhydrase Isozyme Specific Inhibition by Sulfamated 2-Ethylestra Compounds. *Lett. Drug Des. Discov.,* **2011**, *8*, 1-25. http://dx.doi.org/10.2174/157018011796576105

[92] Moeker, J.; Mahon, B.P.; Bornaghi, L.F.; Vullo, D.; Supuran, C.T.; McKenna, R.; Poulsen, S-A. Structural insights into carbonic anhydrase IX isoform specificity of carbohydrate-based sulfamates. *J. Med. Chem.,* **2014**, *57*(20), 8635-8645. http://dx.doi.org/10.1021/jm5012935 PMID: 25254302

[93] Mahon, B.P.; Hendon, A.M.; Driscoll, J.M.; Rankin, G.M.; Poulsen, S-A.; Supuran, C.T.; McKenna, R. Saccharin: a lead compound for structure-based drug design of carbonic anhydrase IX inhibitors. *Bioorg. Med. Chem.,* **2015**, *23*(4), 849-854. http://dx.doi.org/10.1016/j.bmc.2014.12.030 PMID: 25614109

[94] Pinard, M.A.; Aggarwal, M.; Mahon, B.P.; Tu, C.; McKenna, R. A sucrose-binding site provides a lead towards an isoform-specific inhibitor of the cancer-associated enzyme carbonic anhydrase IX. *Acta Crystallogr. F Struct. Biol. Commun.,* **2015**, *71*(Pt 10), 1352-1358. http://dx.doi.org/10.1107/S2053230X1501239X PMID: 26457530

[95] Pinard, M.A.; Boone, C.D.; Rife, B.D.; Supuran, C.T.; McKenna, R. Structural study of interaction between brinzolamide and dorzolamide inhibition of human carbonic anhydrases. *Bioorg. Med. Chem.,* **2013**, *21*(22), 7210-7215. http://dx.doi.org/10.1016/j.bmc.2013.08.033 PMID: 24090602

[96] Shapiro, H.A.; Zwarenstein, H. A Rapid Test for Pregnancy on *Xenopus Lævis. Nature,* **1934**, *133*, 762. http://dx.doi.org/10.1038/133762a0

[97] Gurdon, J.B.; Lane, C.D.; Woodland, H.R.; Marbaix, G. Use of frog eggs and oocytes for the study of messenger RNA and its translation in living cells. *Nature,* **1971**, *233*(5316), 177-182. http://dx.doi.org/10.1038/233177a0 PMID: 4939175

[98] Sasaki, S.; Ishibashi, K.; Nagai, T.; Marumo, F. Regulation mechanisms of intracellular pH of Xenopus laevis oocyte. *Biochim. Biophys. Acta,* **1992**, *1137*(1), 45-51. http://dx.doi.org/10.1016/0167-4889(92)90098-V PMID: 1327152

[99] Terhag, J.; Cavara, N.A.; Hollmann, M. Cave Canalem: how endogenous ion channels may interfere with heterologous expression in Xenopus oocytes. *Methods,* **2010**, *51*(1), 66-74. http://dx.doi.org/10.1016/j.ymeth.2010.01.034 PMID: 20123125

[100] Dumont, J.N. Stages of Oocyte Development in Laboratory Maintained Animals. Oogenesis in Xenopus laevis (Daudin). I. Stages of oocyte development in laboratory maintained animals. *J. Morphol.,* **1972**, *136*(2), 153-179. http://dx.doi.org/10.1002/jmor.1051360203 PMID: 4109871

[101] Wagner, C.A.; Friedrich, B.; Setiawan, I.; Lang, F.; Bröer, S. The Use of Xenopus Laevis Oocytes for the Functional Characterization of Heterologously Expressed Membrane Proteins. *Cellular physiology and biochemistry : international journal of experimental cellular physiology, biochemistry, and pharmacology,,* **2000**, *10*1–12

[102] Bröer, S. Xenopus Laevis Oocytes.*Membrane Transporters in Drug Discovery and Development: Methods and Protocols*; Yan, Q., Ed.; Methods in Molecular Biology; Humana Press: Totowa, NJ, **2010**. http://dx.doi.org/10.1007/978-1-60761-700-6_16

[103] Nakhoul, N.L.; Davis, B.A.; Romero, M.F.; Boron, W.F. Effect of expressing the water channel aquaporin-1 on the CO2 permeability of Xenopus oocytes. *Am. J. Physiol.,* **1998**, *274*(2), C543-C548. http://dx.doi.org/10.1152/ajpcell.1998.274.2.C543 PMID:

9486145

[104] Lu, J.; Daly, C.M.; Parker, M.D.; Gill, H.S.; Piermarini, P.M.; Pelletier, M.F.; Boron, W.F. Effect of human carbonic anhydrase II on the activity of the human electrogenic Na/HCO3 cotransporter NBCe1-A in Xenopus oocytes. *J. Biol. Chem.,* **2006**, *281*(28), 19241-19250. http://dx.doi.org/10.1074/jbc.M602181200 PMID: 16687407

[105] Schueler, C.; Becker, H.M.; McKenna, R.; Deitmer, J.W. Transport activity of the sodium bicarbonate cotransporter NBCe1 is enhanced by different isoforms of carbonic anhydrase. *PLoS One,* **2011**, *6*(11), e27167. http://dx.doi.org/10.1371/journal.pone.0027167 PMID: 22076132

[106] Schneider, H-P.; Alt, M.D.; Klier, M.; Spiess, A.; Andes, F.T.; Waheed, A.; Sly, W.S.; Becker, H.M.; Deitmer, J.W. GPI-anchored carbonic anhydrase IV displays both intra- and extracellular activity in cRNA-injected oocytes and in mouse neurons. *Proc. Natl. Acad. Sci. USA,* **2013**, *110*(4), 1494-1499. http://dx.doi.org/10.1073/pnas.1221213110 PMID: 23297198

[107] Musa-Aziz, R.; Occhipinti, R.; Boron, W.F. Evidence from simultaneous intracellular- and surface-pH transients that carbonic anhydrase II enhances CO2 fluxes across Xenopus oocyte plasma membranes. *Am. J. Physiol. Cell Physiol.,* **2014**, *307*(9), C791-C813. http://dx.doi.org/10.1152/ajpcell.00051.2014 PMID: 24965587

[108] Vilas, G.; Krishnan, D.; Loganathan, S.K.; Malhotra, D.; Liu, L.; Beggs, M.R.; Gena, P.; Calamita, G.; Jung, M.; Zimmermann, R.; Tamma, G.; Casey, J.R.; Alexander, R.T. Increased water flux induced by an aquaporin-1/carbonic anhydrase II interaction. *Mol. Biol. Cell,* **2015**, *26*(6), 1106-1118. http://dx.doi.org/10.1091/mbc.E14-03-0812 PMID: 25609088

[109] Klier, M.; Jamali, S.; Ames, S.; Schneider, H-P.; Becker, H.M.; Deitmer, J.W. Catalytic activity of human carbonic anhydrase isoform IX is displayed both extra- and intracellularly. *FEBS J.,* **2016**, *283*(1), 191-200. http://dx.doi.org/10.1111/febs.13562 PMID: 26470855

[110] Kazokaitė, J.; Ames, S.; Becker, H.M.; Deitmer, J.W.; Matulis, D. Selective inhibition of human carbonic anhydrase IX in Xenopus oocytes and MDA-MB-231 breast cancer cells. *J. Enzyme Inhib. Med. Chem.,* **2016**, *31*(sup4), 38-44. http://dx.doi.org/10.1080/14756366.2016.1217854 PMID: 27557419

[111] Aspatwar, A.; Tolvanen, M.E.E.; Schneider, H-P.; Becker, H.M.; Narkilahti, S.; Parkkila, S.; Deitmer, J.W. Catalytically inactive carbonic anhydrase-related proteins enhance transport of lactate by MCT1. *FEBS Open Bio,* **2019**, *9*(7), 1204-1211. http://dx.doi.org/10.1002/2211-5463.12647 PMID: 31033227

[112] Becker, H.M.; Hirnet, D.; Fecher-Trost, C.; Sültemeyer, D.; Deitmer, J.W. Transport activity of MCT1 expressed in Xenopus oocytes is increased by interaction with carbonic anhydrase. *J. Biol. Chem.,* **2005**, *280*(48), 39882-39889. http://dx.doi.org/10.1074/jbc.M503081200 PMID: 16174776

[113] Becker, H.M.; Klier, M.; Schüler, C.; McKenna, R.; Deitmer, J.W. Intramolecular proton shuttle supports not only catalytic but also noncatalytic function of carbonic anhydrase II. *Proc. Natl. Acad. Sci. USA,* **2011**, *108*(7), 3071-3076. http://dx.doi.org/10.1073/pnas.1014293108 PMID: 21282642

[114] Klier, M.; Schüler, C.; Halestrap, A.P.; Sly, W.S.; Deitmer, J.W.; Becker, H.M. Transport activity of the high-affinity monocarboxylate transporter MCT2 is enhanced by extracellular carbonic anhydrase IV but not by intracellular carbonic anhydrase II. *J. Biol. Chem.,* **2011**, *286*(31), 27781-27791. http://dx.doi.org/10.1074/jbc.M111.255331 PMID: 21680735

[115] Jamali, S.; Klier, M.; Ames, S.; Barros, L.F.; McKenna, R.; Deitmer, J.W.; Becker, H.M. Hypoxia-induced carbonic anhydrase IX facilitates lactate flux in human breast cancer cells by non-catalytic function. *Sci. Rep.,* **2015**, *5*, 13605. http://dx.doi.org/10.1038/srep13605 PMID: 26337752

[116] Ames, S.; Andring, J.T.; McKenna, R.; Becker, H.M. CAIX Forms a Transport Metabolon with Monocarboxylate Transporters in Human Breast Cancer Cells. *Oncogene,* **2019**, 1-14. PMID: 31723238

[117] Becker, H.M.; Deitmer, J.W. Carbonic anhydrase II increases the activity of the human electrogenic Na+/HCO3- cotransporter. *J. Biol. Chem.,* **2007**, *282*(18), 13508-13521. http://dx.doi.org/10.1074/jbc.M700066200 PMID: 17353189

[118] Dahl, N.K.; Jiang, L.; Chernova, M.N.; Stuart-Tilley, A.K.; Shmukler, B.E.; Alper, S.L. Deficient HCO3- transport in an AE1 mutant with normal Cl- transport can be rescued by carbonic anhydrase II presented on an adjacent AE1 protomer. *J. Biol. Chem.,* **2003**, *278*(45), 44949-44958. http://dx.doi.org/10.1074/jbc.M308660200 PMID: 12933803

[119] Becker, H.M Transport of Lactate: Characterization of the Transporters Involved in Transport at the Plasma Membrane by Heterologous Protein Expression in Xenopus Oocytes. In:*Brain Energy Metabolism*; Hirrlinger, J; Waagepetersen, H.S Neuromethods; Springer New York,, **2014**, p. 25–43.

[120] Aspatwar, A.; Becker, H.M.; Parvathaneni, N.K.; Hammaren, M.; Svorjova, A.; Barker, H.; Supuran, C.T.; Dubois, L.; Lambin, P.; Parikka, M.; Parkkila, S.; Winum, J-Y. Nitroimidazole-based inhibitors DTP338 and DTP348 are safe for zebrafish embryos and efficiently inhibit the activity of human CA IX in Xenopus oocytes. *J. Enzyme Inhib. Med. Chem.,* **2018**, *33*(1), 1064-1073. http://dx.doi.org/10.1080/14756366.2018.1482285 PMID: 29909747

[121] Lindskog, S. Purification and properties of bovine erythrocyte carbonic anhydrase. *Biochim. Biophys. Acta,* **1960**, *39*, 218-226. http://dx.doi.org/10.1016/0006-3002(60)90156-6 PMID: 14417215

[122] Nyman, P.O. Purification and properties of carbonic anhydrase from human erythrocytes. *Biochim. Biophys. Acta,* **1961**, *52*, 1-12. http://dx.doi.org/10.1016/0006-3002(61)90898-8 PMID: 14480808

[123] Blackburn, M.N.; Chirgwin, J.M.; James, G.T.; Kempe, T.D.; Parsons, T.; Register, A.M.; Schnackerz, K.D.; Noltmann, E.A. Pseudoisoenzymes of rabbit muscle phosphoglucose isomerase. *J. Biol. Chem.,* **1972**, *247*(4),

1170-1179.
PMID: 5010064
[124] Whitney, P.L.; Briggle, T.V. Membrane-associated carbonic anhydrase purified from bovine lung. *J. Biol. Chem.,* **1982**, *257*(20), 12056-12059.
PMID: 6811592
[125] Wistrand, P.J. Properties of membrane-bound carbonic anhydrase. *Ann. N. Y. Acad. Sci.,* **1984**, *429*, 195-206.
http://dx.doi.org/10.1111/j.1749-6632.1984.tb12333.x
PMID: 6430159
[126] Dodgson, S.J. Inhibition of mitochondrial carbonic anhydrase and ureagenesis: a discrepancy examined. *J. Appl. Physiol.,* **1987**, *63*(5), 2134-2141.
http://dx.doi.org/10.1152/jappl.1987.63.5.2134 PMID: 3121580
[127] Fernley, R.T.; Wright, R.D.; Coghlan, J.P. A novel carbonic anhydrase from the ovine parotid gland. *FEBS Lett.,* **1979**, *105*(2), 299-302.
http://dx.doi.org/10.1016/0014-5793(79)80634-1 PMID: 114424
[128] Murakami, H.; Sly, W.S. Purification and characterization of human salivary carbonic anhydrase. *J. Biol. Chem.,* **1987**, *262*(3), 1382-1388.
PMID: 2433278
[129] Lehtonen, J.; Shen, B.; Vihinen, M.; Casini, A.; Scozzafava, A.; Supuran, C.T.; Parkkila, A-K.; Saarnio, J.; Kivelä, A.J.; Waheed, A.; Sly, W.S.; Parkkila, S. Characterization of CA XIII, a novel member of the carbonic anhydrase isozyme family. *J. Biol. Chem.,* **2004**, *279*(4), 2719-2727.
http://dx.doi.org/10.1074/jbc.M308984200 PMID: 14600151
[130] Hilvo, M.; Baranauskiene, L.; Salzano, A.M.; Scaloni, A.; Matulis, D.; Innocenti, A.; Scozzafava, A.; Monti, S.M.; Di Fiore, A.; De Simone, G.; Lindfors, M.; Jänis, J.; Valjakka, J.; Pastoreková, S.; Pastorek, J.; Kulomaa, M.S.; Nordlund, H.R.; Supuran, C.T.; Parkkila, S. Biochemical characterization of CA IX, one of the most active carbonic anhydrase isozymes. *J. Biol. Chem.,* **2008**, *283*(41), 27799-27809.
http://dx.doi.org/10.1074/jbc.M800938200 PMID: 18703501
[131] Ferrer-Miralles, N.; Domingo-Espín, J.; Corchero, J.L.; Vázquez, E.; Villaverde, A. Microbial factories for recombinant pharmaceuticals. *Microb. Cell Fact.,* **2009**, *8*, 17.
http://dx.doi.org/10.1186/1475-2859-8-17 PMID: 19317892
[132] Narang, A.S.; Desai, D.S. Anticancer Drug Development.*Pharmaceutical Perspectives of Cancer Therapeutics*; Springer: New York, NY, USA, **2009**, pp. 49-92.
http://dx.doi.org/10.1007/978-1-4419-0131-6_2
[133] Pesch, K.; Simmert, U. Combined Assays for Lactose and Galactose by Enzymatic Reactions. *Milchw. Forsch.,* **1929**, *8*, 551.
[134] Twigg, R.S. Oxidation-Reduction Aspects of Resazurin. *Nature,* **1945**, *155*, 401-402.
http://dx.doi.org/10.1038/155401a0
[135] Yajko, D.M.; Madej, J.J.; Lancaster, M.V.; Sanders, C.A.; Cawthon, V.L.; Gee, B.; Babst, A.; Hadley, W.K. Colorimetric method for determining MICs of antimicrobial agents for Mycobacterium tuberculosis. *J. Clin. Microbiol.,* **1995**, *33*(9), 2324-2327.
http://dx.doi.org/10.1128/JCM.33.9.2324-2327.1995 PMID: 7494021
[136] Tiballi, R.N.; He, X.; Zarins, L.T.; Revankar, S.G.; Kauffman, C.A. Use of a colorimetric system for yeast susceptibility testing. *J. Clin. Microbiol.,* **1995**, *33*(4), 915-917.
http://dx.doi.org/10.1128/JCM.33.4.915-917.1995 PMID: 7790460
[137] Yamaguchi, H.; Uchida, K.; Nagino, K.; Matsunaga, T. Usefulness of a colorimetric method for testing antifungal drug susceptibilities of Aspergillus species to voriconazole. *J. Infect. Chemother.,* **2002**, *8*(4), 374-377.
http://dx.doi.org/10.1007/s10156-002-0201-Y PMID: 12525904
[138] Mikus, J.; Steverding, D. A simple colorimetric method to screen drug cytotoxicity against Leishmania using the dye Alamar Blue. *Parasitol. Int.,* **2000**, *48*(3), 265-269.
http://dx.doi.org/10.1016/S1383-5769(99)00020-3 PMID: 11227767
[139] Byth, H.A.; Mchunu, B.I.; Dubery, I.A.; Bornman, L. Assessment of a simple, non-toxic Alamar blue cell survival assay to monitor tomato cell viability. *Phytochem. Anal.,* **2001**, *12*(5), 340-346.
http://dx.doi.org/10.1002/pca.595 PMID: 11705263
[140] O'Brien, J.; Wilson, I.; Orton, T.; Pognan, F. Investigation of the Alamar Blue (resazurin) fluorescent dye for the assessment of mammalian cell cytotoxicity. *Eur. J. Biochem.,* **2000**, *267*(17), 5421-5426.
http://dx.doi.org/10.1046/j.1432-1327.2000.01606.x
PMID: 10951200
[141] de Fries, R.; Mitsuhashi, M. Quantification of mitogen induced human lymphocyte proliferation: comparison of alamarBlue assay to 3H-thymidine incorporation assay. *J. Clin. Lab. Anal.,* **1995**, *9*(2), 89-95.
http://dx.doi.org/10.1002/jcla.1860090203 PMID: 7714668
[142] Mboge, M.Y.; Chen, Z.; Wolff, A.; Mathias, J.V.; Tu, C.; Brown, K.D.; Bozdag, M.; Carta, F.; Supuran, C.T.; McKenna, R.; Frost, S.C. Selective inhibition of carbonic anhydrase IX over carbonic anhydrase XII in breast cancer cells using benzene sulfonamides: Disconnect between activity and growth inhibition. *PLoS One,* **2018**, *13*(11), e0207417.
http://dx.doi.org/10.1371/journal.pone.0207417 PMID: 30452451
[143] Marks, I.S.; Gardeen, S.S.; Kurdziel, S.J.; Nicolaou, S.T.; Woods, J.E.; Kularatne, S.A.; Low, P.S. Development of a Small Molecule Tubulysin B Conjugate for Treatment of Carbonic Anhydrase IX Receptor Expressing Cancers. *Mol. Pharm.,* **2018**, *15*(6), 2289-2296.
http://dx.doi.org/10.1021/acs.molpharmaceut.8b00139 PMID: 29715036
[144] van Kuijk, S.J.A.; Gieling, R.G.; Niemans, R.; Lieuwes, N.G.; Biemans, R.; Telfer, B.A.; Haenen, G.R.M.M.; Yaromina, A.; Lambin, P.; Dubois, L.J.; Williams, K.J. The Sulfamate Small Molecule CAIX Inhibitor S4 Modulates Doxorubicin Efficacy. *PLoS One,* **2016**, *11*(8), e0161040.
http://dx.doi.org/10.1371/journal.pone.0161040 PMID: 27513947
[145] Angeli, A.; Tanini, D.; Peat, T.S.; Di Cesare Mannelli, L.; Bartolucci, G.; Capperucci, A.; Ghelardini, C.; Supuran, C.T.; Carta, F. Discovery of New Selenoureido Analogues of 4-(4-Fluorophenylureido)benzenesulfonamide as Carbonic Anhydrase Inhibitors. *ACS Med. Chem. Lett.,* **2017**, *8*(9), 963-968.
http://dx.doi.org/10.1021/acsmedchemlett.7b00280 PMID: 28947945
[146] Meehan, J.; Ward, C.; Turnbull, A.; Bukowski-Wills, J.; Finch, A.J.; Jarman, E.J.; Xintaropoulou, C.; Martinez-

Perez, C.; Gray, M.; Pearson, M.; Mullen, P.; Supuran, C.T.; Carta, F.; Harrison, D.J.; Kunkler, I.H.; Langdon, S.P. Inhibition of pH regulation as a therapeutic strategy in hypoxic human breast cancer cells. *Oncotarget,* **2017**, *8*(26), 42857-42875. http://dx.doi.org/10.18632/oncotarget.17143 PMID: 28476026

[147] van Kuijk, S.J.A.; Parvathaneni, N.K.; Niemans, R.; van Gisbergen, M.W.; Carta, F.; Vullo, D.; Pastorekova, S.; Yaromina, A.; Supuran, C.T.; Dubois, L.J.; Winum, J-Y.; Lambin, P. New approach of delivering cytotoxic drugs towards CAIX expressing cells: A concept of dual-target drugs. *Eur. J. Med. Chem.,* **2017**, *127*, 691-702. http://dx.doi.org/10.1016/j.ejmech.2016.10.037 PMID: 27823879

[148] McIntyre, A.; Patiar, S.; Wigfield, S.; Li, J.L.; Ledaki, I.; Turley, H.; Leek, R.; Snell, C.; Gatter, K.; Sly, W.S.; Vaughan-Jones, R.D.; Swietach, P.; Harris, A.L. Carbonic anhydrase IX promotes tumor growth and necrosis *in vivo* and inhibition enhances anti-VEGF therapy. *Clin. Cancer Res.,* **2012**, *18*(11), 3100-3111. http://dx.doi.org/10.1158/1078-0432.CCR-11-1877 PMID: 22498007

[149] Chiche, J.; Ilc, K.; Laferrière, J.; Trottier, E.; Dayan, F.; Mazure, N.M.; Brahimi-Horn, M.C.; Pouysségur, J. Hypoxia-inducible carbonic anhydrase IX and XII promote tumor cell growth by counteracting acidosis through the regulation of the intracellular pH. *Cancer Res.,* **2009**, *69*(1), 358-368. http://dx.doi.org/10.1158/0008-5472.CAN-08-2470 PMID: 19118021

[150] Parks, S.K.; Cormerais, Y.; Durivault, J.; Pouyssegur, J. Genetic disruption of the pHi-regulating proteins Na+/H+ exchanger 1 (SLC9A1) and carbonic anhydrase 9 severely reduces growth of colon cancer cells. *Oncotarget,* **2017**, *8*(6), 10225-10237. http://dx.doi.org/10.18632/oncotarget.14379 PMID: 28055960

[151] Puck, T.T.; Marcus, P.I. A Rapid Method for Viable Cell Titration and Clone Production with Hela Cells in Tissue Culture: The Use of X-Irradiated Cells to Supply Conditioning Factors. *Proc. Natl. Acad. Sci. USA,* **1955**, *41*(7), 432-437. http://dx.doi.org/10.1073/pnas.41.7.432 PMID: 16589695

[152] Puck, T.T.; Marcus, P.I.; Cieciura, S.J. Clonal growth of mammalian cells in vitro; growth characteristics of colonies from single HeLa cells with and without a feeder layer. *J. Exp. Med.,* **1956**, *103*(2), 273-283. http://dx.doi.org/10.1084/jem.103.2.273 PMID: 13286432

[153] Liu, Q.; Wang, M.; Kern, A.M.; Khaled, S.; Han, J.; Yeap, B.Y.; Hong, T.S.; Settleman, J.; Benes, C.H.; Held, K.D.; Efstathiou, J.A.; Willers, H. Adapting a drug screening platform to discover associations of molecular targeted radiosensitizers with genomic biomarkers. *Mol. Cancer Res.,* **2015**, *13*(4), 713-720. http://dx.doi.org/10.1158/1541-7786.MCR-14-0570 PMID: 25667133

[154] Zanoni, M.; Piccinini, F.; Arienti, C.; Zamagni, A.; Santi, S.; Polico, R.; Bevilacqua, A.; Tesei, A. 3D tumor spheroid models for *in vitro* therapeutic screening: a systematic approach to enhance the biological relevance of data obtained. *Sci. Rep.,* **2016**, *6*, 19103. http://dx.doi.org/10.1038/srep19103 PMID: 26752500

[155] Baker, B.M.; Chen, C.S. Deconstructing the third dimension: how 3D culture microenvironments alter cellular cues. *J. Cell Sci.,* **2012**, *125*(Pt 13), 3015-3024. http://dx.doi.org/10.1242/jcs.079509 PMID: 22797912

[156] Kimlin, L.C.; Casagrande, G.; Virador, V.M. In vitro three--dimensional (3D) models in cancer research: an update. *Mol. Carcinog.,* **2013**, *52*(3), 167-182. http://dx.doi.org/10.1002/mc.21844 PMID: 22162252

[157] Abo-Ashour, M.F.; Eldehna, W.M.; Nocentini, A.; Bonardi, A.; Bua, S.; Ibrahim, H.S.; Elaasser, M.M.; Kryštof, V.; Jorda, R.; Gratteri, P.; Abou-Seri, S.M.; Supuran, C.T. 3-Hydrazinoisatin-based benzenesulfonamides as novel carbonic anhydrase inhibitors endowed with anticancer activity: Synthesis, in vitro biological evaluation and in silico insights. *Eur. J. Med. Chem.,* **2019**, *184*, 111768. http://dx.doi.org/10.1016/j.ejmech.2019.111768 PMID: 31629164

[158] Dubois, L.; Peeters, S.; Lieuwes, N.G.; Geusens, N.; Thiry, A.; Wigfield, S.; Carta, F.; McIntyre, A.; Scozzafava, A.; Dogné, J-M.; Supuran, C.T.; Harris, A.L.; Masereel, B.; Lambin, P. Specific inhibition of carbonic anhydrase IX activity enhances the *in vivo* therapeutic effect of tumor irradiation. *Radiother. Oncol.,* **2011**, *99*(3), 424-431. http://dx.doi.org/10.1016/j.radonc.2011.05.045 PMID: 21676479

[159] Dubois, L.; Peeters, S.G.J.A.; van Kuijk, S.J.A.; Yaromina, A.; Lieuwes, N.G.; Saraya, R.; Biemans, R.; Rami, M.; Parvathaneni, N.K.; Vullo, D.; Vooijs, M.; Supuran, C.T.; Winum, J-Y.; Lambin, P. Targeting carbonic anhydrase IX by nitroimidazole based sulfamides enhances the therapeutic effect of tumor irradiation: a new concept of dual targeting drugs. *Radiother. Oncol.,* **2013**, *108*(3), 523-528. http://dx.doi.org/10.1016/j.radonc.2013.06.018 PMID: 23849171

[160] Lee, S-H.; McIntyre, D.; Honess, D.; Hulikova, A.; Pacheco-Torres, J.; Cerdán, S.; Swietach, P.; Harris, A.L.; Griffiths, J.R. Carbonic anhydrase IX is a pH-stat that sets an acidic tumour extracellular pH in vivo. *Br. J. Cancer,* **2018**, *119*(5), 622-630. http://dx.doi.org/10.1038/s41416-018-0216-5 PMID: 30206370

[161] Svastová, E.; Hulíková, A.; Rafajová, M.; Zat'ovicová, M.; Gibadulinová, A.; Casini, A.; Cecchi, A.; Scozzafava, A.; Supuran, C.T.; Pastorek, J.; Pastoreková, S. Hypoxia activates the capacity of tumor-associated carbonic anhydrase IX to acidify extracellular pH. *FEBS Lett.,* **2004**, *577*(3), 439-445. http://dx.doi.org/10.1016/j.febslet.2004.10.043 PMID: 15556624

[162] Dubois, L.; Douma, K.; Supuran, C.T.; Chiu, R.K.; van Zandvoort, M.A.M.J.; Pastoreková, S.; Scozzafava, A.; Wouters, B.G.; Lambin, P. Imaging the hypoxia surrogate marker CA IX requires expression and catalytic activity for binding fluorescent sulfonamide inhibitors. *Radiother. Oncol.,* **2007**, *83*(3), 367-373. http://dx.doi.org/10.1016/j.radonc.2007.04.018 PMID: 17502120

[163] Rami, M.; Dubois, L.; Parvathaneni, N-K.; Alterio, V.; van Kuijk, S.J.A.; Monti, S.M.; Lambin, P.; De Simone, G.; Supuran, C.T.; Winum, J-Y. Hypoxia-targeting carbonic anhydrase IX inhibitors by a new series of nitroimidazole--sulfonamides/sulfamides/sulfamates. *J. Med. Chem.,* **2013**, *56*(21), 8512-8520. http://dx.doi.org/10.1021/jm4009532 PMID: 24128000

[164] Silverman, D.N. Carbonic anhydrase catalyzed oxygen-18 exchange between bicarbonate and water. *Arch. Biochem. Biophys.,* **1973**, *155*(2), 452-457.

http://dx.doi.org/10.1016/0003-9861(73)90136-7 PMID: 4196184

[165] Itada, N.; Forster, R.E. Carbonic anhydrase activity in intact red blood cells measured with 18O exchange. *J. Biol. Chem.,* **1977**, *252*(11), 3881-3890. PMID: 405387

[166] Silverman, D.N.; Backman, L.; Tu, C. Role of hemoglobin in proton transfer to the active site of carbonic anhydrase. *J. Biol. Chem.,* **1979**, *254*(8), 2588-2591. PMID: 107161

[167] Endeward, V.; Gros, G. Low carbon dioxide permeability of the apical epithelial membrane of guinea-pig colon. *J. Physiol.,* **2005**, *567*(Pt 1), 253-265. http://dx.doi.org/10.1113/jphysiol.2005.085761 PMID: 15932894

[168] Sultemeyer, D.F.; Queen's , U.; Fock , H.P.; Canvin, D.T. Mass Spectrometric Measurement of Intracellular Carbonic Anhydrase Activity in High and Low Ci Cells of Chlamydomonas. Studies Using 18O Exchange with 13C/18O Labeled Bicarbonate.*Plant physiology (USA)*; , **1990**.

[169] Badger, M.R.; Price, G.D. Carbonic Anhydrase Activity Associated with the Cyanobacterium Synechococcus PCC7942. *Plant Physiol.,* **1989**, *89*(1), 51-60. http://dx.doi.org/10.1104/pp.89.1.51 PMID: 16666546

[170] Fisher, Z.; Hernandez Prada, J.A.; Tu, C.; Duda, D.; Yoshioka, C.; An, H.; Govindasamy, L.; Silverman, D.N.; McKenna, R. Structural and kinetic characterization of active-site histidine as a proton shuttle in catalysis by human carbonic anhydrase II. *Biochemistry,* **2005**, *44*(4), 1097-1105. http://dx.doi.org/10.1021/bi0480279 PMID: 15667203

[171] Ames, S.; Pastorekova, S.; Becker, H.M. The proteoglycan-like domain of carbonic anhydrase IX mediates non-catalytic facilitation of lactate transport in cancer cells. *Oncotarget,* **2018**, *9*(46), 27940-27957. http://dx.doi.org/10.18632/oncotarget.25371 PMID: 29963253

[172] Endeward, V.; Musa-Aziz, R.; Cooper, G.J.; Chen, L-M.; Pelletier, M.F.; Virkki, L.V.; Supuran, C.T.; King, L.S.; Boron, W.F.; Gros, G. Evidence that aquaporin 1 is a major pathway for CO2 transport across the human erythrocyte membrane. *FASEB J.,* **2006**, *20*(12), 1974-1981. http://dx.doi.org/10.1096/fj.04-3300com PMID: 17012249

[173] Arias-Hidalgo, M.; Al-Samir, S.; Weber, N.; Geers-Knörr, C.; Gros, G.; Endeward, V. CO_2 permeability and carbonic anhydrase activity of rat cardiomyocytes. *Acta Physiol. (Oxf.),* **2017**, *221*(2), 115-128. http://dx.doi.org/10.1111/apha.12887 PMID: 28429509

[174] Arias-Hidalgo, M.; Yuan, Q.; Carta, F.; Supuran, C.T.; Gros, G.; Endeward, V. CO2 Permeability of Rat Hepatocytes and Relation of CO2 Permeability to CO2 Production. *Cell. Physiol. Biochem.,* **2018**, *46*(3), 1198-1208. http://dx.doi.org/10.1159/000489070 PMID: 29684917

[175] Arias-Hidalgo, M.; Hegermann, J.; Tsiavaliaris, G.; Carta, F.; Supuran, C.T.; Gros, G.; Endeward, V. CO2 and HCO3- Permeability of the Rat Liver Mitochondrial Membrane. *Cell. Physiol. Biochem.,* **2016**, *39*(5), 2014-2024. http://dx.doi.org/10.1159/000447897 PMID: 27771717

[176] Itel, F.; Al-Samir, S.; Öberg, F.; Chami, M.; Kumar, M.; Supuran, C.T.; Deen, P.M.T.; Meier, W.; Hedfalk, K.; Gros, G.; Endeward, V. CO2 permeability of cell membranes is regulated by membrane cholesterol and protein gas channels. *FASEB J.,* **2012**, *26*(12), 5182-5191. http://dx.doi.org/10.1096/fj.12-209916 PMID: 22964306

[177] Mullard, A. 2019 FDA Drug Approvals. *Nat. Rev. Drug Discov.,* **2020**. http://dx.doi.org/10.1038/d41573-019-00014-x PMID: 30710142

[178] Mullard, A. 2018 FDA drug approvals. *Nat. Rev. Drug Discov.,* **2019**, *18*(2), 85-89. http://dx.doi.org/10.1038/d41573-019-00014-x PMID: 30710142

[179] Hingorani, A.D.; Kuan, V.; Finan, C.; Kruger, F.A.; Gaulton, A.; Chopade, S.; Sofat, R.; MacAllister, R.J.; Overington, J.P.; Hemingway, H.; Denaxas, S.; Prieto, D.; Casas, J.P. Improving the odds of drug development success through human genomics: modelling study. *Sci. Rep.,* **2019**, *9*(1), 18911. http://dx.doi.org/10.1038/s41598-019-54849-w PMID: 31827124

[180] Dowden, H.; Munro, J. Trends in clinical success rates and therapeutic focus. *Nat. Rev. Drug Discov.,* **2019**, *18*(7), 495-496. http://dx.doi.org/10.1038/d41573-019-00074-z PMID: 31267067

[181] Pastoreková, S.; Parkkila, S.; Parkkila, A.K.; Opavský, R.; Zelník, V.; Saarnio, J.; Pastorek, J. Carbonic anhydrase IX, MN/CA IX: analysis of stomach complementary DNA sequence and expression in human and rat alimentary tracts. *Gastroenterology,* **1997**, *112*(2), 398-408. http://dx.doi.org/10.1053/gast.1997.v112.pm9024293 PMID: 9024293

[182] Pastorekova, S.; Gillies, R.J. The role of carbonic anhydrase IX in cancer development: links to hypoxia, acidosis, and beyond. *Cancer Metastasis Rev.,* **2019**, *38*(1-2), 65-77. http://dx.doi.org/10.1007/s10555-019-09799-0 PMID: 31076951

[183] Alterio, V.; Di Fiore, A.; D'Ambrosio, K.; Supuran, C.T.; De Simone, G. Multiple binding modes of inhibitors to carbonic anhydrases: how to design specific drugs targeting 15 different isoforms? *Chem. Rev.,* **2012**, *112*(8), 4421-4468. http://dx.doi.org/10.1021/cr200176r PMID: 22607219

[184] Cecchi, A.; Hulikova, A.; Pastorek, J.; Pastoreková, S.; Scozzafava, A.; Winum, J-Y.; Montero, J-L.; Supuran, C.T. Carbonic anhydrase inhibitors. Design of fluorescent sulfonamides as probes of tumor-associated carbonic anhydrase IX that inhibit isozyme IX-mediated acidification of hypoxic tumors. *J. Med. Chem.,* **2005**, *48*(15), 4834-4841. http://dx.doi.org/10.1021/jm0501073 PMID: 16033263

[185] Lau, J.; Lin, K-S.; Bénard, F. Past, Present, and Future: Development of Theranostic Agents Targeting Carbonic Anhydrase IX. *Theranostics,* **2017**, *7*(17), 4322-4339. http://dx.doi.org/10.7150/thno.21848 PMID: 29158829

[186] Chaturvedi, S.K.; Ma, J.; Zhao, H.; Schuck, P. Use of fluorescence-detected sedimentation velocity to study high--affinity protein interactions. *Nat. Protoc.,* **2017**, *12*(9), 1777-1791. http://dx.doi.org/10.1038/nprot.2017.064 PMID: 28771239

[187] Zhao, H.; Mayer, M.L.; Schuck, P. Analysis of protein interactions with picomolar binding affinity by fluorescence-detected sedimentation velocity. *Anal. Chem.,* **2014**, *86*(6), 3181-3187. http://dx.doi.org/10.1021/ac500093m PMID: 24552356

[188] Jerabek-Willemsen, M.; André, T.; Wanner, R.; Roth, H.M.; Duhr, S.; Baaske, P.; Breitsprecher, D. MicroScale Thermophoresis: Interaction Analysis and Beyond. *J. Mol. Struct.,* **2014**, *1077*, 101-113. http://dx.doi.org/10.1016/j.molstruc.2014.03.009

[189] Zubrienė, A.; Matulienė, J.; Baranauskienė, L.; Jachno, J.; Torresan, J.; Michailovienė, V.; Cimmperman, P.; Matulis, D. Measurement of nanomolar dissociation constants by titration calorimetry and thermal shift assay - radicicol binding to Hsp90 and ethoxzolamide binding to CAII. *Int. J. Mol. Sci.,* **2009**, *10*(6), 2662-2680. http://dx.doi.org/10.3390/ijms10062662 PMID: 19582223

[190] Talibov, V.O.; Linkuvienė, V.; Matulis, D.; Danielson, U.H. Kinetically Selective Inhibitors of Human Carbonic Anhydrase Isozymes I, II, VII, IX, XII, and XIII. *J. Med. Chem.,* **2016**, *59*(5), 2083-2093. http://dx.doi.org/10.1021/acs.jmedchem.5b01723 PMID: 26805033

[191] Koyuncu, I.; Gonel, A.; Durgun, M.; Kocyigit, A.; Yuksekdag, O.; Supuran, C.T. Assessment of the antiproliferative and apoptotic roles of sulfonamide carbonic anhydrase IX inhibitors in HeLa cancer cell line. *J. Enzyme Inhib. Med. Chem.,* **2019**, *34*(1), 75-86. http://dx.doi.org/10.1080/14756366.2018.1524380 PMID: 30362386

[192] Abdelrahman, M.A.; Eldehna, W.M.; Nocentini, A.; Bua, S.; Al-Rashood, S.T.; Hassan, G.S.; Bonardi, A.; Almehizia, A.A.; Alkahtani, H.M.; Alharbi, A.; Gratteri, P.; Supuran, C.T. Novel Diamide-Based Benzenesulfonamides as Selective Carbonic Anhydrase IX Inhibitors Endowed with Antitumor Activity: Synthesis, Biological Evaluation and In Silico Insights. *Int. J. Mol. Sci.,* **2019**, *20*(10), 20. http://dx.doi.org/10.3390/ijms20102484 PMID: 31137489

[193] Svastova, E.; Witarski, W.; Csaderova, L.; Kosik, I.; Skvarkova, L.; Hulikova, A.; Zatovicova, M.; Barathova, M.; Kopacek, J.; Pastorek, J.; Pastorekova, S. Carbonic anhydrase IX interacts with bicarbonate transporters in lamellipodia and increases cell migration via its catalytic domain. *J. Biol. Chem.,* **2012**, *287*(5), 3392-3402. http://dx.doi.org/10.1074/jbc.M111.286062 PMID: 22170054

[194] Swayampakula, M.; McDonald, P.C.; Vallejo, M.; Coyaud, E.; Chafe, S.C.; Westerback, A.; Venkateswaran, G.; Shankar, J.; Gao, G.; Laurent, E.M.N.; Lou, Y.; Bennewith, K.L.; Supuran, C.T.; Nabi, I.R.; Raught, B.; Dedhar, S. The interactome of metabolic enzyme carbonic anhydrase IX reveals novel roles in tumor cell migration and invadopodia/MMP14-mediated invasion. *Oncogene,* **2017**, *36*(45), 6244-6261. http://dx.doi.org/10.1038/onc.2017.219 PMID: 28692057

[195] Parks, S.K.; Chiche, J.; Pouysségur, J. Disrupting proton dynamics and energy metabolism for cancer therapy. *Nat. Rev. Cancer,* **2013**, *13*(9), 611-623. http://dx.doi.org/10.1038/nrc3579 PMID: 23969692

[196] Federici, C.; Lugini, L.; Marino, M.L.; Carta, F.; Iessi, E.; Azzarito, T.; Supuran, C.T.; Fais, S. Lansoprazole and carbonic anhydrase IX inhibitors sinergize against human melanoma cells. *J. Enzyme Inhib. Med. Chem.,* **2016**, *31*(sup1), 119-125. http://dx.doi.org/10.1080/14756366.2016.1177525 PMID: 27142956

[197] Liskova, V.; Hudecova, S.; Lencesova, L.; Iuliano, F.; Sirova, M.; Ondrias, K.; Pastorekova, S.; Krizanova, O. Type 1 Sodium Calcium Exchanger Forms a Complex with Carbonic Anhydrase IX and Via Reverse Mode Activity Contributes to pH Control in Hypoxic Tumors. *Cancers (Basel),* **2019**, *11*(8), 11. http://dx.doi.org/10.3390/cancers11081139 PMID: 31395807

[198] Becker, H.M. Carbonic anhydrase IX and acid transport in cancer. *Br. J. Cancer,* **2020**, *122*(2), 157-167. http://dx.doi.org/10.1038/s41416-019-0642-z PMID: 31819195

[199] McDonald, P.C.; Chafe, S.C.; Brown, W.S.; Saberi, S.; Swayampakula, M.; Venkateswaran, G.; Nemirovsky, O.; Gillespie, J.A.; Karasinska, J.M.; Kalloger, S.E.; Supuran, C.T.; Schaeffer, D.F.; Bashashati, A.; Shah, S.P.; Topham, J.T.; Yapp, D.T.; Li, J.; Renouf, D.J.; Stanger, B.Z.; Dedhar, S. Regulation of pH by Carbonic Anhydrase 9 Mediates Survival of Pancreatic Cancer Cells With Activated KRAS in Response to Hypoxia. *Gastroenterology,* **2019**, *157*(3), 823-837. http://dx.doi.org/10.1053/j.gastro.2019.05.004 PMID: 31078621

[200] Hedlund, E.E.; McDonald, P.C.; Nemirovsky, O.; Awrey, S.; Jensen, L.D.E.; Dedhar, S. Harnessing Induced Essentiality: Targeting Carbonic Anhydrase IX and Angiogenesis Reduces Lung Metastasis of Triple Negative Breast Cancer Xenografts. *Cancers (Basel),* **2019**, *11*(7), 11. http://dx.doi.org/10.3390/cancers11071002 PMID: 31319613

SCIENTIFIC REPORTS
nature research

OPEN

Engineered Carbonic Anhydrase VI-Mimic Enzyme Switched the Structure and Affinities of Inhibitors

Received: 17 February 2019
Accepted: 15 August 2019
Published online: 03 September 2019

Justina Kazokaitė[1,6], Visvaldas Kairys[2], Joana Smirnovienė[1], Alexey Smirnov[1], Elena Manakova[3], Martti Tolvanen[4], Seppo Parkkila[5] & Daumantas Matulis[1]

Secretory human carbonic anhydrase VI (CA VI) has emerged as a potential drug target due to its role in pathological states, such as excess acidity-caused dental caries and injuries of gastric epithelium. Currently, there are no available CA VI-selective inhibitors or crystallographic structures of inhibitors bound to CA VI. The present study focuses on the site-directed CA II mutant mimicking the active site of CA VI for inhibitor screening. The interactions between CA VI-mimic and a series of benzenesulfonamides were evaluated by fluorescent thermal shift assay, stopped-flow CO_2 hydration assay, isothermal titration calorimetry, and X-ray crystallography. Kinetic parameters showed that A65T, N67Q, F130Y, V134Q, L203T mutations did not influence catalytic properties of CA II, but inhibitor affinities resembled CA VI, exhibiting up to 0.16 nM intrinsic affinity for CA VI-mimic. Structurally, binding site of CA VI-mimic was found to be similar to CA VI. The ligand interactions with mutated side chains observed in three crystallographic structures allowed to rationalize observed variation of binding modes and experimental binding affinities to CA VI. This integrative set of kinetic, thermodynamic, and structural data revealed CA VI-mimic as a useful model to design CA VI-specific inhibitors which could be beneficial for novel therapeutic applications.

Human carbonic anhydrases (CAs) are widespread enzymes known for over 80 years[1]. CAs regulate both intracellular and extracellular pH homeostasis through the catalysis of reversible carbon dioxide hydration to bicarbonate and proton. To date, there are twelve catalytically active human CAs, which display diverse sub-cellular localization, tissue-specific expression, and kinetic properties[2,3]. Among a broad spectrum of CA-linked research areas, clinical investigation is a major focus due to the implication of abnormal CA levels or their activities in diseases, such as glaucoma[4], epilepsy[5], obesity[6], and cancer[7]. Therefore, many efforts have been dedicated over years to design CA isoform-selective compounds exhibiting sufficient affinity properties[8]. These derivatives would be prospective for the translation into the clinic because of therapeutic efficacy without inducing undesired side effects caused by inhibited vital off-target CAs. However, it is a challenging task because of the high structural homology among human CAs[9].

CA VI is the only secreted human CA isoform found in saliva[10], serum[11], milk[12], respiratory airways[13], and alimentary canal[14]. Several studies have indicated the immunological CA VI function[15,16] and have presented associations of CA VI with bitter taste perception[17,18] or protection of excess acidity-caused complications, including dental caries[19,20] and injuries of esophageal or gastric epithelium[21]. The link of CA VI with certain cancers, such as that of salivary glands, has been speculated by gene comparison study[22], which have shown close relation of CA VI with CA IX, a marker of tumors[23]. Thus, there is a demand for effective and selective CA VI inhibitors, which would be relevant to determine the exact physiological role of CA VI.

For more than five decades, the most widely applied method in the search of CA isoform selective inhibitors has been the stopped-flow assay of the catalytic activity of CO_2 hydration (SFA)[24,25]. However, SFA has several

[1]Department of Biothermodynamics and Drug Design, Institute of Biotechnology, Vilnius University, Saulėtekio 7, Vilnius, LT-10257, Lithuania. [2]Department of Bioinformatics, Institute of Biotechnology, Vilnius University, Saulėtekio 7, Vilnius, LT-10257, Lithuania. [3]Department of Protein-DNA Interactions, Institute of Biotechnology, Vilnius University, Saulėtekio 7, Vilnius, LT-10257, Lithuania. [4]Department of Information Technology, University of Turku, FI-20520, Turku, Finland. [5]Tampere University, Faculty of Medicine and Health Technology; Fimlab Ltd, Tampere University Hospital, Arvo Ylpön katu 34, FI-33520, Tampere, Finland. [6]Present address: Division of Biochemistry, the Netherlands Cancer Institute, Amsterdam, the Netherlands. Correspondence and requests for materials should be addressed to J.K. (email: kazokaite@ibt.lt)

limitations, such as the largely unknown CO_2 concentration and unfeasibility to measure inhibition constant below several nM[26]. Therefore, biophysical techniques, such as the fluorescent thermal shift assay (FTSA) and isothermal titration calorimetry (ITC), are promising alternatives to screen CA-targeting derivatives. FTSA is a high-throughput method exhibiting minimized biomolecule consumption and low limitations for binding affinity, thereby both strong (picomolar) and weak (millimolar) compounds can be identified during the same experiment[26–29]. ITC allows the direct determination of stoichiometry and thermodynamic parameters, such as affinity, enthalpy, entropy, and heat-capacity, during a single or several titration experiments but it demands relatively large quantities of proteins and has limitations for assessing the binding affinity[26,30,31].

Importantly, two types of variables can be distinguished when binding reactions are carried out by FTSA or ITC: the *observed* parameters obtained from experimental setup and the *intrinsic* values calculated according to the corresponding observed data. Most studies on the development of CA inhibitors usually provide only observed binding parameters, which are dependent on experimental conditions and might be misleading. Both the CA and inhibitor exist in different protonation states in the solution compared with ones in the complex. Therefore, protonation-deprotonation reactions are required to initiate the binding of inhibitor to CA. Only intrinsic values subtract energetic contribution of binding-linked protonation events and thus are relevant for the rational drug design[32–35].

Due to the recent advances in the structural and *in silico* biology, production of target recombinant proteins, including CAs, in large quantities is of high demand for *in vitro* inhibitor screening of drug-candidates during preclinical research. The literature lists a number of host cells for expression of recombinant proteins. Among microorganisms, the enterobacterium *Escherichia coli* (*E. coli*) is selected frequently owing to numerous advantages, such as rapid growth, easy genetic manipulation, and relative cost effectiveness[36,37]. However, the stability of heterologous protein in *E. coli* can be influenced by the several factors, including mRNA instability, codon bias, protein aggregation, toxicity, and lack of post-translational modification[38,39]. Therefore, different, more efficient strategies to obtain functionally active recombinant proteins in high yield are required for screens of chemical compounds with the aim to identify hits in the initial stages of drug discovery.

The goal of the present study was to design a CA II-based CA VI model protein, named as CA VI-mimic, for the search of CA-isoform selective inhibitors. As CA VI-mimic, mutant of CA II containing five point mutations, such as A65T, N67Q, F130Y, V134Q, L203T, was generated via site-directed mutagenesis. CA II was selected as a core for CA VI-mimic because purification yield of CA II from *E. coli* is ~10-fold higher than CA VI, CA II has highest catalytic efficiency among CAs, and CA II is confirmed as a stable CA protein for X-ray crystallography. Here enzymatic activity and inhibition of CA II, CAVI-mimic, and CA VI was determined by SFA. Biophysical studies on inhibitor binding to CA II, CA VI-mimic, and CA VI were carried out by ITC and FTSA. X-ray crystallography and computational modeling were used to compare positions of several inhibitors in the active sites of CA II, CA VI-mimic, and CA VI. Observed and intrinsic thermodynamics were in line with structural results which confirmed the relevance of CA VI-mimic as a CA VI model protein. The most tested benzenesulfonamides bound to CA VI-mimic in a manner corresponding to their interactions with CA VI but not CA II, thereby emphasizing suitability of the investigated CA II mutant mimicking CA VI for inhibitor screening.

Results

Enzymatic activity of CA VI-mimic correlates with CA II, but not CA VI. Studies on inhibitor selectivity towards diverse human CA isoforms are important to develop efficient compounds for the treatment of diseases caused by abnormal levels or activities of a particular CA isoform. Therefore, it is essential to evaluate inhibitor affinity to all human CAs, including CA VI. Since our previous study[40] indicated a low yield of recombinant CA VI from *E. coli*, we generated CA II mutant as a CA VI model protein (CA VI-mimic) for inhibitor screening. Inhibitor affinities towards CA II and CA VI-mimic were expected to differ in the way imitating inhibitor binding to CA VI, but not CA II (Fig. 1A). Thus, negligible differences between inhibitor affinities towards CA VI and CA VI-mimic were presumed. According to computational modeling, five point mutations A65T, N67Q, F130Y, V134Q, L203T were chosen (Figs 1B–D and S1) and introduced into the active site of CA II.

The catalytic activity of CA VI and CA VI-mimic to catalyze CO_2 hydration reaction was measured by SFA (Figs 2A and S3). Analysis of kinetic data showed that site-directed mutagenesis did not significantly affect either the catalytic activity or pK_a of zinc-bound water molecule of CA II. Catalytic constants (k_{cat}) of CA II and CA VI-mimic did not differ (k_{cat} values were $6.0 \times 10^5\,s^{-1}$), whereas k_{cat} for CA VI was lower than CA VI-mimic by 3-fold ($1.9 \times 10^5\,s^{-1}$). In the pH range 5.9–7.0 Michaelis constants (K_M) as well as k_{cat} values of the carbon dioxide hydration reaction were comparable: 7.3 ± 2.9 mM for CA II, 8.8 ± 1.8 mM for CA VI-mimic and 9.9 ± 3.2 mM for CA VI. However, in the pH range 7.1–8.4 K_M values of CA VI-mimic (6.8 ± 2.0 mM) were closer to CA II (4.7 ± 1.0 mM) than to CA VI (11.3 ± 0.7 mM). Interestingly, maximum catalytic activity of CA VI was observed at pH 7.0–8.0 and it decreased at pH above 8.0. The determined pK_a value of zinc-bound water molecule of CA VI was 6.6 ± 0.2. The observed inhibition constants by SFA correlated with dissociation constants determined by FTSA. Typical SFA curves of CA II, CA VI-mimic and CA VI inhibition by compound **39** are shown in Fig. 2B.

Influence of buffer and pH for the observed binding affinity of ethoxzolamide to CA VI-mimic. Biophysical methods, such as ITC and FTSA, enable measurements of observed thermodynamics and thereafter calculations of intrinsic affinities. The observed binding profiles are altered by linked reactions and therefore, only intrinsic binding parameters can be correlated with compound structures, thereby revealing structural reasons for protein-ligand binding affinity.

Binding energetics are significantly affected by several protonation-deprotonation events which are necessary for the binding of sulfonamide derivative to CA. Only deprotonated sulfonamides can interact with the zinc cation in the active site of pronated CA, containing zinc-coordinated water molecule (protonated hydroxy group). In this study, observed and intrinsic affinities of inhibitor binding to CA VI-mimic were determined and compared

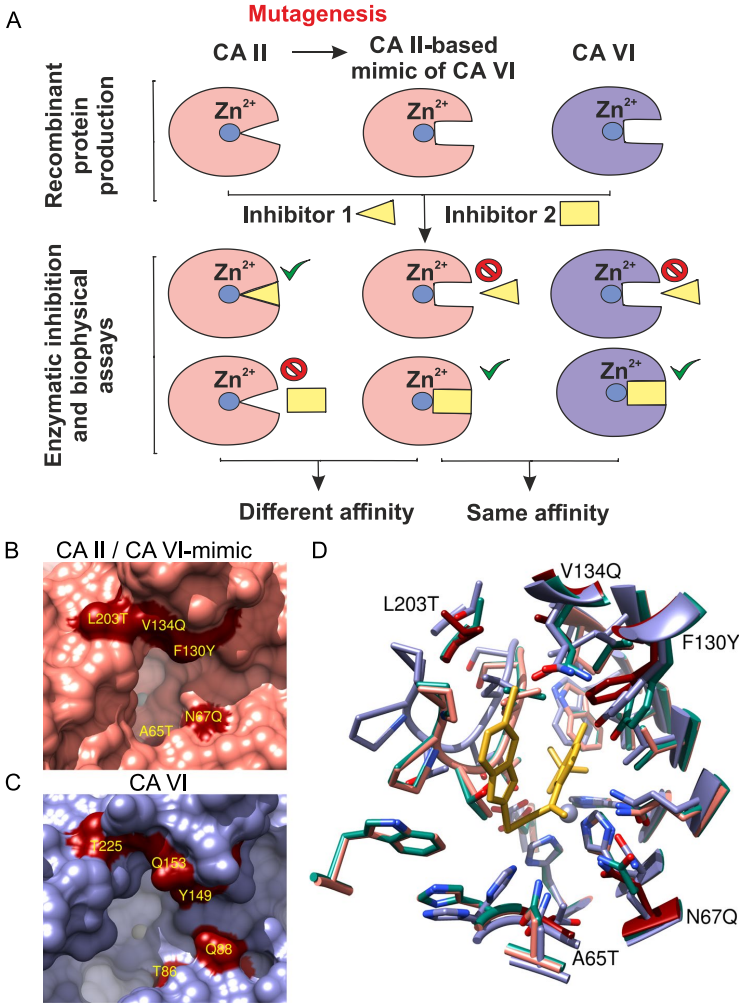


Figure 1. (**A**) The mimic of CA VI was prepared from CA II by site-directed mutagenesis of amino acids that differ between two CA isoforms. The CA VI-mimic protein served as a model of compound binding to CA VI. (**B**) Active site of CA II (PDB ID: 3KS3). Dark red molecular surfaces mark the positions of point mutations introduced in the active site of CA II to resemble CA VI by making a multiple-residue mutant of CA II (CA VI-mimic). (**C**) Active site of CA VI (PDB ID: 3FE4). The light blue areas are buried molecular surfaces between interacting molecules in the homodimeric complex. Dark red molecular surfaces mark the equivalent positions between multiple-residue mutant of CA II (CA VI-mimic) and CA VI. The labels belong to CA VI (CA II numbering). (**D**) Superposed structures of the binding pockets of CA II (rose; PDB ID: 3M96), CA VI (blue; PDB ID: 3FE4), and CA VI-mimic (green; PDB ID: 6QL2). The mutated residues of CA II are colored dark red. The zinc ion in the active site of each CA isoform is shown as a grayish sphere in panels (B–D).

to their affinities towards CA II and CA VI. The obtained experimental data by FTSA on interactions between ethoxzolamide (EZA) and CA VI-mimic in buffers with different pH showed that pH remarkably influenced the observed binding Gibbs energy (Δ_bG_{obs}, Fig. 3A). The dependence of Δ_bG_{obs} on pH has also been observed previously[40,41] when EZA binding to CA II or CA VI was measured. The strongest interaction was determined near neutral pH and became weaker both in acidic and alkaline pH. Sulfonamide group usually has pK_a in the range between 7 and 10, whereas CA isoforms have pK_a around 7. Therefore, diminished EZA affinity in acidic solution was because the fraction of binding-ready deprotonated form of EZA decreased by 10-fold with every pH unit. Similarly, EZA affinity decreased in alkaline solution because the fraction of binding-ready CA with the

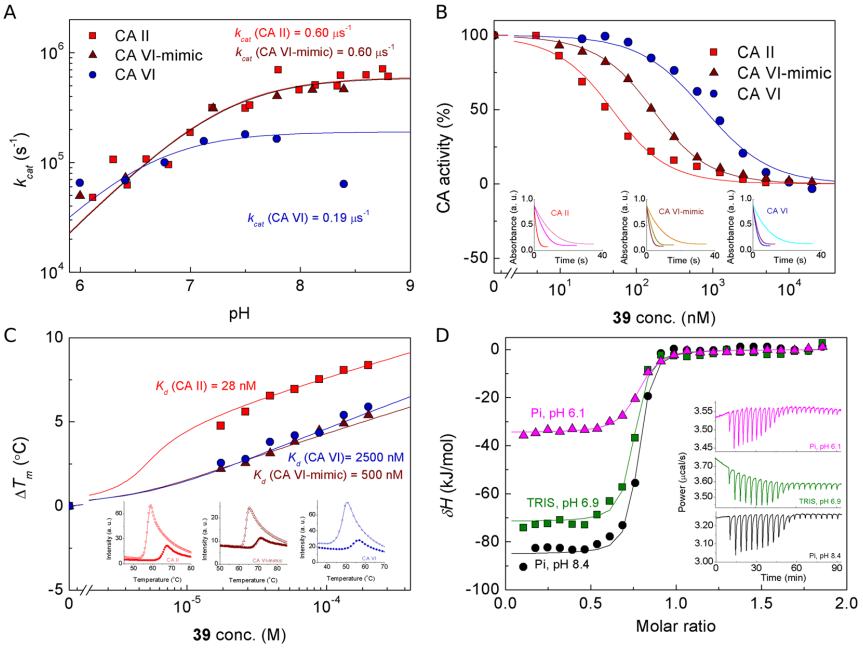


Figure 2. Catalytic activity, inhibition and binding profiles of CA II (red squares), CA VI-mimic (wine triangles) and CA VI (royal circles). (**A**) The plot of k_{cat} dependence on pH by stopped-flow CO_2 hydration assay (SFA). Solid lines were fit using single protonation model. (**B**) Inhibition of CAs by compound **39** using SFA. Data points were fit to the Morrison eq. (solid lines)[74,75]. The insets show raw activity curves of CA catalyzed reaction without added inhibitor (red, wine, royal lines), CA inhibited reaction with 313 nM added compound **39** (magenta, dark yellow, purple lines) and spontaneous CO_2 hydration reaction (pink, orange, cyan lines) in the absence of CA. (**C**) Dosing curves of compound **39** binding to CAs by fluorescent thermal shift assay (FTSA). Data points show the ΔT_m as a function of the total concentration of compound **39** added and the lines are simulated using fitting parameters when temperature is 37 °C, CA concentration is 10 μM, enthalpy of unfolding is 690 kJ/mol for CA II and CA VI-mimic, and 480 kJ/mol for CA VI, enthalpy of binding is −42 kJ/mol, heat capacity of binding is −0.8 J/(molK) and the reference melting temperature is 56.8 °C for CA II, 63.1 °C for CA VI-mimic, and 47.6 °C for CA VI. The ΔT_m shift is equal for CA VI-mimic and CA VI, but K_d's differ due to different enthalpies of unfolding. The insets show CA unfolding curves at 0 and 200 μM inhibitor **39** concentrations. (**D**) Isothermal titration calorimetry (ITC) curves of EZA binding to CA VI-mimic in phosphate (Pi, pH 6.1 (▲) and 8.4 (●)) and TRIS buffer (pH 6.9 (■)) at 25 °C. Lines were fitted using single binding site model. The insets show raw data ITC curves at 10 μM CA VI-mimic concentration. Different observed enthalpies of binding illustrate the presence of binding-linked protonation reactions that must be accounted for the determination of intrinsic binding parameters.

zinc-bound protonated hydroxide (water molecule) decreased. According to U-shaped curve as the global fit of experimental data extrapolated to 25 °C, intrinsic binding Gibbs energy (Δ_bG_{intr}) change upon EZA interaction with CA VI-mimic was determined to be −52.4 kJ/mol which was 7.8 kJ/mol greater than the highest experimentally observed value (−44.6 kJ/mol at pH 7.1). Difference of Δ_bG_{intr} ($\Delta\Delta_bG_{intr}$) between EZA interaction with CA VI-mimic and CA VI were smaller ($\Delta\Delta_bG_{intr}$ = −1.5 kJ/mol) compared to that between CA VI-mimic and CA II ($\Delta\Delta_bG_{intr}$ = 6.1 kJ/mol).

Observed standard enthalpy changes (Δ_bH_{obs}) upon EZA binding to CA VI-mimic formed an X-shaped curve which depended on pH and buffer (Fig. 3B). The same tendency has been found previously[40,41] when Δ_bH_{obs} of EZA binding to CA II or CA VI was analyzed. Results were obtained by ITC titration at 25 °C in two buffers exhibiting different protonation enthalpies: sodium phosphate (Pi) and TRIS. Upon EZA-CA VI-mimic titration, more than 20 kJ/mol difference in Δ_bH_{obs} was observed in same buffer at different pHs (in TRIS buffer: −81.6 kJ/mol at pH 6.5, −57.2 kJ/mol at pH 8.5; in Pi buffer: −38.9 kJ/mol at pH 5.2, −84.9 kJ/mol at pH 8.4). To dissect protonation influence, intrinsic enthalpy (Δ_bH_{intr}) of EZA interaction with CA VI-mimic was globally fitted to be −62.0 kJ/mol. Difference of Δ_bH_{intr} ($\Delta\Delta_bH_{intr}$) between EZA interaction with CA VI-mimic and CA VI were smaller (4.0 kJ/mol) compared to that between CA VI-mimic and CA II (11.0 kJ/mol). Thus, Δ_bH_{intr} were in line with Δ_bG_{intr}, confirming that CA II mutant was mimicking CA VI for EZA binding.

Furthermore, analysis of U- and X-shaped curves obtained by FTSA and ITC, respectively, led to the characterization of two important parameters of CA VI-mimic: ionization constant (pK_a) and enthalpy of protonation

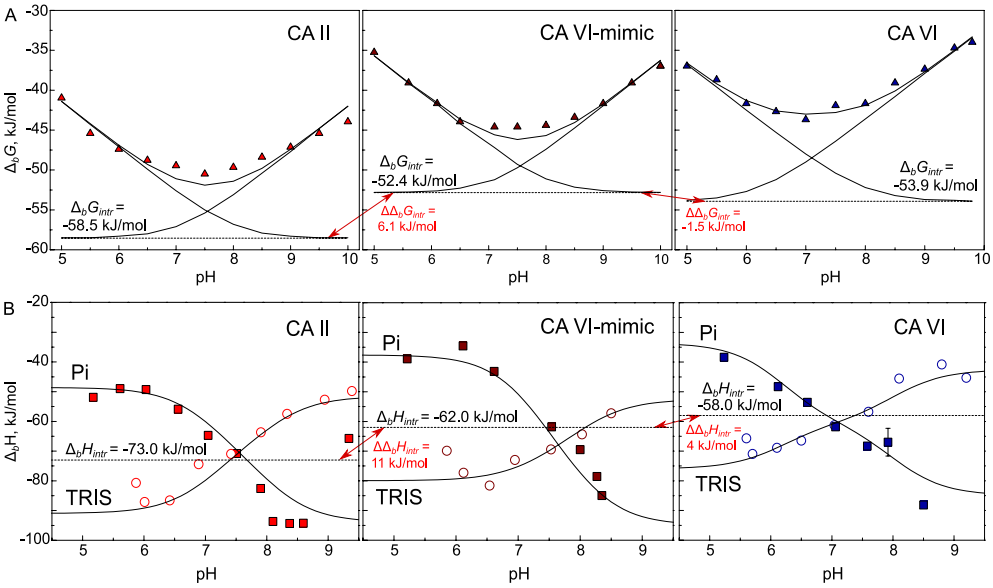


Figure 3. (**A**) Comparison of observed Gibbs energy changes ($\Delta_b G_{obs}$) upon EZA binding to CA II (red), CA VI-mimic (dark red), and CA VI (blue) as a function of pH (25 °C). Experiments were performed by FTSA in universal buffer (50 mM sodium phosphate, 50 mM sodium acetate, and 25 mM sodium borate). The pK_a for CA VI-mimic was determined to be 7.1. (**B**) The observed enthalpy changes ($\Delta_b H_{obs}$) upon EZA binding to CA II (red), CA VI-mimic (dark red), and CA VI (blue) as a function of pH in two different buffers (sodium phosphate (Pi) and TRIS), which have different protonation enthalpies. Experiments were performed by isothermal titration calorimetry (ITC) at 25 °C. The dashed line shows the intrinsic binding enthalpy ($\Delta_b H_{intr}$), which is independent of pH. The pK_a for CA VI-mimic was determined to be 7.3. Thermodynamic binding parameters of EZA binding to CA II and CA VI have been previously published[40,41]. Red arrows indicate difference in $\Delta_b G_{intr}$ or $\Delta_b H_{intr}$ of EZA binding to CA VI-mimic compared to CA II or CA VI.

Protein	pK_a	$\Delta_p G$, kJ/mol	$\Delta_p H$, kJ/mol	$T\Delta_p S$, kJ/mol
CA II[a]	7.1	−40.5	−26.0	14.5
CA VI-mimic	7.2	−41.1	−38.0	3.1
CA VI[b]	6.2	−35.4	−32.0	3.4

Table 1. Thermodynamic parameters of protonation of zinc-bound hydroxide anion of studied CA isoforms as determined by FTSA and ITC at 25 °C. The uncertainty of the pK_a values determined by FTSA and ITC is approximately 0.2 pH units, while for the change in Gibbs energies and enthalpies it is approximately 2 kJ/mol. [a]Data taken from[41]; [b]Data taken from[40].

($\Delta_p H$) of the zinc-bound water molecule (Table 1). The pK_a of CA VI-mimic was determined to be 7.2 at 25 °C as the average of two pK_a values evaluated independently by two techniques: 7.1 by FTSA and 7.3 by ITC. The pK_as of CA II and CA VI-mimic matched each other within the error margin of 0.2 pH unit[42], whereas pK_as of CA VI and CA VI-mimic significantly differed by 1.0 pH (25 °C). Thus, target five point mutations of CA II, which were introduced to design CA VI-mimic, did not affect amino acids surrounding zinc in active sites of CA II at the level causing significant difference of pK_as between CA II and CA VI-mimic. Moreover, $\Delta_p H$ for CA VI-mimic was assessed to be −38.0 kJ/mol at 25 °C. The difference of $\Delta_p H$ between CA VI and CA VI-mimic (6.0 kJ/mol) was 2-fold lower than difference of $\Delta_p H$ between CA II and CA VI-mimic (12.0 kJ/mol). Therefore, experiments with one inhibitor EZA resulted in both pK_a and $\Delta_p H$ for CA VI-mimic, which are essential parameters to determine intrinsic energetics of any other inhibitor binding to CA VI-mimic.

Hydrophobic substituents and fluorine substituents significantly affected intrinsic inhibitor binding affinity for CA VI-mimic. Here 43 benzenesulfonamide derivatives binding to CA VI-mimic was measured by FTSA and inhibition constants of several selected compounds were confirmed by SFA. Trifluoromethanesulfonamide (TFS), EZA, and methazolamide (MZM) were used as controls. Structures of tested compounds are shown in Fig. 4, while dissociation constants (K_d) are listed in Tables 2 and S1 (examples

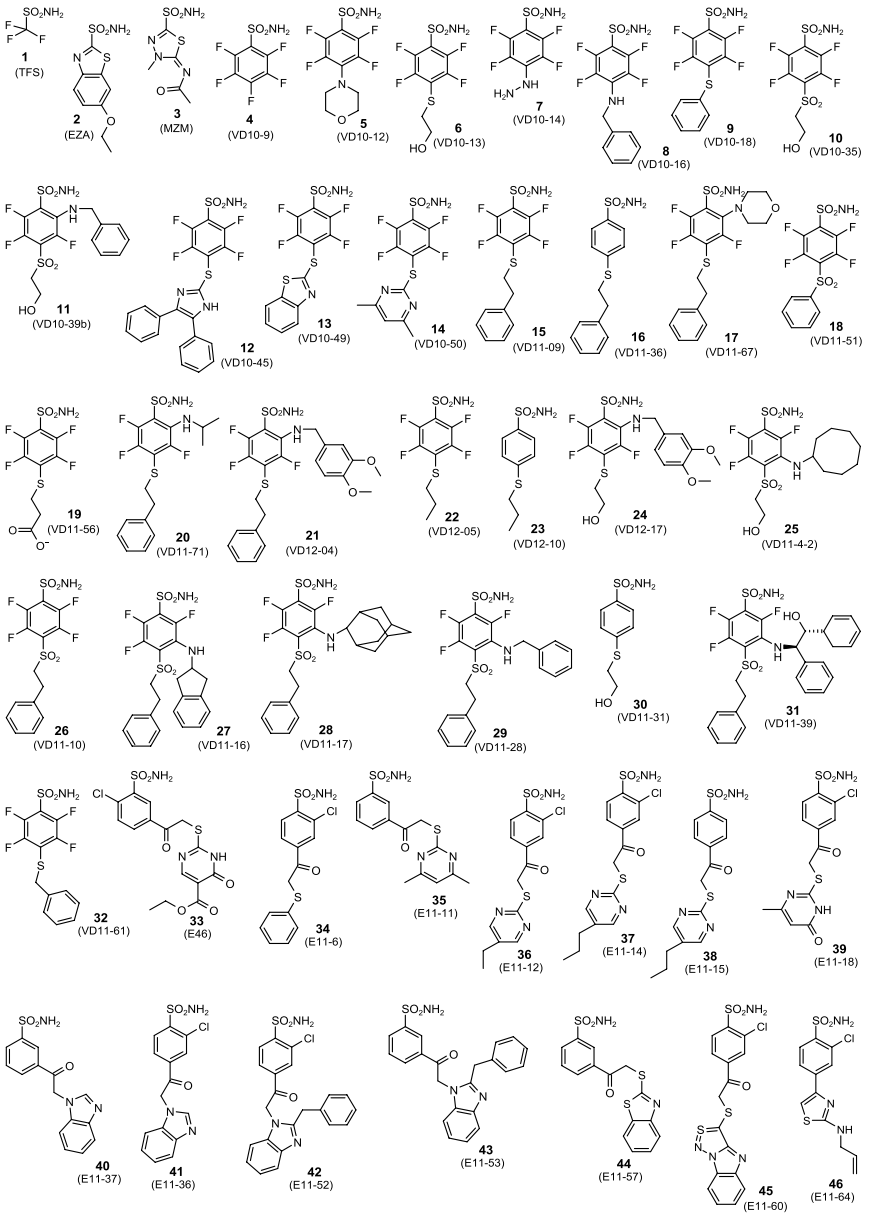


Figure 4. Chemical structures of **1**-**46** compounds designed as CA inhibitors. Compounds **1**-**3** are standard inhibitors of CAs that we used here as control compounds (TFS, EZA, and MZM).

of raw and integrated data of inhibitor binding to CA VI-mimic by FTSA and ITC at different pHs are indicated in Fig. 2C,D, respectively).

According to observed thermodynamics, EZA was shown to be the strongest binder to CA VI-mimic with observed K_d (K_{d_obs}) of 17 nM. From a series of fluorinated benzenesulfonamides, compounds **22** and **26** bearing substituents at *para* position were characterized to be the most potent CA VI-mimic inhibitors bound with observed K_d (K_{d_obs}) in the range of 50–67 nM. The comparison between binding affinities of corresponding fluorinated and nonfluorinated compounds (**6** vs **30**, **15** vs **16**, and **22** vs **23**) showed that fluorination significantly increased observed binding affinity and diminished pK_a of inhibitor sulfonamide amino group. For instance,

Inhibitor	Lab. name	pK_{a_SA}	K_{d_obs} (nM)			K_{d_intr} (nM)		
			CA II	CA VI-mimic	CA VI	CA II	CA VI-mimic	CA VI
1.	TFS	6.02	20	33	14	8.0	15	1.2
2.	EZA	7.82	1.3 (<5.0)	17 (<54)	33 (<54)	0.073	1.1	0.40
3.	MZM	6.86	100	330	830	27	97	44
4.	VD10-9	8.12	46	130	430	1.4	4.7	2.7
5.	VD10-12	8.61	18	100	1100	0.19	1.2	2.4
6.	VD10-13	8.14	11	130	200	0.32	4.2	1.2
7.	VD10-14	8.84	91	330	1000	0.57	2.4	1.3
8.	VD10-16	8.47	9.1	200	1200	0.13	3.3	3.7
9.	VD10-18	7.80	3.4	140	200	0.20	9.8	2.5
10.	VD10-35	7.28	17	130	67	2.5	22	2.1
11.	VD10-39b	7.85	83	140	130	4.6	8.8	1.5
12.	VD10-45	7.69	5.8	140	140	0.43	12	2.2
13.	VD10-49	7.83	0.65	110	200	0.037	7.2	2.3
14.	VD10-50	8.02	9.6 (<43)	330 (140)	1000 (630)	0.37	15	7.9
15.	VD11-9	8.05	1.7	100	400	0.061	4.1	3.0
16.	VD11-36	10.1	12	500	1100	0.0039	0.20	0.077
17.	VD11-67	8.67	5900	100 000	100 000	55	1000	190
18.	VD11-51	7.07	3.3	130	160	0.68	31	6.6
19.	VD11-56	7.97	20	330	500	0.86	16	4.4
20.	VD11-71	8.67	500	2500	3300	4.6	26	6.3
21.	VD12-04	8.67	1800	3300	20 000	17	35	38
22.	VD12-05	8.15	2.2	50	140	0.065	1.7	0.86
23.	VD12-10	10.2	25 (<36)	500 (200)	830 (3900)	0.0070	0.16	0.048
24.	VD12-17	8.67	1300	5000	11 000	12	52	21
25.	VD11-4-2	8.01	56	100	67	2.2	4.5	0.54
26.	VD11-10	7.22	1.2	67	140	0.21	13	4.8
27.	VD11-16	7.87	35	1000	2000	1.9	59	22
28.	VD11-17	7.87	50	140	330	2.6	8.5	3.6
29.	VD11-28	7.87	6.7	200	110	0.35	12	1.2
30.	VD11-31	9.96	140	1000	5000	0.070	0.55	0.50
31.	VD11-39	7.87	33	2000	1000	1.8	120	11
32.	VD11-61	8.53	3.3	140	330	0.042	2.1	0.87
33.	E46	8.90	50	50	200	0.28	0.31	0.23
34.	E11-6	8.70	5.6	330	1100	0.048	3.3	2.0
35.	E11-11	9.40	1000	2000	13 000	1.8	4.0	4.5
36.	E11-12	8.90	8.5	500	5000	0.047	3.1	5.7
37.	E11-14	8.90	7.1	330	3300	0.039	2.1	3.8
38.	E11-15	9.40	560	1300	5000	0.98	2.5	1.8
39.	E11-18	8.90	28 (<54)	500 (300)	2500 (1600)	0.15	3.1	2.8
40.	E11-37	9.60	3600	3300	6700	4.0	4.2	1.5
41.	E11-36	8.30	8.3	500	3300	0.16	12	14
42.	E11-52	8.70	2.9	330	1400	0.025	3.3	2.5
43.	E11-53	9.60	1700	3300	10 000	1.9	4.2	2.3
44.	E11-57	9.60	140	500	3300	0.16	0.63	0.75
45.	E11-60	8.70	250	500	3300	2.2	4.9	5.9
46.	E11-64	9.40	100	1100	17 000	0.16	2.2	5.5

Table 2. The K_{d_obs} and K_{d_intr} values (nM) for interactions between inhibitor and three CA proteins: CA II, CA VI-mimic, and CA VI. The observed inhibitor affinities for CA VI-mimic were obtained experimentally by FTSA (pH 7.0, 37 °C), whereas the intrinsic parameters were calculated from the corresponding observed data using pK_a of 7.0 for CA VI-mimic at 37 °C as explained in the methods part. The standard error of K_d measurements is ±2-fold. The pK_a values of applied sulfonamide amino group (pK_{a_SA}) and inhibitor affinities towards CA II and CA VI have been already reported[58,86]. Dissociation constants K_ds of selected compounds were confirmed by SFA (pH 7.5). Experiments were performed at 23 °C and observed K_ds were extrapolated to 37 °C using van't Hoff equation when enthalpy of binding is −42 kJ/mol. The values at 37 °C are given in parentheses. The determined K_ds at 23 °C are given in Table S2.

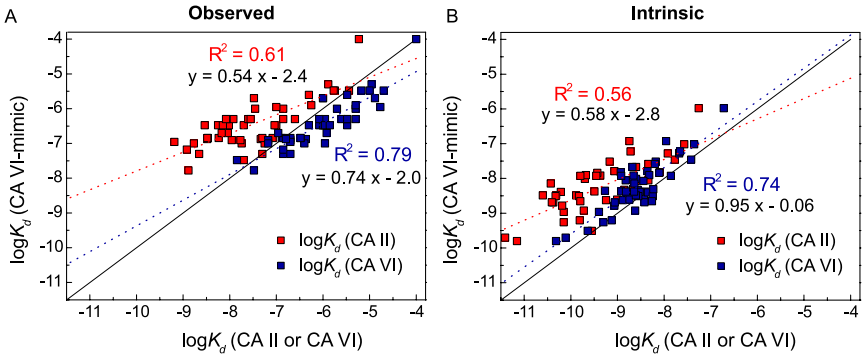


Figure 5. Comparison of logK_d values representing observed (**A**) and intrinsic (**B**) inhibitor binding affinities towards CA VI-mimic and CA II (red squares) or CA VI-mimic and CA VI (blue squares). Straight line represents a model of equal affinity of inhibitor binding to pairwise proteins. Red and blue dashed lines show linear regression models for inhibitor binding to CA II and CA VI, respectively. R^2 values and linear equations are indicated. Experiments were performed by FTSA (pH 7.0, 37 °C).

K_{d_obs} for **30** and **6** binding to CA VI-mimic increased 8-fold upon fluorination (from 1000 nM to 130 nM), whereas K_{d_obs} for **23** and **22** increased affinity 10-fold (from 500 nM to 50 nM). Fluorines reduced pK_a of sulfonamide group significantly: from 9.96 to 8.14 for inhibitors **30** and **6**, respectively, and from 10.2 to 8.15 for compounds **23** and **22**, respectively (Table 2). Correspondingly, chlorine in most compounds also increased observed affinity and reduced pK_a of inhibitor sulfonamide amino group. For example, upon chlorination K_{d_obs} for **40** and **41** interaction with CA VI-mimic increased 430-fold (from 3600 nM to 8.3 nM, respectively), while pK_a values were lowered by 1.30 unit (from 9.60 to 8.30, respectively).

To investigate structure-activity relationships, intrinsic K_d (K_{d_intr}) values for interactions between CA VI-mimic and investigated series of compounds were calculated. The largest differences between K_{d_obs} and K_{d_intr} values were determined for nonfluorinated benzenesulfonamides (**16**, **23**, and **30**), where the binding to CA VI-mimic differed 2500, 3200, and 1800-fold, respectively. Only five compounds (**10**, **18**, **26**, TFS, and MZM) exhibited lower than 10-fold difference between the K_{d_obs} and K_{d_intr}. According to intrinsic thermodynamics, the strongest binders were inhibitors **16**, **23**, **30**, and **33** with K_{d_intr} in the range of 0.16–0.55 nM. Therefore, the strongest intrinsic interaction between inhibitor and CA VI-mimic was observed when inhibitor did not possess any fluorines in benzenesulfonamide scaffold and contained a hydrophobic substituent at *para* position, such as SCH2CH2CH3 (K_{d_intr} for inhibitor **23** was 0.16 nM) and SCH2CH2Ph (K_{d_intr} for inhibitor **16** was 0.20 nM). Exceptionally, inhibitor **33** was the strongest binder to CA VI-mimic with chlorine at *ortho* position and large hydrophilic group at *meta* position (K_{d_intr} was 0.31 nM). Replacement of the methyl group (inhibitor **23**) by hydrophilic hydroxyl group (inhibitor **30**) weakened intrinsic binding affinity more than 3-fold (from to 0.16 nM to 0.55 nM). Moving on to the structural analysis of fluorinated benzenesulfonamides, two inhibitors were determined to be the strongest binders to CA VI-mimic: compound **5** bearing 4-Morpholinyl group at *para* position (K_{d_intr} was 1.2 nM) and **22** with SCH2CH2CH3 group at *para* position (K_{d_intr} was 1.7 nM). In line with results obtained from nonfluorinated compounds, hydrophobic contacts between inhibitors and CA VI were identified to be significant because the exchange of methyl group (inhibitor **22**) by hydroxyl group (inhibitor **6**) or carboxyl group (inhibitor **19**) weakened intrinsic interaction by 2 and 9-fold, respectively. Apparently, the number of methyl groups of substituents at *para* position had significant effect on intrinsic binding affinity. The inhibitor **32** with SCH2Ph bound to CA VI-mimic 2-fold stronger than inhibitor **15** with SCH2CH2Ph and 4-fold stronger than inhibitor **9** with SPh. Most often, introducing diverse substituents at *meta* position did not change intrinsic binding affinity significantly (**6** vs **25**, **26** vs **28**, and **26** vs **29**), except for **26** vs **31** bearing large hydrophobic group which weakened interaction 9-fold. The compound **17** bearing two large and highly hydrophobic substituents at *ortho* and *para* positions was the weakest binder not only according to the observed parameters (K_{d_obs} was 100 µM), but also intrinsic data (K_{d_intr} of 1000 nM).

Thermodynamically CA VI-mimic binds benzenesulfonamides similarly to CA VI but differing from CA II. To evaluate if CA VI-mimic based on CA II is a suitable CA VI model protein for inhibitor screening, observed and intrinsic affinities represented by logarithmic K_d values of inhibitor binding to CA II, CA VI-mimic, and CA VI were compared by applying linear regression. A higher linear correlation was determined between observed affinities of inhibitor binding to CA VI and CA VI-mimic ($R^2 = 0.79$) compared to the observed affinities of inhibitor interaction with CA II and CA VI ($R^2 = 0.61$; Fig. 5A). Analysis of the calculated intrinsic parameters were in line with experimentally measured observed data, emphasizing a stronger correlation of the intrinsic thermodynamics of inhibitor binding to CA VI and CA VI-mimic ($R^2 = 0.74$) compared to that of CA II and CA VI-mimic ($R^2 = 0.56$; Fig. 5B). Furthermore, regression line slopes indicating the comparison of inhibitor binding to CA VI and CA VI-mimic (0.74 for observed affinity, 0.95 for intrinsic affinity) were larger than the corresponding slopes for CA II and CA VI (0.54 for observed affinity, 0.58 for intrinsic affinity),

thereby indicating a lower difference between the inhibitor binding towards CA VI-mimic and CA VI compared to CA II.

The influence of investigated CA II mutations on inhibitor binding thermodynamics was further analyzed by calculating the absolute error (AE) values from logarithmic observed or intrinsic K_ds of inhibitor binding to CA VI-mimic, CA II, and CA VI. According to the observed thermodynamics, binding affinities of only 12 inhibitors out of 46 tested compounds towards CA VI-mimic was more similar to CA II than CA VI. For the intrinsic data, only 6 compounds were identified as CA VI-mimic binders with the affinity more alike CA II compared to CA VI. Moreover, mean absolute errors (MAEs) as the averages for each AE were also evaluated. MAEs of $AE_{obs,CA\ II}$ and $AE_{intr,CA\ II}$ were equal to 1.1, while MAEs of $AE_{obs,CA\ VI}$ and $AE_{intr,CA\ VI}$ were significantly smaller, 0.47 and 0.41, respectively. Therefore, CA VI-mimic designed via site-directed mutagenesis from CA II was characterized to be a proper model of CA VI for observed and intrinsic inhibitor binding reactions.

Differences in inhibitor binding affinities are due different binding modes as determined by crystallographic analysis of CA II and CA VI-mimic. Despite numerous attempts, the crystal structures of recombinant CA VI complexes with sulfonamide-based inhibitors were not obtained by soaking. Even though CA VI crystals survived soaking procedure, crystals did not contain the clear electron densities of inhibitors. The co-crystallization of CA VI protein with several inhibitors failed, as we did not obtain any crystals suitable for X-ray diffraction experiment. Most likely, CA VI complexes with sulfonamide-based inhibitors cannot be crystallized using crystallization conditions that are effective for the unbound CA VI protein.

To structurally investigate the binding of benzenesulfonamides with CA VI, we have engineered CA VI-mimic and applied in crystallographic studies. We have solved crystal structures of CA VI-mimic complexes with three inhibitors (Fig. S2): EZA (PDB ID: 6QL2), inhibitor **14** (PDB ID: 6QL1), and **25** (PDB ID: 6QL3). These complexes were compared with the corresponding complexes composed of CA II and same ligands (EZA (PDB IDs: 3CAJ (X-ray), 6BCC (neutron diffraction)), inhibitor **14** (PDB ID: 4HT0), and **25** (4PYY)). The space groups and unit cell parameters of CA VI-mimic crystals were similar to those of CA II (Table 3). There was one unique protein-ligand complex in the asymmetric unit. CA VI-mimic binding pocket was found to be similar to CA VI according to crystallographic studies (Fig. 1D) followed by thermodynamic analysis. For this reason, the insights into the compound binding mode to CA VI-mimic are likely to be valid for analyzing the ligand binding data to CA VI.

The comparison of binding mode of inhibitor **14** in the active sites of CA VI-mimic and CA II is shown in Fig. 6A. Inhibitor **14** in the active site of CA VI-mimic had two alternative binding modes characterized by different positions of the fluorinated ring: the ring was either lodged between Leu198 and Thr200 side chains (colored cyan in Fig. 6A), or located in the hydrophilic part of active site (colored blue). On the other hand, in the active site of CA II we had only one position of fluorinated ring – between Leu198 and Thr200. It looks like the replacement of Phe130 in CA II with tyrosine in CA VI-mimic enabled additional position of fluorinated ring of ligand due to a steric collision between the fluorine atom of fluorinated ring and the oxygen atom of Tyr130 side chain (the close contact found in the structure was 2.5 Å). The alternative position of the fluorinated ring of compound **14** in the active site of CA VI-mimic probably was available only due to spatial fluctuations of Tyr130 side chain. Also, due to a significantly larger size and the hydrophilicity of the side chain of Gln134 in CA VI-mimic compared to Val134 in CA II, the hydrophobic dimethylpyrimidine tail of inhibitor **14** was repelled in CA VI-mimic (see *para*-group of the cyan ligand, Fig. 6A). Therefore, the change of size and the hydrophobicity/hydrophilicity of the residues 130 and 134 upon mutation could be rationalized as the main causes for the relatively significant difference in the binding affinities: inhibitor **14** bound to CA II 40-fold better than to CA VI-mimic (K_{d_intr} values were 0.37 nM and 15 nM for CA II and CA VI-mimic, respectively; Table 2).

The model compound EZA was bound similarly in active sites of CA II and CA VI-mimic (Fig. 6B). Some discrepancy was present only in the positions of highly flexible ethoxy moiety. The aliphatic-aromatic interactions between the methyl group of Leu198 and the first ring of EZA was present in both cases. The larger side chain of Tyr130 slightly changed the position of EZA aromatic ring in CA VI-mimic as compared with CA II due to steric conflicts. It is important also to note the role of the residue 134 interacting with the hydrophobic tail of EZA, similarly to the observation for inhibitor **14** above. The hydrophobic Val134 sidechain in CA II was mutated into hydrophilic Gln134 in CA VI, leading to the worsening of the interaction. Thus, the mutations of residues 130 and 134 were the likely reasons for 15-fold stronger binding of EZA to CA II, as determined by intrinsic thermodynamics (K_{d_intr} values were 0.073 nM and 1.1 nM for CA II and CA VI-mimic, respectively; Table 2).

The intrinsic binding parameters of inhibitor **25** towards CA II and CA VI-mimic were comparable (2.2 nM vs 4.5 nM, respectively; Table 2). In contrast, the binding modes of the compound found in crystal structures were different in these active sites. In CA II, inhibitor **25** had two alternative conformations: (1) the fluorinated ring located between Leu198 and Thr200, whereas the cyclooctyl ring replaced the side chain of Phe130 (Fig. 6C, pink ligand); (2) the fluorinated ring positioned in the hydrophobic part of active site, while the cyclooctyl ring – in the hydrophilic part (Fig. 6D, pink ligand). In CA VI-mimic, compound **25** had one well-defined conformation (Fig. 6C, D, blue) in which the cyclooctyl ring replaced the Tyr130 side chain, whereas the fluorinated ring occupied the hydrophilic part of active site. We can explain the presence of the single conformation of inhibitor **25** bound to CA VI-mimic. It seems that the mutation in position 67 (asparagine to glutamine) allows the position of fluorinated ring in hydrophilic part of active site when the *para*-substituent of ligand does not have sterical collision with side chain of residue 67 (compare side chain conformations of asparagine (CA II) and glutamine (CA VI-mimic), Fig. 6C, D). The same position of glutamine is found in the complexes of CA VI-mimic with inhibitor **14** and EZA ligands which means that compound **25** does not influence the position of side chain of residue 67 in CA VI-mimic. The replacement of asparagine (CA II) to glutamine (CA VI-mimic) creates the additional free space in the active site and allows for another binding mode.

Isoform-ligand	CA VI-mimic – inhibitor 14	CA VI-mimic - EZA	CA VI-mimic – inhibitor 25
PDB ID	6QL1	6QL2	6QL3
Data-collection statistics			
Space group	$P12_11$	$P12_11$	$P12_11$
Unit-cell parameters (Å)	a = 42.3, b = 41.4, c = 71.2, β = 104.3°	a = 42.1, b = 41.3, c = 71.4, β = 104.2°	a = 42.2, b = 41.4, c = 71.9, β = 104.2°
Resolution range (Å)	1.42–69.0	1.30–40.9	1.35–69.7
Wavelength (Å)	0.976300	0.975522	0.975522
Radiation source	EMBL, P14	EMBL, P14	EMBL, P14
Unique reflections number	42097	56403	52382
R_{merge}, overall (outer shell)	0.042(0.241)	0.067 (0.334)	0.088 (0.338)
I/σ overall (outer shell)	22.7(7.2)	13.1 (5.0)	10.8 (4.1)
Multiplicity overall (outer shell)	7.0 (6.6)	6.9 (6.9)	6.8 (6.7)
Completeness (%) overall (outer shell)	92.8 (74.1)	96.4 (94.5)	98.8 (99.0)
Wilson B-factor	13.2	13.1	9.3
Refinement statistics:			
R_{work}	0.157	0.119	0.116
R_{free}	0.185	0.157	0.156
RMSD bond lengths, (Å)	0.011	0.013	0.033
RMSD bond angles (°)	2.000	1.991	2.195
Average B factors (Å^2):			
all	16.7	20.4	15.0
main-chain	13.5	16.3	10.3
side-chain	16.2	21.7	14.8
inhibitors	26.9	13.3	17.3
waters	27.6	33.1	31.3
zinc	7.7	9.1	4.7
other molecules	40.5	37.0	36.9
Number of atoms:			
all	2562	2380	2482
protein	2181	2111	2127
inhibitor	69	16	28
water	287	226	275
zinc	1	1	1
other molecules	24	26	51
Ramachandran statistics (%):			
most favored regions	96	97	97
additionally allowed regions	4	3	3
outliers	0	0	0

Table 3. Data collection and refinement statistics of human CA VI-mimic and its complexes with inhibitors inhibitor **14**, **25**, and EZA. All datasets were collected at 100 K, test set size was 10%.

Discussion

Nowadays enzymes encompass over one-third of drug targets investigated by large pharmaceutical companies[43], thereby emphasizing the relevance of target-based drug approach. This strategy aims to identify the compounds which would exhibit the most therapeutically beneficial effect via modulating catalytic activity or expression levels of disease-associated enzymes. The present study is focused on CA VI isoform as a drug target due to the link of CA VI with several pathologies[19,20,22]. Even though several studies on the design of compounds targeting CA VI have been reported[40,44,45], CA VI-selective inhibitor has not been discovered so far. Therefore, there is an interest in inhibitors with high affinity and selectivity against CA VI which would be crucial to reveal biological function of CA VI.

During preclinical development, numerous high-throughput screening assays are employed to design and optimize hits toward a target protein. Therefore, *in vitro* techniques require high quantities of recombinant proteins for the proper evaluation of compound quality, efficacy, and safety before testing in humans. Despite recent advances in molecular sciences, difficulties in the production of recombinant proteins in large scale are observed. Our previous study[40] indicated low yield of CA VI from *E. coli*. Here we have presented a strategy to apply CA VI-mimic as CA VI model protein for the investigation on enzymatic inhibition and inhibitor binding thermodynamics. The CA VI-mimic was designed via site-directed mutagenesis from CA II by introducing five point mutations, such as A65T, N67Q, F130Y, V134Q, and L203T. Such approach to obtain CA protein based on the CA II mutant for the search of CA-selective inhibitors has been successfully applied previously. It was due to troubles to obtain sufficient amounts of recombinant CA isoforms and enabled by high structural homology between human

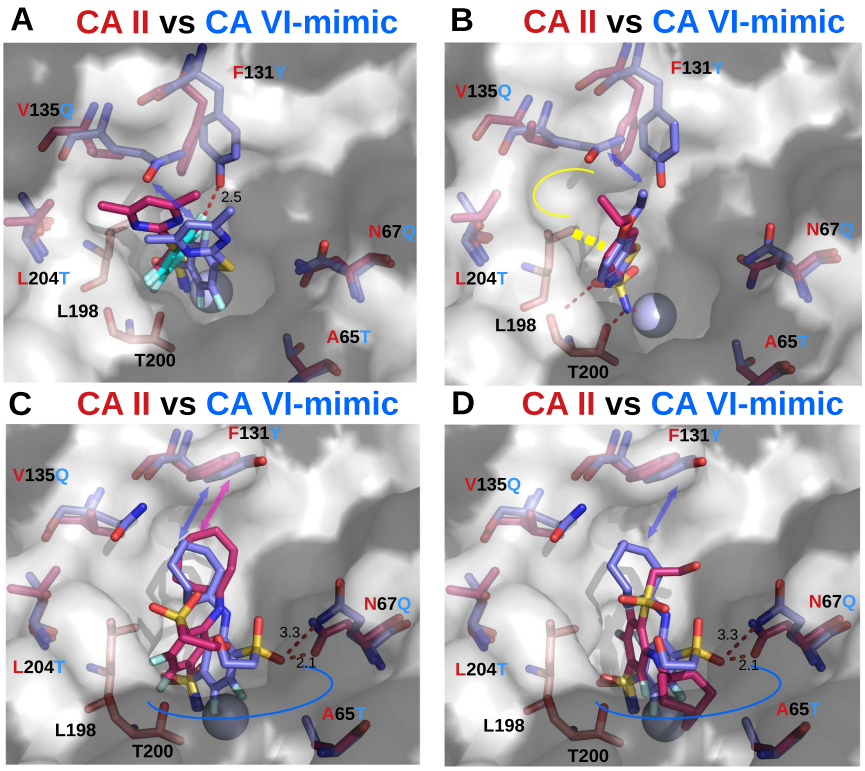


Figure 6. Differences in the binding structural modes of three compounds in CA II and CA VI-mimic as determined by X-ray crystallography. The zinc ion in active sites of CAs is shown as a light blue sphere. CA II side chain residues and ligands bound to CA II are colored pink and are shown transparent. CA VI-mimic side chains as well as its ligands are colored blue and also shown transparent. Mutated CA II side chains are labeled red for CA II, blue for CA VI-mimic. Hydrogen bonds are shown as dashed lines and distances are marked. Hydrophobic part of active site is shown as white surface, whereas hydrophilic part is shown as gray surface. (**A**) Compound **14** bound to active sites of CA VI-mimic (two alternative conformations of **14** are shown in cyan and blue, PDB ID: 6QL1) and CA II. The second ring of the "cyan" conformation of **14** in CA VI-mimic is not resolved in crystal structure, and not shown. (**B**) EZA bound to active site of CA VI-mimic (PDB ID: 6QL2) and CA II (PDB ID 3CAJ). Interaction of L198 with the first ring of compound is marked by thick dashed yellow line. Yellow line designates hydrophobic pocket for binding of *para*-substituent. The typical interactions for sulfonamide moiety are indicated, whereas they are omitted for clarity in other panels. (**C**, **D**) Compound **25** bound to active site of CA VI-mimic (PDB ID: 6QL3) and CA II (two alternative conformations of the ligand are indicated, PDB ID 4PYY). Blue line designates a hydrophilic part of the active site of CA VI-mimic.

CAs. McKenna's group reported a number of structural studies on CA IX-mimic based on CA II mutant with 2 mutations (S65A, Q67N)[46–48], 7 mutations (A65S, N67Q, E69T, I91L, F131V, K170E, L204A)[49–51] or 8 mutations (A9K, S65A, Q67N, T69E, L91I, V131F, E170K, A204L)[52]. Our group also published the exploration on inhibition parameters and binding thermodynamics via the application of CA IX-mimic as CA II mutant with 6 mutations (S65A, Q67N, L91I, V130F, L134V, A203L) and CA XII-mimic as CA II mutant with 6 mutations (S65A, K67N, T91I, A130F, S134V, N203L)[53]. The significant findings of the listed studies promoted the present investigation of CA II mutant mimicking CA VI. Over 10-fold higher purification yield of CA VI-mimic compared to CA VI from *E. coli* allowed kinetic, thermodynamic, and structural analyses of 43 benzenesulfonamides binding to CA VI-mimic. Even though the most tested inhibitors exhibited moderate affinities towards CA VI-mimic, this study provided insight into the structure-based design of inhibitors with better affinity and selectivity towards CA VI.

The observed kinetic parameters of CA VI and CA VI-mimic are consistent with previous works. The determined catalytic constant of CA VI compares reasonable well to published k_{cat} value ($3.4 \times 10^5\ s^{-1}$)[44]. The difference of k_{cat} values most likely arise from the uncertain CO_2 concentration in the previous work. The CA VI-mimic had the same catalytic activity as CA II ($k_{cat} - 6.0 \times 10^5\ s^{-1}$) and confirmed previously published results that A65, N67, F130, V134, L203 amino acids in the active site of CA II are not important for catalytic activity[54–56]. Three

times higher catalytic activity of CA VI-mimic than CA VI is an advantage in measuring nanomolar inhibition constants by SFA, because similar to all enzymatic methods it is limited by both CA activity and concentration[26].

The relevance of protonation-deprotonation reactions occurring additionally upon inhibitor binding to CA has been reviewed by several groups[57,58]. Such protonation events have been recently confirmed by neutron crystallography[59,60]. To generate compounds with great affinities by rational design, it is essential to understand the structural reasons for the changes in binding affinities of the investigated compounds towards the target. Only intrinsic parameters subtract the contribution of protonation reactions occurring in conjunction with the binding reaction between the CA and inhibitor. In the present study, nonfluorinated benzenesulfonamides exhibited stronger intrinsic and weaker observed binding affinity than corresponding fluorinated compounds. This result is in line with the previous investigation[34], emphasizing the impact of fluorine electronegativity on the lowering of the pK_a of inhibitor sulfonamide group but not the direct recognition of CA VI-mimic surface. The diminished pK_a of fluorinated inhibitors led to the elevated observed affinity due to the increased fraction of inhibitor in the deprotonated form that bound to CA VI-mimic with the protonated zinc-bound hydroxide ion in the active site. Furthermore, substituents at *ortho* and *para*, but not *meta* positions were identified to be significant for the molecular recognition between the compound and CA VI. However, *ortho* and *meta*-substituted benzenesulfonamides have been recently shown to act as tight CA IX binders[32]. Therefore, such findings confirmed that intrinsic, but not observed parameters should be applied to analyze the dependence of binding efficiency on compound chemical structures, thereby allowing important structure-thermodynamics correlations to design CA-isoform selective inhibitors.

Inhibitor binding affinity can be significantly affected by structural properties of CA VI which have been widely investigated. The crystal structure of recombinant CA VI catalytic domain, lacking signal sequence and C-terminal region, has revealed its dimeric arrangement with the active sites of monomers facing each other and directed towards the center of the dimer[61]. Interestingly, the recent study[62] has indicated that pentraxin domain (PTX) is present in non-mammalian CA VI, whereas PTX-coding exon is not found in mammalian *CA6* gene most likely due to rearrangements occurring upon the duplication of the adjacent glucose transporter genes. Instead of the PTX domain, mammalian CA VI contains a C-terminal region of at least 25 residues which is not detected in other vertebrate CA isoforms. This part of CA VI may be important to form oligomers and bind other proteins affecting CA VI enzymatic activity or causing biological effect as a consequence of CA VI-protein interactions. Therefore, *in vitro* and *in vivo* studies on targeting CA VI can yield discrepancies in results because of the structural differences between recombinant CA VI applied for inhibitor screening and endogenous CA VI of live model organisms, such as mice or zebrafish.

The combination of data obtained from enzymatic inhibition and biophysical binding methods, such as FTSA and ITC, significantly strengthens the conclusions of compound structure-activity relationships. Since techniques are based on different strategies to characterize inhibitor efficacies, the precision and accuracy of the measurements are necessary to reliably select the most potent and strongest inhibitors/binders. The uncertainty and repeatability of FTSA[42] and ITC[63,64] measurements have been previously discussed. Furthermore, correlation between the affinities determined by FTSA and SFA or FTSA and ITC have been recently reported[26,58] and confirmed in the present study. Therefore, both enzymatic inhibition and biophysical binding techniques are necessary for precise identification of inhibitors with great affinity and selectivity towards the particular CA isoform, thereby leading to the success in clinical development.

In conclusion, this study on site-directed mutagenesis of residues in the active site of CA II to resemble CA VI gave clues to the basis for isoform specificity of benzenesulfonamides towards CA VI over CA II. The characterization of numerous properties, such as kinetics of binding, inhibition profiles and the mechanism of action, provided the deeper insight into the efficacy of CA VI-targeting inhibitors. This *in vitro* step is crucial because only sufficiently characterized compound can result in the success on translating experimental data to a clinical disease setting. Moreover, the present kinetic, thermodynamic, and structural information is important for experiments *in silico*, such as machine learning, when current binding information will be determined, filtered, and extracted.

Methods

Synthesis of CA inhibitors. The synthesis of CA inhibitors has been previously described[65–68]. EZA, MZM and TFS were purchased from Sigma-Aldrich (St. Louis, MO, USA) and were used without further purification.

Production of CA VI-mimic protein. The structural superpositions of proteins for Figs 1D and 6(A–D) were performed using UCSF Chimera v. 1.12[69]. The residues within 5 Å from the typical CA II inhibitor in PDB entry 3M96 in both isoforms were analyzed, and five residues which were different between the isoforms were selected to create CA VI-mimic. The structure-based alignment was generated using PROMALS3D web server[70]. The sequence alignment figure was prepared using TeXshade package[71].

The expression vector pET15b-CA II[72], encoding full length CA II (1-260), was used in site-directed mutagenesis. The residues located in CA II active site, A65, N67, F130, V134, and L203, were replaced to T, Q, Y, Q, and T, respectively. For each mutagenesis reaction two oligonucleotide primers (sense and antisense) with target mutation were used: **A65T_s**: 5'CTC AAC AAT GGT CAT ACT TTC AAC GTG GAG3' and **A65T_a**: CTC CAC GTT GAA AGT ATG ACC ATT GTT GAG; **N67Q_s**: CAA TGG TCA TAC TTT CCA GGT GGA GTT TGA TGA C and **N67Q_a**: GTC ATC AAA CTC CAC CTG GAA AGT ATG ACC ATT G; **F130Y_s**: CCA AAT ATG GGG ATT ATG GGA AAG CTG TGC AG and **F130Y_a**: CTG CAC AGC TTT CCC ATA ATC CCC ATA TTT GG; **V134Q_s**: GAT TAT GGG AAA GCT CAG CAG CAA CCT GAT GG and **V134Q_a**: CCA TCA GGT TGC TGC TGA GCT TTC CCA TAA TC; **L203T_s**: GAC CAC CCC TCC TCT TAC GGA ATG TGT GAC CTG and **L203T_a**: CAG GTC ACA CAT TCC GTA AGA GGA GGG GTG GTC. PCR was carried out with high fidelity *Pfu* DNA polymerase (Thermo Fisher Scientific), except V134Q created with Phusion DNA polymerase (Thermo Fisher Scientific). Composition of PCR: 1× polymerase buffer, 50 ng template DNA, 0.2 mM dNTPmix, 125 ng

each sense and antisense primer, and 1.5 U DNA polymerase. Thermal cycling conditions: initial denaturation – 95 °C for 10 min, then 18 cycles: 95 °C for 3 min, annealing – 66 °C (A65T and F130Y), 63 °C (N67Q), 71 °C (V134Q), or 72 °C (L203T) for 2 min, extension – 72 °C for 8 min, final extension – one time 72 °C for 10 min. After temperature cycling, PCR product was treated with *Dpn I* restriction endonuclease in order to digest the parental DNA template and to select new synthesized mutated DNA[73]. The mutations were confirmed by DNA sequencing.

Expression of CA VI-mimic protein was carried out in *E. coli* BL21(DE3) strain. Transformed cells colony was transferred to LB medium, containing 100 µg/ml ampicillin, grown at 37 °C and 220 rpm for 16 h. Then the saturated culture was diluted (1:50) in fresh LB medium, containing 100 µg/ml ampicillin and 60 µM $ZnSO_4$ and grown to $OD_{600} \approx 0.8$. The expression of CA VI-mimic protein was induced with 0.2 mM isopropyl-β-D-thiogalactoside (IPTG) and 0.4 mM $ZnSO_4$. The cells were grown over night at 19 °C, 220 rpm and harvested by centrifugation at 4000 g for 20 min at 4 °C.

The biomass was suspended in the lysis buffer (20 mM HEPES, 0.15 M NaCl, and 1 mM PMSF, pH 7.4), incubated at 4 °C for 60 min and then disrupted by sonication. Debris of cells and insoluble proteins precipitated after centrifugation at 30 000 g for 25 min. The soluble CA VI-mimic protein was purified using a metal chelate and CA-affinity chromatography. For the metal chelate chromatography the column was equilibrated with 20 mM HEPES, 0.15 M NaCl (pH 7.4). For elution of CA VI-mimic protein, solution composed of 20 mM HEPES, 0.15 M NaCl, and 0.2 M imidazole (pH 7.4) was used. Eluted protein was purified using a CA-affinity column containing *p*-aminomethylbenzene sulfonamide-agarose (Sigma-Life Science Aldrich). Sorbent was equilibrated with 20 mM HEPES, 0.15 M NaCl (pH 7.4). For the protein elution, solution composed of 0.1 M sodium acetate and 0.5 M sodium perchlorate (pH 5.6) was used. Eluted CA VI-mimic protein was dialyzed into storage buffer containing 20 mM HEPES, 0.05 M NaCl, pH 7.4, and stored at −80 °C.

The purity of CA VI-mimic protein was analyzed by SDS-PAGE. Protein concentrations were determined by UV-vis spectrophotometry using extinction coefficient $\varepsilon_{280} = 51910\ M^{-1}\ cm^{-1}$ and confirmed by standard Bradford method. Molecular mass of CA VI-mimic protein was confirmed by Mass spectrometer: observed – 29192.4 Da, theoretically predicted – 29323.0 Da. The difference is due to Met residue removed during production.

Enzymatic activity and inhibition by SFA. Enzymatic activity and inhibition experiments were performed using an Applied Photophysics SX.18MV-R stopped-flow spectrophotometer at 23 °C. Saturated CO_2 solution was prepared by bubbling the CO_2 gas in Milli-Q water at 23 °C for 1 h. The concentration of CO_2 was determined using a model described previously[26].

Catalytic constants k_{cat} and Michaelis constants K_M of CA VI and CA VI-mimic were determined in a pH range from 6.0 to 8.4 using 25 mM buffer and 30–300 µM indicator systems with similar pK_a values: MES (pK_a 6.1) and Bromocresol Purple (pK_a 6.4, λ - 590 nm, pH 6.0–6.4), MOPS (pK_a 7.2) and Bromothymol Blue (pK_a 7.1, λ - 615 nm, pH 6.8–7.1), HEPES (pK_a 7.5) and Phenol Red (pK_a 7.5, λ - 557 nm, pH 7.2–7.8), TRIS (pK_a 8.06) and *m*-Cresol Purple (pK_a 8.3, λ - 575 nm, pH 8.0–8.4). CA VI and CA VI -mimic concentration was 50–100 nM. The ionic strength of solution was maintained at 0.2 M by the addition of sodium sulfate. Maximal velocities v_{max} were obtained using Lineweaver-Burk coordinates, and k_{cat}, pK_a values were determined using single ionization model:

$$k_{cat} = \frac{k_{cat-max}}{1 + 10^{pH-pK_a}}$$

Enzyme inhibition experiments were performed using 25 mM HEPES buffer containing 0.2 M sodium sulfate and 50 µM Phenol Red indicator, pH 7.5. Enzyme concentration was 10–30 nM for CA II, and 50 nM for CA VI and 50–107 nM CA VI-mimic. Inhibitor concentration was 0–20 µM in <0.2% DMSO. Raw curves were fitted using a single exponential model and the inhibition constants were determined using Morrison equation[74,75]:

$$CA\ act.\ (\%) = 1 - \frac{([CA] + [I] + IC_{50} - \sqrt{([CA] + [I] + IC_{50})^2 - 4[CA][I]})}{2[CA]} \cdot 100\%$$

where [CA] is the total concentration of the active CA molecules, [I] is the total added inhibitor concentration, and IC_{50} is the concentration of inhibitor that achieves 50% inhibition of enzymatic activity. A dose-response curve was fitted using fixed CA concentration and assuming that it is equal to the active enzyme concentration.

Inhibitor binding by FTSA. FTSA measurements were performed using a Corbett Rotor-Gene 6000 (Qiagen Rotor-Gene Q) instrument using the blue channel (excitation 365 ± 20 nm, detection 460 ± 15 nm). Samples contained 10 µL of 10 µM CA VI-mimic protein, 10 µL of 0–200 µM inhibitor in 50 mM phosphate buffer at pH 7.0 containing 100 mM NaCl, 50 µM solvatochromic dye 8-anilino-1-naphthalene sulfonate (ANS) and a final DMSO concentration of 2%. The applied heating rate was 1 °C/min. The pH dependence of the observed binding constant was measured in universal buffer containing 50 mM sodium phosphate, 50 mM sodium acetate, 25 mM sodium borate at pH 5.0–10.0. Data were fitted and analyzed as previously described[72,76]. Experiments were repeated at least twice.

Inhibitor binding by ITC. ITC measurements were performed using a VP-ITC instrument (Microcal Inc., Northampton, USA) with 1.4 mL of 4–6 µM CA VI-mimic protein solution in the cell and 300 µL of 40–60 µM ligand solution in the syringe. A typical experiment consisted of 25–30 injections (10 µL each) added at 200–240 s intervals. In order to determine the pH dependence of the observed binding enthalpy, experiments were performed at 25 °C in 50 mM phosphate or 50 mM TRIS buffer containing 100 mM NaCl at pH 5.0–10.0 with a final DMSO concentration of 1%, equal in the syringe and the cell. Data were integrated, fitted and analyzed as previously described[77]. Experiments were repeated at least twice.

Calculation of the intrinsic thermodynamics. The enzymatic or biophysical assays allow the determination of *observed* inhibitor affinity for CA. However, observed parameters depend on buffer or pH. Therefore, observed values are only relevant for the comparison of inhibitor binding affinities towards the target using the same experimental conditions and should not be used in structure-thermodynamics correlations in drug design.

Several protonation events take place upon the interaction between the inhibitor and CA: protonation of zinc-bound hydroxide in the active site of CA, deprotonation of inhibitor sulfonamide group, bond formation between CA and inhibitor, and compensating protonation-deprotonation reactions of buffer. To develop compounds with great affinities in the rational drug design, *intrinsic* parameters must be determined by subtracting the contribution of protonation reactions occurring in the conjunction with the inhibitor binding to CA[58].

The parameter of K_{d_intr} is directly related to K_{d_obs} and fractions of deprotonated sulfonamide-based inhibitor ($f_{RSO_2NH^-}$) and CA with protonated zinc-bound hydroxide (water molecule) in the active site (f_{CAZnH_2O}).

$$K_{d_intr} = K_{d_obs} \times f_{RSO_2NH^-} \times f_{CAZnH_2O}$$

The fractions of binding-ready inhibitor and CA depend on the pK_a of sulfonamide amino group (pK_{a_SA}) and the pK_a of water molecule in the active site of CA (pK_{a_CA}), respectively.

$$f_{RSO_2NH^-} = \frac{10^{pH-pK_{a_SA}}}{1 + 10^{pH-pK_{a_SA}}}$$

$$f_{CAZnH_2O} = 1 - \frac{10^{pH-pK_{a_CA}}}{1 + 10^{pH-pK_{a_CA}}}$$

The intrinsic Gibbs energy change ($\Delta_b G_{intr}$) is associated with the change in K_{d_intr} for the binding reaction.

$$\Delta_b G_{intr} = RT \ln K_{d_intr}$$

The K_{d_intr} values for the tested benzenesulfonamide binding to CA VI-mimic were calculated using the pK_a of 7.0 for CA VI-mimic at 37 °C.

The $\Delta_b H_{obs}$ was measured by ITC as the sum of enthalpies caused by inhibitor binding to CA and protonation events, such as protonation enthalpies of buffer ($\Delta_p H_{buf}$), sulfonamide inhibitor ($\Delta_p H_{SA}$), and hydroxide bound to zinc in the active site of CA ($\Delta_p H_{CA}$):

$$\Delta_b H_{intr} = \Delta_b H_{obs} - n_{SA}\Delta_p H_{SA} - n_{CA}\Delta_p H_{CA} + n_{buf}\Delta_p H_{buf},$$

where $n_{SA} = f_{RSO_2NH^-} - 1$ is the number of protons released from the inhibitor to buffer, $n_{CA} = 1 - f_{CAZnH_2O}$ is the number of protons bound to zinc-bound hydroxide of CA, and $n_{buf} = n_{CA} + n_{SA}$ is the sum of uptaken or released protons by buffer. The enthalpy of protonation of TRIS and sodium phosphate buffers at 25 °C is equal to −47.4 kJ/mol and −5.1 kJ/mol, respectively[78].

Crystallization. The CA VI-mimic was concentrated by ultrafiltration to 19 mg/mL. Crystallization condition (buffer) was 0.1 M sodium BICINE (pH 9.0), 0.2 M ammonium sulfate and 2 M sodium malonate (pH 7.0). The ligand solutions for crystal soaking were made by mixing of 50 µL of corresponding reservoir solution and 1 µL of 50 mM ligand solution (in DMSO).

Data collection and crystallographic structure determination. Three datasets of X-ray diffraction (CA VI-mimic in complex with inhibitor **14** (VD10-50), **25** (VD11-4-2), and EZA) were collected at the EMBL beamline P14. The datasets were processed by XDS program[79]. The molecular replacement was made by MOLREP program[80] using as initial model 4HT0. The 3D models of compounds were created by AVOGADRO program[81]. The library files which contain complete chemical and geometric descriptions of compounds were created using LIBCHECK program[82,83]. The models were prepared using COOT[84] and refined using REFMAC[85]. All represented graphics were made using Pymol programs (PyMOL, version 1.8.4.0). Coordinates and structure factors have been deposited to the RCSB Protein Data Bank (PDB). The PDB access codes are listed in Table 3.

References

1. Meldrum, N. & Roughton, F. Some properties of carbonic anhydrase, the CO_2 enzyme present in blood. *J Physiol* **75**, 15–6 (1932).
2. Frost, S. C. Physiological functions of the alpha class of carbonic anhydrases. *Subcell. Biochem.* **75**, 9–30 (2014).
3. Aggarwal, M., Boone, C. D., Kondeti, B. & McKenna, R. Structural annotation of human carbonic anhydrases. *J Enzyme Inhib Med Chem* **28**, 267–277 (2013).
4. Mincione, F. *et al*. Carbonic anhydrase inhibitors: design of thioureido sulfonamides with potent isozyme II and XII inhibitory properties and intraocular pressure lowering activity in a rabbit model of glaucoma. *Bioorg. Med. Chem. Lett.* **15**, 3821–3827 (2005).
5. Thiry, A., Dogné, J.-M., Supuran, C. T. & Masereel, B. Carbonic anhydrase inhibitors as anticonvulsant agents. *Curr Top Med Chem* **7**, 855–864 (2007).
6. Scozzafava, A., Supuran, C. T. & Carta, F. Antiobesity carbonic anhydrase inhibitors: a literature and patent review. *Expert Opinion on Therapeutic Patents* **23**, 725–735 (2013).
7. Mboge, M. Y., Mahon, B. P., McKenna, R. & Frost, S. C. Carbonic Anhydrases: Role in pH Control and Cancer. *Metabolites* **8** (2018).
8. Alterio, V., Di Fiore, A., D'Ambrosio, K., Supuran, C. T. & De Simone, G. Multiple Binding Modes of Inhibitors to Carbonic Anhydrases: How to Design Specific Drugs Targeting 15 Different Isoforms? *Chem. Rev.* **112**, 4421–4468 (2012).
9. Pinard, M. A. *et al*. Probing the Surface of Human Carbonic Anhydrase for Clues towards the Design of Isoform Specific Inhibitors, Probing the Surface of Human Carbonic Anhydrase for Clues towards the Design of Isoform Specific Inhibitors. *BioMed Research International*, *BioMed Research International* **2015**, **2015**, e453543 (2015).

10. Murakami, H. & Sly, W. S. Purification and characterization of human salivary carbonic anhydrase. *J. Biol. Chem.* **262**, 1382–1388 (1987).
11. Kivelä, J. *et al*. Secretory carbonic anhydrase isoenzyme (CA VI) in human serum. *Clin. Chem.* **43**, 2318–2322 (1997).
12. Karhumaa, P. *et al*. The identification of secreted carbonic anhydrase VI as a constitutive glycoprotein of human and rat milk. *Proc Natl Acad Sci USA* **98**, 11604–11608 (2001).
13. Leinonen, J. S., Saari, K. A., Seppänen, J. M., Myllylä, H. M. & Rajaniemi, H. J. Immunohistochemical demonstration of carbonic anhydrase isoenzyme VI (CA VI) expression in rat lower airways and lung. *J. Histochem. Cytochem.* **52**, 1107–1112 (2004).
14. Kaseda, M., Ichihara, N., Nishita, T., Amasaki, H. & Asari, M. Immunohistochemistry of the bovine secretory carbonic anhydrase isozyme (CA-VI) in bovine alimentary canal and major salivary glands. *J. Vet. Med. Sci.* **68**, 131–135 (2006).
15. Pan, P. *et al*. Gene expression profiling in the submandibular gland, stomach, and duodenum of CAVI-deficient mice. *Transgenic Res.* **20**, 675–698 (2011).
16. Patrikainen, M. S., Pan, P., Barker, H. R. & Parkkila, S. Altered gene expression in the lower respiratory tract of Car6 (−/−) mice. *Transgenic Res.* **25**, 649–664 (2016).
17. Patrikainen, M., Pan, P., Kulesskaya, N., Voikar, V. & Parkkila, S. The role of carbonic anhydrase VI in bitter taste perception: evidence from the Car6−/− mouse model. *J Biomed Sci* **21**, 82 (2014).
18. Melis, M. *et al*. The gustin (CA6) gene polymorphism, rs2274333 (A/G), as a mechanistic link between PROP tasting and fungiform taste papilla density and maintenance. *PLoS One* **8**, e74151 (2013).
19. Kivela, J., Parkkila, S., Parkkila, A. K., Leinonen, J. & Rajaniemi, H. Salivary carbonic anhydrase isoenzyme VI. *J. Physiol. (Lond.)* **520**(Pt 2), 315–320 (1999).
20. Kimoto, M., Kishino, M., Yura, Y. & Ogawa, Y. A role of salivary carbonic anhydrase VI in dental plaque. *Arch. Oral Biol.* **51**, 117–122 (2006).
21. Parkkila, S. *et al*. Salivary carbonic anhydrase protects gastroesophageal mucosa from acid injury. *Dig. Dis. Sci.* **42**, 1013–1019 (1997).
22. Hassan, M. I., Shajee, B., Waheed, A., Ahmad, F. & Sly, W. S. Structure, function and applications of carbonic anhydrase isozymes. *Bioorg Med Chem* **21**, 1570–1582 (2013).
23. Pastorek, J. & Pastorekova, S. Hypoxia-induced carbonic anhydrase IX as a target for cancer therapy: From biology to clinical use. *Seminars in Cancer Biology* **31**, 52–64 (2015).
24. Gibbons, B. H. & Edsall, J. T. Rate of Hydration of Carbon Dioxide and Dehydration of Carbonic Acid At 25 Degrees. *J. Biol. Chem.* **238**, 3502–3507 (1963).
25. Khalifah, R. G. The carbon dioxide hydration activity of carbonic anhydrase. I. Stop-flow kinetic studies on the native human isoenzymes B and C. *J. Biol. Chem.* **246**, 2561–2573 (1971).
26. Smirnovienė, J., Smirnovas, V. & Matulis, D. Picomolar inhibitors of carbonic anhydrase: Importance of inhibition and binding assays. *Anal. Biochem.* **522**, 61–72 (2017).
27. Kranz, J. K. & Schalk-Hihi, C. Protein thermal shifts to identify low molecular weight fragments. *Meth. Enzymol.* **493**, 277–298 (2011).
28. Niesen, F. H., Berglund, H. & Vedadi, M. The use of differential scanning fluorimetry to detect ligand interactions that promote protein stability. *Nat Protoc* **2**, 2212–2221 (2007).
29. Matulis, D., Kranz, J. K., Salemme, F. R. & Todd, M. J. Thermodynamic stability of carbonic anhydrase: measurements of binding affinity and stoichiometry using ThermoFluor. *Biochemistry* **44**, 5258–5266 (2005).
30. Rogez-Florent, T. *et al*. Label-free characterization of carbonic anhydrase-novel inhibitor interactions using surface plasmon resonance, isothermal titration calorimetry and fluorescence-based thermal shift assays. *J. Mol. Recognit.* **27**, 46–56 (2014).
31. Garbett, N. C. & Chaires, J. B. Thermodynamic studies for drug design and screening. *Expert Opin Drug Discov* **7**, 299–314 (2012).
32. Zubrienė, A. *et al*. Intrinsic Thermodynamics and Structures of 2,4- and 3,4-Substituted Fluorinated Benzenesulfonamides Binding to Carbonic Anhydrases. *ChemMedChem* **12**, 161–176 (2017).
33. Linkuvienė, V. *et al*. Intrinsic thermodynamics of inhibitor binding to human carbonic anhydrase IX. *Biochimica et Biophysica Acta (BBA) - General Subjects* **1860**, 708–718 (2016).
34. Zubrienė, A. *et al*. Intrinsic thermodynamics of 4-substituted-2,3,5,6-tetrafluorobenzenesulfonamide binding to carbonic anhydrases by isothermal titration calorimetry. *Biophys. Chem.* **205**, 51–65 (2015).
35. Baranauskienė, L. & Matulis, D. Intrinsic thermodynamics of ethoxzolamide inhibitor binding to human carbonic anhydrase XIII. *BMC Biophys* **5**, 12 (2012).
36. Rosano, G. L. & Ceccarelli, E. A. Recombinant protein expression in Escherichia coli: advances and challenges. *Front Microbiol* **5** (2014).
37. Jia, B. & Jeon, C. O. High-throughput recombinant protein expression in Escherichia coli: current status and future perspectives. *Open Biol* **6** (2016).
38. Gopal, G. J. & Kumar, A. Strategies for the production of recombinant protein in Escherichia coli. *Protein J.* **32**, 419–425 (2013).
39. Idicula-Thomas, S. & Balaji, P. V. Understanding the relationship between the primary structure of proteins and its propensity to be soluble on overexpression in Escherichia coli. *Protein Sci.* **14**, 582–592 (2005).
40. Kazokaitė, J., Milinavičiūtė, G., Smirnovienė, J., Matulienė, J. & Matulis, D. Intrinsic binding of 4-substituted-2,3,5,6-tetrafluorobenezenesulfonamides to native and recombinant human carbonic anhydrase VI. *FEBS J.* **282**, 972–983 (2015).
41. Morkūnaitė, V. *et al*. Intrinsic thermodynamics of sulfonamide inhibitor binding to human carbonic anhydrases I and II. *J Enzyme Inhib Med Chem* **30**, 204–211 (2015).
42. Cimmperman, P. & Matulis, D. Chapter 8:Protein Thermal Denaturation Measurements via a Fluorescent Dye. In *Chapter 8:Protein Thermal Denaturation Measurements via a Fluorescent Dye* 247–274 (2011).
43. Holdgate, G. A., Meek, T. D. & Grimley, R. L. Mechanistic enzymology in drug discovery: a fresh perspective. *Nature Reviews Drug Discovery* **17**, 115–132 (2018).
44. Nishimori, I. *et al*. Carbonic anhydrase activators: the first activation study of the human secretory isoform VI with amino acids and amines. *Bioorg. Med. Chem.* **15**, 5351–5357 (2007).
45. Winum, J.-Y., Montero, J.-L., Vullo, D. & Supuran, C. T. Carbonic anhydrase inhibitors: glycosylsulfanilamides act as subnanomolar inhibitors of the human secreted isoform VI. *Chem Biol Drug Des* **74**, 636–639 (2009).
46. Tars, K. *et al*. Sulfocoumarins (1,2-Benzoxathiine-2,2-dioxides): A Class of Potent and Isoform-Selective Inhibitors of Tumor-Associated Carbonic Anhydrases. *J. Med. Chem.* **56**, 293–300 (2013).
47. Genis, C. *et al*. Design of a carbonic anhydrase IX active-site mimic to screen inhibitors for possible anticancer properties. *Biochemistry* **48**, 1322–1331 (2009).
48. Sippel, K. H. *et al*. Characterization of Carbonic Anhydrase Isozyme Specific Inhibition by Sulfamated 2-Ethylestra Compounds. *Lett. Drug Des. Discovery* **8**, 1–25 (2011).
49. Moeker, J. *et al*. Structural Insights into Carbonic Anhydrase IX Isoform Specificity of Carbohydrate-Based Sulfamates. *Journal of Medicinal Chemistry* **57**, 8635–8645 (2014).
50. Pinard, M. A., Aggarwal, M., Mahon, B. P., Tu, C. & McKenna, R. A sucrose-binding site provides a lead towards an isoform-specific inhibitor of the cancer-associated enzyme carbonic anhydrase IX. *Acta Crystallogr F Struct Biol Commun* **71**, 1352–1358 (2015).
51. Mahon, B. P. *et al*. Saccharin: A lead compound for structure-based drug design of carbonic anhydrase IX inhibitors. *Bioorganic & Medicinal Chemistry* **23**, 849–854 (2015).

52. Pinard, M. A., Boone, C. D., Rife, B. D., Supuran, C. T. & McKenna, R. Structural study of interaction between brinzolamide and dorzolamide inhibition of human carbonic anhydrases. *Bioorg Med Chem* **21**, 7210–7215 (2013).
53. Dudutienė, V. *et al*. Discovery and characterization of novel selective inhibitors of carbonic anhydrase IX. *J. Med. Chem.* **57**, 9435–9446 (2014).
54. Krebs, J. F. & Fierke, C. A. Determinants of catalytic activity and stability of carbonic anhydrase II as revealed by random mutagenesis. *J. Biol. Chem.* **268**, 948–954 (1993).
55. Behravan, G., Jonasson, P., Jonsson, B. H. & Lindskog, S. Structural and functional differences between carbonic anhydrase isoenzymes I and II as studied by site-directed mutagenesis. *Eur. J. Biochem.* **198**, 589–592 (1991).
56. Sjöblom, B., Polentarutti, M. & Djinovic-Carugo, K. Structural study of X-ray induced activation of carbonic anhydrase. *Proc. Natl. Acad. Sci. USA* **106**, 10609–10613 (2009).
57. Krishnamurthy, V. M. *et al*. Carbonic anhydrase as a model for biophysical and physical-organic studies of proteins and protein-ligand binding. *Chem. Rev.* **108**, 946–1051 (2008).
58. Linkuvienė, V. *et al*. Thermodynamic, kinetic, and structural parameterization of human carbonic anhydrase interactions toward enhanced inhibitor design. *Quarterly Reviews of Biophysics* **51** (2018).
59. Kovalevsky, A. *et al*. 'To Be or Not to Be' Protonated: Atomic Details of Human Carbonic Anhydrase-Clinical Drug Complexes by Neutron Crystallography and Simulation. *Structure* **26**, 383–390.e3 (2018).
60. Koruza, K. *et al*. Using neutron crystallography to elucidate the basis of selective inhibition of carbonic anhydrase by saccharin and a derivative. *Journal of Structural Biology*, https://doi.org/10.1016/j.jsb.2018.12.009 (2019).
61. Pilka, E. S., Kochan, G., Oppermann, U. & Yue, W. W. Crystal structure of the secretory isozyme of mammalian carbonic anhydrases CA VI: implications for biological assembly and inhibitor development. *Biochem. Biophys. Res. Commun.* **419**, 485–489 (2012).
62. Patrikainen, M. S. *et al*. Identification and characterization of a novel zebrafish (Danio rerio) pentraxin-carbonic anhydrase. *PeerJ* **5**, e4128 (2017).
63. Linkuvienė, V., Krainer, G., Chen, W.-Y. & Matulis, D. Isothermal titration calorimetry for drug design: Precision of the enthalpy and binding constant measurements and comparison of the instruments. *Anal. Biochem.* **515**, 61–64 (2016).
64. Paketurytė, V., Linkuvienė, V., Krainer, G., Chen, W.-Y. & Matulis, D. Repeatability, precision, and accuracy of the enthalpies and Gibbs energies of a protein–ligand binding reaction measured by isothermal titration calorimetry. *European Biophysics Journal*, https://doi.org/10.1007/s00249-018-1341-z (2018).
65. Dudutienė, V. *et al*. Functionalization of fluorinated benzenesulfonamides and their inhibitory properties toward carbonic anhydrases. *ChemMedChem* **10**, 662–687 (2015).
66. Zubrienė, A. *et al*. Benzenesulfonamides with benzimidazole moieties as inhibitors of carbonic anhydrases I, II, VII, XII and XIII. *J Enzyme Inhib Med Chem* **29**, 124–131 (2014).
67. Dudutienė, V. *et al*. 4-Substituted-2,3,5,6-tetrafluorobenzenesulfonamides as inhibitors of carbonic anhydrases I, II, VII, XII, and XIII. *Bioorg. Med. Chem.* **21**, 2093–2106 (2013).
68. Čapkauskaitė, E. *et al*. Benzenesulfonamides with pyrimidine moiety as inhibitors of human carbonic anhydrases I, II, VI, VII, XII, and XIII. *Bioorganic & Medicinal Chemistry* **21**, 6937–6947 (2013).
69. Pettersen, E. F. *et al*. UCSF Chimera–a visualization system for exploratory research and analysis. *J Comput Chem* **25**, 1605–1612 (2004).
70. Pei, J., Kim, B.-H. & Grishin, N. V. PROMALS3D: a tool for multiple protein sequence and structure alignments. *Nucleic Acids Res* **36**, 2295–2300 (2008).
71. Beitz, E. TeXshade: shading and labeling of multiple sequence alignments using LaTeX2e. *Bioinformatics* **16**, 135–139 (2000).
72. Cimmperman, P. *et al*. A quantitative model of thermal stabilization and destabilization of proteins by ligands. *Biophys. J.* **95**, 3222–3231 (2008).
73. Carrigan, P. E., Ballar, P. & Tuzmen, S. Site-directed mutagenesis. *Methods Mol. Biol.* **700**, 107–124 (2011).
74. Morrison, J. F. Kinetics of the reversible inhibition of enzyme-catalysed reactions by tight-binding inhibitors. *Biochim. Biophys. Acta* **185**, 269–286 (1969).
75. Williams, J. W. & Morrison, J. F. The kinetics of reversible tight-binding inhibition. *Meth. Enzymol.* **63**, 437–467 (1979).
76. Baranauskienė, L. *et al*. Inhibition and binding studies of carbonic anhydrase isozymes I, II and IX with benzimidazo[1,2-c][1,2,3] thiadiazole-7-sulphonamides. *J Enzyme Inhib Med Chem* **25**, 863–870 (2010).
77. Kazlauskas, E. *et al*. Thermodynamics of Aryl-Dihydroxyphenyl-Thiadiazole Binding to Human Hsp90. *PLoS One* **7**, e36899 (2012).
78. Goldberg, R. N., Kishore, N. & Lennen, R. M. Thermodynamic Quantities for the Ionization Reactions of Buffers. *Journal of Physical and Chemical Reference Data* **31** (2002).
79. Kabsch, W. XDS. *Acta Cryst D* **66**, 125–132 (2010).
80. Vagin, A. & Teplyakov, A. MOLREP: an Automated Program for Molecular Replacement. *J Appl Cryst, J Appl Crystallogr* **30**, 1022–1025 (1997).
81. Hanwell, M. D. *et al*. Avogadro: An advanced semantic chemical editor, visualization, and analysis platform. *J Cheminform* **4**, 17 (2012).
82. Vagin, A. A. *et al*. REFMAC5 dictionary: organization of prior chemical knowledge and guidelines for its use. *Acta Crystallogr D Biol Crystallogr* **60**, 2184–95 (2004).
83. Winn, M. D. *et al*. Overview of the CCP4 suite and current developments. *Acta Crystallogr D Biol Crystallogr* **67**, 235–242 (2011).
84. Emsley, P., Lohkamp, B., Scott, W. G. & Cowtan, K. Features and development of Coot. *Acta Crystallogr. D Biol. Crystallogr.* **66**, 486–501 (2010).
85. Murshudov, G. N., Vagin, A. A. & Dodson, E. J. Refinement of macromolecular structures by the maximum-likelihood method. *Acta Crystallogr. D Biol. Crystallogr.* **53**, 240–255 (1997).
86. Čapkauskaitė, E. *et al*. Combinatorial Design of Isoform-Selective N-Alkylated Benzimidazole-Based Inhibitors of Carbonic Anhydrases. *ChemistrySelect* **2**, 5360–5371 (2017).

Acknowledgements

Authors thank Gleb Bourenkov for the help with data collection at P14 EMBL beamline at PETRA III ring of the DESY synchrotron. The access to the beamline was supported by iNEXT (grant number 653706) funded by the Horizon 2020 program of the European Commission. The study was also supported by the grant S-MIP-17-87 from the Research Council of Lithuania.

Author Contributions

J.K., J.S., V.K., A.S., M.T., S.P. and D.M. participated in the conception or design of the study; J.K. produced recombinant proteins, carried out biophysical assays and analyzed thermodynamic parameters; V.K. performed computational modelling; J.S. carried out enzymatic activity and inhibition measurements; A.S. and E.M. were responsible for X-ray crystallographic analysis; J.K. wrote the first version of manuscript; J.K., V.K., J.S., A.S., E.M., M.T., S.P. and D.M. contributed to manuscript drafting and approved the final version of manuscript.

Additional Information

Supplementary information accompanies this paper at https://doi.org/10.1038/s41598-019-49094-0.

Competing Interests: D.M. declares that he has patents and patent applications pending on CA inhibitors.

Publisher's note: Springer Nature remains neutral with regard to jurisdictional claims in published maps and institutional affiliations.

Open Access This article is licensed under a Creative Commons Attribution 4.0 International License, which permits use, sharing, adaptation, distribution and reproduction in any medium or format, as long as you give appropriate credit to the original author(s) and the source, provide a link to the Creative Commons license, and indicate if changes were made. The images or other third party material in this article are included in the article's Creative Commons license, unless indicated otherwise in a credit line to the material. If material is not included in the article's Creative Commons license and your intended use is not permitted by statutory regulation or exceeds the permitted use, you will need to obtain permission directly from the copyright holder. To view a copy of this license, visit http://creativecommons.org/licenses/by/4.0/.

© The Author(s) 2019

Check for updates

Chemistry Europe
European Chemical Societies Publishing

Switching the Inhibitor-Enzyme Recognition Profile via Chimeric Carbonic Anhydrase XII

Joana Smirnovienė,[a] Alexey Smirnov,[a] Audrius Zakšauskas,[a] Asta Zubrienė,[a] Vytautas Petrauskas,[a] Aurelija Mickevičiūtė,[a] Vilma Michailovienė,[a] Edita Čapkauskaitė,[a] Elena Manakova,[b] Saulius Gražulis,[b] Lina Baranauskienė,[a] Wen-Yih Chen,[c] John E. Ladbury,[d] and Daumantas Matulis*[a]

A key part of the optimization of small molecules in pharmaceutical inhibitor development is to vary the molecular design to enhance complementarity of chemical features of the compound with the positioning of amino acids in the active site of a target enzyme. Typically this involves iterations of synthesis, to modify the compound, and biophysical assay, to assess the outcomes. Selective targeting of the anti-cancer carbonic anhydrase isoform XII (CA XII), this process is challenging because the overall fold is very similar across the twelve CA isoforms. To enhance drug development for CA XII we used a reverse engineering approach where mutation of the key six amino acids in the active site of human CA XII into the CA II isoform was performed to provide a protein chimera (chCA XII) which is amenable to structure-based compound optimization. Through determination of structural detail and affinity measurement of the interaction with over 60 compounds we observed that the compounds that bound CA XII more strongly than CA II, switched their preference and bound more strongly to the engineered chimera, chCA XII, based on CA II, but containing the 6 key amino acids from CA XII, behaved as CA XII in its compound recognition profile. The structures of the compounds in the chimeric active site also resembled those determined for complexes with CA XII, hence validating this protein engineering approach in the development of new inhibitors.

1. Introduction

The development of selective inhibitors targeted at structurally highly similar enzyme isoforms is a challenging task in drug discovery. Enzyme-inhibitor binding interactions occur via key amino acids at defined positions, usually in the active site of the enzyme. Identifying the bonding patterns of the residues participating in the intermolecular interactions provides insight into the catalytic mechanism and the opportunity for inhibitor recognition.[1] In the case of inhibition of protein isoforms, detecting the distinguishing amino acid interactions is crucial for the design of isoform-selective inhibitors.

Carbonic anhydrases (CAs, EC 4.2.1.1) catalyze reversible hydration of carbon dioxide to bicarbonate and protons. Their isoforms play roles in numerous physiological and pathological processes by regulating the pH and bicarbonate balance.[2–5] CA inhibitors have been used as therapeutic options in a number of disease areas including anti-glaucoma agents,[6,7] diuretics[8] and antiepileptics.[9–12] However, most of the clinically used inhibitors lack selectivity towards targeted CA isoforms and exhibit various side effects. There is thus, a demand for selective inhibitors that target only the disease-associated CA isoform, for instance, isoforms IX or XII, which regulate the pH of a tumor microenvironment.[13]

Design and development of CA isoform-selective inhibitors is challenging due to the high amino acid sequence homology between isoforms. Humans have twelve catalytically active CA isoforms: CA I, CA II, CA III, CA VII, CA XIII (cytosolic), CA VA and CA VB (mitochondrial), CA VI (secreted), CA IV, CA IX, CA XII, CA XIV (membrane-bound). Active sites of CA isoforms are cone-shaped and differ from each other by several residues.

CA XII is an important isoform since it controls the extracellular pH of cancer cells under physiological conditions

[a] J. Smirnovienė, Dr. A. Smirnov, A. Zakšauskas, Dr. A. Zubrienė, Dr. V. Petrauskas, A. Mickevičiūtė, V. Michailovienė, Dr. E. Čapkauskaitė, Dr. L. Baranauskienė, Prof. D. Matulis
Department of Biothermodynamics and Drug Design
Institute of Biotechnology, Life Sciences Center
Vilnius University, Saulėtekio 7
Vilnius 10257 (Lithuania)
E-mail: daumantas.matulis@bti.vu.lt
[b] Dr. E. Manakova, Prof. S. Gražulis
Department of Protein-DNA Interactions
Institute of Biotechnology
Life Sciences Center
Vilnius University
Saulėtekio 7
Vilnius 10257 (Lithuania)
[c] Prof. W.-Y. Chen
Department of Chemical and Materials Engineering
Institute of Systems Biology and Bioinformatics
National Central University (Taiwan)
[d] Prof. J. E. Ladbury
School of Molecular and Cellular Biology
University of Leeds
LC MiaII Building
Leeds, LS2 9JT (UK)

Supporting information for this article is available on the WWW under https://doi.org/10.1002/open.202100042

© 2021 The Authors. Published by Wiley-VCH GmbH. This is an open access article under the terms of the Creative Commons Attribution Non-Commercial NoDerivs License, which permits use and distribution in any medium, provided the original work is properly cited, the use is non-commercial and no modifications or adaptations are made.

and acts as a hypoxia-induced tumor marker. CA XII is regulated by estrogen receptor in breast cancer.[14] High expression of CA XII correlates with favorable survival of patients having invasive breast[15] or resectable non-small cell lung cancers.[16] However, it is associated with poor prognosis in patients with colorectal,[17] hepatocellular[18] carcinomas, and diffuse astrocytomas.[19] Furthermore, CA XII is considered as a pharmacological target to overcome chemoresistance in cancer cells.[20] The lower wide-spread expression of CA XII has also been detected in human eye,[21] gut,[22] kidney,[23] pancreas,[24] gastric mucosa,[25] epithelial components of skin,[26] endometrial epithelium[27] and male excurrent ducts.[28] Additional roles of CA XII in the human body include glaucoma progression,[21] salt uptake in sweat glands,[29] and pH regulation of nucleus pulposus cells.[30] CA XII function in disease is reviewed in detail by Waheed and Sly.[31]

CA XII is an important but highly challenging drug target. Traditional screening and drug design protocols are limited because it is a membrane-associated dimeric enzyme containing N-terminal extracellular catalytic domain, a membrane-spanning α-helix, and a 30-residue small intracellular C-terminal region. CA XII has been the focus of numerous studies to determine its structure and function down to the atomic level. The first crystallographic structure of CA XII at 1.55 Å resolution was solved in 2001.[32] The protein has GXXXG and GXXXS dimerization motifs in the transmembrane segment, two glycosylation sites, Asn52 and Asn136, exposed on the surface and a single disulfide linkage between Cys23 and Cys203. The active site composition is analogous to the most studied CA II: the zinc ion is coordinated by His94, His96, His119 and a water molecule. The pK_a of the zinc-bound water molecule at 25 °C is 7.0–7.1.[33,34] A large body of work has resulted in the deposition of structural data for 24 crystal structures of chlorinated/fluorinated *mono-/di*-substituted benzenesulfonamides bound to CA XII complexes[35–42] to the PDB. This forms a valuable resource for CA XII inhibitor design.

The high-resolution structural data is complemented by a wealth of thermodynamic, kinetic and structural analysis of interactions between more than 400 inhibitors and 12 CA isoforms. These reveal that minor structural differences between CA isoforms can cause unpredictable effects to the changes of selective recognition between a ligand and target isoform.[43] Most conserved residues are found deep within the active site (close to the zinc ion),[44] whilst the top of the binding site is more variable.

Here we use a protein engineering approach to produce a chimeric version based on the CA II isoform which is soluble and highly amenable to drug development strategies. In an earlier study we showed that CA II-based mutant with six CA XII-specific residues (A65S, N67K, I91T, F130A, V134S, and L203N), resembled the active site of CA XII.[39] We, therefore, produced a chimeric CA XII protein (chCA XII) which recapitulates the CA XII enzyme activity and function. We have characterized the catalytic activity and thermal stability of chCA XII, as well as conducted ligand binding and inhibition studies with 63 small molecule compounds by enzymatic and biophysical assays. For the design of novel and selective anticancer drug candidates we have analyzed the structural differences between the targeted CA XII and off-target, ubiquitously expressed, CA II, which share 34% sequence identity.[45] We have obtained nine crystal structures of inhibitors bound to chCA XII and compared the binding modes together with binding affinities of inhibitors to CA II and CA XII. The detailed analysis validates the protein engineering a route to selective inhibitors of the CA XII isoform.

2. Results

The principal hypothesis and approach in constructing chCA XII is shown in Figure 1. The chimeric protein produced is essentially the same CA II, except that it would recognize inhibitors that would be normally recognized by CA XII. The sequences of CA II and CA XII were aligned (supplementary Figure S1) and six amino acids (A65S, N67K, I91T, F130A, V134S, and L203N) in the vicinity of the ligand binding site that differ between CA II and CA XII were mutated resulting in a chimeric form of CA II (chCA XII) whose ligand recognition mirrored that of CA XII.

2.1. Catalytic Properties of chCA XII Closely Mimic CA XII

To ascertain the role of key amino acids in the active site of CA XII, the thermal stability and catalytic activity of the chCA XII was measured in a wide pH range and compared to the properties of CA II and CA XII.[46,47] Six mutations (A65S, N67K, I91T, F130A, V134S and L203N) in the active site of CA II resulted in increased thermal stability by 0.5 °C in the pH range 4.5–10.0 (Figure 2A). The CA II and chCA XII were most stable at pH 6.0–8.0 with melting temperature T_m 55.6 ± 0.1 °C and 56.1 ± 0.1 °C, respectively. The CA XII had different stability profile with the maximum T_m = 53.6 ± 0.2 °C at pH 6.0. In addition, the chCA XII had similar maximal catalytic activity as CA II (k_{cat} = 6.0 × 10^5 s^{-1}), but larger pK_a value of His64 by 0.6 units (pK_a = 7.9 ± 0.2 for chCA XII and pK_a = 7.3 ± 0.2 for CA II) as shown in Figure 2B. The determined maximal catalytic constant of CA XII was (4.1 ± 0.9) × 10^5 s^{-1} with pK_a of 7.6 ± 0.2. Interestingly, the Michaelis-Menten constant of chCA XII (K_M = 3.6 ± 2.0 mM) was

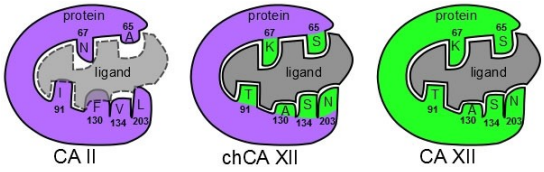


Figure 1. The general scheme of engineering the chimeric CA XII (chCA XII). The CA XII-selective inhibitor is shown in gray. The hypothetical inhibitor is unable to bind to CA II (violet) but is supposed to bind well to chCA XII (violet-green) and CA XII (green). To obtain chCA XII, six residues in the active site of CA II were replaced by the ones present in CA XII at the same locations of the active site (N67→K67, A65→S65, I91→T91, F130→A130, V134→S134, and L203→N203).

© 2021 The Authors. Published by Wiley-VCH GmbH

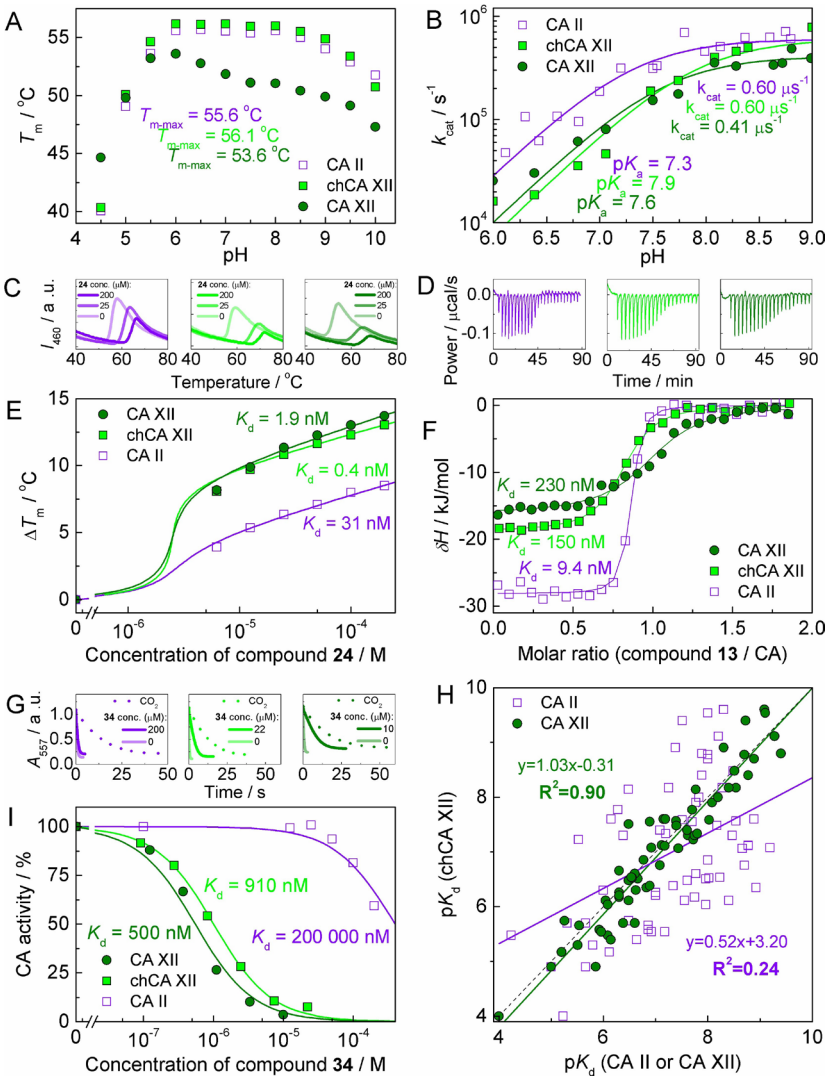


Figure 2. Experimental data of stability, catalytic activity and inhibitor binding of CA II (violet squares), CA XII (dark green circles) and chCA XII (light green squares) by FTSA (panels A, C, E, H), ITC (panels D, F) and SFA (panels G, I) techniques. (A) Thermal stability profiles of CA's at pH 4.5–10.0. (B) Catalytic constant of CA dependence on pH in the range 6.0–9.0. (C) Unfolding curves of the proteins at 0, 25 and 200 µM inhibitor **24** concentrations. (D) Raw curves of CA titrations with inhibitor **13**. (E) Thermal shifts of CA melting temperature at increasing inhibitor **24** concentrations up to 200 µM. (F) Integrated titration curves for inhibitor **13** binding to CA. (G) Acidification curves of spontaneous and catalyzed CO_2 hydration reaction by CA at several inhibitor **34** concentrations. (H) Correlations of observed pK_d's between chCA XII and CA XII (R^2 = 0.90) or CA II (R^2 = 0.24). The theoretically perfect positive correlation is represented as a black dashed line and linear regression models are shown as green (y = 1.03x–0.31) and violet (y = 0.52x + 3.20) lines. (I) Dose-response curves of inhibition of CA enzymatic activity by **34**. Overall, all shown figures here confirm that the chCA XII protein is recognized by compounds similarly to CA XII, but different from CA II.

similar to CA XII (K_M = 3.6 ± 1.5 mM) and differed from CA II (K_M = 4.7 ± 1.0 mM) in the pH range 6.8–9.0 (Figure S2). The site-directed mutagenesis of CA II slightly stabilized the enzyme and retained the catalytic efficiency (k_{cat} has not changed), but the pK_a of a proton shuttle His64 has increased while the K_M value decreased to approach the CA XII.

© 2021 The Authors. Published by Wiley-VCH GmbH

2.2. chCA XII Structure-Affinity Data Recapitulate Wild Type Interactions

To understand the reasons for affinity and selectivity of inhibitors targeting CA II and CA XII, we measured interactions between a series of 63 sulfonamide-based inhibitors and chCA XII by fluorescent thermal shift assay (FTSA, also called Thermofluor® or differential scanning fluorimetry) and compared the binding constants to those of CA II and CA XII.[43] We also used stopped-flow CO_2 hydration assay (SFA) to confirm the inhibitory properties of chemical compounds and isothermal titration calorimetry (ITC) to determine the thermodynamic parameters of binding. As control compounds, we used commercially available inhibitors - ethoxzolamide (EZA), acetazolamide (AZM), methazolamide (MZM), naphthalene-2-sulfonamide (2-NSA) and 1-(4-fluorophenyl)-3-(4-sulfamoylphenyl)urea (U-104/SLC-0111). Figure 2 shows representative experimental data by FTSA (panels C, E), ITC (panels D, F) and SFA (panels G, I).

X-ray crystallographic structures of chCA XII were solved in complex with nine compounds (**6**, **9**, **11**, **13**, **43**, **44**, **48**, **50**, and **52**). Electron densities of compounds are shown in Figure S3 and data collection and refinement statistics are presented in the Table S1. Several compounds bound to CA II and CA XII have been characterized previously, so we compared the binding of inhibitors by chCA XII with parental CA II and CA XII isoforms. Inhibitors used in the study could be arranged to 3 groups according to binding affinities: first that possessed more than 10-fold selectivity towards CA II over CA XII, second that possessed more than 10-fold selectivity for CA XII over CA II, and third that bound CA II and CA XII with similar dissociation constants. The binding affinities determined by FTSA were in good agreement with ITC and SFA assays as previously discussed.[43,46,48] As shown there, we use the K_d values obtained by FTSA method since this technique provides the most accurate results.

2.3. CA II-Selective Compounds

The compounds analyzed formed three broad groups. The first group comprised drug ethoxzolamide (**1**), non-halogenated, chlorinated, or fluorinated benzensulfonamides with substituents at *para*- (**2**–**16**), *ortho*- (**17**) or *meta*- (**18**–**22**) positions (Figure 3, upper part) that bind to CA II more strongly than CA XII. The binding affinities are provided in Table 1. The majority of chemical compounds **1**–**22** (with exception of **2**, **4** and **17**) are strong nanomolar inhibitors of CA II (K_d 0.65–67 nM) possessing up to 200-fold selectivity over CA XII (K_d 37–1100 nM) and chCA XII (K_d 25–2900 nM). Ureidosulfonamide **2** (U104/SLC-0111) has been previously published as a strong inhibitor of CA XII with $K_i = 4.5$ nM and a moderate inhibitor of CA II with $K_i = 96$ nM.[49] However, we have observed that the binding affinities of compound **2** were stronger for CA II (K_d 330 nM by FTSA, 150 nM by SFA, 200 nM by ITC) than for CA XII (K_d 5500 nM by FTSA, 1900 nM by SFA, unobservable K_d by ITC due to weak binding). According to our results, this compound inhibits CA II, chCA XII and CA XII weaker than other *para*-substituted compounds **3**–**16**.

The observed binding affinities of nonfluorinated compounds **3** and **4** were approximately ten-fold lower than analogous fluorinated compounds **9** and **10** due higher pK_a value of sulfonamide group of inhibitors **3** and **4**.[41] Modification of methyl group in **3** and **9** to hydroxy group (compounds **4** and **10**) of *para*-substituent weakened the binding by several times. The additional morpholine substituent at *ortho*- position (compound **17**) decreased the binding affinity for CA II by over 1000-fold (K_d 5.9 μM) and chCA XII, CA XII (K_d 100 μM). However, additional substituents at *meta*- position (compounds **18**–**21**) did not have notable change of binding affinity or selectivity. Dichloro *meta*-substituted compound **22** also bound CA II 14–17-fold stronger than chCA XII or CA XII. The binding affinities of compounds **1**–**22** representing the first group were similar for chCA XII and CA XII, thus chCA XII closely mimicked the CA XII.

Crystal structures of four *para*-substituted compounds (**6**, **9**, **11**, and **13**) bound to chCA XII were solved and compared to the complexes of CA II and CA XII with these inhibitors. The superimposed binding modes of compounds **6**, **9**, **11** and **13** in the active sites of CA II, CA XII and chCA XII are shown in Figure 4. This group of compounds bound CA II stronger than CA XII (as well as chCA XII): 6–75-fold (11 vs 830 nM), 9–17-fold (2.2 vs 37 nM), 11–15-fold (17 vs 250 nM), and 13–29-fold (9.6 vs 280 nM). The fluorinated ring of *para*-substituted benzenesulfonamides (**9**, **11**, **13**) could be found in two orientations in the active site of CA II, chCA XII and CA XII. For example, compound **13** (Figure 4D) had identical orientation of fluorinated ring in CA II and chCA XII active sites, whereas in CA XII we found two alternative positions of fluorinated ring. Despite such differences in the binding mode of compound **13** to CA XII and chCA XII, the binding affinities were similar. The stronger binding to CA II could be due to dimethyl pyrimidine interaction with the phenylalanine side chain Phe131, whereas in chCA XII and CA XII the position of dimethyl pyrimidine varied. The electron density of the dimethyl pyrimidine in the crystal structure of chCA XII was rather weak, suggesting mobility. Compound **11** had two alternative positions of fluorinated ring in active site of chCA XII, whereas in the crystal structures of CA II and CA XII it had a single but different position of fluorinated ring (Figure 4C). In CA II, the side chain of Phe130 reduced the mobility of the flexible tail. In chCA XII, the electron density of the tail was also weak. The electron density of **9** bound in chCA XII was well-defined and compound was modeled in a single orientation. In the crystal structures of CA II, the position of the ligand was different. Compound bound in all four subunits of asymmetric unit of CA XII is found in multiple conformations with variable positions of the tail (Figure 4B). The position of the chlorinated benzene ring of compound **6** as in the case of other chlorosubstituted benzenesulfonamide derivatives was fixed.[38,50]

There were differences of binding mode in the position of *para*-substituent. The positions of the pyrimidine ring in CA XII differed from that in CA II and chCA XII (Figure 4A). Despite the differences in the position of *para*-substituent, compound **6**

© 2021 The Authors. Published by Wiley-VCH GmbH

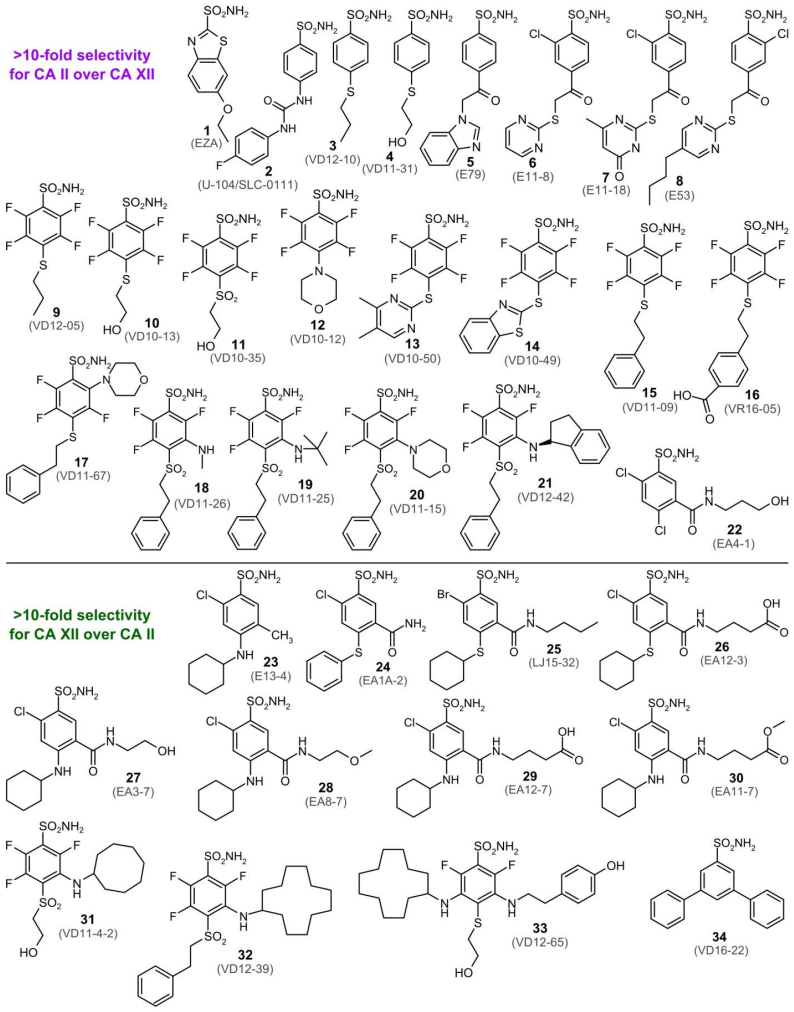


Figure 3. Chemical structures of compounds **1**–**34** used in this study arranged according to their selectivity. Benzenesulfonamides **1**–**22** bound more than 10-fold stronger to CA II than to CA XII, while compounds **23**–**34** were more than 10-fold stronger binders of CA XII.

showed the same binding affinities towards chCA XII and CA XII. Note that the affinities of compound **6** for CA II and CA XII differed 75-fold. The reason for this was that pyrimidine substituent of compound **6** in CA II is located in the hydrophobic cavity formed by side chains of Phe130, Val134, Leu203 and conservative between CA II and CA XII-Pro201 and Leu197. The *para*-substituents of compounds **9** and **13** also had close interactions with this hydrophobic cavity in active site of CA II. Active site of CA XII does not contain such hydrophobic cavity and has alanine instead Phe130 (in CA II), serine instead Val134 and asparagine instead Leu203.

2.4. CA XII-Selective Compounds

The second group of compounds included halogenated benzensulfonamides **23**–**34** that possess higher than ten-fold selectivity for anticancer target CA XII over off-target CA II (Figure 3 lower part). The chemical compounds are nanomolar inhibitors of CA XII (as well as chCA XII) as listed in Table 1. Inhibitors **23**–**29** have Cl– or Br– atom at the *ortho*- position, cyclohexylamino or cyclohexylsulfanyl tail at *para*- position and varying tail with amide linkage (except **23**) at *meta*- position. Compound **23** with methyl substituent at *meta*- position bound CAs with K_d 420–5000 nM while compounds **24**–**29** with amide linkage at the same position strengthens the binding up to

© 2021 The Authors. Published by Wiley-VCH GmbH

Table 1. The *observed* dissociation constants (K_d, nM) of CA II-selective compounds **1**–**22** and CA XII-selective compound **23**–**34** binding to recombinant human CA II, chCA XII and CA XII, determined by fluorescent thermal shift assay (pH 7.0, 37 °C) and confirmed by isothermal titration calorimetry (shown in the parentheses, pH 7.0, 37 °C) and stopped-flow CO_2 hydration assay (shown in the parentheses as second value in italic font, pH 7.5, 24 °C).

Compound No.	Lab. name	Carbonic anhydrase K_d [nM][a] CA II	chCA XII	CA XII	K_d ratio CA XII/CA II
>10-fold selectivity for CA II over CA XII					
1	EZA	1.3	25	71	55
2	U-104/ SLC-0111	330 (200, *150*)	1800 (780, *300*)	5500 (NA, *1900*)	17
3	VD12-10	25	330	330	13
4	VD11-31	140 *(100)*	2200 *(330)*	2900 *(5000)*	21
5	E79	4.0	770	910	228
6	E11-8	11 (38)	910 (920)	830 (600)	75
7	E11-18	28	770	330	12
8	E53	67	2860	1100	16
9	VD12-05	2.2 (≤ 12)	86 (44)	37 (47)	17
10	VD10-13	11	310	220	20
11	VD10-35	17 (≤ 12)	250 (180)	250 (140)	15
12	VD10-12	18	670	500	28
13	VD10-50	9.6 (≤ 12)	300 (150)	280 (230)	29
14	VD10-49	0.65	84	120	185
15	VD11-9	1.7	75	76	45
16	VR16-05	2.0	175	83	42
17	VD11-67	5900	100000	100000	17
18	VD11-26	5.9	290	290	49
19	VD11-25	1.7	77	67	39
20	VD11-15	1.2	450	150	125
21	VD12-42	2.9	27	41	14
22	EA4-1	10	140	170	17
>10-fold selectivity for CA XII over CA II CA II/ CA XII					
23	E13-4	5000	2000	420	12
24	EA1A-2	31	0.4	1.9	16
25	LJ15-32	6.3	0.77	0.53	12
26	EA12-3	13	1.6	0.4	33
27	EA3-7	420	50 (≤ 12)	24 (≤ 12)	17
28	EA8-7	330 (120)	7.2 (≤ 12)	17 (19)	20
29	EA12-7	3000 (*500*)	59 (21, *< 25)*	19 *(≤ 12, < 25)*	160
30	EA11-7	530	17 (25)	20 (56)	27
31	VD11-4-2	56	6.7	2.9	19
32	VD12-39	710	25	65	11
33	VD12-65	> 200000	220	500	> 400
34	VD16-22	58000 (*200000*)	3330 *(910)*	830 (*500*)	70

[a] FTSA data for CA II and CA XII were taken from,[43] except for compounds **23**, **25**,[36] **34**,[52] **2** (U-104/SLC-0111) and **16**-determined in this study; NA-not available due to weak binding, below the level of detection by ITC.

5000-fold. The strongest binders **24**–**26** (K_d 0.4–1.9 nM for CA XII, K_d 0.4-1.6 for chCA XII, and K_d 6.3–31 nM for CA II) bear phenylsulfanyl or cyclohexylsulfanyl substituent at *para* position. Replacement of cyclohexylsulfanyl to cyclohexylamino tail decreased the binding affinities approximately ten-fold. In this study we have synthesized two new inhibitors - **29** (EA12-7) and **30** (EA11-7) that were analogues to lead compound **26** (EA12-3).[36] We have measured binding affinities towards all 12 catalytically active CAs (Figure 5, Table S2) and showed that compound **29** (EA12-7) bound all CAs with decreased affinity compared to **26** (EA12-3), but significantly increased selectivity. It has 155-fold selectivity towards CA XII (K_d = 19 nM) over CA II (K_d = 3000 nM) and bound very weakly or did not bind CAs I, III, VA, VB, VI, VII and CA XII ($K_d \geq$ 10000–200000 nM). Methylation of carboxy group at *meta*-substituent (compound **30**) did not increase affinity or selectivity in comparison to **26** and **29**.

In our previous study we showed that fluorinated compounds with bulky substituents on benzensulfonamide ring have greater affinity for CA XII than CA II.[40] The lead compound **31** (VD11-4-2) of anticancer target CA IX (K_d = 50 pM)[39] bound CA XII and chCA XII stronger than CA II (K_d = 2.9, 6.7 and 56 nM, respectively). Replacement of cyclooctylamino group to cyclododecylamino substituent at *meta*- position and addition of phenyl ring to *para*- position (**32**) decreased the affinity for all tested CAs. However, the same displacement of hydrophobic ring and addition of 2-(4-hydroxyphenyl)ethylamino group at second *meta*- position with $SO_2CH_2CH_2OH$ tail (**33**) increased the size of inhibitor so that it could not fit in the active site of CA II, but bound to CA XII and chCA XII (K_d 500 and 220 nM). Another di-*meta*-substituted benzenesulfonamide bearing phenyl groups **34** also very weakly bound CA II (K_d 58000 nM) but stronger to CA XII and chCA XII (K_d = 830 and 3300 nM). Overall, the chCA XII was a suitable model for screening of CA XII-selective inhibitors. It bound halogenated benzenesulfonamides **23**–**34** with similar affinities as CA XII and accommodated large compounds with bulky substituents in the active site that hardly or did not fit in the active site of CA II.

© 2021 The Authors. Published by Wiley-VCH GmbH

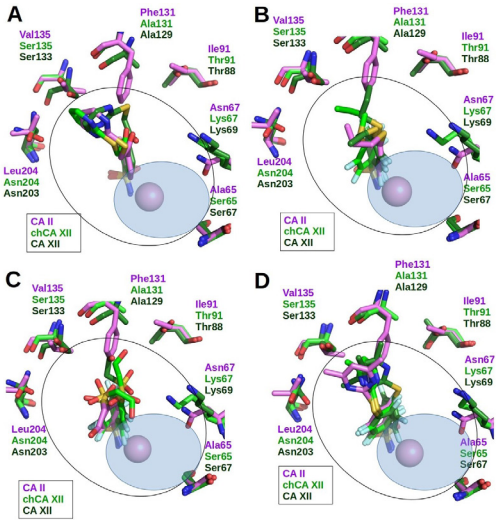


Figure 4. X-ray crystallographic structures of CA II-selective compounds bound to CA II, chCA XII and CA XII. Zn(II) is shown as magenta sphere. Black line denotes the shape of the active site, whereas blue transparent ellipse denotes the hydrophilic part of active site which contains water molecules. Protein side chains and ligands bound to CA II are colored magenta, chCA XII-light green, CA XII-dark green. (A) Compound **6** bound in the active site of CA II (PDB: 4KNJ), chCA XII (PDB: 6YH5) and CA XII (PDB: 4KP5). (B) Compound **9** bound in the active site of CA II (PDB: 4WW6), chCA XII (PDB: 6YHA) and CA XII (PDB: 5MSA). (C) Compound **11** bound in the active site of CA II (PDB: 4PZH), chCA XII (PDB: 6YH4) and CA XII (PDB: 5MSB). (D) Compound **13** bound in the active site of CA II (PDB: 4HT0), chCA XII (PDB: 6YHB) and CA XII (PDB: 4HT2).

2.5. Nonselective Inhibitors

The third group incorporated inhibitors **35**–**63** that bound to CA II, chCA XII and CA XII with affinities differing by up to ten-fold (Figure 6, Table 2). Drugs acetazolamide (**35**) and methazolamide (**36**) were nanomolar inhibitors of CA II (K_d 46 and 100 nM) and bound up to 9-fold stronger than chCA XII or CA XII, while naphthalene-2-sulfonamide (**37**) similarly bound CA II stronger than chCA XII and CA XII (K_d for CA II was 770 nM, while for chCA XII and CA XII - 6700 and 6300 nM, respectively). The chlorinated benzensulfonamides bearing thiazole (**38**), benzimidazole (**39**) or pyrimidine (**40**, **41**) fragments at *para*-position were weaker inhibitors of CA II, chCA XII and CA XII than acetazolamide (**35**) and 2,3,5,6-tetrafluoro-4-(phenylthio) benzensulfonamide (**42**). The weak binding for CA XII and chCA XII also shown by *ortho*-substituted with bulky hydrophobic groups fluorinated benzenesulfonamides **43** (K_d 10000 and 12500 nM), **44** (K_d 720 and 4000 nM).

Structural arrangement of **43** and **44** in the active site of chCA XII is compared in Figure 7A. Compounds differed in the position of the sulfonamide group at Zn(II). Compound **43** contains relatively rigid hydrophobic group in the *ortho*-position. Due to its geometry, **43** could not occupy the canonical position of sulfonamide group in the active site. Only the positions of the sulfonamide nitrogen atoms of both compounds coincided. The sulfonamide nitrogen atom of **43** also formed the hydrogen bond with hydroxyl of Thr199 and the coordination bond with Zn(II). Compound **44** contains in the *ortho*-position bulky but flexible hydrophobic cyclooctylamino group. The sulfonamide group of this compound occupies the canonical position of sulfonamide-based inhibitors in the active site of human CA isoforms (sulfonamide made two hydrogen bonds with Thr199 and coordinated Zn(II)).

Fluorinated benzensulfonamides **45**–**47** with cyclooctylamino substituents at *ortho*- position and varying tails at *para*-position also exhibited moderate affinity towards tested CAs (K_d 240–12500 nM). Stronger binders of CA II, chCA XII and CA XII were *meta-, para*- di-substituted tri-fluorinated, or chlorinated/brominated at *ortho*- position benzensulfonamides **48**–**63**. They showed similar binding affinities for all three proteins (K_d 3.3–88 nM for CA II, 0.25–46 nM for chCA XII, and K_d = 0.8–330 nM for CA XII). The crystal structures of compounds **48**, **50**, **52** bound to chCA XII were determined.

The compound **50** was synthesized by modifying **11**: the hydrophobic substituent was added to the *meta*- position of fluorinated ring. Compounds **50** and **11** have similar binding affinities to CA II (K_d 17 nM) so the impact of additional surface was not detected. The additional hydrophobic surface at the *meta*-position of fluorinated ring has improved the binding affinity (K_d) of the **50** for CA XII and chCA XII by 20-fold and 30-

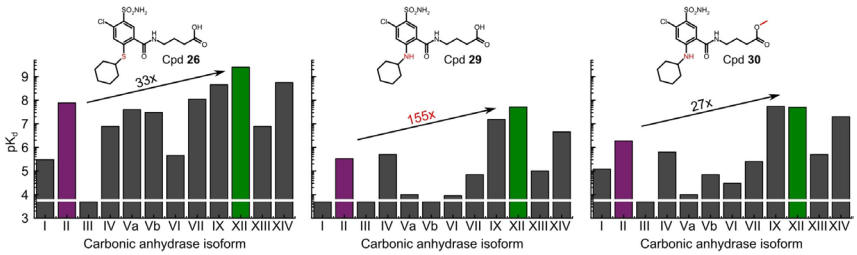


Figure 5. CA XII-selective inhibitors: **26** (EA12-3), **29** (EA12-7) and **30** (EA11-7) and their affinities for all twelve human CA isoforms determined by fluorescent thermal shift assay. The white line on the bars represents the limit of affinity determination (K_d 200 μM). Substitution of sulfur atom to nitrogen atom in the *para* position decreased the binding affinity for all 12 CAs, but increased inhibitor selectivity for CA XII over CA II from 33-fold to 155-fold and up to 10000-fold over remaining 10 CA isoforms. However, additional methylation of carboxy group at *meta* substituent increased the binding affinity for all CAs up to 25-fold, but reduced selectivity towards CA XII.

© 2021 The Authors. Published by Wiley-VCH GmbH

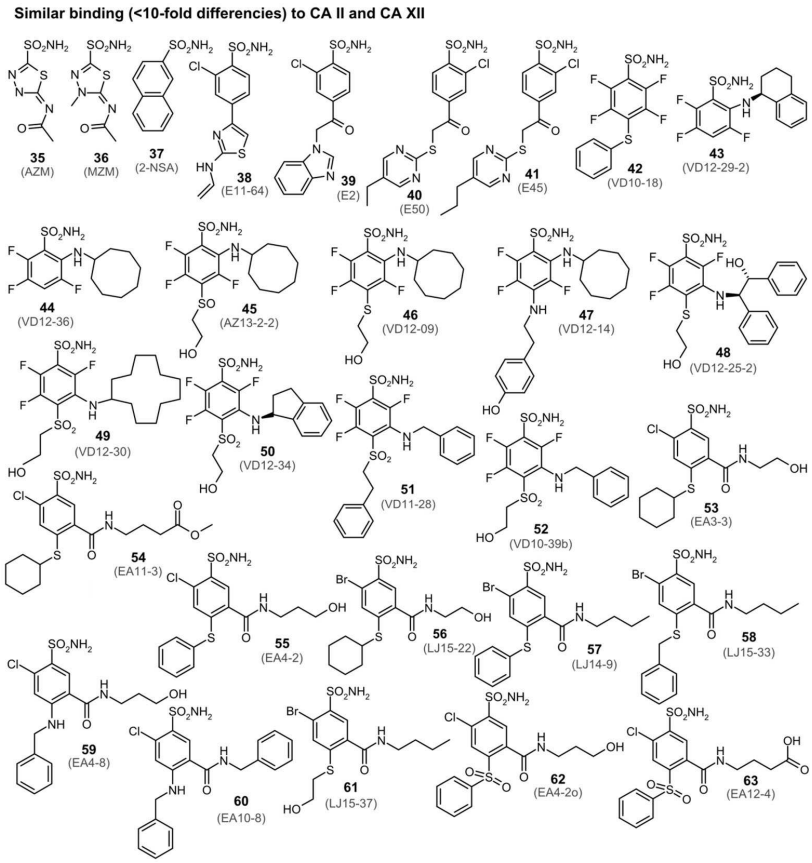


Figure 6. Chemical structures of compounds **35**–**63**, that bound to CA II and CA XII with similar binding affinities (< 10-fold differences). Their binding affinities were also close for chCA XII and thus were uninformative about the switch of affinities in the chimeric protein.

fold, respectively. The binding mode of **50** was the same in the active sites of CA XII and chCA XII, whereas in CA II the position of the compound was different (Figure 7C). The binding affinities of **48** and **52** for CA XII were 5–6-fold higher compared to **11** (10–16-fold for chCA XII). Despite the similar binding affinities of the compound **52** for CA II, CA XII and chCA XII, the binding modes also differed as in case of **50**. The binding mode of compound **52** was similar only in the active sites of CA XII and chCA XII (Figure 7D). The binding mode of **48** was the same in the active sites of CA II and chCA XII and in one protein chain out of four in CA XII. In the other three protein chains of CA XII, the *meta*-substituent of the compound was located on the opposite side (Figure 7B). The bulky **48** molecule fully occupied the middle part of the active site cavity closing the access of water molecules to the deeper parts of active site. The consequence of this could be a decreased dissociation rate.[37] The possible reasons of similar binding affinities of **11** and **50** to CA II have been analyzed,[37] and the enthalpy-entropy compensation was observed for this pair of compounds. Compounds **11** and **50** bound to CA XII differently (compare Figure 4C and Figure 7C). Compound **50** efficiently filled the active site of CA XII. Thus, the *meta*-substituent of **50** was located in the hydrophobic environment and sterically displaced the remaining part of the compound into the hydrophilic part of CA XII active site, where the formation of hydrogen bonds with protein surface is more likely. Such explanation could be also applicable to the comparison of **11** and **52**.

The binding, inhibition and structural studies revealed that the engineered chCA XII protein mimicked the active site of CA XII. The experimental dosing/titration curves of chCA XII were closer to CA XII, but not CA II (Figure 2E, F, I). Figure 2H summarizes the binding data and shows the correlations between observed pK_d's of chCA XII and CA II or CA XII. There is a strong correlation between pK_d's of chCA XII and CA XII with coefficient of determination $R^2 = 0.90$, and nearly absent correlation between binding affinities of chCA XII and CA II with $R^2 = 0.24$. The correlations of intrinsic values were also similar to

© 2021 The Authors. Published by Wiley-VCH GmbH

Table 2. The *observed* dissociation constants (K_d, nM) of nonselective compound **35**–**63** binding to recombinant human CA II, chCA XII and CA XII, determined by fluorescent thermal shift assay (pH 7.0, 37 °C).

Compound No.	Lab. name	Carbonic anhydrase K_d [nM][a]			K_d ratio
Similar binding (< 10-fold selectivity)		CA II	chCA XII	CA XII	CA XII/CA II
35	AZM	46	415	130	2.8
36	MZM	100	550	500	5.0
37	2-NSA	770	6700	6300	8.2
38	E11-64	100	625	500	5.0
39	E2	1600	5000	3100	1.9
40	E50	140	2600	1200	8.6
41	E45	120	2900	1100	9.2
42	VD10-18	3.4	50	18	5.3
43	VD12-29-2	2200	12500	10000	4.5
44	VD12-36	230	4000	720	3.1
45	AZ13-2-2	2200	2000	250	0.1
46	VD12-09	1000	500	240	0.2
47	VD12-14	10000	12500	1400	7.0
48	VD12-25-2	64	46	16	0.3
49	VD12-30	42	1.25	5.0	0.1
50	VD12-34	17	12.5	8.3	0.5
51	VD11-28	6.7	33	40	6.0
52	VD10-39b	83	40	25	0.3
53	EA3-3	10	1.7	2.0	0.2
54	EA11-3	10	2.0	1.3	8.0
55	EA4-2	5.0	0.25	0.83	0.2
56	LJ15-22	13	4.0	1.7	7.6
57	LJ14-9	10	0.29	0.8	0.1
58	LJ15-33	5.3	6.7	4.0	0.8
59	EA4-8	20	28	130	6.5
60	EA10-8	40	31	330	8.3
61	LJ15-37	31	26	9.5	0.3
62	EA4-2o	3.3	3.3	3.1	0.9
63	EA12-4	15	10	6.4	0.4

[a] FTSA data for CA II and CA XII were taken from,[43] except for **37** (2-NSA) from,[52] **55**, **56**, **58**, and **63** from.[36]

observed ones and were provided in Figure S4. The binding affinities of several compounds were closer between CA II and chCA XII, than between chCA XII and CA XII, but all of them belonged to the group of nonselective inhibitors.

3. Discussion

This study has used a reverse engineering approach to provide an opportunity to develop selective inhibitors to the difficult target CA XII. In achieving this it has shed light on outstanding questions surrounding protein-ligand recognition. Despite decades of effort on drug development aimed at the carbonic anhydrases even the apparently most basic questions remain open. For example, is carbonic anhydrase behaving as rather rigid protein that does not undergo significant conformational or other structural changes upon ligand binding, or is the protein rather flexible where motions of substantial parts are essential for ligand recognition? Recent studies indicated that motion is important even for an allegedly "rigid protein", a prototypical textbook example such as CA II.[51] In our opinion, carbonic anhydrase active sites are rather rigid and recognize ligands primarily via a Lock-and-Key mechanism.[52] However, the question is largely open and requires further studies to understand the principles of recognition and enable truly rational design of high-affinity and high-selectivity compounds.

Several studies[44,45,53] have distinguished the active site residues that differ between CA II and CA XII and could be exploited for selective inhibitor design. The first active site mutants of CA II were generated in the early 1990 s.[54,55] CA II was used as a model isoform due to simple expression and purification, ultra-high catalytic activity ($k_{cat} = 0.6–1.4 \times 10^6$ s^{-1}), moderate thermal stability (T_m 55–59 °C)[56,57] and off-target function - it is found in erythrocytes and regulates blood ion concentrations.[58]

By engineering chCA XII we have shown that six mutations in the active site of CA II (A65S, N67K, I91T, F130A, V134S, and L203N) were sufficient to switch its inhibitor recognition profile to the CA XII. The kinetic studies showed that these mutations did not affect the catalytic activity (k_{cat} of CA II and chCA XII is 6.0×10^5 s^{-1}) but increased the pK_a value of the proton shuttle His64 from 7.3 to 7.9. The observed maximal catalytic constant of CA XII was $(4.1 \pm 0.9) \times 10^5$ s^{-1} and pK_a of His64 was 7.6 ± 0.1. The parameters closely matched the previously published k_{cat} value of $(4.0 \pm 1.7) \times 10^5$ s^{-1} and pK_a of 8.0 ± 0.2 by stopped-flow spectrophotometry and 7.5 ± 0.1 by ^{18}O-mass spectrometry.[34] Our previous study showed, that A65T, N67Q, F130Y, V134Q, and L203T mutations did not affect the pK_a value of His64 in CA II.[59] For this reason, we assumed that I91T mutation increased the pK_a of mutant enzyme and Thr88 (CA XII numbering) was a key member in catalytic mechanism of CA XII.

© 2021 The Authors. Published by Wiley-VCH GmbH

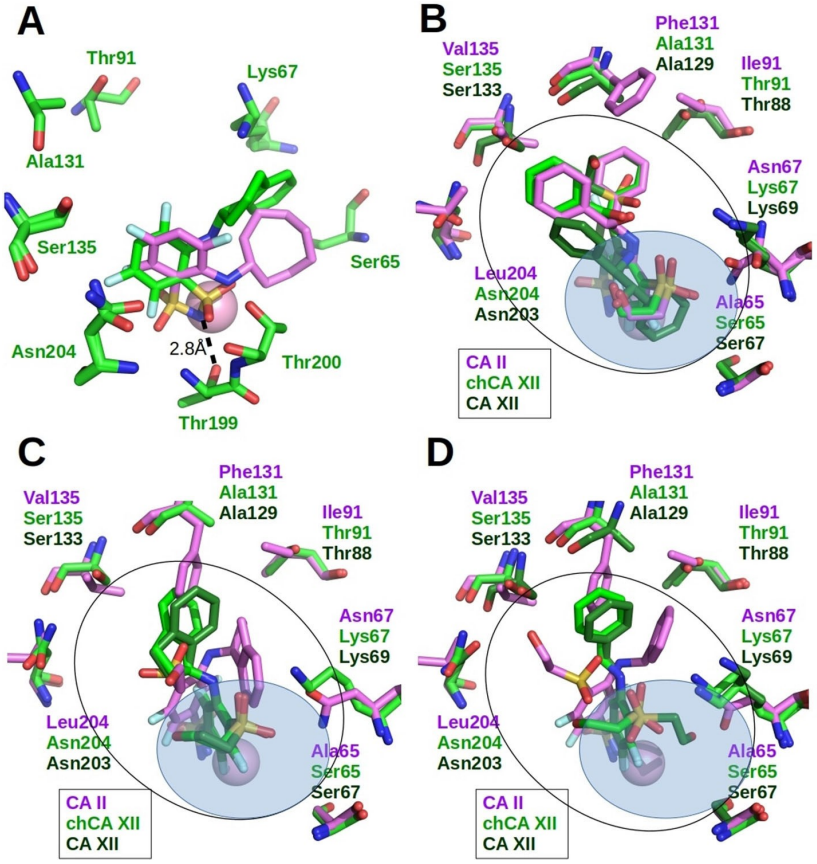


Figure 7. X-ray crystallographic structures of several nonselective compounds bound to CA II, chCA XII and CA XII. Zn(II) is shown as magenta sphere. Black line denotes the shape of active site, whereas blue transparent area marked the hydrophilic part of active site which contains water molecules. Protein side chains and ligands bound to CA II are colored magenta, chCA XII-light green, CA XII-dark green. (A) Compounds **43** (PDB: 6YH8) and **44** (magenta, PDB: 6YH6) bound in chCA XII. (B) Compound **48** bound in CA II (PDB: 4QIY), chCA XII (PDB: 6YH9) and CA XII (PDB: 4QJ0, main orientation (from 4 protein subunits: 3 vs 1)). (C) Compound **50** bound in CA II (PDB: 5DRS), chCA XII (PDB: 6YH7) and CA XII (PDB: 5LLO). (D) Compound **52** bound in CA II (PDB: 5EHE), chCA XII (PDB: 6YHC) and CA XII (PDB: 4QJW).

The chCA XII recognized the substrate with similar K_M constant as CA XII ($K_M = 3.6$ mM) as well as observed pK_d's of 63 inhibitors binding to chCA XII were significantly more similar to CA XII ($R^2 = 0.90$) than to CA II ($R^2 = 0.24$). Compounds **9**, **11**, **13**, **48** and **50** occupied similar positions in the active sites of CA XII and chCA XII, and binding modes differed from CA II. These crystal structures supported the similar binding by CA XII and chCA XII, as suggested by binding data. However, several cases demonstrated different binding modes of the ligand in chCA XII and CA XII, and the binding modes in chCA XII resembled CA II. Despite similar position, the key residues interacting with ligand in CA II and chCA XII differed and contacts between ligand and protein differed. Detailed interaction analysis of multiple binding modes as in CA XII could be helpful here.

In this study we have compared inhibitor binding properties of CA II, chCA XII and CA XII using the observed parameters, because both isoforms have similar pK_a value of zinc-bound water equal to 7.0–7.1 ± 0.2 at 25 °C.[33,34,60] The binding of sulfonamide compound to CA occurs only when sulfonamide group is in the deprotonated form and zinc-bound water in the active site is protonated.[43,61] For this reason, attention should be paid to the pK_a's of zinc-bound water molecule and sulfonamide group of an inhibitor when comparing binding affinities of several CAs or inhibitors. Structure-affinity correlation analysis should be performed using intrinsic parameters of binding[41,50,62–66] that are independent on experimental condition (pH, buffer, etc.). Our previous studies with chimeric carbonic anhydrase VI revealed that intrinsic binding affinities had a better linear correlation between chCA VI and CA VI than the observed affinities.[59]

However, in the case of chimeric chCA XII, the pK_a of the Zn(II)-bound water molecule did not differ from CA II or CA XII.

© 2021 The Authors. Published by Wiley-VCH GmbH

The pK_a values were 6.9 for CA II, 6.9 for chCA XII and 6.8 for CA XII at 37 °C. Therefore, in the calculation of intrinsic binding constants, the only reason for the differences from the observed constants remained the pK_a of the compound sulfonamide amino group. Furthermore, when comparing binding to these three proteins, the relative ratio of observed or intrinsic values remained essentially the same and thus Figure 2H compares the switch of the observed values, while the corresponding intrinsic constants and their switch is provided in the supplementary materials. The switch was equally well observed in both approaches.

When studying correlations between compound's chemical structure and *observed* binding affinity for CA II or CA XII, the studied *para*-substituted benzenesulfonamides bound to CA II with more than ten-fold higher affinity than to CA XII. The data were consistent with other published studies.[42,48,67–69] Despite the fact that 4-(4-fluorophenylureido)benzenesulfonamide U-104/SLC-0111[49] (**2** in this study) has been tested in patients with advanced solid tumors and has finished Phase 1 clinical trial,[70] our study indicates, that as confirmed by three different assays (FTSA, ITC and SFA), the U-104/SLC-0111 exhibits rather weak, micromolar, affinity for anticancer target CA XII and binds it 17-fold weaker than off-target CA II. Recently, Jonsson and Liljas have expressed doubts about proper experimental data for promoting the U-104/SLC-0111 compound into preclinical studies.[71] Our results show that lead compound EA12-3 (**26**)[36] is a significantly stronger inhibitor of CA XII (K_d = 0.4 nM) and its newly synthesized analogue EA12-7 (**29**) possessed significant selectivity for CA XII. Further studies are needed, by as many techniques as possible, to confirm the validity of the affinities, especially because the enzyme inhibition assay is limited by the concentration of the enzyme and is therefore difficult to apply it for determination of sub-nanomolar affinities.

4. Conclusions

The detailed thermodynamic and kinetic profiling combined with X-ray structural studies revealed that CA II-based chimeric protein chCA XII resembled the active site of CA XII. Amino acids S67, K69, T88, A129, S133, and N203 were confirmed as key residues of CA XII for inhibitor recognition, while T88 played a major role in the catalytic mechanism. A series of 63 sulfonamide compounds bound chCA XII with similar affinities to CA XII, but not CA II. Structurally, the switch from CA II to CA XII was very sensitive and therefore both alternative inhibitor binding positions were observed in the crystal structures of chCA XII. As a result, chCA XII was shown as a suitable model for designing CA XII-selective inhibitors, such as compound EA12-3 and a newly synthesized analogue EA12-7. Our study provided additional insight to the basis for isoform selectivity of sulfonamides binding to CA XII, over CA II. The strategy could potentially be applied to other drug design projects in medicinal chemistry if the protein was sufficiently rigid.

Experimental Section

Protein Preparation

Carbonic anhydrase protein isoforms I–XIV, including chCA XII were expressed and purified as described previously.[39] The molecular weight of enzymes was confirmed by mass-spectrometry, purity was analyzed by SDS-PAGE and concentrations were determined by UV-Vis spectrophotometry.

Synthesis of Chemical Compounds

Ethoxzolamide (EZA), acetazolamide (AZM), methazolamide (MZM), naphthalene-2-sulfonamide (2-NSA), and all starting materials and reagents were purchased from Sigma-Aldrich (St. Louis, MO, USA). Compounds **2**, **23**, **29** and **30** were newly designed and synthesis is reported in electronic supplementary information. Synthesis of other chemical compounds was described earlier.[35,36,38–40,42,52,67,72–74] All compounds were dissolved in dimethyl sulfoxide (DMSO) at 10–30 mM concentration and diluted in aqueous buffers just prior to the FTSA, ITC or SFA experiments.

Crystallization

The chCA XII protein was concentrated by ultrafiltration to 28 mg/mL. Crystallization buffer contained 0.1 M sodium bicine (pH 9.0), 0.2 M ammonium sulfate and 2 M sodium malonate (pH 7.0). The ligand solutions for crystal soaking were made by mixing of 50 μL of corresponding reservoir solution and 3 μL of 50 mM ligand solution (in DMSO).

Data Collection and Structure Determination

All datasets of X-ray diffraction were collected at the EMBL beamline P13. The datasets were processed by XDS program[75] and scaled with SCALA.[76] The molecular replacement was made using MOLREP program.[77] The initial phases were received from PDB entry 4HT0. The 3D models of compounds were built by AVOGADRO program.[78] The library files with complete chemical and geometric descriptions of compounds were generated using LIBCHECK program.[79,80] The models were built using COOT[81] and refined by REFMAC.[82,83] Coordinates and structure factors have been deposited to the RCSB Protein Data Bank (PDB). The PDB access codes, data collection and refinement statistics are listed in supporting information Table S1.

Fluorescent Thermal Shift Assay

Thermal stability of chCA XII and inhibitor binding affinities were determined using fluorescent thermal shift assay, also known as ThermoFluor® or differential scanning fluorimetry (DSF). QIAGEN Rotor-Gene Q (Corbett Rotor-Gene 6000) cycler with the blue channel (365 ± 20 nm excitation and 460 ± 15 nm detection) was used to monitor the fluorescence of *1-anilino-8-naphthalene sulfonate* (ANS) upon carbonic anhydrase unfolding. The temperature of samples was elevated from 25 to 99 °C at a heating rate of 1 °C/min.

Thermal stability experiments at different pH's (from pH 4.5 to 10.0) were performed using 10 μM chCA XII in universal buffer (50 mM sodium acetate, 25 mM sodium borate, 50 mM sodium phosphate and 50 mM sodium chloride) containing 2% DMSO compound and 50 μM ANS. The melting temperature T_m was determined using a model for fluorescence yield upon protein unfolding.[84,85]

© 2021 The Authors. Published by Wiley-VCH GmbH

Inhibitor binding affinities were determined upon addition of 0–200 μM (in 2% DMSO) to the 5 μM CA (except 10 μM for CA IV) solution in 50 mM sodium phosphate, 100 mM sodium chloride buffer (pH 7.0). The thermal shift data were fitted using a quantitative model[85,86] yielding the K_d values.

Isothermal Titration Calorimetry

Isothermal titration calorimetry experiments were carried out at 37 °C using VP-ITC and iTC-200 calorimeters. The solution containing 6–20 μM carbonic anhydrase in the cell was titrated with 60–200 μM inhibitor solution in the syringe. Experiments were performed in 50 mM sodium phosphate buffer containing 100 mM sodium chloride at pH 7.0 with a final DMSO concentration of 2%. CAs were dialyzed in the reaction buffer before the titrations. Experimental setup used for VP-ITC instrument: 25 injections of 10 μL every 180 s at reference power of 4 μcal/s and stirring speed of 260 rpm; iTC200 instrument: 19 injections of 2 μL every 180 s at reference power of 5 μcal/s and stirring speed of 750 rpm. The thermodynamic parameters of binding were determined using NITPIC,[87] SEDPHAT[88] and/or MicroCal Origin software. The first injection point was deleted in the integrated data and a single binding model was applied to fit the data.

Stopped-Flow CO_2 Hydration Assay

Catalytic properties of chCA XII, CA XII and inhibition constants were determined using the stopped-flow CO_2 hydration assay. Experiments were performed using Applied Photophysics SX.18 MV-R Stopped-Flow Spectrometer at 24 °C temperature. Saturated substrate solution was prepared by bubbling CO_2 gas into milli-Q water for 1 hour at room temperature.

The catalytic constant k_{cat} and Michaelis-Menten constant K_M of chCA XII and CA XII in pH range 6.0–9.0 was determined using 25 mM buffer and 30–100 μM indicator pairs with similar pK_a values: Mes and Bromocresol purple (λ 590 nm, pH 6.0–6.4), Mops and Bromothymol blue (λ 615 nm, pH 6.8–7.1), Hepes and Phenol red (λ 557 nm, pH 7.2–7.8), Tris and *m*-Cresol purple (λ 575 nm, pH 8.1–8.4), Ches and Thymol blue (λ 595 nm, pH 8.6–9.0). Solutions also contained 0.2 M sodium sulfate to maintain ionic strength. Enzyme concentration was 150–200 nM for chCA XII and 50–150 nM for CA XII. The saturated substrate solution was diluted with milli-Q water and final carbon dioxide concentrations were determined according to Ref.[46] The kinetic parameters were obtained using Lineweaver-Burk and Michaelis-Menten plots. The pK_a values of His64 were determined by fitting k_{cat} dependence on pH data using a single ionization event model:

$$k_{cat} = \frac{k_{cat-max}}{1 + 10^{pH-pK_a}} \quad (1)$$

Inhibition of enzymatic activity experiments were performed in 25 mM Hepes buffer, containing 30 μM Phenol red indicator, 0.2 M sodium sulfate, pH 7.5. The samples consisted of 30–100 nM CA II, 50–200 nM chCA XII, 50–100 nM CA XII and 0–100 μM inhibitor (in <1% DMSO). The raw curves of time-dependent absorbance change were fitted using a single exponential model. The rates of spontaneous CO_2 hydration reaction were subtracted from the observed catalyzed reaction rates. The K_d values were calculated by fitting dose-response curves to a Morrison equation:[89,90]

$$CA\ act.(\%) = \left(1 - \frac{([CA] + [I] + K_d - \sqrt{([CA] + [I] + K_d)^2 - 4[CA][I]})}{2[CA]}\right) \cdot 100\,\% \quad (2)$$

Supporting information

Synthesis of chemical compounds **2**, **23**, **29** and **30**; sequence alignment of CA II and CA XII; the dependence of Michelis-Menten constant on pH; the electron densities of inhibitors bound to CAs of the crystal structures described in this study; correlations of intrinsic pK_d's between chCA XII and either CA XII or CA II; data collection and refinement statistics of chimeric CA XII complexes with inhibitors **6**, **9**, **11**, **13**, **43**, **44**, **48**, **50**, and **52**; the observed dissociation constants (K_d, nM) of compounds **26**, **29** and **30** binding to recombinant human carbonic anhydrases I–XIV; the pK_a values of compound's sulfonamide group and the intrinsic dissociation constants of compounds **1**–**63** binding to recombinant human CA II, chCA XII and CA XII.

Contributor Roles

D. M., J. S., L. B., J. E. L.-designed and supervised the project; J. S., L.B., A. Zu.-performed the enzymatic and biophysical experiments; J. S., V. P., L. B., A. Zu.-derived the models and analyzed the data; A.S., E. M., S. G.-determined the crystal structures of CA-inhibitor complexes, wrote the crystallography part; A. M., V. M.-expressed and purified the CA proteins; A. Za., E. Č.-synthesized the inhibitors and wrote the synthesis part; J. S., D. M., J. E. L.-wrote the paper; W-Y. C., J. E. L., V. P.-provided critical feedback. All authors have read and approved the final version of the manuscript.

Acknowledgements

Authors thank Gleb Bourenkov for the help with data collection at P13 EMBL beamline at PETRA III ring of the DESY synchrotron (access to the DESY synchrotron EMBL beam line P13), supported by iNEXT grant number 653706 (to A. S., E. M., S. G.) funded by the Horizon 2020 program of the European Commission. This research was supported by the grant MSF-JM-6 from Vilnius University. A. Za. was supported by the grant S-SEN-20-10 from the Research Council of Lithuania.

Conflict of Interest

The authors declare no conflict of interest.

Keywords: drug design · enzyme models · fluorescence spectroscopy · sulfonamides · X-ray diffraction

[1] J. Zhao, Y. Cao, L. Zhang, *Comput. Struct. Biotechnol. J.* **2020**, *18*, 417–426.

© 2021 The Authors. Published by Wiley-VCH GmbH

[2] A. J. Esbaugh, B. L. Tufts, *Respir. Physiol. Neurobiol.* **2006**, *154*, 185–198.
[3] D. Lee, J. H. Hong, *Int. J. Mol. Sci.* **2020**, *21*, 339.
[4] D. Sterling, R. A. Reithmeier, J. R. Casey, *Jop* **2001**, *2*, 165–70.
[5] W. F. Widdas, G. F. Baker, P. Baker, *Cytobios* **1994**, *80*, 7–24.
[6] C. J. Ingram, R. F. Brubaker, *Am. J. Ophthalmol.* **1999**, *128*, 292–296.
[7] L. H. Silver, *Am. J. Ophthalmol.* **1998**, *126*, 400–408.
[8] D. Wile, *Ann. Clin. Biochem.* **2012**, *49*, 419–431.
[9] F. Brigo, S. Lattanzi, S. C. Igwe, M. Behzadifar, N. L. Bragazzi, *Cochrane Database Syst. Rev.* **2018**, *10*, CD001416.
[10] S. V. Kothare, J. Kaleyias, *Expert Opin. Drug Metab. Toxicol.* **2008**, *4*, 493–506.
[11] T. Leniger, J. Thöne, M. Wiemann, *Br. J. Pharmacol.* **2004**, *142*, 831–842.
[12] E. Perucca, *Pharmacol. Res.* **1997**, *35*, 241–256.
[13] M. Y. Mboge, R. McKenna, S. C. Frost, in *Top. Anti-Cancer Res.* (Eds.: Atta-ur-Rahman, K. Zaman), Bentham Science Publishers, **2016**, pp. 3–42.
[14] D. H. Barnett, S. Sheng, T. H. Charn, A. Waheed, W. S. Sly, C.-Y. Lin, E. T. Liu, B. S. Katzenellenbogen, *Cancer Res.* **2008**, *68*, 3505–3515.
[15] P. H. Watson, S. K. Chia, C. C. Wykoff, C. Han, R. D. Leek, W. S. Sly, K. C. Gatter, P. Ratcliffe, A. L. Harris, *Br. J. Cancer* **2003**, *88*, 1065–1070.
[16] M. I. Ilie, V. Hofman, C. Ortholan, R. E. Ammadi, C. Bonnetaud, K. Havet, N. Venissac, J. Mouroux, N. M. Mazure, J. Pouyssegur, P. Hofman, *Int. J. Cancer* **2011**, *128*, 1614–1623.
[17] P. Viikilä, A. J. Kivelä, H. Mustonen, S. Koskensalo, A. Waheed, W. S. Sly, E. A. Doisy, J. Pastorek, S. Pastorekova, S. Parkkila, C. Haglund, *World J. Gastroenterol.* **2016**, *22*, 8168.
[18] X.-F. Gu, C.-B. Shi, W. Zhao, *Int. J. Clin. Exp. Pathol.* **2019**, *12*, 2173–2183.
[19] J. Haapasalo, M. Hilvo, K. Nordfors, Hannu Haapasalo, S. Parkkila, A. Hyrskyluoto, I. Rantala, A. Waheed, W. S. Sly, S. Pastorekova, Jaromir Pastorek, A.-K. Parkkila, *Neurooncology* **2008**, *10*, 131–138.
[20] J. Kopecka, I. Campia, A. Jacobs, A. P. Frei, D. Ghigo, B. Wollscheid, C. Riganti, *Oncotarget* **2015**, 6(9):6776-6793.
[21] S.-Y. Liao, *J. Med. Genet.* **2003**, *40*, 257–261.
[22] A. Kivelä, S. Parkkila, J. Saarnio, T. J. Karttunen, J. Kivelä, A.-K. Parkkila, A. Waheed, W. S. Sly, J. H. Grubb, G. Shah, Ö. Türeci, H. Rajaniemi, *Am. J. Pathol.* **2000**, *156*, 577–584.
[23] S. Parkkila, A.-K. Parkkila, J. Saarnio, J. Kivelä, T. J. Karttunen, K. Kaunisto, A. Waheed, W. S. Sly, Ö. Türeci, I. Virtanen, H. Rajaniemi, *J. Histochem. Cytochem.* **2000**, 48(12):1601-1608.
[24] A. J. Kivelä, S. Parkkila, J. Saarnio, T. J. Karttunen, J. Kivelä, A.-K. Parkkila, S. Pastoreková, J. Pastorek, A. Waheed, W. S. Sly, H. Rajaniemi, *Histochem. Cell Biol.* **2000**, *114*, 197–204.
[25] M. Leppilampi, J. Saarnio, T. J. Karttunen, J. Kivela, S. Pastorekova, J. Pastorek, A. Waheed, W. S. Sly, S. Parkkila, *World J. Gastroenterol.* **2003**, *9*, 1398–403.
[26] L. Syrjänen, T. Luukkaala, M. Leppilampi, M. Kallioinen, S. Pastorekova, J. Pastorek, A. Waheed, W. S. Sly, S. Parkkila, T. Karttunen, *APMIS Acta Pathol. Microbiol. Immunol. Scand.* **2014**, *122*, 880–889.
[27] P. Karhumaa, *Mol. Hum. Reprod.* **2000**, *6*, 68–74.
[28] P. Karhumaa, K. Kaunisto, S. Parkkila, A. Waheed, S. Pastorekov´, J. Pastorek, W. S. Sly, H. Rajaniemi, *Mol. Hum. Reprod.* **2001**, *7*, 611–616.
[29] E. Muhammad, N. Leventhal, G. Parvari, A. Hanukoglu, I. Hanukoglu, V. Chalifa-Caspi, Y. Feinstein, J. Weinbrand, H. Jacoby, E. Manor, T. Nagar, J. C. Beck, V. C. Sheffield, E. Hershkovitz, R. Parvari, *Hum. Genet.* **2011**, *129*, 397–405.
[30] K. A. Power, S. Grad, J. P. H. J. Rutges, L. B. Creemers, M. H. P. van Rijen, P. O'Gaora, J. G. Wall, M. Alini, A. Pandit, W. M. Gallagher, *Arthritis Rheum.* **2011**, *63*, 3876–3886.
[31] A. Waheed, W. S. Sly, *Gene* **2017**, *623*, 33–40.
[32] D. A. Whittington, A. Waheed, B. Ulmasov, G. N. Shah, J. H. Grubb, W. S. Sly, D. W. Christianson, *Proc. Natl. Acad. Sci. USA* **2001**, *98*, 9545–9550.
[33] V. Jogaitė, A. Zubrienė, V. Michailovienė, J. Gylytė, V. Morkūnaitė, D. Matulis, *Bioorg. Med. Chem.* **2013**, *21*, 1431–1436.
[34] B. Ulmasov, A. Waheed, G. N. Shah, J. H. Grubb, W. S. Sly, C. Tu, D. N. Silverman, *Proc. Natl. Acad. Sci. USA* **2000**, *97*, 14212–14217.
[35] A. Zakšauskas, E. Čapkauskaitė, L. Jezepčikas, V. Linkuvienė, M. Kišonaitė, A. Smirnov, E. Manakova, S. Gražulis, D. Matulis, *Eur. J. Med. Chem.* **2018**, *156*, 61–78.
[36] A. Zakšauskas, E. Čapkauskaitė, L. Jezepčikas, V. Linkuvienė, V. Paketurytė, A. Smirnov, J. Leitans, A. Kazaks, E. Dvinskis, E. Manakova, S. Gražulis, K. Tars, D. Matulis, *Eur. J. Med. Chem.* **2020**, *185*, 111825.
[37] A. Smirnov, A. Zubrienė, E. Manakova, S. Gražulis, D. Matulis, *PeerJ* **2018**, *6*, e4412.
[38] E. Čapkauskaitė, A. Zubrienė, A. Smirnov, J. Torresan, M. Kišonaitė, J. Kazokaitė, J. Gylytė, V. Michailovienė, V. Jogaitė, E. Manakova, S. Gražulis, S. Tumkevičius, D. Matulis, *Bioorg. Med. Chem.* **2013**, *21*, 6937–6947.
[39] V. Dudutienė, J. Matulienė, A. Smirnov, D. D. Timm, A. Zubrienė, L. Baranauskienė, V. Morkūnaite, J. Smirnovienė, V. Michailovienė, V. Juozapaitienė, A. Mickevičiūtė, J. Kazokaitė, S. Bakšytė, A. Kasiliauskaitė, J. Jachno, J. Revuckienė, M. Kišonaitė, V. Pilipuitytė, E. Ivanauskaitė, G. Milinavičiūtė, V. Smirnovas, V. Petrikaitė, V. Kairys, V. Petrauskas, P. Norvaišas, D. Lingė, P. Gibieža, E. Capkauskaitė, A. Zakšauskas, E. Kazlauskas, E. Manakova, S. Gražulis, J. E. Ladbury, D. Matulis, *J. Med. Chem.* **2014**, *57*, 9435–9446.
[40] V. Dudutienė, A. Zubrienė, A. Smirnov, D. D. Timm, J. Smirnovienė, J. Kazokaitė, V. Michailovienė, A. Zakšauskas, E. Manakova, S. Gražulis, D. Matulis, *ChemMedChem* **2015**, *10*, 662–687.
[41] A. Zubrienė, J. Smirnovienė, A. Smirnov, Vaida Morkūnaitė, V. Michailovienė, J. Jachno, V. Juozapaitienė, P. Norvaišas, E. Manakova, S. Gražulis, D. Matulis, *Biophys. Chem.* **2015**, *205*, 51–65.
[42] V. Dudutienė, A. Zubrienė, A. Smirnov, J. Gylytė, D. Timm, E. Manakova, S. Gražulis, D. Matulis, *Bioorg. Med. Chem.* **2013**, *21*, 2093–2106.
[43] V. Linkuvienė, A. Zubrienė, E. Manakova, V. Petrauskas, L. Baranauskienė, A. Zakšauskas, A. Smirnov, S. Gražulis, J. E. Ladbury, D. Matulis, *Q. Rev. Biophys.* **2018**, *51*, DOI 10.1017/S0033583518000082.
[44] M. A. Pinard, B. Mahon, R. McKenna, *BioMed Res. Int.* **2015**, *2015*, 1–15.
[45] A. Bhatt, B. P. Mahon, V. W. D. Cruzeiro, B. Cornelio, M. Laronze-Cochard, M. Ceruso, J. Sapi, G. A. Rance, A. N. Khlobystov, A. Fontana, A. Roitberg, C. T. Supuran, R. McKenna, *ChemBioChem* **2017**, 18(2):213-222 .
[46] J. Smirnovienė, V. Smirnovas, D. Matulis, *Anal. Biochem.* **2017**, *522*, 61–72.
[47] A. Zubrienė, D. Matulis, in *Carbonic Anhydrase Drug Target Thermodyn. Struct. Inhib. Bind.* (Ed.: D. Matulis), Springer International Publishing, Cham, **2019**, pp. 51–59.
[48] B. Balandis, G. Ivanauskaitė, J. Smirnovienė, K. Kantminienė, D. Matulis, V. Mickevičius, A. Zubrienė, *Bioorg. Chem.* **2020**, *97*, 103658.
[49] F. Pacchiano, F. Carta, P. C. McDonald, Y. Lou, D. Vullo, A. Scozzafava, S. Dedhar, C. T. Supuran, *J. Med. Chem.* **2011**, *54*, 1896–1902.
[50] M. Kišonaitė, A. Zubrienė, E. Čapkauskaitė, A. Smirnov, J. Smirnovienė, V. Kairys, V. Michailovienė, E. Manakova, S. Gražulis, D. Matulis, *PLoS One* **2014**, *9*, e114106.
[51] H. Singh, C. K. Das, S. K. Vasa, K. Grohe, L. V. Schäfer, R. Linser, *Angew. Chem. Int. Ed.* **2020**, 59(51):22916-22921.
[52] V. Dudutienė, A. Zubrienė, V. Kairys, A. Smirnov, J. Smirnovienė, J. Leitans, A. Kazaks, K. Tars, L. Manakova, S. Gražulis, D. Matulis, *Biophys. J.* **2020**, 119(8):1513-1524.
[53] C. L. Lomelino, J. T. Andring, R. McKenna, *Int J Med Chem* **2018**, *2018*, 9419521.
[54] G. Behravan, P. Jonasson, B.-H. Jonsson, S. Lindskog, *Eur. J. Biochem.* **1991**, *198*, 589–592.
[55] X. Ren, B.-H. Jonsson, S. Lindskog, *Eur. J. Biochem.* **1991**, *201*, 417–420.
[56] B. S. Avvaru, S. A. Busby, M. J. Chalmers, P. R. Griffin, B. Venkatakrishnan, M. Agbandje-McKenna, D. N. Silverman, R. McKenna, *Biochemistry* **2009**, *48*, 7365–7372.
[57] Z. Fisher, C. D. Boone, S. M. Biswas, B. Venkatakrishnan, M. Aggarwal, C. Tu, M. Agbandje-McKenna, D. Silverman, R. McKenna, *Protein Eng. Des. Sel.* **2012**, *25*, 347–355.
[58] R. P. Henry, *Am. Zool.* **1984**, *24*, 241–251.
[59] J. Kazokaitė, V. Kairys, J. Smirnovienė, A. Smirnov, E. Manakova, M. Tolvanen, S. Parkkila, D. Matulis, *Sci. Rep.* **2019**, *9*, 12710.
[60] V. Morkūnaitė, J. Gylytė, A. Zubrienė, L. Baranauskienė, M. Kišonaitė, V. Michailovienė, V. Juozapaitienė, M. J. Todd, D. Matulis, *J. Enzyme Inhib. Med. Chem.* **2015**, *30*, 204–211.
[61] V. M. Krishnamurthy, G. K. Kaufman, A. R. Urbach, I. Gitlin, K. L. Gudiksen, D. B. Weibel, G. M. Whitesides, *Chem. Rev.* **2008**, *108*, 946–1051.
[62] L. Baranauskienė, D. Matulis, *BMC Biophys.* **2012**, *5*, 12.
[63] J. Kazokaitė, G. Milinavičiūtė, J. Smirnovienė, J. Matulienė, D. Matulis, *FEBS J.* **2015**, *282*, 972–983.
[64] V. Linkuvienė, J. Matulienė, V. Juozapaitienė, V. Michailovienė, J. Jachno, D. Matulis, *Biochim. Biophys. Acta Gen. Subj.* **2016**, *1860*, 708–718.
[65] A. Zubrienė, D. Matulis, in *Carbonic Anhydrase Drug Target Thermodyn. Struct. Inhib. Bind.* (Ed.: D. Matulis), Springer International Publishing, Cham, **2019**, pp. 107–123.
[66] A. Zubrienė, A. Smirnov, V. Dudutienė, D. D. Timm, J. Matulienė, V. Michailovienė, A. Zakšauskas, E. Manakova, S. Gražulis, D. Matulis, *ChemMedChem* **2017**, *12*, 161–176.
[67] E. Čapkauskaitė, A. Zubrienė, V. Paketurytė, D. D. Timm, S. Tumkevičius, D. Matulis, *Bioorg. Chem.* **2018**, *77*, 534–541.

© 2021 The Authors. Published by Wiley-VCH GmbH

[68] K. Rutkauskas, A. Zubrienė, I. Tumosienė, K. Kantminienė, M. Kažemėkaitė, A. Smirnov, J. Kazokaitė, V. Morkūnaitė, E. Čapkauskaitė, E. Manakova, S. Gražulis, Z. Beresnevičius, D. Matulis, *Molecules* **2014**, *19*, 17356–17380.
[69] K. Rutkauskas, A. Zubrienė, I. Tumosienė, K. Kantminienė, V. Mickevičius, D. Matulis, *Med. Chem. Res.* **2017**, *26*, 235–246.
[70] P. C. McDonald, S. Chia, P. L. Bedard, Q. Chu, M. Lyle, L. Tang, M. Singh, Z. Zhang, C. T. Supuran, D. J. Renouf, S. Dedhar, *Am. J. Clin. Oncol.* **2020**, *1*.
[71] B.-H. Jonsson, A. Liljas, *Biophys. J.* **2020**, *119*, 1275–1280.
[72] E. Čapkauskaitė, A. Zubrienė, L. Baranauskienė, G. Tamulaitienė, E. Manakova, V. Kairys, S. Gražulis, S. Tumkevičius, D. Matulis, *Eur. J. Med. Chem.* **2012**, *51*, 259–270.
[73] J. Kazokaitė, R. Niemans, V. Dudutienė, H. M. Becker, J. Leitāns, A. Zubrienė, L. Baranauskienė, G. Gondi, R. Zeidler, J. Matulienė, K. Tārs, A. Yaromina, P. Lambin, L. J. Dubois, D. Matulis, *Oncotarget* **2018**, *9*, DOI 10.18632/oncotarget.25508.
[74] A. Zubrienė, E. Čapkauskaitė, J. Gylytė, M. Kišonaitė, S. Tumkevičius, D. Matulis, *J. Enzyme Inhib. Med. Chem.* **2014**, *29*, 124–131.
[75] W. Kabsch, *Acta Crystallogr. Sect. D* **2010**, *D66*, 125–132.
[76] P. Evans, *Acta Crystallogr. Sect. D.* **2006**, 62, 72–82.
[77] A. Vagin, A. Teplyakov, *Acta Crystallogr. Sect. D* **2010**, *66*, 22–25.
[78] M. D. Hanwell, D. E. Curtis, D. C. Lonie, T. Vandermeersch, E. Zurek, G. R. Hutchison, *J. Cheminf.* **2012**, *4*, 17.
[79] A. A. Vagin, R. A. Steiner, A. A. Lebedev, L. Potterton, S. McNicholas, F. Long, G. N. Murshudov, *Acta Crystallogr.* **2004**, *60*, 2184–95.
[80] M. D. Winn, C. C. Ballard, K. D. Cowtan, E. J. Dodson, P. Emsley, P. R. Evans, R. M. Keegan, E. B. Krissinel, A. G. W. Leslie, A. McCoy, S. J. McNicholas, G. N. Murshudov, N. S. Pannu, E. A. Potterton, H. R. Powell, R. J. Read, A. Vagin, K. S. Wilson, *Acta Crystallogr. Sect. D* **2011**, *67*, 235–242.
[81] P. Emsley, B. Lohkamp, W. G. Scott, K. Cowtan, *Acta Crystallogr. Sect. D* **2010**, *66*, 486–501.
[82] G. N. Murshudov, A. A. Vagin, E. J. Dodson, *Acta Crystallogr.* **1997**, *53*, 240–55.
[83] G. N. Murshudov, P. Skubák, A. A. Lebedev, N. S. Pannu, R. A. Steiner, R. A. Nicholls, M. D. Winn, F. Long, A. A. Vagin, *Acta Crystallogr. Sect. D* **2011**, *67*, 355–367.
[84] D. Matulis, J. K. Kranz, F. R. Salemme, M. J. Todd, *Biochemistry* **2005**, *44*, 5258–5266.
[85] V. Petrauskas, A. Zubrienė, M. J. Todd, D. Matulis, in *Carbonic Anhydrase Drug Target Thermodyn. Struct. Inhib. Bind.* (Ed.: D. Matulis), Springer International Publishing, Cham, **2019**, pp. 63–78.
[86] P. Cimmperman, L. Baranauskienė, S. Jachimovičiūtė, J. Jachno, J. Torresan, V. Michailovienė, J. Matulienė, J. Sereikaitė, V. Bumelis, D. Matulis, *Biophys. J.* **2008**, *95*, 3222–3231.
[87] S. Keller, C. Vargas, H. Zhao, G. Piszczek, C. A. Brautigam, P. Schuck, *Anal. Chem.* **2012**, *84*, 5066–5073.
[88] H. Zhao, G. Piszczek, P. Schuck, *Methods* **2015**, *76*, 137–148.
[89] J. F. Morrison, *Biochim. Biophys. Acta Enzymol.* **1969**, *185*, 269–286.
[90] J. W. Williams, J. F. Morrison, in *Methods Enzymol.*, Academic Press, **1979**, pp. 437–467.

Manuscript received: February 17, 2021
Revised manuscript received: March 8, 2021

© 2021 The Authors. Published by Wiley-VCH GmbH

Biophysical Journal
Article

Biophysical Society

Isoform-Selective Enzyme Inhibitors by Exploring Pocket Size According to the Lock-and-Key Principle

Virginija Dudutienė,[1] Asta Zubrienė,[1] Visvaldas Kairys,[2] Alexey Smirnov,[1] Joana Smirnovienė,[1] Janis Leitans,[3] Andris Kazaks,[3] Kaspars Tars,[3] Lena Manakova,[4] Saulius Gražulis,[4] and Daumantas Matulis[1,*]
[1]Department of Biothermodynamics and Drug Design and [2]Department of Bioinformatics, Institute of Biotechnology, Life Sciences Center, Vilnius University, Vilnius, Lithuania; [3]Latvian Biomedical Research and Study Centre, Riga, Latvia; and [4]Department of Protein-DNA Interactions, Institute of Biotechnology, Life Sciences Center, Vilnius University, Vilnius, Lithuania

ABSTRACT In the design of high-affinity and enzyme isoform-selective inhibitors, we applied an approach of augmenting the substituents attached to the benzenesulfonamide scaffold in three ways, namely, substitutions at the 3,5- or 2,4,6-positions or expansion of the condensed ring system. The increased size of the substituents determined the spatial limitations of the active sites of the 12 catalytically active human carbonic anhydrase (CA) isoforms until no binding was observed because of the inability of the compounds to fit in the active site. This approach led to the discovery of high-affinity and high-selectivity compounds for the anticancer target CA IX and antiobesity target CA VB. The x-ray crystallographic structures of compounds bound to CA IX showed the positions of the bound compounds, whereas computational modeling confirmed that steric clashes prevent the binding of these compounds to other isoforms and thus avoid undesired side effects. Such an approach, based on the Lock-and-Key principle, could be used for the development of enzyme-specific drug candidate compounds.

SIGNIFICANCE In the design of isoform-selective enzyme inhibitors, a series of homologous compounds with augmented substituent groups was designed. Larger inhibitors bound with greater affinity until reaching a limit of accommodation to the active site followed by an abrupt decrease in affinity upon further augmentation of the substituent, thus demonstrating the validity of the Lock-and-Key principle in determining the affinity and selectivity of protein-ligand recognition.

INTRODUCTION

Compounds may bind to proteins via different mechanisms, ranging from a rigid "Lock-and-Key" to flexible "induced fit" or "conformational selection" (1,2) modes. The induced fit emphasizes ligand ability to alter protein structure and dynamics upon binding. The ligand-bound and ligand-free states of a protein would differ significantly. The conformational selection, however, postulates that protein exists in multiple conformational states in solution, and the ligand selects and binds to the most favored conformation. In this case, ligand binding does not "induce" a conformational change. On the other hand, the Lock-and-Key principle may be valid when the protein is conformationally rather rigid and does not substantially change its structure upon ligand binding. In this case, it is important to design ligands that would fit the active site pocket of the disease target protein, being not too small and not too large in size to fit the pocket as closely as possible.

Here, we designed a series of compounds of increasing sizes until the ligand compound could not fit in the active site and the affinity dropped thousands of fold. Modulating the size of the ligand yielded both high-affinity and high-selectivity compounds, and the principle could be applied to drug design to a much greater extent than is currently used. To demonstrate this approach, we have used a family of enzymes that possesses the following important features: 1) a family consists of 12 highly similar structural isoforms (isozymes) with essentially the same fold; 2) the active site pocket of all isoforms is highly similar, differing from each other by only several amino acids; and 3) the Zn(II) metal ion, bound in tetrahedral geometry to four nitrogen atoms, three protein histidines, and the nitrogen of sulfonamide group, forming a coordination bond between the ligand

Submitted April 27, 2020, and accepted for publication August 21, 2020.
*Correspondence: matulis@ibt.lt
Editor: Alexandr Kornev.
https://doi.org/10.1016/j.bpj.2020.08.037
© 2020 Biophysical Society.

and protein, increasing the affinity, orienting the ligand, and allowing the prediction of how to increase the molecule size to fully fit the active site pocket.

The family of zinc metalloenzymes used in this study is carbonic anhydrase (CA), an enzyme that catalyzes the reversible hydration of CO_2 and maintains various physiological functions in essentially every cell of any living organism, from bacteria to humans. Humans express 15 CA isoforms, but only 12 of these forms contain Zn(II) and are catalytically active (3,4). The 12 active isoforms have different subcellular localizations and can be found as cytosolic (I, II, III, VII, and XIII), mitochondrial (VA and VB), extracellularly oriented but membrane-bound via a transmembrane helix (IX, XII, and XIV) or via a lipid anchor (IV), and secreted (VI). Some of these isoforms have been therapeutic drug targets for decades and are currently used as targets for the development of antiglaucoma, diuretic, antiobesity, and anticonvulsant drugs. The isoforms CA IX and CA XII have emerged as possible targets against cancer (5–8). However, many of the current clinical CA inhibitors, mostly used to treat glaucoma and high altitude sickness, demonstrate little selectivity for a particular CA isoform and, as a consequence, indiscriminately inhibit most of the isoforms.

The first CA was purified in 1933 (9), whereas the first determination that sulfonamides inhibit CA was made in 1940 (10). The first x-ray crystal structure of a carbonic anhydrase was solved by Liljas et al. in 1972, showing the presence of Zn(II) in the active site (11–13). The removal of Zn(II) from the native holoCA II decreased the affinity of primary sulfonamides to apoCA II (missing Zn(II)) by ~6 kcal/mol (14). The Whitesides group determined that approximately −8 kcal/mol of benzenesulfonamide binding energy is contributed by the Zn-N bond and only −1 kcal/mol by the hydrogen bonding network. The contacts between CA II and the un-substituted benzene ring contributed only −2.9 kcal/mol (15). The introduction of substituents on the benzene ring could significantly influence the orientation and binding mode of compounds in the active site and consequently strengthened the interaction with CA and enabled the generation of inhibitors with increased affinity and selectivity for several CA isoforms (16).

The group of R. McKenna has made significant efforts into designing human CA isoform-specific inhibitors by determining and reviewing the x-ray crystallographic structures of CA-ligand complexes (4,17,18). The deepest part of the active site pocket has been called the "conserved pocket" because of high similarity among isoforms. A group of amino acids that differ among isoforms and could form a basis for selective recognition has been called a "selective pocket" and is situated somewhat further from the active site. Any ligand has to make contacts with those amino acids to exhibit a selective binding profile. Furthermore, differences in amino acids change the pocket size as well as the maximal ligand sizes that can be accommodated.

Isoforms CA I and CA II exhibit more occluded active site entrance than CA IX and CA XII (CA I and CA II have Tyr204 and Phe131 at the entrance of the binding pocket, whereas CA IX and CA XII have Val131 and Ala131 at isostructural positions), and these differences have been used to design selective inhibitors (7).

In addition, selective inhibitors have been made by exploiting different subcellular locations of CAs. This strategy was especially useful for increasing compound selectivity for extracellularly bound CA IX and CA XII by making membrane-impermeable inhibitors through the addition of cationic or other groups (19,20).

We have previously designed a series of fluorinated benzenesulfonamides bearing substituents at the para, para/ortho, and para/meta positions with respect to the sulfonamide group (21–23) and concluded that bulky hydrophobic groups at the ortho or meta positions are crucial for selectivity toward CA IX. For example, compound VR16-09, bearing a bulky aminocyclododecyl group at the ortho position and another polar tail at the para position exhibited a selectivity that was more than a millionfold higher for CA IX than for CA I and CA II (23). Crystallographic studies rationalized the selectivity of the compound, showing that the bulky 12-member carbon ring occupies the hydrophobic part of the CA IX active site, whereas binding to CA II was not favorable because of the clash with Phe131 (24).

CA isoforms are relatively rigid enzymes and based on crystallographic data seem to not undergo substantial conformational changes upon ligand binding. Recently we have compared 24 crystal structures of CA isoforms in the absence and presence of various benzenesulfonamides (25). The resultant RMSD values of the peptide backbone between proteins without inhibitor and complexes with inhibitor were in the range of 0.17–0.51 Å, showing that no significant conformational changes occurred upon ligand binding. Other studies reviewed in (16) showed the RMSD around 0.2–0.4 Å between ligand-free and ligand-bound forms of CA II.

Here, we have synthesized di-ortho- and di-meta-substituted benzenesulfonamides with hydrophobic substituents of a systematically increasing size. The augmentation of the inhibitor size allowed determination of the maximal contact area and maximal size that could fit in the protein pocket. Variation of the substituent size and bulkiness allowed us to explore the features of CA active site cavities, giving new insights into the rational design of CA-selective inhibitors.

MATERIALS AND METHODS

Protein preparation

Production and purification of 12 catalytically active human CA isoforms (CA I, II, III, IV, VA, VB, VI, VII, IX, XII, XIII, and XIV) were performed

as previously described (26). The catalytic domain of CA IX used for co-crystallization with inhibitor was produced in methylotrophic yeast *Pichia pastoris* as described in (27).

The purity of all recombinant CAs was analyzed by SDS-PAGE, and the molecular weights were confirmed by HR-MS.

Fluorescent thermal shift assay

Fluorescent thermal shift assay (FTSA) determinations of compound affinities were performed by heating the protein samples containing various concentrations of an inhibitor from 25 to 99°C while recording extrinsic fluorescence of the solvatochromic dye 8-anilino-1-naphthalene sulfonate (ANS) or Sypro Orange and determining the protein melting temperatures at each compound concentration by fitting the melting curves to a two-state model of the protein unfolding (28,29). The resultant melting temperatures were plotted as a function of added ligand concentration, and the binding constants were obtained according to the model, taking into account the thermodynamics of protein unfolding and ligand binding (28,29).

The FTSA experiments were performed in a Corbett Rotor-Gene 6000 (QIAGEN Rotor-Gene Q, Hilden, Germany) instrument using the blue channel (excitation 365 ± 20 nm, detection 460 ± 15 nm). Samples contained 5–10 μM protein, 0–400 μM ligand, 50 μM ANS or 2000-3000-fold diluted Sypro Orange, and 50 mM sodium phosphate buffer containing 100 mM NaCl at pH 7.0, with a final dimethyl sulfoxide (DMSO) concentration of 2%. The applied heating rate was 1°C/min. All experiments were repeated at least twice.

Stopped-flow CO_2 hydration assay

Carbonic anhydrase inhibition experiments were performed by applying the stopped-flow CO_2 hydration assay (SFA) by using an Applied Photophysics (Leatherhead, UK) SX.18MV-R stopped-flow spectrophotometer at 24°C. Reaction buffer contained 25 mM Hepes, 0.2 M sodium sulfate and 50 μM Phenol Red indicator (λ-557 nm) (pH 7.5). Saturated CO_2 solution was prepared by bubbling the CO_2 gas in Milli-Q water for 1 h at 24°C. The enzyme concentration was 200 nM for CA I, 50–100 nM for CA II, 300 nM for CA III, 100–200 nM for CA IV, 113 nM for CA VA, 264–300 nM for CA VB, 100 nM for CA VI, 50 nM for CA VII, 10–50 nM for mammalian CA IX, 150 nM for yeast CA IX, 50–200 nM for CA XII, 200–500 nM for CA XIII, and 40–45 nM for CA XIV. The inhibitor concentration was 0–150 μM (in a row of twofold or threefold serial dilution) in ≤ 1.5% DMSO. Raw curves were fitted using a single exponential model, and the inhibition constants were determined using the Morrison equation:

$$CA\ act.(\%) = \left(1 - \frac{\left([CA] + [I] + K_d - \sqrt{([CA] + [I] + K_d)^2 - 4[CA][I]}\right)}{2[CA]}\right) \times 100\%,$$

where [CA] is the total added CA concentration, assuming that it is equal to the active enzyme concentration, [I] is the total added inhibitor concentration, and K_d is the dissociation constant. Fixed CA concentration was used to fit dose-response curves.

Determination of the pK_a of compound sulfonamide group

Compound was added to a series of 50 mM universal buffer solutions (ranging from pH 7.5 to 12.0 at every half pH unit) at the concentration of 60–200 μM, containing 2% DMSO. The UV-VIS spectra were recorded for each compound buffer solution at 25°C. The ratio of normalized absorbances (typically 10 nm above and below the isosbestic point) was plotted as a function of pH. The pK_a-value was determined by fitting the curve to the Henderson-Hasselbach equation. The pK_a-values determined at 25°C were recalculated to 37°C by using the Van't Hoff equation.

Intrinsic binding thermodynamics

Experimentally observed affinity constants and the IC_{50}-values or inhibition constants K_i are dependent on variables, such as pH, because of ligand-binding-linked protonation/deprotonation reactions occurring simultaneously with inhibitor binding. These dependencies may mislead the chemical reasons for the structure-affinity relationships. Therefore, the experimentally observed constants are called "observed," and these constants should not be used to explain the compound structural reasons for drug design, as previously explained (30). Instead, the intrinsic binding constant $K_{b,intr}$ should be calculated by dividing the experimentally determined observed binding constant K_b by the available fractions of

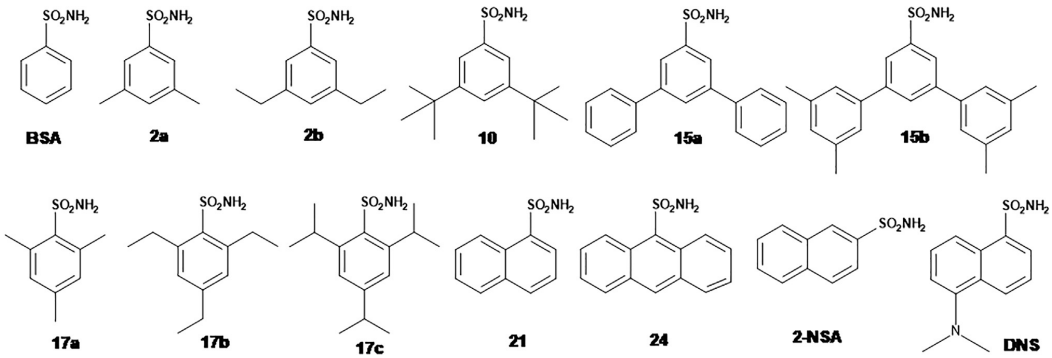


FIGURE 1 Series of benzenesulfonamide-bearing compounds designed for probing of CA enzyme active sites. Top line includes di-meta-substituted benzenesulfonamides; the bottom line shows the tri-substituted (di-ortho and para) benzenesulfonamides and ligands containing conjugated benzene ring systems. Compound synthesis is described in the Supporting Materials and Methods.

deprotonated inhibitor and protonated Zn(II)-bound water form of CA as follows:

$$K_{b,intr} = \frac{K_b}{\left(f_{RSO_2NH^-} f_{CAZnH_2O}\right)} \quad (1)$$

The fractions of the deprotonated inhibitor and the Zn(II)-bound water form of CA depend on the pK_a of the sulfonamide amino group (pK_{a_sulf}) and the pK_a of the water molecule attached to Zn(II) in the active site of CA (pK_{a_CA}), respectively:

$$f_{RSO_2NH^-} = \frac{10^{pH-pK_{a_sulf}}}{1 + 10^{pH-pK_{a_sulf}}} \text{ and} \quad (2)$$

$$f_{CAZnH_2O} = 1 - \frac{10^{pH-pK_{a_CAZnH_2O}}}{1 + 10^{pH-pK_{a_CAZnH_2O}}} \quad (3)$$

The pK_a-values of water molecules coordinated to Zn(II) in the active site of CA isoforms were taken from the following (30): CA isoform, pK_a: CA I, 8.1; CA II, 6.9; CA III, 6.5; CA IV, 6.6; CA VA, 7.3; CA VB, 7.0; CA VI, 6.0; CA VII, 6.8; CA IX, 6.6; CA XII, 6.8; CA XIII, 8.0; and CA XIV, 6.8).

The intrinsic Gibbs energy of binding was calculated using Eq. 4:

$$\Delta G_{intr} = -RT\ln(K_{b,intr}) \quad (4)$$

The maps listing the intrinsic Gibbs energies of compound binding to each isoform and the differences after applying functional group additions are shown in Figs. 3 and S3. The intrinsic $K_{d,intr}$-values for all CA isoforms are presented in Table S1. It is important that intrinsic rather than observed values are listed. However, the observed affinities are listed in Table 1 for the convenience of the reader who is accustomed to evaluating the observed constants at particular experimental conditions such as pH 7.0.

Molecular docking in silico

Molecular docking was performed using Smina (31), a fork of AutoDock Vina (32), because it supports a variety of scoring functions, including user-defined custom functions. Vinardo scoring function (33) was employed during the docking. Because of the importance of the coordination bond between Zn(II) and sulfonamide nitrogen, a pseudoatom was generated using the AutoDock4$_{Zn}$ tool (34) at a tetrahedral Zn(II) coordination site, and an additional quadratic potential between the generated pseudoatom and the sulfonamide nitrogen with −10 weight was added on top of the default Vinardo scoring function. A 22.5 × 22.5 × 22.5 Å^3-size grid box was used during the docking. The search exhaustiveness during the docking was increased to 50 instead of the default 8. After the docking, the lowest energy docked pose was rescored using the unmodified Vinardo scoring function (33) as well as the Convex-PL v0.3 scoring function (35). The human CA isoforms CA VA and CA VB, which did not have structures in the Protein Data Bank (PDB) were built using SWISS-MODEL web server (36), based on murine CA V template (PDB: 1KEQ). For the rest of catalytic human CAs, the receptor models were taken from the PDB (chain A except where noted): 1AZM (CA I), 3HS4 (CA II), 3UYQ (CA III), chain C of 5JN8 (CA IV), 3FE4 (CA VI), 6H38 (CA VII), 3IAI (CA IX), 1JD0 (CA XII), 3CZV (CA XIII), and 4LU3 (CA XIV). In the PDB structure, PDB: 3FE4 of CA VI the magnesium ion was present instead of zinc; therefore, it was replaced by Zn for the purposes of docking. Additional dockings were also performed into CA VI-mimic, PDB: 6QL2 (37). The receptor was kept rigid during the docking, except for the cases noted in the text in which one or two specified side chains were mobilized. The protein structures were prepared using UCSF Chimera v1.13.1 (38). The ligands were optimized using MMFF94s force field (39) within Avogadro program v1.2.0 (40). The conversions of the files into various formats were done with AutoDock Tools version 01.26.2015 (labeled as "latest") (41) and Open Babel v2.4.1 (42). Open Babel Application Programming Interface was used to calculate heavy atom RMSDs between the docked and x-ray structures.

Crystallization of CA-compound complexes

The proteins were concentrated by ultrafiltration to 20–38 mg/mL (CA II), 25 mg/mL (CA XII), and 10 mg/mL (CA IX prepared in yeast). Crystallization conditions (buffers) are listed in Table S7. The

TABLE 1 The Observed Dissociation Constants K_d (μM) for Compound Interaction with Human Recombinant CA Isoforms Are Listed as Determined by FTSA at 37°C and pH 7.0

	Dissociation Constants K_d (μM) of CA Isoforms											
Cmpd	CA I	CA II	CA III	CA IV	CA VA	CA VB	CA VI	CA VII	CA IX	CA XII	CA XIII	CA XIV
BSA	7.1	1.8	>400	17	8.3	33	14	6.7	1.5	13	7.5	8.7
2a	21	18	>400	28	17	2.5	110	25	8.3	83	6.3	5.0
2b	67	3.8	>400	6.7	>400	0.13	33	4.6	0.33 (1.9)	17	0.91	1.7
10	>200	2.5 (1.25)	>200	11	>200	4.4	83	2.0	0.056 (0.18)	5.9 (1.1)	0.50	1.4
15a	>200	58 (>100)	>400	1.3	>400	>400	125	>400	0.0065 (0.067)	0.83 (0.50)	1.4	0.40
15b	>200	>200 (>100)	>200	>200	>200	>200	>200	>200	0.091 (0.33)	>200	>200	>200
17a	29	14	>600	50	25	18	125	50	17	100	17	5.0
17b	>400	>400	>400	>400	>400	100	>400	>400	50	>400	>400	10
17c	>400	>400	>400	>400	>400	>400	>400	>400	>400	>400	>400	>400
21	2.6	2.9	>400	2.5	3.3	0.83	5.0	1.6	0.33	2.5	0.83	0.56
24	>400	6.7	>400	5.0 (5.9)	>400	0.067 (<0.15)	8.3	10	1.0 (1.1)	9.8 (12.5)	1.3	1.3 (1.1)
2-NSA	0.91	0.77	>400	10	13	5.0	17	2.2	0.24 (0.13)	6.3	5.0	0.29
DNS	0.40 (<0.05)	2.0 (2.5)	>400	1.9 (0.67)	10 (2.8)	1.0 (4.0)	12.5 (5.0)	3.2 (1.7)	0.0040 (<0.015)	0.50 (0.03)	0.50 (<0.1)	0.17 (0.22)
AZM (30)	2.4 (0.29)	0.046 (0.010)	40	0.087	0.84	0.14	0.22	0.013	0.021 (0.0067)	0.13 (0.025)	0.12 (<0.01)	0.063

Uncertainties of the FTSA and SFA measurements are ∼1.6-fold in K_d. For comparison, the dissociation constants K_d (μM) were determined by the SFA at 24°C and pH 7.5.

ligand solutions for crystal soaking were made by mixing of 50 μL of corresponding reservoir solution and 0.5 μL of 50 mM ligand solution (in DMSO). In the case of CA IX, the ligands were added via co-crystallization. The protein was incubated for an hour in a 5 mM ligand solution dissolved in DMSO before mixing it with the crystallization buffer.

X-ray data collection and structure determination

Two data sets of CA II-17a, CA II-2-NSA were collected at the European Molecular Biology Laboratory (DESY, Hamburg, Germany) beamline P14; four data sets CA II-2a, CA II-24, CA XII-10, CA XII-15a were collected at beamline P13; CA II-21 was collected at beamline X11. The data set of CA IX-15a was collected at BESSY II (Berlin, Germany) beamline 14.1, and CA IX-2-NSA was collected at MAX IV (Lund, Sweden) beamline BioMAX. Most of the data sets were processed using the XDS (43) program, whereas data sets of CA II-21, CA IX-15a were processed by MOSFLM (44). The molecular replacement was made by the MOLREP (45) program, using the following initial models: 3HLJ for CA II, 1JD0 for CA XII, and 6FE2 for CA IX. The three-dimensional models of compounds were created using the AVOGADRO (40) program. The library files, which contain complete chemical and geometric descriptions of compounds, were created using the LIBCHECK program (46). The models were prepared using COOT (47) and refined by REFMAC (48). All represented graphics were made using PyMOL programs (version 1.8.x; PyMOL). Coordinates and structure factors have been deposited to the Research Collaboration for Structural Biology (RCSB). Data processing, refinement, and validation statistics are shown in Table S3.

RESULTS

Compound binding and structure-affinity relationship

The binding of synthesized compounds (Fig. 1) to 12 catalytically active human CA isoforms was determined by the FTSA. The K_d-values for all compounds are listed in Table 1. Because FTSA only demonstrates binding and does not determine inhibition of enzymatic activity, the compound inhibitory properties were confirmed by the SFA of enzymatic inhibition of the CO_2 hydration (data are listed in the parentheses in Table 1).

Augmentation of substituents was performed on the benzenesulfonamide scaffold in three directions: 1) substituting 3,5-positions; 2) substituting 2,4,6-positions; and 3) extending the condensed ring system, having a significant effect on the binding affinities to the CA isoforms (Fig. 2). Substitution of 3,5-positions had an important effect on the CA IX, an anticancer drug target, binding profile. The affinity

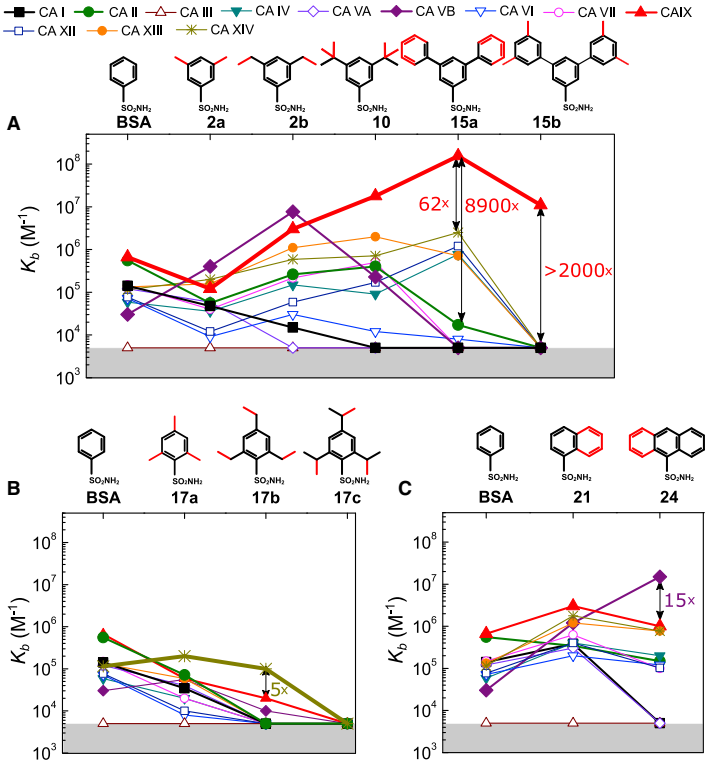


FIGURE 2 The observed binding constants of compound interactions with 12 CA isoforms of 3,5-substituted compounds (*A*), 2,4,6-substituted compounds (*B*) and ligands with fused benzene rings (*C*). Compound structures are shown on the top of each panel, and the gradual increase in the compound size and hydrophobicity compared with that of the neighboring compound is shown in red. A higher position means greater affinity, and the ratios of affinities (*colored numbers* inside the plots) show the selectivity over other isoforms. The gray area at the bottom of each plot shows the limit of detection of the assay. To see this figure in color, go online.

toward CA IX increased some 10-fold when changing from methyl (**2a**) to ethyl (**2b**), to tert-butyl (**10**), and to phenyl (**15a**) modifications from 8300 to 330, to 56, and 6.5 nM, respectively (Fig. 2 *A*). The last modification of 3,5-diphenyl groups (**15a**) to 3,5-dimethylphenyl groups (**15b**) decreased the affinity for CA IX by a factor of 10 (K_d = 91 nM). However, the bulky **15b** did not bind to any other CA isoform, making it the most selective for CA IX in the whole series of compounds presented in this study. Its selectivity for CA IX exceeded 2000-fold compared with that for any other isoform.

The second series of compounds involved variation of the length and the branching of the alkyl chain in the 2,4,6- positions in benzenesulfonamide (**BSA**). Compounds bearing methyl (**17a**), ethyl (**17b**), and isopropyl (**17c**) groups were investigated. Unexpectedly, methyl substitution with ethyl led to the almost completely inactive compound **17b**. Compound **17c** with isopropyl groups failed to bind any CA isoforms, indicating that two isopropyl substituents in ortho positions make it impossible for the sulfonamide to find a binding-suitable position in any CA isoform. It also means that the active site arrangement is rather rigid. Because the binding affinity is substantially reduced with the size of the substituent at the 2,4,6- positions (methyl < ethyl < isopropyl), the available space for the ligand is increasingly limited.

In the third series of compounds containing fused aromatic rings, the bulkiest anthracene-9-sulfonamide **24** was found to be a nanomolar inhibitor of CA VB (K_d = 67 nM), selective over the remaining CAs, in which the affinity was micromolar or lower.

The overall tendency was that the substituents of increased size bound with higher affinity, presumably due to better contacts with the protein until they filled the available space. Further increase in the size of the compound led to a sharp decrease in affinity due to inability to fit in the active site.

To investigate the structure-affinity relationship, intrinsic dissociation constants ($K_{d,intr}$) and intrinsic Gibbs energy (ΔG_{intr})-values for interactions between CA isoforms and compounds were calculated (Tables S1 and S2). The intrinsic parameters represent the actual binding reaction between the sulfonamide with a deprotonated amino group and the Zn-bound water form of CA. Such a binding reaction has been confirmed by neutron diffraction crystallography as the reaction taking place when sulfonamides bind to CA (49–51). In the compound structure-affinity correlation analysis, only intrinsic parameters are meaningful, providing insight into molecular recognition.

Using ΔG_{intr}-values, we constructed compound structure-affinity correlation maps (Figs. 3 and S3). The modification of the simplest compound **BSA** by introducing hydrophobic substituents at di-meta positions in the direction of **2a**→**2b**→**10**→**15a** was the most favorable for CA IX, with the absolute value of ΔG_{intr} gradually increasing from −54.1 kJ/mol for **2a** to −71.9 kJ/mol for **15a**. Compound **15a** with the diphenyl groups at the meta positions of benzenesulfonamide was the strongest binder of CA IX ($K_{d,intr}$ of 0.8 pM). Compound **15a** was the optimal compound for efficient CA IX inhibition, and further modification to **15b** was unfavorable for binding to CA IX and all other CAs.

The binding affinity increased slightly for CAs in the direction **2a**→**17a** (dimethyl→trimethyl groups) but decreased for all isoforms in the direction **17a**→**17b**→**17c** (from trimethyl to triethyl and triisopropyl substituents), showing that such compounds are too bulky to fit in the active sites of CAs or that the positions of the two ortho-methyl groups make the arrangement of the inhibitor energetically unfavorable.

The interaction thermodynamics of the synthesized compounds with the 12 CA isoforms clearly showed that the active site cavities of the CA isoforms differ in volume and shape. The variation of substituent size and bulkiness in the benzene ring allowed us to determine the optimal inhibitor diameter and shape for the efficient inhibition of cancer-related isoform CA IX and mitochondrial CA VB, which is implicated in obesity-related pathologies.

X-ray crystal structures of compound-CA complexes

Nine x-ray crystallographic structures of the inhibitors bound in the active sites of several CA isoforms were determined to study the structure-thermodynamics correlations and the binding recognition (Figs. 4 and S5). The structures show the most energetically favorable orientations of the bound ligand. In each case, the sulfonamide amino group formed a direct coordination bond with the Zn(II), whereas the hydrophobic part of each compound was exposed to the solvent.

CA II exhibits a narrower active site than CA IX because CA II contains Phe131 instead of Val (Fig. 4). The limitation of the size of the binding pocket was likely the main reason for the differences in the binding affinities of bulky compounds to CA II and CA IX.

The sulfonamide group of compounds **21** and **17a,** bearing either the naphthalene ring (in **21**) or 2,4,6-trimethylbenzene (in **17a**), occupied similar positions in both crystal structures of CA II (Fig. 4 *A*). Both crystal structures had comparable resolutions of 1.4 and 1.8 Å, respectively, and therefore, the solvent molecules in both structures could be compared. Water molecules in the hydrophilic part of the active site in these structures could be found in very similar positions (marked by *yellow circles* in Fig. 4). Sulfonamides **17a** and **21** had similar intrinsic binding affinities to CA II, and the $K_{d,intr}$-values were equal to 0.65 and 1.7 nM, respectively (Table S1). Interestingly, binding of compound **21** to CA II induced rotation of the Leu141 and Leu198 side chains to better accommodate the ligand in the binding site compared

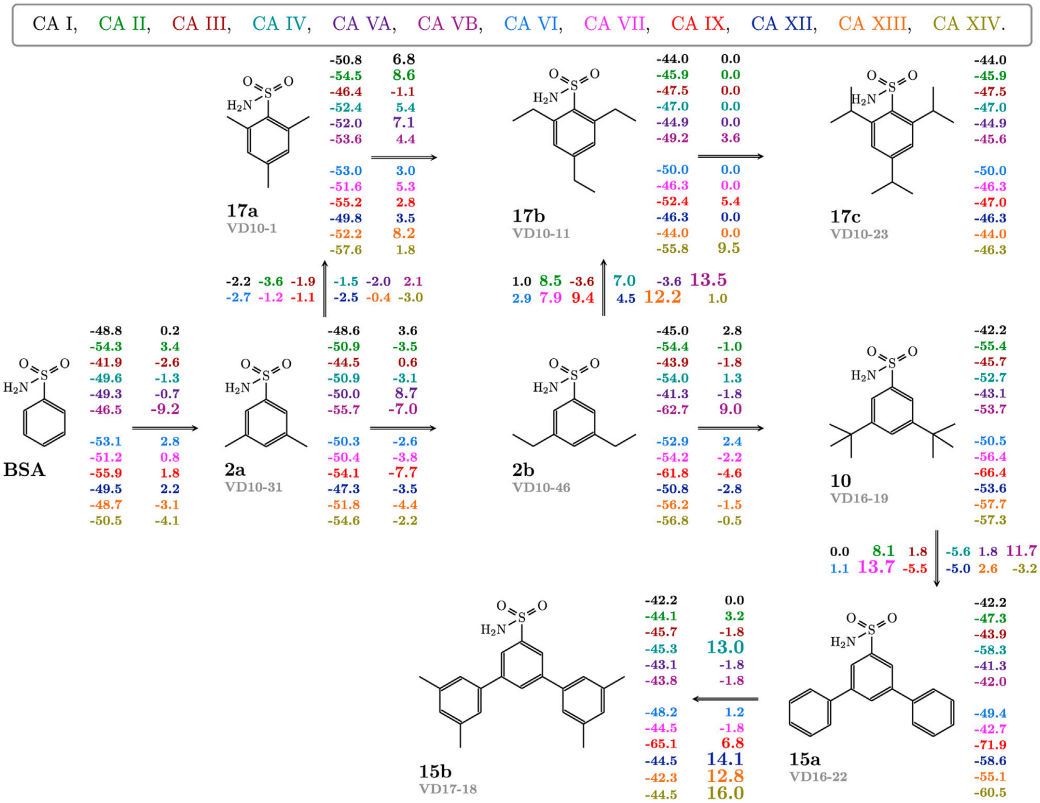


FIGURE 3 The map of correlations between the compound chemical structures and the intrinsic standard Gibbs energy changes upon compound binding to all 12 CA isoforms is shown. Chemical structures of compounds are listed according to their similarities while growing in molecular size in the direction of arrows. Intrinsic Gibbs energies of binding are listed next to the chemical structures. Differences in the intrinsic Gibbs energies upon binding between the structurally similar compounds are shown next to the arrows. The values are in kJ/mol. Negative values show tighter binding, whereas positive values indicate weaker affinities. Colors represent the 12 catalytically active human CA isoforms. This map shows how small changes in compound structure lead to relatively large changes in the binding energy and, at the same time, provide the selectivity of binding to a particular CA isoform. To see this figure in color, go online.

with the Leu141 and Leu198 geometries in CA II complexes with compounds **17a, 2a**, **2-NSA**, and **24**, solved in this study, as well as other smaller ligands, including **AZM** (PDB: 3HS4) and **BSA** (PDB: 6GDC).

The next pair of compounds to be compared is **2-NSA** and **2a** (Fig. 4 *B*). Naphthalene derivative **2-NSA** differed from **21** by the position of sulfonamide on the naphthalene ring, and benzenesulfonamide derivative **2a** differs from **17a** by the positioning of the methyl groups. The **2-NSA** in CA II was modeled by two alternate conformations, but the electron density of the second conformation (Fig. S4 *A*) is weak. Benzene rings of benzenesulfonamide of both compounds formed aliphatic-aromatic interactions with the side chain of residue Leu141. The positions of sulfonamides are similar in both crystal structures. The distribution of water molecules in the hydrophilic parts of the CA II active site was similar (Fig. 4 *B*), as were the conformations of the active site residues. The intrinsic binding affinities of both compounds were also comparable (Table S1, $K_{d,intr}$ 0.57 nM (**2-NSA**) vs. 2.6 nM (**2a**)). Two alternate conformations of naphthalene derivative **2-NSA** could be due to a quasisymmetry of the shape of the naphthalene ring when it is flipped around the sulfonamide C-S bond.

Fig. 4 *C* compares the binding modes of naphthalene derivatives **2-NSA** and **21** in CA II. These inhibitors differed by the position of sulfonamide on the naphthalene ring. Because of the fixed position of sulfonamide specifically bound to the zinc atom, the positions of the naphthalene substituent were determined by the geometry of the active site cavity. The narrower compound **2-NSA** was found in an

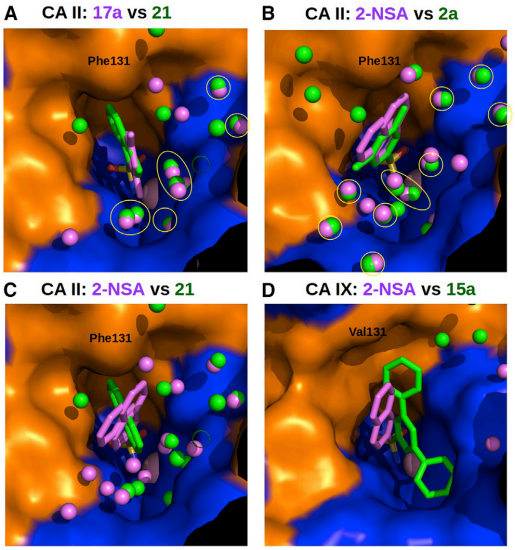


FIGURE 4 Pair-wise comparison of the structural arrangement of related compounds bound to CA II and CA IX as determined by x-ray crystallography. Inhibitors bound to CA II are all shown in the same orientation. The structures and names of the inhibitors in pairs are shown in pink or green. Water molecules found in corresponding crystal structures are shown as green or pink spheres. The Zn(II) ion is shown as a pink sphere at the bottom of the active site. The CA protein surface is colored orange for hydrophobic residues (Val, Ile, Leu, Phe, Met, Ala, Gly, and Pro) and blue for residues with charged and polar side chains (Arg, Asp, Asn, Glu, Gln, His, Lys, Ser, Thr, Tyr, Trp, and Cys). (*A*) Compounds **17a** (PDB: 6T4N, *pink*) and 21 (PDB: 6T4P, *green*) bound to the active site of CA II. (*B*) Compounds **2-NSA** (two alternately oriented positions, PDB: 6T81, *pink*) and **2a** (PDB: 6T4O, *green*) bound to the active site of CA II. (*C*) Compounds **2-NSA** (two alternately oriented positions, PDB: 6T81, *pink*) and **21** (PDB: 6T4P, *green*) bound to the active site of CA II. (*D*) Compound **2-NSA** (PDB: 6TL6, *pink*) and **15a** (PDB: 6TL5, *green*) bound to the active site of CA IX. Electron density maps, the refinement statistics, and additional figures are provided in the Supporting Materials and Methods. To see this figure in color, go online.

alternate conformation in the crystal structure. The naphthalene ring of compound **21** was located in the hydrophobic environment beneath the Phe131 side chain, whereas the naphthalene ring of compound **2-NSA** could not have the same orientation because both alternate conformations should clash sterically with Phe131. Despite dissimilar orientations of naphthalene rings and different positions of water molecules, these compounds had comparable affinity to CA II ($K_{d,intr}$: 1.7 nM for **21** vs. 0.57 nM for **2-NSA**; Table S1). The resolution of the crystal structure of CA II with the naphthalene derivative **2-NSA** was much better than of the complex with **21** (1.0 Å vs. 1.8 Å, respectively). As shown in Fig. 4 *C*, compound **21** rather tightly filled the hydrophobic part of the active site cavity.

Fig. 4 *D* compares the binding mode between compounds **2-NSA** and **15a** in the active site of CA IX. The sulfonamide groups in both compounds were slightly tilted (the S-C bond was tilted by ~30°) with respect to each other because of spatial restraints imposed by the cavities on the hydrophobic ring systems. Compound **2-NSA** occupied the hydrophobic part of the active site of CA IX in a manner similar to that in complexes with CA II (Fig. 4 *B* or Fig. 4 *C*). Sulfonamide **15a** more efficiently occupied the active site of CA IX, and the benzene ring of one meta-substituent was located in the hydrophilic part of the active site, where it displaced water molecules. The meta-terphenyl derivative **15a** bound to CA IX 143-fold stronger than the naphthalene derivative **2-NSA**. The $K_{d,intr}$ were 0.00077 and 0.11 nM, respectively (Table S1). The large difference between the two binding affinities was due to different binding modes and better filling of the binding pocket by compound **15a**. The displaced water molecules from the hydrophilic part of the active site could not reach the sulfonamide group during Zn(II)-**15a** dissociation, as discussed in (52).

The binding mode of compound **15a** was similar in the active sites of CA XII and CA IX (compare Fig. 4 *D* (*green*) and Fig. S5 *D* (*pink*)). Compound **15a** bound significantly better to CA IX than to CA XII ($K_{d,intr}$ 0.00077 and 0.13 nM, respectively; Table S1). The active site of CA XII is more hydrophilic than that of CA IX (compare *blue* (hydrophilic) and *orange* (hydrophobic) *surfaces* in Figs. 4 *D* and S5 *D*). The binding is weaker to CA XII than to CA IX, likely because of hydrophobic compound **15a** binding to a more hydrophilic binding site of CA XII.

In silico docking of the compounds to the active sites of enzymes

Molecular docking can often give useful insight about the ligand-receptor structural arrangement, especially if the experimental structures are not available, and also provide the binding energy estimates. For this purpose, all studied compounds were docked to all 12 CA isoforms by using Smina (31), a fork of AutoDock (32), using Vinardo (33) and Convex-PL (35) scoring functions. In many cases, the best binders for the isoforms were correctly predicted by docking. The full analysis of the docking results can be found in the Supporting Materials and Methods. Below, we describe some of the insights into the binding of two highest-affinity compounds for CA IX revealed by docking.

An example of the docked structures of CA IX-selective ligands **15a** and **15b** compared with the x-ray structure of **15a** in the CA IX binding site is shown in Fig. 5. The picture displays superposed solvent-accessible surfaces of CA IX with CA I (Fig. 5 *A*) and CA II (Fig. 5 *B*) and shows the clashes of CA I and CA II surfaces with the two terminal rings of the bifurcated ligand in Fig. 5, *C* and *D*. Compounds **15a** and **15b** could not bind to CA I because of clashes with Phe91, Leu131, His67, and His200 or to CA II because of clashes with Phe131 and Asn67. The smaller Asn67 of CA II clashes with the ligand more than the bulkier Gln67 does

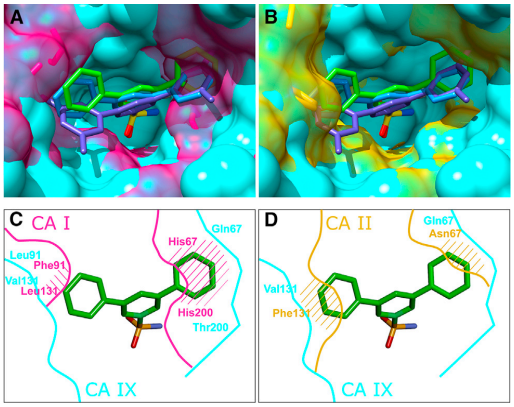


FIGURE 5 X-ray crystal structure of **15a** (*green sticks*) bound to CA IX (protein shown in *opaque cyan surface*) superimposed with the structures of CA I (*pink*) or CA II (*yellow*), showing that the compound cannot bind in the same orientation to either CA I or CA II because of steric clashes, shown as dashed areas in the bottom panels. The docked orientations of two CA IX-selective compounds **15a** (*blue sticks*) and **15b** (*purple sticks*) to CA IX closely resembled the x-ray position of **15a**. The solvent-accessible surface for CA IX is shown as an opaque cyan surface. The solvent-accessible surfaces of CA I (*transparent pink* in *A*) and CA II (*transparent yellow* in *B*) are shown, and the CA I and CA II protein atoms that extend out beyond the CA IX surface are visible as pink and yellow sticks. (*C*) and (*D*) show compound **15a** in the same orientation as that in the crystal structure, and the protein surfaces of CA I and CA II (in the same coloring) show clashes with both terminal rings of the bifurcate ligands. The numbering of amino acids in CA I and CA IX is presented according to CA II. Correlations between experimentally determined and calculated binding affinities are provided in the Figs. S6 and S7. To see this figure in color, go online.

in the same position in CA IX because Gln67 is flipped and its CO group forms a hydrogen bond with the amino group of Gln92. Interestingly, in some zones, CA IX is bulkier than CA I and CA II, but there are no clashes with the ligands. The docking in these cases fully reproduced the experimental crystallographic and thermodynamic binding data.

DISCUSSION

Despite the numerous studies concerning enzyme isoform-specific inhibitors, we do not have sufficiently well-defined tools for rational design of selective inhibitors. In this work, we present a method of CA isoform cavity investigation in which a benzenesulfonamide series with a substituted hydrophobic group of increasingly larger size was used. When the ligand size is incrementally increased, there ought to be a limiting size after which the molecule cannot fit into the binding site. This size limit should vary for every isoform and could be employed to search for isoform-selective inhibitors. Additionally, the aim was to increase the size of the ligand until, hopefully, it cannot fit in the binding pocket of some CA isoforms that we would not want to target. In particular, ubiquitous isoform CA II has a bulky Phe131 side chain pointing toward the binding site, whereas in clinically relevant isoform CA IX it is replaced by a smaller valine residue.

Variation of the substituent length and bulkiness was performed on the benzenesulfonamide scaffold by three approaches: 1) substituting 3,5-positions; 2) substituting 2,4,6-positions; and 3) extending the condensed ring system. This strategy proved to be successful and led to the discovery of several inhibitors specific for CA IX and CA VB. Promising CA IX inhibitors were revealed, namely **15a** (observed $K_d = 6.5$ nM, 60-fold higher selectivity than that of the next best binding isoform), **10** ($K_d = 56$ nM, 9-fold higher selectivity), and **15b** ($K_d = 91$ nM, >2000-fold higher selectivity). For **15b**, no binding was detected to any other catalytically active CA isoform; it bound solely to CA IX. Anthracene-9-sulfonamide **24** turned out to be a selective inhibitor for CA VB ($K_d = 67$ nM, 15-fold selectivity).

Some other compounds among the investigated series appear to be promising scaffolds for further development. For example, compared with **BSA**, naphthalene-1-sulfonamide **21** and **2-NSA** bound better to most CA isoforms; therefore, compared with **BSA**, they could potentially be better lead compounds in designing new CA inhibitors because the solved crystal structures with these compounds show that certain positions on these ligands could be advantageously expanded as substituents. **DNS** is an example of such improvement for **21**. The addition of a 5-(dimethylamino) group led to another selective nanomolar CA IX inhibitor ($K_d = 4$ nM, 40-fold higher selectivity).

It appears that the dominating mechanism or mode of action of the inhibitors followed the Lock-and-Key principle, in which the protein is structurally rather rigid and the conformations of the unliganded and ligand-bound protein are similar. The analysis of numerous available crystallographic structures of unliganded CA enzymes and enzyme-ligand complexes largely indicate that there is no major conformational change upon ligand binding (16,25). However, a previous study has indicated otherwise and preferred to conclude that the binding mechanism is occurring primarily according to the conformational selection principle (53).

Searching for leads or improving their selectivity is a routine approach in drug discovery. However, to the best of our knowledge, systematic exploration by increasing the ligand size in search of the expansion limit for a particular CA isoform is a novel approach that has not been attempted before for enzyme inhibition. Certainly, this approach would not have been possible without the presence of a sulfonamide group, which serves as an "anchor" group ensuring binding to the zinc ion situated in the deep cleft of the active site. The first and general rule was that the sulfonamide group had to achieve a favorable position for interaction in the active site of the CA isoform. The coordination bond between the nitrogen atom of the sulfonamide group and Zn(II) and the two hydrogen bonds between sulfonamide and the residues of the active site make the right conditions for tight interaction. Another part of the inhibitor is important for

the formation of additional interactions between the inhibitor and active site of the protein and to some extent affects the binding geometry of the sulfonamide moiety. The successful results herein were obtained by using exclusively hydrophobic substituents (except the dimethylamino substituent in **DNS**) in benzenesulfonamides, which simplified the task by avoiding the concern about matching hydrogen bond donors and acceptors in the receptors, etc. On the other hand, the obtained selective inhibitors were merely frameworks consisting of carbon atoms, and the properties of the obtained leads can be further improved by substituting some of the carbon atoms with other elements (nitrogen, oxygen, etc.) or by attaching additional, more finely tailored, or hydrophilic substituents.

The use of large, bulky hydrophobic substituents is not new (54,55). However, in similar cases, the hydrophobic groups targeted a specific position somewhere in the fringes of the binding pocket. In this study, the large hydrophobic group was targeted to fill the whole binding pocket as much as possible to probe its limits and to discover essential differences between the isoforms.

The x-ray structure of the best binding compound/receptor combination **15a**-CA IX provided insights into the origin of the strong binding, as well as the selectivity toward CA IX. The bulky Phe131 side chain in CA II is replaced by a smaller valine side chain in CA IX, allowing for a good fit of compound **15a** in the CA IX binding site. CA XII has an even smaller alanine side chain in that position, and the **15a**/CA XII complex exhibited a binding mode similar to that of the complex with CA IX. However, the ∼130-fold weaker binding of the hydrophobic ligand **15a** to CA XII than to CA IX was probably attributable to the more hydrophilic character of the binding pocket in CA XII than in CA IX.

X-ray crystallographic analysis of several compounds bound to CA II, CA IX, and CA XII essentially confirmed that the most successful ligands nearly completely filled the binding site. X-ray crystallography confirmed that the selectivity of **15a** toward CA IX was due to the combination of the optimal size of the binding site at a strategically important distance from zinc (e.g., because of the decreased size of residue 131, which is mutated from Phe in many CA isoforms to Val in CA IX).

Because only some crystal structures involving investigated compound/receptor complexes were available, docking of all compounds to all CA isoforms was employed to test the extent to which we could predict the structural positions and the binding energetics. To obtain two slightly different results for the binding affinities, docking was performed using two scoring functions with different underpinnings (Vinardo is a physics-based fitting function, and Convex-PL is a knowledge-based potential). The docking calculations were able to correctly reproduce the binding modes of larger ligands, such as **24**, **10**, and **15a**, with mixed success in reproducing the binding modes of the smaller ligands. For the smaller ligands, it can be argued that the accurate reproduction of the binding mode was not essential for the success of the undertaken task of finding selective inhibitors because of the following: 1) the observed small ligand scores are relatively close to each other, irrespective of geometry, and 2) the small ligands turned out to have a low isoform selectivity and therefore were less interesting. For the important CA IX and CA XII isoforms, the docking essentially confirmed conclusions drawn from the x-ray structures. It is concluded that docking has a predictive capability that can be used to design better drugs.

CONCLUSIONS

The carbonic anhydrase model enzyme active site cavity was explored with sulfonamide ligands by gradually augmenting their hydrophobic substituents. The funnel-like binding pockets in the 12 catalytically active human CA isoforms were able to differently accommodate ligands containing hydrophobic substituents at the benzene ring of the sulfonamide. Benzenesulfonamides bearing bulky hydrophobic substituents at meta positions yielded promising CA IX inhibitors, and di-meta compounds filled well the CA IX active site cavity. Extension of the condensed ring system allowed the discovery of new CA VB-selective inhibitors. The application of di-meta compounds distinguished the CA IX isoform as having the most spacious active site cavity. In contrast, substitution of ortho positions with more bulky substituents than methyl groups led to loss of interaction, revealing a rather narrow "neck" of the CA active site cavities not far from the zinc ion. All these observations indicate that the primary mechanism of ligand binding occurs according to the rigid Lock-and-Key principle. Optimal inhibitor and active site cavity sizes appear to be of great importance for the design of novel selective inhibitors for CA enzymes, and the approach could find use in drug design for other ligand-enzyme systems.

SUPPORTING MATERIAL

Supporting Material can be found online at https://doi.org/10.1016/j.bpj.2020.08.037.

AUTHOR CONTRIBUTIONS

V.D. and D.M. conceived and designed the experiments. V.D. performed the synthesis. A.Z. and J.S. performed the binding and inhibition studies. V.K. performed the molecular modeling studies. A.S., J.L., K.T., L.M., and S.G. performed and analyzed the x-ray crystallography data. A.K. produced CA IX in yeast. V.D., A.Z., V.K., A.S., and D.M. wrote the manuscript. The manuscript was written through contributions of all authors. All authors have given approval to the final version of the manuscript.

ACKNOWLEDGMENTS

The authors thank Gleb Bourenkov and Guillaume Pompidor for help with data collection at the P14 and P13 European Molecular Biology Laboratory beamlines at PETRA III ring of the DESY synchrotron.

This research was supported by Grant S-MIP-17-87 from the Research Council of Lithuania. This work has been supported in part by iNEXT (grant number 653706), funded by the Horizon 2020 program of the European Commission. This work was supported by the European Regional Development Fund (ERDF) grant No. 1.1.1.2/VIAA/3/19/464 "Structural and kinetic studies of human carbonic anhydrases as multiple drug targets".

SUPPORTING CITATIONS

References (56–58) appear in the Supporting Material.

REFERENCES

1. Holyoak, T. 2013. Molecular recognition: lock-and-key, induced fit, and conformational selection. *In* Encyclopedia of Biophysics. G. C. K. Roberts, ed. Springer, pp. 1584–1590.
2. Boehr, D. D., R. Nussinov, and P. E. Wright. 2009. The role of dynamic conformational ensembles in biomolecular recognition. *Nat. Chem. Biol.* 5:789–796.
3. McKenna, R., and S. C. Frost. 2014. Overview of the carbonic anhydrase family. *Subcell. Biochem.* 75:3–5.
4. Aggarwal, M., B. Kondeti, and R. McKenna. 2013. Insights towards sulfonamide drug specificity in α-carbonic anhydrases. *Bioorg. Med. Chem.* 21:1526–1533.
5. Chiche, J., J.-E. Ricci, and J. Pouysségur. 2013. Tumor hypoxia and metabolism – towards novel anticancer approaches. *Ann. Endocrinol. (Paris).* 74:111–114.
6. Monti, S. M., C. T. Supuran, and G. De Simone. 2012. Carbonic anhydrase IX as a target for designing novel anticancer drugs. *Curr. Med. Chem.* 19:821–830.
7. Singh, S., C. L. Lomelino, …, R. McKenna. 2018. Cancer drug development of carbonic anhydrase inhibitors beyond the active site. *Molecules.* 23:1045.
8. Mboge, Y., M. R. McKenna, and S. C. Frost. 2016. Advances in anticancer drug development targeting carbonic anhydrase IX and XII. *In* Topics in Anti-Cancer Research. A.-u. Rahman and K. Zaman, eds. Bentham Science Publishers, pp. 3–42.
9. Meldrum, N. U., and F. J. W. Roughton. 1933. Carbonic anhydrase. Its preparation and properties. *J. Physiol.* 80:113–142.
10. Mann, T., and D. Keilin. 1940. Sulphanilamide as a specific inhibitor of carbonic anhydrase. *Nature.* 146:164–165.
11. Liljas, A., K. K. Kannan, …, M. Petef. 1972. Crystal structure of human carbonic anhydrase C. *Nat. New Biol.* 235:131–137.
12. Tilander, B., B. Strandeberg, and K. Fridborg. 1965. Crystal structure studies on human erythrocyte carbonic anhydrase C. (II). *J. Mol. Biol.* 12:740–760.
13. Fridborg, K., K. K. Kannan, …, G. Wirén. 1967. Crystal structure of human erythrocyte carbonic anhydrase C. 3. Molecular structure of the enzyme and of one enzyme-inhibitor complex at 5-5 A resolution. *J. Mol. Biol.* 25:505–516.
14. King, R. W., and A. S. Burgen. 1976. Kinetic aspects of structure-activity relations: the binding of sulphonamides by carbonic anhydrase. *Proc. R. Soc. Lond. B Biol. Sci.* 193:107–125.
15. Krishnamurthy, V. M., B. R. Bohall, …, G. M. Whitesides. 2007. Thermodynamic parameters for the association of fluorinated benzenesulfonamides with bovine carbonic anhydrase II. *Chem. Asian J.* 2:94–105.
16. Krishnamurthy, V. M., G. K. Kaufman, …, G. M. Whitesides. 2008. Carbonic anhydrase as a model for biophysical and physical-organic studies of proteins and protein-ligand binding. *Chem. Rev.* 108:946–1051.
17. Pinard, M. A., B. Mahon, and R. McKenna. 2015. Probing the surface of human carbonic anhydrase for clues towards the design of isoform specific inhibitors. *BioMed Res. Int.* 2015:453543.
18. Lomelino, C. L., J. T. Andring, and R. McKenna. 2018. Crystallography and its impact on carbonic anhydrase research. *Int. J. Med. Chem.* 2018:9419521.
19. Casey, J. R., P. E. Morgan, …, C. T. Supuran. 2004. Carbonic anhydrase inhibitors. Design of selective, membrane-impermeant inhibitors targeting the human tumor-associated isozyme IX. *J. Med. Chem.* 47:2337–2347.
20. Supuran, C. T., A. Scozzafava, …, M. D. Banciu. 1998. Carbonic anhydrase inhibitors — Part 53. Synthesis of substituted-pyridinium derivatives of aromatic sulfonamides: the first non-polymeric membrane-impermeable inhibitors with selectivity for isozyme IV. *Eur. J. Med. Chem.* 33:577–594.
21. Dudutienė, V., A. Zubrienė, …, D. Matulis. 2015. Functionalization of fluorinated benzenesulfonamides and their inhibitory properties toward carbonic anhydrases. *ChemMedChem.* 10:662–687.
22. Dudutienė, V., J. Matulienė, …, D. Matulis. 2014. Discovery and characterization of novel selective inhibitors of carbonic anhydrase IX. *J. Med. Chem.* 57:9435–9446.
23. Kazokaitė, J., R. Niemans, …, D. Matulis. 2018. Novel fluorinated carbonic anhydrase IX inhibitors reduce hypoxia-induced acidification and clonogenic survival of cancer cells. *Oncotarget.* 9:26800–26816.
24. Tars, K., and D. Matulis. 2019. X-ray crystallographic structures of high-affinity and high-selectivity inhibitor complexes with CA IX that plays a special role in cancer. *In* Carbonic Anhydrase as Drug Target: Thermodynamics and Structure of Inhibitor Binding. D. Matulis, ed. Springer International Publishing, pp. 203–213.
25. Smirnov, A., E. Manakova, and D. Matulis. 2019. Correlations between inhibitor binding thermodynamics and co-crystal structures with carbonic anhydrases. *In* Carbonic Anhydrase as Drug Target: Thermodynamics and Structure of Inhibitor Binding. D. Matulis, ed. Springer International Publishing, pp. 249–261.
26. Mickevičiūtė, A., V. Juozapaitienė, …, D. Matulis. 2019. Recombinant production of 12 catalytically active human CA isoforms. *In* Carbonic Anhydrase as Drug Target: Thermodynamics and Structure of Inhibitor Binding. D. Matulis, ed. Springer International Publishing, pp. 15–37.
27. Leitans, J., A. Kazaks, …, K. Tars. 2015. Efficient expression and crystallization system of cancer-associated carbonic anhydrase isoform IX. *J. Med. Chem.* 58:9004–9009.
28. Matulis, D., J. K. Kranz, …, M. J. Todd. 2005. Thermodynamic stability of carbonic anhydrase: measurements of binding affinity and stoichiometry using ThermoFluor. *Biochemistry.* 44:5258–5266.
29. Petrauskas, V., A. Zubrienė, …, D. Matulis. 2019. Inhibitor binding to carbonic anhydrases by fluorescent thermal shift assay. *In* Carbonic Anhydrase as Drug Target: Thermodynamics and Structure of Inhibitor Binding. D. Matulis, ed. Springer International Publishing, pp. 63–78.
30. Linkuvienė, V., A. Zubrienė, …, D. Matulis. 2018. Thermodynamic, kinetic, and structural parameterization of human carbonic anhydrase interactions toward enhanced inhibitor design. *Q. Rev. Biophys.* 51:e10.
31. Koes, D. R., M. P. Baumgartner, and C. J. Camacho. 2013. Lessons learned in empirical scoring with smina from the CSAR 2011 benchmarking exercise. *J. Chem. Inf. Model.* 53:1893–1904.
32. Trott, O., and A. J. Olson. 2010. AutoDock Vina: improving the speed and accuracy of docking with a new scoring function, efficient optimization, and multithreading. *J. Comput. Chem.* 31:455–461.
33. Quiroga, R., and M. A. Villarreal. 2016. Vinardo: a scoring function based on Autodock Vina improves scoring, docking, and virtual screening. *PLoS One.* 11:e0155183.
34. Santos-Martins, D., S. Forli, …, A. J. Olson. 2014. AutoDock4(Zn): an improved AutoDock force field for small-molecule docking to zinc metalloproteins. *J. Chem. Inf. Model.* 54:2371–2379.
35. Kadukova, M., and S. Grudinin. 2017. Convex-PL: a novel knowledge-based potential for protein-ligand interactions deduced from structural databases using convex optimization. *J. Comput. Aided Mol. Des.* 31:943–958.
36. Waterhouse, A., M. Bertoni, …, T. Schwede. 2018. SWISS-MODEL: homology modelling of protein structures and complexes. *Nucleic Acids Res.* 46:W296–W303.

37. Kazokaitė, J., V. Kairys, …, D. Matulis. 2019. Engineered carbonic anhydrase VI-mimic enzyme switched the structure and affinities of inhibitors. *Sci. Rep.* 9:12710.

38. Pettersen, E. F., T. D. Goddard, …, T. E. Ferrin. 2004. UCSF Chimera–a visualization system for exploratory research and analysis. *J. Comput. Chem.* 25:1605–1612.

39. Halgren, T. A. 1999. MMFF VI. MMFF94s option for energy minimization studies. *J. Comput. Chem.* 20:720–729.

40. Hanwell, M. D., D. E. Curtis, …, G. R. Hutchison. 2012. Avogadro: an advanced semantic chemical editor, visualization, and analysis platform. *J. Cheminform.* 4:17.

41. Morris, G. M., R. Huey, …, A. J. Olson. 2009. AutoDock4 and AutoDockTools4: automated docking with selective receptor flexibility. *J. Comput. Chem.* 30:2785–2791.

42. O'Boyle, N. M., M. Banck, …, G. R. Hutchison. 2011. Open Babel: an open chemical toolbox. *J. Cheminform.* 3:33.

43. Kabsch, W. 2010. XDS. *Acta Crystallogr. D Biol. Crystallogr.* 66:125–132.

44. Battye, T. G. G., L. Kontogiannis, …, A. G. W. Leslie. 2011. iMOSFLM: a new graphical interface for diffraction-image processing with MOSFLM. *Acta Crystallogr. D Biol. Crystallogr.* 67:271–281.

45. Vagin, A., and A. Teplyakov. 2010. Molecular replacement with MOLREP. *Acta Crystallogr. D Biol. Crystallogr.* 66:22–25.

46. Vagin, A. A., R. A. Steiner, …, G. N. Murshudov. 2004. REFMAC5 dictionary: organization of prior chemical knowledge and guidelines for its use. *Acta Crystallogr. D Biol. Crystallogr.* 60:2184–2195.

47. Emsley, P., B. Lohkamp, …, K. Cowtan. 2010. Features and development of Coot. *Acta Crystallogr. D Biol. Crystallogr.* 66:486–501.

48. Murshudov, G. N., P. Skubák, …, A. A. Vagin. 2011. REFMAC5 for the refinement of macromolecular crystal structures. *Acta Crystallogr. D Biol. Crystallogr.* 67:355–367.

49. Kovalevsky, A., M. Aggarwal, …, R. McKenna. 2018. "To be or not to be" protonated: atomic details of human carbonic anhydrase-clinical drug complexes by neutron crystallography and simulation. *Structure.* 26:383–390.e3.

50. Koruza, K., B. P. Mahon, …, S. Z. Fisher. 2019. Using neutron crystallography to elucidate the basis of selective inhibition of carbonic anhydrase by saccharin and a derivative. *J. Struct. Biol.* 205:147–154.

51. Fisher, S. Z., M. Aggarwal, …, R. McKenna. 2012. Neutron diffraction of acetazolamide-bound human carbonic anhydrase II reveals atomic details of drug binding. *J. Am. Chem. Soc.* 134:14726–14729.

52. Smirnov, A., A. Zubrienė, …, D. Matulis. 2018. Crystal structure correlations with the intrinsic thermodynamics of human carbonic anhydrase inhibitor binding. *PeerJ.* 6:e4412.

53. Ma, H., A. Li, and K. Gao. 2017. Network of conformational transitions revealed by molecular dynamics simulations of the carbonic anhydrase II apo-enzyme. *ACS Omega.* 2:8414–8420.

54. Ashton, M. J., D. C. Cook, …, N. Vicker. 1994. Selective type IV phosphodiesterase inhibitors as antiasthmatic agents. The syntheses and biological activities of 3-(cyclopentyloxy)-4-methoxybenzamides and analogues. *J. Med. Chem.* 37:1696–1703.

55. Ilies, M. A., B. Masereel, …, C. T. Supuran. 2004. Carbonic anhydrase inhibitors: aromatic and heterocyclic sulfonamides incorporating adamantyl moieties with strong anticonvulsant activity. *Bioorg. Med. Chem.* 12:2717–2726.

56. Smirnovienė, J., V. Smirnovas, and D. Matulis. 2017. Picomolar inhibitors of carbonic anhydrase: Importance of inhibition and binding assays. *Anal. Biochem.* 522:61–72.

57. Grudinin, S., P. Popov, …, G. Cheremovskiy. 2016. Predicting binding poses and affinities in the CSAR 2013–2014 docking exercises using the knowledge-based Convex-PL potential. *J. Chem. Inf. Model.* 56:1053–1062.

58. Kadukova, M., and S. Grudinin. 2018. Docking of small molecules to farnesoid X receptors using AutoDock Vina with the Convex-PL potential: lessons learned from D3R Grand Challenge 2. *J Comput Aided Mol Des.* 32:151–162.

Vilniaus universiteto leidykla
Saulėtekio al. 9, III rūmai, LT-10222 Vilnius
El. p. info@leidykla.vu.lt, www.leidykla.vu.lt
Tiražas 15 egz.